FINAL REPORT

UPDATED SITE-SPECIFIC SEISMIC HAZARD AND DEVELOPMENT OF TIME HISTORIES FOR RESOLUTION COPPER'S NEAR WEST SITE, SOUTHERN ARIZONA

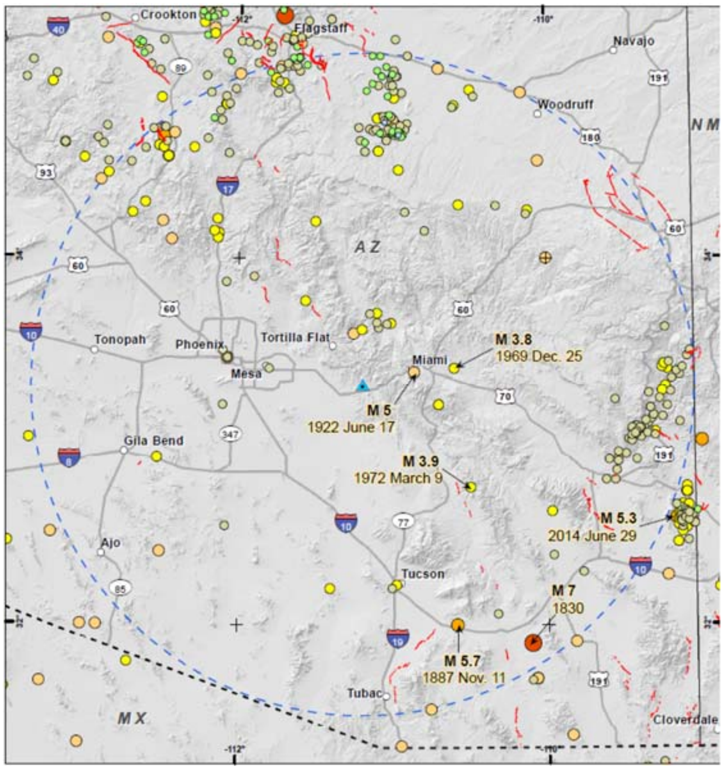

Prepared for
Resolution Copper

27 November 2017

Prepared by
Ivan Wong, Patricia Thomas, and Nora Lewandowski
Lettis Consultants International, Inc.
1981 N. Broadway, Suite 330, Walnut Creek, California 94596

Scott Lindvall
Lettis Consultants International, Inc.
27441 Tourney Road, Suite 220, Valencia, California 91355

and
Andrew Seifried
Lettis Consultants International, Inc.
4155 Darley Ave., Suite A, Boulder, California 94596

TABLE OF CONTENTS

TABLE OF CONTENTS

Tables

Figures

TABLE OF CONTENTS

TABLE OF CONTENTS

TABLE OF CONTENTS

TABLE OF CONTENTS

ABBREVIATIONS AND ACRONYMS

ABSMOOTH	LCI proprietary software that computes recurrence parameters from earthquake catalogs
BADCT	Arizona Mining Guidance Manual (Best Available Demonstrated Control Technology)
BHP	BHP Copper
BRPEWGII	Basin and Range Province Earthquake Working Group II
CMS	Conditional Mean Spectrum
DBM	Design Basis Memorandum
DSHA	Deterministic seismic hazard analysis
EPRI/DOE/NRC	Electric Power Research Institute/Department of Energy/ Nuclear Regulatory Commission
GMM	Ground motion model
HAZ45	PSHA computer program developed by Norm Abrahamson
KCB	Klohn Crippen Berger
MMI	Modified Mercalli intensity
M	Moment magnitude
m_b	Body-wave magnitude
M_D	Coda duration magnitude
M_I	Intensity-based magnitude
M_L	Richter local Magnitude
M_N	Nuttli magnitude
NEHRP	National Earthquake Hazards Reduction Program
NGA	Next Generation of Attenuation
NSHM	National Seismic Hazard Maps
PEER	Pacific Earthquake Engineering Research
PGA	Peak horizontal ground acceleration
PSHA	Probabilistic seismic hazard analysis
SA	Spectral acceleration
SBR	Southern Basin and Range Province
UCERF2	Uniform California Earthquake Rupture Forecast, Version 2
UCERF3	Uniform California Earthquake Rupture Forecast, Version 3
UHS	Uniform Hazard Spectrum
USGS	United States Geological Survey
V_S	Shear-wave velocity
V_S30	Time-averaged V_S in top 30 m
WGUEP	Working Group on Utah Earthquake Probabilities

EXECUTIVE SUMMARY

At the request of Resolution Copper, this report presents the results of a site- specific probabilistic seismic hazard analysis (PSHA) and deterministic seismic hazard analysis (DSHA) for the Near West site in southern Arizona. This study is an update of the 2013 study by Wong *et al.* ("Site-Specific Seismic Hazard Analyses for the Resolution Mining Company Tailings Storage Facilities Options, Southern Arizona") to incorporate comments from public scoping and newly collected baseline information. Since that study, site-specific shear-wave velocity (V_S) measurements have been made and there has been an update to the Next Generation of Attenuation (NGA)-West1 ground motion models (GMMs). Site conditions vary at the Near West site with facilities founded on a range of geologic units including Pinal schist, Gila conglomerate, rhyolite and diabase. Based on the recent site investigations and to cover the range of site conditions, the hazard is computed for two site conditions: (1) Pinal schist and Gila conglomerate (V_S30 [time-averaged V_S in the top 30 m] of 700 to 1,050 m/sec) and (2) rhyolite and diabase (V_S30 1,200 m/sec).

The objective of this study is to estimate the levels of ground motions that could be exceeded at specified annual frequencies (or return periods) for the two site conditions and to compare the site-specific PSHA results with the results of a DSHA. The site is located in the Basin and Range Province of southern Arizona. Southern Arizona has a low level of seismicity compared to the rest of the western U.S. The Near West site is located about 49 km southeast of the nearest Quaternary active fault, the Sugarloaf fault zone. Because of the low level of seismicity in southern Arizona, this study also assessed whether very active faults such as those in southern California could contribute to the hazard at long periods at sites such as Near West.

In this study, geologic and seismologic data were used to evaluate and characterize potential seismic sources, the likelihood of earthquakes of various magnitudes occurring on those sources, and the likelihood of the earthquakes producing ground motions over a specified level. Uncertainties in models and parameters are incorporated into the PSHA through the use of logic trees. Based on the PSHA, Uniform Hazard Spectra (UHS) and Conditional Mean Spectra (CMS), and time histories were developed. The study was performed in accordance with Appendix E "Engineering Design Guidance" of the Arizona Mining BADCT Guidance Manuelt.

The inputs into the PSHA consists of a seismic source characterization model, ground motion models, and the two site condition V_S30 values mentioned above. The seismic source includes both crustal faults capable of generating large surface-faulting earthquakes and an areal source zone to account for background seismicity that cannot be attributed to identified faults explicitly already included in the seismic source model. All known Quaternary active or potentially active faults within 200 km of the site were included in the analysis. We also included longer, more active faults beyond 200 km in southern California and Baja California such as tge San Andreas fault. A total of 47 faults are included in the seismic source model. For each fault, (1) rupture scenarios, (2) probability of activity, (3) fault geometry including rupture length, rupture width, orientation, and sense of slip, (4) maximum or characteristic magnitude and (5) earthquake recurrence including both recurrence model and rates were included in the seismic source model.

The Next Generation of Attentuation (NGA)-West2 GMMs were used in the hazard analyses to estimate ground motions as a function of magnitude, distance, and site condition among other parameters.

The results of the PSHA in terms of peak horizontal ground acceleration (PGA) are tabulated below for a range of return periods for the two site conditions. Also shown are the PGA values that were calculated in the 2013 study for a single site condition (V_S30 500 ± 100 m/sec). The major differences in approaches between the two studies were: (1) V_S data collected as part of this study was used in the updated study; (2) the more recent NGA-West2 GMMs were implemented; and (3) a more robust approach to assessing the hazard from background earthquakes was used. The probabilistic seismic hazard at the site is low consistent with the observations of low levels of tectonic activity and historical seismicity in the surrounding area. The PGA values in the updated study are lower than those from the 2013 analysis for a V_S30 of 1200 m/sec. The decrease at least at PGA is not significant.

Return Period (yrs)	This Study		2013
	Pinal Schist/Gila Conglomerate (V_S30 700 to 1050 m/sec)	Rhyolite/Diabase (V_S 1200 m/sec)	Gila Conglomerate (V_S30 1200 m/sec)
1,000	0.042	0.032	0.051
2,500	0.076	0.059	0.078
4,750	0.107	0.085	0.105
10,000	0.150	0.120	0.142

A DSHA for a scenario **M** 6.6 earthquake on the Sugarloaf fault, the nearest active fault to the site, at a rupture distance of 48.5 km was performed. The 84th percentile PGA was 0.079 g for Pinal schist/Gila conglomerate and 0.062 g for rhyolite/diabase.

In addition to the results of the PSHA and DSHA, CMS for a return period of 10,000 years for the two site conditions were calculated. Seven horizontal-component time histories for the same return period were also developed.

At the request of Resolution Copper, this report presents the results of a site- specific probabilistic seismic hazard analysis (PSHA) and deterministic seismic hazard analysis (DSHA) for its Near West Tailings Storage Facility (TSF) site in southern Arizona. This study is an update of the 2013 study by Wong *et al.* ("Site-Specific Seismic Hazard Analyses for the Resolution Mining Company Tailings Storage Facilities Options, Southern Arizona") to incorporate comments from public scoping and newly collected baseline information. Since that study, site-specific shear-wave velocity (V_S) measurements have been made and there has been an update to the Next Generation of Attenuation (NGA)-West1 GMMs. Site conditions vary at the Near West site with facilities founded on a range of geologic units including Pinal schist, Gila conglomerate, rhyolite and diabase. Based on the recent site investigations and to cover the range of site conditions, the hazard is computed for two site conditions: (1) Pinal schist and Gila conglomerate and (2) rhyolite and diabase.

1.1 PURPOSE

The objective of this study is to estimate the levels of ground motions that could be exceeded at specified annual frequencies (or return periods) for two site conditions and to compare the site-specific PSHA results with the results of a DSHA. The site is located in the Basin and Range Province of southern Arizona (Figure 1). Southern Arizona has a low level of seismicity compared to the rest of the western U.S. (Figure 2). The Near West site is located about 49 km southeast of the nearest Quaternary active fault, the Sugarloaf fault zone (Figure 3). Because of the low level of seismicity in southern Arizona, this study also assessed whether very active faults such as those in southern California could contribute to the hazard at long periods at sites such as Near West (Figure 4).

In this study, geologic and seismologic data were used to evaluate and characterize potential seismic sources, the likelihood of earthquakes of various magnitudes occurring on those sources, and the likelihood of the earthquakes producing ground motions over a specified level. This updated study builds upon numerous studies that have been performed for dams and other mining facilities in central and southern Arizona.

The PSHA methodology is used in this study for assessing ground motion hazard. The evaluation of seismic hazard required the explicit inclusion of the range of possible interpretations of components in the seismic hazard model, including seismic source characterization and ground motion estimation. These uncertainties particularly in areas like Arizona can be large for several reasons but primarily due to lack of comprehensive studies. Uncertainties in models and parameters are incorporated into the PSHA through the use of logic trees (Figure 5). The following report presents the seismic source characterization, the ground motion models used in the PSHA and DSHA, the probabilistic and deterministic ground motion hazard results, calculation of Uniform Hazard Spectra (UHS) and Conditional Mean Spectra (CMS), and development of time histories. As stated above, the hazard was calculated for two site conditions: Pinal schist and Gila conglomerate characterized by a V_S30 (time-averaged shear-wave velocity in the top 30 m) of 700 to 1,050 m/sec and rhyolite and diabase characterized by a V_S30 of 1,200 to 1,500 m/sec.

1.2 DESIGN GUIDANCE

As stated in Appendix E "Engineering Design Guidance" of the Arizona Mining BADCT Guidance Manuel:

The minimum design earthquake is the maximum probable earthquake (MPE). The MPE is defined as the maximum earthquake that is likely to occur during a 100-year interval (80% probability of not being exceeded in 100 years) and shall not be less than the maximum historical event. The design earthquake may apply to structures with a relatively short design life (e.g., 10 years) and minimum potential threat to human life or the environment.

Where human life is potentially threatened, the maximum credible earthquake (MCE) should be used. MCE is the maximum earthquake that appears capable of occurring under the presently known tectonic framework.

- *Potential threat to human life or the environment*
- *Facility life*
- *Potential future property development downstream of the embankment or earth structure*
- *Seismic history in the area*

The MPE 80% probability of not being exceeded in 100 years has an equivalent return period of about 450 years.

1.3 SCOPE OF WORK

The following scope of work was performed as described in our proposal dated 15 May 2017.

Task 1 – Update of the PSHA

A site-specific PSHA for two ranges of site conditions as characterized by Vs30 (time-averaged shear-wave velocity [V_S] in the top 30 m) was performed. The results of multiple downhole V_S surveys and MASW (multi-channel-analysis-of-surface-waves) have been provided to us and an inspection of the data indicates that the velocity structure at the Near West site is quite variable.

The PSHA was also updated with the NGA-West2 ground motion prediction models. The NGA-West1 models were used in the 2013 study. The historical seismicity record was also updated.

Task 2 – Calculate CMS

CMS for a return period of 10,000 years at high and low frequencies were calculated for the Near West site.

Task 3 – Time History Development

Seven horizontal-component time histories were developed using the approach of spectral matching. The time histories were partitioned between the CMS.

1.4 ACKNOWLEDGMENTS

Our appreciation to Claire Unruh, Melody Wade and Åse Mitchell for their assistance in the preparation of this report and to Phil Pearthree of the Arizona Geological Survey for providing information.

The PSHA approach used in this study is based on the model developed principally by Cornell (1968). The occurrence of earthquakes on a fault is assumed to be a Poisson process. The Poisson model is widely used and is a reasonable assumption in regions where data are sufficient to provide only an estimate of average recurrence rate (Cornell, 1968). When there are sufficient data to permit a real-time estimate of the occurrence of earthquakes, the probability of exceeding a given value can be modeled as an equivalent Poisson process in which a variable average recurrence rate is assumed. The occurrence of ground motions at the site in excess of a specified level is also a Poisson process, if (1) the occurrence of earthquakes is a Poisson process, and (2) the probability that any one event will result in ground motions at the site in excess of a specified level is independent of the occurrence of other events.

The probability that a ground motion parameter "Z" exceeds a specified value "z" in a time period "t" is given by:

$$p(Z > z) = 1\text{-}e^{-\nu(z)\bullet t} \tag{1}$$

where $\nu(z)$ is the annual mean number (or rate) of events in which Z exceeds z. It should be noted that the assumption of a Poisson process for the number of events is not critical. This is because the mean number of events in time t, $\nu(z)\bullet t$, can be shown to be a close upper bound on the probability $p(Z > z)$ for small probabilities (less than 0.10) that generally are of interest for engineering applications. The annual mean number of events is obtained by summing the contributions from all sources, that is:

$$\nu(z) = \sum_{n} \nu_n(z) \tag{2}$$

where $\nu_n(z)$ is the annual mean number (or rate) of events on source n for which Z exceeds z at the site. The parameter $\nu_n(z)$ is given by the expression:

$$\nu_n(z) = \sum_{i}\sum_{j} ß_n(m_i)\bullet p(R{=}r_j|m_i)\bullet p(Z{>}z|m_i,r_j) \tag{3}$$

where:

$ß_n(m_i)$ = annual mean rate of recurrence of earthquakes of magnitude increment m_i on source n;

$p(R=r_j|m_i)$ = probability that given the occurrence of an earthquake of magnitude m_i on source n, r_j is the closest distance increment from the rupture surface to the site;

$p(Z > z|m_i,r_j)$ = probability that given an earthquake of magnitude m_i at a distance of r_j, the ground motion exceeds the specified level z.

Calculations were made using the computer program HAZ45 developed by Norm Abrahamson, which has been validated using the test cases in the Pacific Earthquake Engineering Research (PEER) Center-sponsored “Validation of PSHA Computer Programs” Project (Thomas *et al.*, 2010) as well as the follow-on PEER PSHA Computer Program Validation Project (Hale *et al.*, in review).

2.1 SEISMIC SOURCE CHARACTERIZATION

Two types of earthquake sources are characterized in this PSHA: (1) fault sources; and (2) areal source zones (Section 4.1). Fault sources are modeled as three-dimensional fault surfaces and details of their behavior are incorporated into the source characterization. Areal source zones are regions where earthquakes are assumed to occur randomly. Seismic sources are modeled in the hazard analysis in terms of geometry and earthquake recurrence.

The geometric source parameters for faults include fault location, segmentation model, dip, and thickness of the seismogenic zone. The recurrence parameters include recurrence model, recurrence rate (slip rate or average recurrence interval for the maximum event), slope of the recurrence curve (*b*-value), and maximum magnitude. Clearly, the geometry and recurrence are not totally independent. For example, if a fault is modeled with several small segments instead of large segments, the maximum magnitude is lower, and a given slip rate requires many more small earthquakes to accommodate a cumulative seismic moment. For areal source zones, only the areas, maximum magnitude, and recurrence parameters (based on the historical earthquake record) need to be defined.

Uncertainties in the seismic source parameters as described below were incorporated into the PSHA using a logic tree approach (Figure 5). In this procedure, values of the source parameters are represented by the branches of logic trees with weights that define the distribution of values. A sample logic tree for a fault is shown on Figure 5. In general, three values for each parameter were weighted and used in the analysis. Statistical analyses by Keefer and Bodily (1983) indicate that a three-point distribution of 5th, 50th, and 95th percentiles weighted 0.185, 0.63, and 0.185 (rounded to 0.2, 0.6, and 0.2), respectively, is the best discrete approximation of a continuous distribution. Alternatively, they found that the 10th, 50th, and 90th percentiles weighted 0.3, 0.4, and 0.3, respectively, can be used when limited available data make it difficult to determine the extreme tails (i.e., the 5th and 95th percentiles) of a distribution. Note that the weights associated with the percentiles are not equivalent to probabilities for these values, but rather are weights assigned to define the distribution. We generally applied these guidelines in developing distributions for seismic source parameters with continuous distributions (e.g., M_{max}, fault dip, slip rate or recurrence) unless the available data suggested otherwise. Estimating the 5th, 95th, or even 50th percentiles is typically challenging and involves subjective judgment given limited available data.

Source Geometry

In the PSHA, it is assumed that earthquakes of a certain magnitude may occur randomly along the length of a given fault or segment. The distance from an earthquake to the site is dependent on the source geometry, the size and shape of the rupture on the fault plane, and the likelihood of the earthquake occurring at different points along the fault length. The distance to the fault is defined to be consistent with the specific ground motion model used to calculate the ground motions. The distance, therefore, is dependent on both the dip and depth of the fault plane, and a separate distance function is calculated for each geometry and each GMM. The size and shape of the rupture on the fault plane are dependent on the magnitude of the earthquake; larger events rupture longer and wider portions of the fault plane. The rupture dimensions were modeled following the magnitude-rupture area and rupture-width relationships of Wells and Coppersmith (1994).

Recurrence

The recurrence relationships for the seismic sources are modeled using the truncated-exponentially Gutenberg-Richter, characteristic earthquake, and the maximum magnitude recurrence models (Section 4.1). These models are weighted (Figure 5) to represent our judgment on their applicability to the sources. For areal source zones, only a truncated exponential recurrence relationship is assumed to be appropriate.

The general approach of Molnar (1979) and Anderson (1979) was used to arrive at the recurrence for the truncated exponential model. The number of events exceeding a given magnitude, N(m), for the truncated exponential relationship is

$$N(m) = \alpha(m^o)\frac{10^{-b(m-m^o)} - 10^{-b(m^u-m^o)}}{1 - 10^{-b(m^u-m^o)}} \qquad (4)$$

where $\alpha(m^o)$ is the annual frequency of occurrence of earthquakes greater than the minimum magnitude, m^o; b is the Gutenberg-Richter parameter defining the slope of the recurrence curve; and m^u is the upper-bound magnitude event that can occur on the source. A m^o of **M** 5.0 was used for the hazard calculations because smaller events are not considered likely to produce ground motions with sufficient energy to damage well-designed structures.

The model where faults rupture with a "characteristic" magnitude on specific segments was included as described by Aki (1983) and Schwartz and Coppersmith (1984). For the characteristic model, the numerical model of Youngs and Coppersmith (1985) was used. In the characteristic model, the number of events exceeding a given magnitude is the sum of the characteristic events and the non-characteristic events. The characteristic events are distributed uniformly over a $\pm$ 0.25 magnitude unit around the characteristic magnitude, and the remainder of the moment rate is distributed exponentially using the equation (4) with a maximum magnitude 0.25 unit lower than the characteristic magnitude (Youngs and Coppersmith, 1985).

The maximum magnitude model can be regarded as an extreme version of the characteristic model and the model proposed by Wesnousky (1986) was used in the PSHA. In the maximum magnitude model, there is no exponential portion of the recurrence curve, i.e., no events can occur between the minimum magnitude of **M** 5.0 and the distribution about the maximum magnitude.

The recurrence rates for the fault sources are defined by either the slip rate or the average return time for the maximum or characteristic event and the recurrence *b*-value. The slip rate is used to calculate the moment rate on the fault using the following equation defining the seismic moment:

$$M_o = \mu A D \qquad (5)$$

where M_o is the seismic moment, μ is the shear modulus, A is the area of the rupture plane, and D is the slip on the plane. Dividing both sides of the equation by time results in the moment rate as a function of slip rate:

$$\dot{M}_o = \mu A S \qquad (6)$$

where $\dot{M}_o$ is the moment rate and S is the slip rate. M_o has been related to moment magnitude,

M, by Hanks and Kanamori (1979):

$$\mathbf{M} = 2/3 \log M_o - 10.7 \qquad (7)$$

Using this relationship and the relative frequency of different magnitude events from the recurrence model, the slip rate can be used to estimate the absolute frequency of different magnitude events.

The average return time for the characteristic or maximum magnitude event defines the high magnitude (low likelihood) end of the recurrence curve. When combined with the relative frequency of different magnitude events from the recurrence model, the recurrence curve is established.

2.2 GROUND MOTION PREDICTION

To characterize the ground motions at a specified site as a result of the seismic sources considered in the PSHA and DSHA, empirical GMMs for spectral accelerations were used. The models used in this study were selected on the basis of the appropriateness of the site conditions and tectonic environment for which they were developed (Figure 5; Section 4.3).

The uncertainty in GMMs was included in the PSHA by using the lognormal distribution about the median values as defined by the standard error associated with each model. Per standard practice, five standard errors about the median value were included in the analysis.

The seismotectonic setting and historical seismicity of the Near West site are discussed below.

3.1 SEISMOTECTONIC SETTING

The Resolution Copper Near West site is located in southern Arizona; east of Phoenix (Figures 1 and 2). Arizona is divided into three physiographic and seismotectonic provinces: the Colorado Plateau in the northeast, the Southern Basin and Range (SBR) in the south and southwest, and the intervening Transition Zone that is roughly 40 to 100-km-wide and northwest-southeast trending (Figure 6). All three provinces are characterized by relatively few late Quaternary faults and low rates of seismicity. These regions are bounded to the east by the Rio Grande Rift, and to the west by the Salton Trough Province (Figure 6). The Near West site is located in the SBR near the boundary with the Transition Zone.

The Southern Basin and Range Province is a block-faulted terrain of alternating mountain ranges and intervening valleys, bounded by moderately to steeply dipping normal faults. The mountains comprise igneous, metamorphic, and indurated sedimentary rocks of Precambrian through Tertiary age; the valleys are filled with undeformed sequences of fluvial and lacustrine sediments of Oligocene to Pleistocene age. There are differing estimates on the timing of initiation of Basin and Range extension; McQuarrie and Wernicke (2005) suggest that deformation began at 25 Ma, whereas Menges and Pearthree (1989) indicate that deformation may have commenced during the Miocene at 15 Ma. However, there is general consensus that major extension ceased at some time in the late Miocene or Pliocene, and the modern landscape is dominated by geomorphological landforms that indicate tectonic inactivity (Menges and McFadden, 1981). Relative tectonic quiescence in southern Arizona is also reflected by the low levels of historical seismicity and sparse evidence for Quaternary faulting. The Southern Basin and Range Province is dominated by northwest-southeast-striking normal faults; however, the site region encompasses the transition from this northwest-southeast structural grain to a more north-south orientation as the province extends into northern Mexico.

The Transition Zone represents a tectonic transition from the relatively thin (~15 to 20 km) extended crust of the SBR to the thick (~40 km) crust of the Colorado Plateau. Bedrock in the region consists primarily of Precambrian metamorphic and granitic plutonic rocks and Paleozoic sediments. The composition of late Cenozoic basin-fill sediments reflects widespread Tertiary volcanism in the region. The Transition Zone is characterized by north- to northwest-trending mountain ranges and intervening basins related mainly to Miocene and younger normal faulting (Menges and McFadden, 1981; Mack *et al.*, 2003). The topography of the Transition Zone is more subdued than that of the Southern Basin and Range Province to the south: the ranges are less pronounced and the basins are smaller and less well-defined. The relatively subdued landforms, low to moderate levels of seismicity (Brumbaugh, 1987; Bausch and Brumbaugh, 1997), and relative lack of significant late Quaternary faulting (Pearthree *et al.*, 1983) have been interpreted to indicate geologically recent tectonic cessation of major extension in the region (Menges and McFadden, 1981). The few Quaternary normal faults that are mapped in the region generally trend northwest-southeast and are likely reactivated faults that originated during Basin and Range extension (Lockridge *et al.,* 2012). Based on reconnaissance mapping and limited paleoseismic studies, these faults have average recurrence intervals of tens to hundreds of thousands of years (Pearthree, 1998; Piety and Anderson, 1991).

The Colorado Plateau in northern Arizona is part of a large region that extends across southeastern Utah, northwestern New Mexico, and western Colorado. Physiographically and geologically distinct from the highly deformed Rocky Mountains to the north and east and the Basin and Range region to the south and west, the Colorado Plateau is characterized by relative tectonic stability and elevated topography dissected by rivers. Whereas major crustal deformation of the Colorado Plateau ceased at the end of Laramide orogeny (40 Ma), the region has been subject to about 2 km of epeirogenic uplift during the Cenozoic (Morgan and Swanberg, 1985). During uplift, the plateau acted as a coherent block, with only minor differential movements creating northerly-trending monoclines and associated structural basins. Contemporary seismicity in the Colorado Plateau Province is low to moderate, with widespread, generally small events that cannot be correlated with surface geological features (Wong and Humphrey, 1989).

The Salton Trough to the west of the Basin and Range marks the transition between ocean-floor spreading in the Gulf of California and right-lateral strike-slip faulting along the San Andreas fault zone. This region is one of the most seismically active areas in the western United States, characterized by right-lateral strike-slip faulting and elevated levels of contemporary seismicity with repeated events of **M** 6 to 7 during the period of historical record (Figure 4). Slip rates on faults in this region are as high as 30 mm/yr (Working Group on California Earthquake Probabilities, 2008).

3.2 HISTORICAL SEISMICITY

A historical seismicity catalog was compiled for an area that encompassed over 200 km around the site, extending from a latitude of approximately 31°N to 36.3°N and a longitude of approximately 115°W to 107.5°W (Figure 2). The catalog extends from 1830 to April 2017 and the majority of the catalog consists of the compilation presented in Thomas *et al*. (2015). Primary data sources used in that compilation include the Northern Arizona University regional catalog (1830 through 2005) and the Advanced National Seismic Service (ANSS) (1931 through 2017) catalog. In addition to the Thomas *et al.* (2015) compilation, more recent events from the ANSS catalog were included.

The site is located in the SBR in an area of low historical seismicity. This area, however, has had poor seismographic coverage (Thomas *et al.*, 2015). In addition to the SBR, the catalog includes seismicity to the north in the area of the Transition Zone physiographic province as well as the southern Colorado Plateau (Section 3.1). The catalog includes 26 events of magnitude **M** 5 to 5.9, three events of magnitude **M** 6 to 6.9, and three events of **M** 7 and greater (Figure 2). One of the **M** 7 events is documented as having occurred in 1830, though it is based on one report made in the mid-1850's and is therefore considered suspect and poorly constrained and documented (DuBois *et al.*, 1982). Wong *et al.* (2013) note that this event continues to be included in some catalogs but has been removed from the Arizona Geological Survey catalog because it is poorly dated, dubious, and because no physical evidence has been found to corroborate such a reportedly high intensity and relatively young event (Phil Pearthree, Arizona Geological Survey written communication to I. Wong, 2013). The event appears on Figure 2, but it was excluded from the earthquake recurrence calculations. Three historic events whose effects were likely felt at the location of the site, are described in the next section below.

3.2.1 Significant Earthquakes

This section describes three significant historical earthquakes that have occurred in or near the site region whose effects were likely felt at the location of the site.

1887 Sonora Earthquake

The largest event in the catalog was an earthquake of **M** 7.4 that occurred on 3 May 1887 in northern Sonora, Mexico, approximately 330 km southeast of the site (Dubois *et al*., 1982; Suter and Contreras, 2002) (Figure 7). The earthquake ruptured three major normal faults (Otates, Teras, and Pitáycachi faults) and was felt throughout Arizona and New Mexico and as far south as Mexico City (Dubois *et al*., 1982; Suter and Contreras, 2002). The maximum felt intensity was between Modified Mercalli intensity (MMI) XI and XII and intensity MMI VI would have been observed at the site (Figure 7; DuBois *et al*., 1982).

1922 Miami Earthquake

In the historical seismicity catalog, the closest earthquake to the Near West site was a **M** 5.0 event that occurred on 17 June 1922 in the vicinity of Miami, Arizona, approximately 32 km east-northeast of the site (DuBois *et al*., 1982) (Figure 8). Although the felt intensity at the site location was not included by DuBois *et al*. (1982), the felt intensity likely would have been MMI IV based on the proximity to the MMI V contour. Although the event was felt throughout the town of Miami, no structural damage was reported (DuBois *et al*., 1982). Wong *et al.* (2008) noted that this event was recorded on a seismograph in Tucson and that the location and size of the event are highly uncertain.

2014 Southeastern Arizona Earthquake

A more recent **M** 5.3 event occurred on 29 June 2014 approximately 206 km east-southeast of the site, near the town of Duncan, Arizona and near the Arizona-New Mexico border (Figure 9). This event was recorded on the USGS Did You Feel It website (http://earthquake.usgs.gov/earthquakes/eventpage/usc000rnfe#dyfi). The maximum reported intensity of MMI V was reported near the epicenter. Based on reported intensities surrounding the site, an intensity between MMI II and III would have been observed at the site (Figure 9). The earthquake occurred at a depth of 6.4 km and the moment tensor solution reported by the USGS shows that the event is consistent with northeast-striking oblique-normal faulting. Subsequent to this event, there have been over 40 likely aftershocks ranging in magnitude from **M** 2.0 to 4.0.

3.2.2 Local Seismicity

The largest event within 50 km of the site was the 17 June 1922 **M** 5.0 earthquake. This event is the second closest earthquake to the site in the catalog; the closest event was an **M** 4.3 earthquake that occurred on 15 September 1980, 31 km north of the site (Figure 10). Other events within 50 km of the site include an **M** 4.1 earthquake and an **M** 3.5 earthquake that occurred on 11 September 1963 and 21 October 1963, respectively, 48 km east-southeast of the site; an **M** 3.1 earthquake that occurred on 25 June 2010, 33 km north of the site; an **M** 3.2 earthquake that occurred on 20 September 2014, 41 km northeast of the site; and an **M** 3.7 earthquake that occurred on 11 December 1979, 44 km north-northeast of the site.

The following section discusses the characterization of the seismic sources and the ground motion models selected and used in the PSHA and DSHA. The seismic source model used in this study was based on previous studies in the region performed by the authors (e.g., Wong *et al*., 2013) including the evaluation performed for the update of the Arizona Public Services (APS) Palos Verdes nuclear power plant. Velocity surveys were performed in 2017 at Near West to support this evaluation (Section 4.2).

4.1 SEISMIC SOURCES

Seismic source characterization is concerned with three fundamental elements: (1) the identification, location and geometry of significant sources of earthquakes; (2) the maximum size of the earthquakes associated with these sources; and (3) the rate at which the earthquakes occur. The seismic source model includes crustal faults capable of generating large surface-faulting earthquakes (Section 4.1.1), and an areal source zone, which accounts for background crustal seismicity that cannot be attributed to identified faults explicitly included in the seismic source model (Section 4.1.2).

4.1.1 Crustal Fault Sources

Fault parameters required in the PSHA include: (1) rupture model (including independent single plane and potentially linked models); (2) probability of activity; (3) fault geometry including rupture length, rupture width, fault orientation, and sense of slip; (4) maximum or characteristic magnitude [M_{max}]; and (5) earthquake recurrence including both recurrence model and rates. These parameters are generally discussed further below. Selected faults that contribute the most to the hazard are specifically discussed in subsequent sections. We have explicitly incorporated the uncertainties in each parameter through the use of logic trees, as exemplified in Figure 5.

All known active or potentially active faults were included in the analyses within 200 km of the site (Figure 3). We included known faults showing evidence for late Quaternary (≤ 130,000 years) activity or repeated Quaternary (≤ 1.6 million years) activity. In the 2013 study (Wong *et al*., 2013), two faults in the vicinity of the Near West site, the Concentrator and Conley Springs faults, were examined and judged to be pre-Quaternary in age and were not included in our hazard analysis. At the request of the Independent Technical Review Board, a reconnaissance-level fault investigation was performed at the Near West site to evaluate possible faulting that may represent a surface-faulting hazard (Hartleb and Wong, 2017). The study concluded that Quaternary-active faults are highly unlikely at the site although the limited extent and relatively young age of Quaternary deposits precluded a definitive conclusion.

We also included longer, more active faults in southern California and Baja California, such as the southern San Andreas fault, because from previous analyses in the region (e.g., Wong *et al*., 2013), we know that these major fault sources can be significant contributors to the hazard at longer periods, despite their great distances (Figure 4). The Pitaycachi fault, source of the 1887 Sonora earthquake, was also included in the hazard analysis because although it is distant (190 km away) and its slip rate is slow (< ~0.1 mm/ yr), it is the source of the largest earthquake in the region (Figure 4).

Faults are generally modeled as single, independent, planar sources, simplified from the complex zones shown on Figure 3. Table 1 shows the parameters for the faults. Our fault characterization is based on our previous probabilistic seismic hazard analyses in Arizona, the APS study, and from data compiled in the USGS Quaternary Fault and Fold Database (http://earthquake.usgs.gov/hazards/qfaults/) and sources listed in Table 1.

Maximum magnitudes were estimated for the local faults using the empirical relationships of: (1) Wells and Coppersmith (1994), for all fault types; (2) the Stirling *et al.* (2002) censored relationship for all fault types; and (3) Wesnousky (2008) for all fault types, as noted in the footnotes of Table 1. None of the local faults are blind, and minimum seismogenic depths were assumed to be 0 km. We assumed maximum seismogenic depths of 12 km (weighted 0.3), 15 km (weighted 0.5), and 17 km (weighted 0.2), primarily based on the maximum depth of historical seismicity in the region (e.g., Lockridge *et al*., 2012).

Fault dips are averages over the entire seismogenic crust. Although near-surface fault dip data are available for many of the faults, crustal dip data are lacking. We assumed default dips of 50° (weighted 0.6) ±15° (weighted 0.2) for all the local faults, which all show dominantly normal slip. This default fault dip distribution is after recommendations made by the Basin and Range Province Earthquake Working Group II (BRPEWGII; Lund, 2012; see Issue G4) to the USGS regarding crustal-scale dips for typical range-bounding normal faults in the Basin and Range Province used in the 2014 update of the National Seismic Hazard Maps. This distribution was based on focal plane and aftershock data for historical surface-rupturing earthquakes in the Basin and Range Province, as well as normal faults worldwide (see presentation by Crone at: http://geology.utah. gov/ghp/workgroups /pdf/brpewg/BRPEWGII_Presentations.pdf).

Recurrence models can significantly impact hazard calculations and we considered truncated exponential, maximum magnitude, and characteristic recurrence models for this analysis. Observations of historical seismicity and paleoseismic investigations suggest that characteristic behavior is more likely for individual faults, whereas seismicity in areal zones best fits a truncated exponential model (Schwartz and Coppersmith, 1984; Youngs and Coppersmith, 1985). The maximum magnitude model is an extreme version of the characteristic model (Wesnousky, 1986). We favored (weighted 0.6) the characteristic model for all local fault sources and assigned equal weights of 0.2 to the exponential and maximum magnitude models.

In assigning probabilities of activity for local fault sources, we considered both the likelihood that the fault is structurally capable of independently generating earthquakes, and the likelihood that it is still active within the modern stress field. We incorporated many factors in assessing these likelihoods, such as: orientation in the modern stress field, fault geometry (length, continuity, and dip), relation to other faults, age of youngest movement, rates of activity, geomorphic expression, amount of cumulative offset, and any evidence for a non-tectonic origin. Faults with definitive evidence for repeated Quaternary activity were generally assigned probabilities of being active (seismogenic) of 1.0 (Table 1). The probability of activity for faults that do not show definitive evidence for repeated Quaternary activity was individually judged based on available data and the criteria explained above. Resulting values range from 0.5 to 1.0 (Table 1) and the specific reasons for assigning probabilities less than 1.0 to a particular fault are generally given in the comments column of Table 1.

As recurrence interval data are generally lacking for local faults, we used slip rates to characterize rates of fault activity (Table 1). We considered all available long- (≤ 1.6 Ma) and short-term (≤ 130 ka) data in developing slip rate distributions, but we preferred short-term data whenever possible. In addition to the time period, we also considered the type and quality of data in determining rates. Preferred slip rates (generally weighted 0.6) are primarily based on data in the USGS Quaternary fault database and as noted in the comments column of Table 1. Maximum and minimum values (each generally weighted 0.2) are typically selected to represent 95th and

5th percentile values as previously discussed in Section 2, unless the available data suggest otherwise as noted in the comments column of Table 1. Note that from our previous hazard analyses in the area we found that none of the local faults contributed significantly to the hazard so we do not include detailed local fault specific discussions herein.

Our characterization of southern California faults was modified from our recent hazard analysis in the region (Wong *et al*., 2011). Based on previous analyses, we included the San Andreas, San Jacinto, and Cerro Prieto. These plate- boundary structures are all long, complex, and highly-active fault zones or systems that have been extensively studied. They are included in the PSHA because their potential to generate very large (up to **M** 8 or larger) and relatively frequent events compared to the local faults (Figure 4). The source characterization of these faults follows that used by the USGS in the 2008 National Hazard Maps (Petersen *et al*., 2008). This seismic source model is referred to as the Uniform California Earthquake Rupture Forecast, Version 2 (or UCERF2), which was developed by the Working Group on California Earthquake Probabilities and was documented by Wills *et al*. (2008) and Field *et al*. (2008). The parameters of the more significant regional faults included here are summarized in Tables 2a through 2c. The UCERF2 model did not include the Cerro Prieto fault, but we added it here because it is a major transform structure south of the U.S.-Mexico border that appears to be accommodating significant slip comparable to the Imperial fault and is included in the UCERF3 model (Figure 4).

The southern Cerro Prieto and southern San Andreas faults are significant fault sources to the hazard at the site, and so they are discussed below (Figure 4). The Sugarloaf fault zone is the closest Quaternary fault to the site, so it is also discussed (Figure 3).

Cerro Prieto Fault

Our characterization of the Cerro Prieto fault is taken from Thomas *et al.* (2015). Although it is not included in either the USGS Quaternary Fault and Fold Database, or the California Geological Survey 2010 Fault Activity Map (http://www.quake.ca.gov/gmaps /FAM/faultactivitymap.html), the Cerro Prieto fault was included in Jennings' (1994) earlier Fault Activity Map of California and Adjacent Areas after original mapping by Gastil *et al*. (1975). It is now included in the UCERF3 model, which is the basis for the 2014 USGS NSHMs. The Cerro Prieto fault is a northwest-striking dextral-slip transform fault that extends for over 115 km and is part of where the East Pacific Rise comes onshore (Figure 4). It extends from the Wagner Basin spreading center in the Gulf of California to at least the Cerro Prieto spreading center (and volcano and geothermal field), near Mexicalli, Mexico. It is approximately 350 km southwest of the site. It has not been mapped or studied paleoseismically in any detail and the Southern California Earthquake Data Center lists the slip rate as uncertain with the fault being "difficult to trace in alluvium of the Colorado River delta" (http://www.data.scec.org/significant/cerroprieto.html).

The Cerro Prieto fault does have linear trends of associated microseismicity that extend northwest of the fault as mapped by Jennings (1994), well beyond the Cerro Prieto volcano, prompting Magistrale (2002) to suggest the fault extends another 35 km to the northwest into southern California. Based on this, the model includes two scenarios for the northern end of the fault (Table 2a): Scenario A, at the Cerro Prieto Volcano (weighted 0.6); and, Scenario B, extending into southern California after the microseismicity trend defined by Magistrale (weighted 0.4).

The Cerro Prieto geothermal field at the northern end of the fault has been the focus of much investigation, including the **M** 5.4 earthquake that occurred on 24 May 2006 and ruptured the Morelia fault, a small cross-fault at the northern end of the Cerro Prieto fault (Suarez-Vidal *et al*., 2007). There is also suggestion that multiple large historical surface ruptures (about **M** 7.1) have occurred on the southern Cerro Prieto fault, including one in 1915 and 1934, but they are not as well- documented (Biehler *et al*., 1964; Merriam, 1965; Allen *et al*., 1965). Due to lack of other published information on previous ruptures and the large uncertainties on rupture behavior, the model assumes a floating rupture model for the Cerro Prieto fault with a preferred characteristic magnitude of **M** 7.1 (Table 2a), but included a broad distribution (+0.5 and -0.3) due to the large uncertainties. The upper bound of **M** 7.6 allows the entire fault to rupture.

Rates are unknown for the Cerro Prieto fault. Several investigators have postulated that it is a principal plate-bounding structure, with slip from the San Jacinto fault being transferred to the Cerro Prieto fault via the Imperial fault (Magistrale, 2002; Suarez-Vidal *et al*., 2007; T. Rockwell, San Diego State University, written communication, cited in Table B-1 of Field *et al*., 2013). The Imperial fault has an estimated rate of 15 to 40 mm/yr, with paleoseismic trench data indicating 5 m of slip occurred between the 1940 and 1690 fault ruptures (Thomas and Rockwell, 1996). The UCERF3 model uses an input range of 35 ± 5 mm/yr for the Cerro Prieto fault (Table B-1), which is geodetically based, whereas the modeled mean rates are lower, ranging from 11 to 15 mm/yr (Field *et al*., 2013). Given the very large uncertainty, this study uses a broad slip rate distribution of: 15 mm/yr (weighted 0.25), 20 mm/yr (weighted 0.35), 35 mm/yr (weighted 0.25), 40 mm/yr (weighted 0.15).

Southern San Andreas Fault Zone

The right-lateral strike-slip San Andreas fault zone is the most significant structure accommodating North American-Pacific plate motion, accounting for up to 70% of the relative plate motion along most of its length. The southern San Andreas fault zone includes the section of the fault south of the creeping segment in central California (Figure 4). This part of the fault has generated two large historical earthquakes, the 1857 **M** 7.8 to 8 Ft. Tejon that ruptured the Parkfield through Mojave South sections, and an **M** ~7½ earthquake in 1812 that ruptured the North San Bernardino and Mojave South and possibly Mojave North sections. In addition, the northernmost Parkfield section has experienced numerous moderate earthquakes (**M** ~6) in the historical period, the most recent of which occurred in 2004.

The Working Group on California Earthquake Probabilities (WGCEP) (Field *et al*., 2008) developed a new characterization of the San Andreas fault as part of the Uniform California Earthquake Rupture Forecast (UCERF)2 that differs considerably from that of previous working groups (e.g., WGCEP, 1988; 1995; Cao *et al*., 2003). We use a simplified version of their fault characterization and earthquake recurrence models to model the southern San Andreas fault. They include three alternative deformation models to describe how slip is distributed between the southern San Andreas and other faults in the area including the San Jacinto fault; we use only their preferred model. UCERF3 was released in 2013 by Field *et al*. (2013) but we have not adopted this model because of issues regarding fault segmentation and multi-segment ruptures that we cannot agree with because we find earthquake scenarios in the model that are not supported by paleoseismic data.

Changes in the UCERF2 model (Field *et al*., 2008) from the 2002 model of Cao *et al.* (2003) include modification to the sectioning, geometry, recurrence and slip rates on the fault. Field *et al.* (2008) divide the southern San Andreas fault zone into 10 sections, a departure from earlier working groups who divided it into six rupture segments (e.g., WGCEP, 1988, 1995; Cao *et al*., 2003). The sections defined by the Field *et al.* (2008) are not necessarily rupture segments and do not imply a specific earthquake model; rather, they are defined based on distinct geological characteristics that may or may not relate to earthquake rupture characteristics. We have adopted the divisions of UCERF2, with the following sections: Parkfield (PK), a 36-km-long section extending from Parkfield to the town of Cholame; Cholame (CH), extending southeast 62 km from Cholame; Carrizo (CC), a 59-km-long segment extending to the southern end of the Carrizo Plain; Big Bend (BB), a 50-km-long stretch ending at the intersection with the east-west-striking Garlock fault; Mojave North (NM), which extends 40 km from the Garlock fault to Elizabeth Lake, the northern end of the "Mojave segment" used by previous working groups; Mojave South (SM), a 100-km-long section similar to the former "Mojave segment", that traverses the southeastern edge of the Mojave desert from Elizabeth Lake to near Cajon Pass, about halfway between Wrightwood and Lost Lake; San Bernardino Mountains North (NSB), which extends about 35 km southeast from Cajon Pass to the intersection with the Mill Creek fault and the northern end of an region of structural complexity called the San Gorgonio Pass knot (Field *et al.*, 2008); San Bernardino South (SSB) and San Gorgonio Pass-Garnet Hill, also referred to as Banning-Garnet Hill (BG), which pass through the complex San Gorgonio Pass region and are northwest-striking strike-slip and slightly more west-striking reverse oblique-slip faults, respectively; and last, Coachella Valley (CO), which starts at the junction with the Mission Creek fault where the SAF again regains its northwest strike, and ends at the Salton Sea (Field *et al.*, 2008).

Slip rates on several of the newly defined sections also have changed in the UCERF2 model, reflecting both the new sectioning and more recent geologic and geodetic data. The San Andreas fault zone has the highest slip rate of any fault in California. On the Parkfield, Cholame, Carrizo and Big Bend sections, the average late Holocene slip rate is about 34 to 35 mm/yr, consistent with previous estimates (Sieh and Jahns, 1984; Sims, 1994). The slip rate decreases southward as more slip is transferred to other structures of the San Andreas fault system, especially the San Jacinto fault. As a consequence, the average slip rate on the southern sections of the fault decreases from about 27 ± 7 mm/yr in the Mojave North section to about 20 ± 6 mm/yr on the southernmost Coachella Valley section.

Field *et al*. (2008) used the recurrence interval data determined from paleoseismic studies and a method of assessing the probability that a specific rupture scenario is consistent with the paleoseismic record to determine a rupture recurrence rate for each of the ten sections. They used slip rates to moment balance the *a priori* recurrence rates to develop final moment-balanced rupture rates for all possible rupture scenarios. These rates have been adopted for use in the model. The table of rupture rates appears in Table 2b.

Sugarloaf Fault Zone

The Sugarloaf fault zone is expressed as a low, fairly continuous east-facing fault scarp as much as 5 m high at the contact between Precambrian granite and Tertiary basin fill sediments along the western margin of the small sedimentary basin on the flank of the Mazatzal Mountains (Pearthree *et al*., 1995) (Figure 3). It is the closest Quaternary fault to the site at 49 km (Figure 3). The relief across the fault is minimal, indicating relatively little Quaternary activity (Pearthree, 1998). Stream bank exposures show down-to-the-east displacement on a northwest-striking fault plane dipping 70° to 80° to the northeast. Fault scarps on alluvium are rare and are poorly preserved. Paleoseismic trenching shows that the fault offsets late to latest Pleistocene deposits, but middle to upper Holocene deposits are not displaced (Pearthree *et al*., 1995). There is evidence for multiple Quaternary events, yet, the timing of individual events cannot be constrained (Pearthree *et al*., 1995; Pearthree, 1998). A preferred slip rate of 0.02 ± 0.01 mm/yr is calculated from ~ 1 m of vertical displacement in late Pleistocene (ca. 50 to 100 ka) deposits. A preferred maximum magnitude of **M** 6.5, the minimum magnitude for surface-faulting, was assumed for this 8-km long short fault in the PSHA. A slightly larger magnitude, **M** 6.6, was assumed for the DSHA.

4.1.2 Crustal Background Earthquakes

In state-of-the-practice seismic hazard evaluations, the hazard from background earthquakes is addressed. Background earthquakes are those events that do not appear to be associated with known geologic structures. They occur on crustal faults that exhibit no surficial expression (buried faults) or are unmapped due to inadequate studies. In this source characterization, we address the hazard from background earthquakes through: (1) a gridded seismicity model, where locations of past seismicity appear to be likely locations of future seismicity (stationarity); and (2) the use of a regional seismic source zone for the SBR, where earthquakes are assumed to occur randomly (Figure 11). For both approaches, the background earthquakes are assumed to occur uniformly from 2 km to the bottom of the seismogenic crust. The maximum depths of the seismogenic crust is the same distribution used for the crustal faults (Section 4.1.1).

Earthquake recurrence estimates in the site region are required in order to assess the hazard from background earthquakes. A declustered SBR background zone catalog was developed by Thomas *et al*. (2015) and updated for this report (Section 3.2; Figure 11). The SBR zone, as defined in this report, incorporates seismicity from the SBR and the Transition Zone (as defined by Peirce [1984]), because the number of earthquakes in each of these two zone was deemed insufficient to independently determine earthquake recurrence parameters. The recurrence parameters for the SBR were developed using the historical seismicity record for the period of 1830 to April 2017.

Completeness intervals were modified from Thomas *et al.* (2015) and Wong *et al.* (2008) by developing Stepp (1972) plots using the updated earthquake catalog. These plots were developed by calculating the average annual number of independently occurring events in each half-magnitude increment for the SBR catalog (Figure 12). Completeness estimates and number of earthquakes within each interval used in the recurrence calculations are listed below in Table 3.

In the western U.S., the conventional approach has been to assume that the minimum threshold for surface faulting represents the upper size limit for background earthquakes. In the Basin and Range Province, this threshold ranges from **M** 6 to 6.75 (e.g., dePolo, 1994). It is believed that larger earthquakes will be accompanied by surface rupture, and repeated events of this size will produce recognizable fault-related geomorphic features. We have adopted a maximum magnitude distribution of **M** 6.2 [0.101], **M** 6.35 [0.244], **M** 6.5 [0.310], **M** 6.65 [0.244], and **M** 6.8 [0.101] for the SBR. This distribution is consistent with previous site-specific PSHAs completed in central and southern Arizona where all known Quaternary faults within the region are modeled (e.g., Wong *et al*., 2008; Thomas *et al.,* 2015). Note that the USGS NSHM distribution of maximum magnitude extends to larger magnitudes, but is designed in part to account for the fact that the NSHM model only includes fault for which sufficient paleoseismic history has been established. Our range of background maximum magnitudes in the Basin and Range Province is similar to what is used in other areas of the western U.S. that possess a moderate to high level of heat flow and hence moderate to high crustal temperatures that constrain the thickness of the seismogenic crust to less than 15 to 20 km (e.g., Wong and Chapman, 1990). In the recent WGUEP (2016) study, the maximum magnitude of background seismicity was estimated at **M** 6.75 ± 0.25.

We estimated recurrence for the background earthquakes for both the gridded seismicity and uniform source zone. In both cases, recurrence parameters (*b*-values and rates) were calculated using a modified version of the program ABSMOOTH (EPRI/DOE/NRC, 2012). For the gridded seismicity, the program divides the source zone into cells of a selected size (0.2-degree cells in this report) and calculates the *b*-value and rate in each cell using the likelihood function of the data in that cell along with penalty functions. These penalty functions smooth the cell-to-cell variation in the rate and/or the *b*-value, therefore optimizing these values. The program outputs both mean values and eight alternative sets ("realizations") of the recurrence parameters in order to characterize epistemic uncertainty in the rates and *b*-values (EPRI/DOE/NRC, 2012). The uniform source zone recurrence parameters were computed for the entire area as one cell.

Figure 13 shows the gridded seismicity results generated from ABSMOOTH for the SBR. Recurrence parameters for the uniform seismic source zone were adopted from the eight realizations generated for the gridded seismicity, such that the total rates generated for each realization were assumed to apply uniformly across the SBR zone (Figure 5).

In general, earthquake recurrence for the SBR zone is not well constrained. There are too few earthquakes (99 independent events; Table 3) even at magnitudes less than **M** 4.0 and the historical record is short (< 200 years). Because of the limited seismographic coverage of the SBR, the recurrence is highly uncertain. To incorporate uncertainty into the hazard analysis, we implemented the eight realizations (which include eight *b*-values and rates) generated by ABSMOOTH, with equal weight applied to each realization (Figure 5). Table 4 provides the rates of events for **M** 5 and above for the corresponding *b*-values for use in the PSHA. Figure 14 shows the resulting recurrence curves for **M** ≥ 5.0 and the range of *b*-values and our maximum magnitude distribution (**M** 6.2, **M** 6.35, **M** 6.5, **M** 6.75, and **M** 6.8) compared to the historical seismicity. Although spanning a broad range, the eight realizations do not always envelope the historical seismicity; this is likely due to the paucity of events in the catalog and their large uncertainties.

An inspection of the resulting recurrence intervals for **M** 5 and 6 events was performed to check the reasonableness of the eight *b*-values and rates for the SBR (Figure 14). To do this, using the mean maximum magnitude and the mean of the eight realizations of the recurrence parameters, the resulting recurrence intervals were evaluated. The mean rate at **M** 5.0 was 0.0636, or a recurrence interval of 16 years, and the mean rate at **M** 6.0 was 0.0060, or a recurrence interval of 137 years. The average *b*-value of the eight realizations was 0.73.

The use of the uniform and gridded seismic source zones were weighted equally at 0.5 and 0.5, respectively (Figure 5). Recent seismicity may be considered more likely representative of seismicity occurring in the next 100 years. However, given the short 187-year long and incomplete historical record the possibility exists that the catalog is not representative of the long-term record of seismicity and thus the two approaches were implemented with equal weight.

4.2 SITE CHARACTERISTICS

The site geology across the Near West site is quite variable with several facilities and structures founded on a range of surficial geology. In 2016, hydroGEOPHYSICS Inc. (HGI) performed downhole S-wave and P-wave measurements in six boreholes distributed across the Near West area: GT-1, GT-4, GT-14, GT-21, GT-31, and GT-41 (HGI, 2016) (Figure 15). The depths of the downhole surveys ranged from 50 to 125 ft. In addition, MASW surveys were also performed. There is considerable variation between the downhole and MASW surveys and based on discussions with HGI, the MASW results were used (Figure 15).

The site geology at Near West was divided into two categories based on the Vs30 values estimated from the MASW surveys: Pinal schist and Gila conglomerate grouped together and rhyolite and diabase. The respective ranges of Vs30 used for the two categories was 700 to 1,050 m/sec and 1,200 to 1,500 m/sec. There were two measured Vs30 values for both the Gila conglomerate and Pinal schist and one measurement each for the rhyolite and diabase. Thus there is uncertainty associated with the Vs30 values. The above ranges were used in the hazard analyses.

4.3 GROUND MOTION MODELS

To predict ground motions in hazard analyses, recently developed empirical ground motion models appropriate for tectonically active crustal regions were used. These models, developed as part of the NGA Project sponsored by PEER Center Lifelines Program, have been published and are available on the PEER website (http://peer.berkeley.edu/).

The NGA-West1 Project began in 2003, and the first set of five models became available in 2008. The NGA-West 1 models had a substantially better scientific basis than past relationships, which generally dated around 1997 (e.g., Abrahamson and Silva, 1997), because they involve: (a) an expanded and improved database of strong ground motion recordings and supporting information on the causative earthquakes, the source-to-site travel path characteristics, and the site and structure conditions at ground motion recording stations; (b) improved understanding of the effects of various parameters and effects on ground motions that are used to constrain models; and (c) improved statistical methods to develop ground motion relationships including uncertainty quantification. The models benefited greatly from a large amount of new strong motion data from large earthquakes (**M** > 7) at short distances (< 25 km). Data include records from the 1999 **M** 7.6 Chi Chi, Taiwan, 1999 **M** 7.4 Kocaeli, Turkey, and 2002 **M** 7.9 Denali, Alaska earthquakes.

In 2010, the NGA-West2 Project began as a follow-up to the original NGA-West1 Project. The NGA-West2 models were developed based on an expanded database, with a number of more recent well recorded earthquakes added including Wenchuan, China, numerous moderate magnitude California events down to **M** 3.0, and several Japanese, New Zealand, and Italian earthquakes. The NGA-West2 models are now state-of-the-practice. For example, the models were used in the 2014 USGS National Seismic Hazard Maps. In this study, the models of Campbell and Bozorgnia (2014), Chiou and Youngs (2014), Abrahamson *et al.* (2014), and Boore *et al.* (2014) are used. The models are weighted equally in the PSHA and DSHA. As described above, a range in VS30 of 700 to 1,050 m/sec was used in the NGA models for the Pinal schist and Gila conglomerate category. For the rhyolite and diabase category, a VS30 value of 1,200 m/sec was used because it is the upper bound value in the NGA-West2 models. Thus for sites which have higher VS30 values, the ground motion hazard is likely conservative.

The aleatory variability in the four NGA-West2 models used in this analysis is generally a function of period, magnitude, and VS30. Details of the individual aleatory variability models can be found in the four NGA-West2 models. For example, for the Abrahamson *et al*. (2014) model and a VS30 of 760 m/sec, sigma varies from 0.67 to 0.81, 0.65 to 0.72 and 0.62 to 0.69 for magnitude **M** 5, 6, and 7, respectively.

Other input parameters include $Z_{2.5}$, the depth of a V_S of 2.5 km/sec (a proxy for basin effects) which is only used in one model, Campbell and Bozorgnia (2014). Abrahamson *et al.* (2014) and Chiou and Youngs (2014) use $Z_{1.0}$ for the depth to the V_S of 1.0 km/sec. In the absence of site-specific data, the authors provide an equation for default values based on the V_S30 at the site. Other parameters such as depth to the top of rupture (zero for all surficial faults unless specified otherwise), dip angle, and rupture width are specified for each fault or calculated within the PSHA code.

As noted by Al Atik and Youngs (2014), the development of the NGA-West2 models was a collaborative effort with many interactions and exchanges of ideas among the developers and the developers indicated that an additional epistemic uncertainty needs to be incorporated into the median ground motions in order to more fully represent an appropriate level of epistemic uncertainty on the median. The three-point distribution and model of Al Atik and Youngs (2014) was applied. The model is a function of magnitude, style of faulting and spectral period.

The hazard results for ground motions are described below and shown in Figures 16 to 57.

5.1 PSHA RESULTS

The results of the PSHA for the two site conditions are presented in terms of ground motion as a function of annual exceedance frequency. The annual exceedance frequency is the reciprocal of the average return period. The results for the Pinal schist and Gila conglomerate sites for a V_S30 of 700 m/sec and rhyolite and diabase site for a V_S30 of 1,200 m/sec are presented. For each of the sites, these results which use the lowest V_S30 of the range for each site, control the hazard at all periods. Figures 16 and 17 show the mean, median (50th percentile), 5th, 15th, 85th, and 95th percentile hazard curves for peak horizontal ground acceleration (PGA). The range of uncertainty between the 5th and 95th percentile (fractiles) is about a factor of 3.4 at a return period of 10,000 years. These fractiles indicate the range of epistemic uncertainty about the mean hazard. The 1.0 sec horizontal spectral acceleration (SA) hazard is shown on Figures 18 and 19. At the return periods of 1,000, 2,500, 4,750, and 10,000 years, the mean spectral values are listed in Table 5. The hazard can be characterized as low to moderate even at a long return period of 10,000 years.

The contributions of the various seismic sources to the mean PGA and 1.0 sec SA hazard are shown on Figures 20 to 27. At PGA, the contribution from the SBR background earthquakes dominates the hazard (Figures 20 to 23). At 1.0 sec SA, the background seismicity controls the hazard for return periods greater than 200 to 300 years, but there are also contributions from the relatively distant Cerro Prieta fault and southern San Andreas fault (Figures 24 to 27).

The hazard can also be deaggregated in terms of the joint magnitude-distance-epsilon probability conditional on the ground motion parameter (PGA or SA exceeding a specific value). Epsilon is the difference between the logarithm of the ground motion amplitude and the mean logarithm of ground motion (for that M and R) measured in units of standard deviation (σ). Thus positive epsilons indicate larger than average ground motions. By deaggregating the PGA and 1.0 sec SA hazard by magnitude, distance and epsilon bins, we can illustrate the contributions by events at various periods. Figures 28 to 35 illustrate the contributions by events for return periods of 1,000, 2,500, 4,750 and 10,000 years. At PGA and all return periods, background earthquakes within 50 km of the site are dominant (Figures 28 to 31). At 1.0 sec SA, the contributions from more distant faults are shown in Figures 32 to 35.

Based on the magnitude and distance bins (Figures 28 to 35), the controlling earthquakes as defined by the mean magnitude (M-bar) and modal magnitude (M*) and mean distance (D-bar) and modal distance (D*) can be calculated. Table 6 lists the M-bar, M*, D-bar, and D* for the four return periods (1,000, 2,500, 4,750, and 10,000 years) and for PGA and 1.0 sec horizontal SA.

Uniform Hazard Spectra (UHS) for the four return periods are shown for the two site conditions on Figures 36 and 37, respectively. A UHS depicts the ground motions at all spectral periods with the same annual exceedance frequency or return period. Figure 38 compares the UHS for both site conditions for the four return periods. As expected, the ground motions are larger for the softer Pinal schist and Gila conglomerate site conditions than the rhyolite/diabase for the same return period.

5.1.1 Hazard Sensitivities

In this section, sensitivities to the hazard due to the minimum magnitude Mmin, the GMMs, and major components of the seismic source model are examined. Sensitivities were performed for the Pinal schist and Gila conglomerate site condition, but the relative results are applicable to all site conditions.

In this study, as is typical in site-specific PSHAs and in the USGS National Seismic Hazard Maps (NSHM), we use a Mmin of **M** 5.0. However, due to the significant contribution to the hazard from events of **M** 5.0 to 6.0, we investigated the impact of a lower Mmin. Figures 39 and 40 compare the total mean PGA and 1.0 sec SA hazard for Mmin of **M** 4.0 and 5.0. The maximum difference at PGA is at very short return periods (Figure 39). As the return period increases, the hazard curves converge. At 1.0 sec SA, there is almost no difference in hazard (Figure 40).

In addition to the sensitivity to Mmin, sensitivities of the hazard to the GMMs and the most significant portions of the seismic source model were performed. In these sensitivity analyses, the total mean hazard curves are conditioned on specific nodes in the logic tree having a full weight of 1.0. Figures 41 to 44 illustrate the sensitivity of the mean PGA and 1.0 sec horizontal SA hazard to the choice of GMMs. At the 10,000-year return period, there is a factor of 2 difference between the models giving the largest and smallest ground motion. This is a typical value for current GMMs in tectonically active regions and is a significant source of uncertainty in the hazard.

On Figures 45 and 46, the sensitivity in the PGA and 1.0 sec SA hazard is shown between the gridded and the uniform background zone which were weighted equally in the PSHA. The hazard is nearly identical for the two models due to the location of Near West in an area of average seismicity for the SBR (Figures 2 and 13).

Figures 47 and 48 show the sensitivity in hazard to the Mmax for the background earthquakes. There is very little difference in PGA hazard for the range of Mmax (Figure 47), but some difference in the 1.0 sec SA hazard (Figure 48). This is a typical result since earthquake rates at lower magnitudes are more important (see further discussion).

Figures 49 and 50 show the sensitivity to the differences in the gridded seismicity rates computed by ABSMOOTH. There are significant differences between the different rates with realization 6 giving much lower hazard. This reflects the large uncertainties incorporated into the rates for the background seismicity due to the short and incomplete historical record (Figure 13).

Tornado plots are provided to summarize the sensitivity analyses. The plots show the effects of the dominant seismic hazard model components (on vertical axis) on the total mean hazard specified in terms of the ground motion at a given return period. For each key element of the seismic hazard model, sensitivity analyses are performed assigning a weight of 1.0 to one of the epistemic alternatives (nodes on the logic tree) for that element of the seismic hazard model, as discussed above. The ground motion (PGA and 1.0 sec SA) at 10,000-year return period is computed from each sensitivity analysis. The tornado plot shows the ratio of these ground motions to the ground motion from the full analysis using the entire logic tree.

Figures 51 and 52 show tornado plots at a return period of 10,000 years. At PGA, the gridded seismicity rates are the source of the largest uncertainty in the hazard followed by the GMMs. At 1.0 sec SA, the GMMs are the largest source of uncertainty. Mmax of the background earthquakes and the choice of uniform versus gridded seismicity are not that significant to the mean hazard.

5.2 COMPARISON WITH NATIONAL SEISMIC HAZARD MAPS

In 1996, the USGS released a "landmark" set of National Hazard Maps for earthquake ground shaking, which was a significant improvement from previous maps they had developed (Frankel *et al*., 1996). These maps have been revised and updated, and the most current version was released in 2014 (Petersen *et al*., 2014). These maps were the result of the most comprehensive analyses of seismic sources and ground motion prediction ever undertaken on a national scale and they make use of the five NGA-West2 relationships. The 2008 maps are the basis for the current International Building Code. The maps are for NEHRP site class B/C (firm rock) or V_S30 of 760m/sec.

For a 2,475-year return period, the 2014 USGS National Hazard Maps indicate a firm rock PGA and 1.0 sec SA of 0.12 and 0.071 g, respectively, for the site compared to the site-specific values of 0.065 and 0.046 g for a V_S30 of 700 m/sec. The difference is due mainly to the difference in rates for the background seismicity. The USGS uses a minimum rate or floor for the region covered by the SBR based on uniform smoothing of seismicity. The region for which the background rates are computed is much larger and includes higher seismicity regions to the north. In addition, the USGS uses a higher maximum magnitude (**M** 7.45) and a large smoothing kernel (50 km) in their Gaussian smoothing approach.

5.3 COMPARISON WITH PREVIOUS STUDY

In 2013, a PSHA was performed for the Near West site using the NGA-West1 GMMs and assuming a V_S30 of 500 ± 100 m/sec for the Gila conglomerate (Wong *et al*., 2013). Figure 53 compares the 5,000 and 10,000-year return period UHS from the current PSHA results with the results from the 2013 study. The current study uses updated GMMs (NGA-West2), an updated source model, and updated site conditions (V_S30 for Gila conglomerate is 700 to 1,050 m/sec based on V_S measurements). The UHS for sites on Gila conglomerate are larger than the 2013 UHS for short periods (periods < 0.2 sec) and lower at longer periods.

5.4 DSHA RESULTS

The most significant seismic source to the site in a deterministic sense is the Sugarloaf fault although this fault is quite distant (Figure 3). The maximum event that was modeled in the DSHA is a **M** 6.6 on the Sugarloaf fault at a rupture distance of 48.5 km. Figure 54 shows the median and 84th percentile 5%- damped horizontal acceleration response spectra and the individual spectra from each of the GMMs for the 84th percentile for the Pinal schist and Gila conglomerate site condition. Figure 55 is a similar plot for the rhyolite and diabase site condition.

Figures 56 and 57 show comparisons of the horizontal deterministic spectra with UHS for a range of return periods. The 84th percentile spectra has an equivalent return period of between 2,500 and 4,750 years for both site conditions. The equivalent return period of the deterministic ground motions is controlled by the level of the probabilistic hazard at the site. For this site, the low seismicity around the site results in relatively long equivalent return periods for the deterministic ground motions.

The following describes the CMS approach and CMS calculated for the site.

6.1 APPROACH

The UHS represents the spectral accelerations at each period based on the rates of occurrence of all nearby sources, the GMMs and the uncertainties in these models. It is a broader spectrum than is expected for any single event. This uniform hazard can be represented by a suite of spectra that individually more closely represent the spectral shape of expected events contributing to the UHS. At a given period, a spectrum can be computed based on the deaggregated magnitude, distance and epsilon at that period. Depending on the epsilon required to match the spectrum to the UHS, the expected shape of this spectrum is not necessarily the median predicted spectral shape. Given the epsilon at a target period, epsilon at all other periods can be determined using a correlation function. Thus, a CMS represents a more realistic shape of an event likely to cause the target spectral acceleration at the target period.

The CMS approach was developed for the purpose of using the results of a PSHA to develop input to the seismic evaluation of structures (i.e., performing dynamic response calculations). The approach provides a method for defining the ground motion response spectrum input to a structural response analysis, where the estimated response is linked to the PSHA result (the hazard curve for a spectral acceleration at a given period), and where the estimate of structural response is mean-centered (i.e., non-conservative). The CMS response spectrum is associated with a Sa level for a single-structure period or narrow period range (e.g. the fundamental period of the structure to be analyzed), at a specified annual frequency of exceedance or return period. By linking a response spectrum suited to input to structure response analyses to the PSHA results, it is possible to make statements about the likelihood of observing levels of structural response and potential damage.

The procedure to implement the CMS approach is described in Baker (2011) and is summarized here. The steps in the process as defined by Baker (2011) are:

Step 1: Determine the Target Sa at a Given Period, and the Associated M, R and ε

For a specified annual frequency of exceedance (AFE) or return period, determine the target Sa from the mean hazard curve for Sa for the fundamental period of the structure to be analyzed. This period is denoted *T**. For this ground motion, obtain the mean magnitude (*M)*, distance (R), and ε from the PSHA deaggregation results. Depending upon the response characteristics of the structure or structures to be analyzed, CMS may need to be developed for several values of *T**.

Step 2: Compute the Mean and Standard Deviation of the Response Spectrum, Given M and R

For the mean M and R determined in Step 1, compute the mean and standard deviation of logarithmic spectral acceleration at all periods for the mean magnitude and distance. These are provided by standard ground motion prediction (attenuation) models. The predicted mean and standard deviation, given magnitude, distance, period, etc., are denoted $\overline{\ln Sa}(M, R, T)$ and $\sigma_{\ln Sa}(T)$, respectively. The mean and standard deviation of the log spectral acceleration can be computed using the GMMs that were used in the PSHA itself. Since multiple GMMs were used in the PSHA, a weighted estimate of the mean log Sa and the standard deviation can be used. Alternatively, a CMS can be developed for each GMM and a weighted average taken to produce the final CMS.

Step 3: Compute* ε *at Other Periods, Given* ε*(T*)

Compute the "conditional mean" ε at other periods. The conditional mean ε at ε (T^*) was determined in Step 1. The conditional mean at other periods, T_i, is determined by,

$$\mu_{\varepsilon(Ti)|\varepsilon(T*)} = \rho(T_i, T^*)\varepsilon(T^*) \quad (6\text{-}1)$$

where $\rho(T_i,T^*)$ is the correlation coefficient between ε for periods T_i and T^*. The correlation coefficients of Baker and Jayaram (2008), which are developed using the NGA-West database and is applicable to periods in the range 0.01 – 10 sec are used to compute the conditional mean ε at other periods.

Step 4: Compute the Conditional Mean Spectrum

The CMS is computed using the estimated log mean and standard deviation from Step 2 and the conditional mean ε(Ti) values determined in Step 3. The CMS is estimated according to:

$$\mu_{\ln S_a(T_i)|\ln(S_a(T^*)} = \mu_{\ln S_a}(M, R, T_i) + \rho(T_i, T^*)\varepsilon(T^*)\sigma_{\ln S_a}(T_i) \quad (6\text{-}2)$$

The CMS is,

$$S_{a,CMS}(T) = \exp(\mu_{\ln(S_a(T_i)|\ln(S_a(T^*)}) \quad (6\text{-}3)$$

The standard deviation of $\ln S_a$ (T_i) is

$$\sigma_{\ln Sa(T_i)|\ln Sa(T*)} = \sigma_{\ln Sa(T_i)}\sqrt{1-\rho^2(T_i, T^*)} \quad (6\text{-}4)$$

6.2 CMS

CMS conditioned to the UHS at 0.2 and 1.5 sec have been computed for the 10,000-year return periods for both site conditions (Figures 58 to 59). As discussed in Section 5.1, the hazard at the site at a 10,000-year return period is controlled by the background seismicity. At the 10,000-year return period, the M-bar and D-bar at 0.2 sec is **M** 5.8 at 18 km for both site conditions. The M-bar and D-bar at 1.5 sec are **M** 6.2 at 20 km and **M** 6.1 at 28 km for the Pinal schist and Gila conglomerate and the rhyolite and diabase sites, respectively. The CMS are tabulated in Table 7.

In consultation with KCB, we developed seven horizontal-component time histories for the UHS at a return period of 10,000 years. Because the response spectrum of a time history has peaks and valleys that deviate from the design response spectrum (target spectrum), it is necessary to modify the motion to improve its response spectrum compatibility. The procedure proposed by Lilhanand and Tseng (1988), as modified by Al Atik and Abrahamson (2010) and contained in the computer code RSPMatch09, was used to develop the acceleration time histories through spectral matching to the target (seed) spectrum. This time-domain procedure has been shown to be superior to previous frequency-domain approaches because the adjustments to the time history are only done at the time at which the spectral response occurs resulting in only localized perturbations on both the time history and the spectra (Lilhanand and Tseng, 1988).

To match the target spectrum, seed time histories should be from events of similar magnitude, distance (for duration), to a lesser extent site condition, and most importantly, spectral shape as the earthquake dominating the spectrum. The seed time-histories selected are based on the controlling earthquakes (Table 6). Table 8 lists the seed time histories.

The spectral matches and the resulting time histories for the Pinal Schist and Gila Conglomerate site conditions are shown on Figures 60 to 87 with the response spectra calculated from the matched time histories. Shown with each set of time histories is the normalized Arias intensity or Husid plot, which provides an appropriate duration measure independent of the absolute amplitude level of the acceleration time history. The properties of the spectrally-matched time histories are listed in Table 9.

Abrahamson, N.A. and Silva, W.J., 1997, Empirical response spectral attenuation relations for shallow crustal earthquakes: Seismological Research Letters, v. 68, p. 94-127.

Abrahamson, N.A. and Silva, W.J., and Kamai, R., 2014, Summary of the ASK14 ground-motion relation for active crustal regions: Earthquake Spectra, v. 30, p. 1025-1055.

Akciz, S.O., Grant Ludwig, L., Arrowsmith, J R., and Zielke, O., 2010, Century-long average time intervals between earthquake ruptures of the San Andreas fault in the Carrizo Plain, California: Geology, v. 38, p. 787-790.

Aki, K., 1983, Seismological evidence in support of the existence of "Characteristic Earthquakes": Earthquake Notes, v. 54, p. 60-61.

Al Atik, L. and Youngs, R., 2014, Epistemic uncertainty for NGA-West2 models: Earthquake Spectra: v. 30, p. 1301-1318.

Al Atik, L. and Abrahamson, N., 2010, An improved method for nonstationary spectral matching: Earthquake Spectra: v. 26, p. 601-617.

Anderson, J.G., 1979, Estimating the seismicity from geological structure for seismic risk studies: Bulletin of the Seismological Society of America, v. 69, p. 135-158.

Baker, J.W., 2011, The conditional mean spectrum: A tool for ground motion selection: American Society of Civil Engineers, Journal of Structural Engineering, v. 137, p. 322-331.

Baker J.W. and Cornell C.A., 2006, Correlation of response spectral values for multi-component ground motions: Bulletin of the Seismological Society of America, v. 96, p. 215-227.

Baker, J.W. and Jayaram, N., 2008, Correlation of Spectral Acceleration Values from NGA Ground Motion Models: Earthquake Spectra, v. 24, p. 299-317.

Bausch, D. and Brumbaugh, D.A., 1997, Relocation study of early Arizona earthquakes: Events of 1906, 1910, and 1912: unpublished report prepared for Arizona Division of Emergency Management, Earthquake Program, 65 p. + Appendices.

Boore, D.M., Stewart, J.P., Seyhan, E., Atkinson, G.M., 2014, NGA-West2 equations for predicting PGA, PGV, and 5%-damped PSA for shallow crustal earthquakes: Earthquake Spectra, v. 32, p. 979-1004.

Brumbaugh, D. S., 1987, A tectonic boundary for the Southern Colorado Plateau: Tectonophysics, v. 136, p. 125-136.

Bull, W.B., and Pearthree, P.A., 1988, Frequency and size of Quaternary surface ruptures of the Pitaycachi fault, northeastern Sonora, Mexico: Bulletin of the Seismological Society of America, v. 78, p. 956-978.

Campbell, K.W. and Bozorgnia, Y., 2014, NGA-West2 ground motion model for the average horizontal components of PGA, PGV, and 5%-damped linear acceleration response spectra: Earthquake Spectra, v. 30, p. 1087-1115.

Cao, T.C., Bryant, W.A., Rowshandel, B., Branum, D., and Wills, C.J., 2003, The revised 2002 California probabilistic seismic hazard maps, June 2003: California Geological Survey website.

Chiou, B-S.J. and Youngs, R.R., 2014, Update of the Chiou and Youngs NGA ground motion model for average horizontal component of peak ground motion and response spectra:

Earthquake Spectra, v. 30, p. 1117-1153.

Cornell, C.A., 1968, Engineering seismic risk analysis: Bulletin of the Seismological Society of America, v. 58, p. 1583-1606.

Demsey, K.A., and Pearthree, P.A., 1994, Surficial and environmental geology of the Sierra Vista area, Cochise County, Arizona: Arizona Geological Survey Open-File Report 83-22, 14 p., scale 1: 500,000.

dePolo, C.M., 1994, The maximum background earthquake for the Basin and Range Province, western North America: Bulletin of the Seismological Society of America, v. 84, p. 466-472.

Drewes, H., Houser, B.B., Hedlund, D.C., Richter, D.H., Thorman, C.H., and Finnell, T.L., 1985, Geologic map of the Silver City 10 x 20 Quadrangle, New Mexico and Arizona: U.S. Geological Survey Miscellaneous Investigations Series Map 1-310-C, scale 1: 250,000.

DuBois, S.M., Smith, A.W., Nye, N.K., and Nowak, T.A., 1982, Arizona earthquakes, 1776-1980: Arizona Bureau of Geology and Mineral Technology Bulletin, v. 192, 456 p.

EPRI/DOE/NRC, 2012, Technical Report: Central and Eastern United States Seismic Source Characterization for Nuclear Facilities. EPRI, Palo Alto, CA, U.S. DOE, and U.S. NRC: 2012.

Euge, K.M., Schell, B.A., and Lam, I.P., 1992, Development of seismic acceleration maps for Arizona: Arizona Department of Transportation Report No. AZ92-344, 327 p., 5 sheets, scale 1: 1,000,000.

Field, E.H., Biasi, G.P., Bird, P., Dawson, T.E., Felzer, K.R., Jackson, D.D., Johnson, K.M., Jordan, T.H., Madden, C., Michael, A.J., Milner, K.R., Page, M.T., Parsons, T., Powers, P.M., Shaw, B.E., Thatcher, W.R., Weldon, R.J., II, and Zeng, Y., 2013, Uniform California Earthquake Rupture Forecast, Version 3 (UCERF3) – The Time-Independent Model: U.S. Geological Survey Open-File Report 2013-1165, California Geological Survey Special Report 228, and Southern California Earthquake Center Publication 1792.

Foley, L.L., LaForge, R.C., and Piety, L.A., 1988, Seismotectonic study for Elephant and Caballo Dams, Rio Grande Project, New Mexico: U.S. Bureau of Reclamation Seismotectonic Report 88-9, 60 p., 1 pl., scale 1: 24,000.

Frankel, A., 1995, Mapping seismic hazard in the central and eastern United States: Seismological Research Letters, v. 66, p. 8-21.

Grant, L.B. and Donnellan, A., 1994, 1855 and 1991 surveys of the San Andreas Fault; implications for fault mechanics: Bulletin of the Seismological Society of America, v. 84, p. 241-246.

Grant, L. and Sieh, K., 1993, Stratigraphic evidence for 7 meters of dextral slip on the San Andreas fault during the great 1857 earthquake in the Carrizo Plain: Bulletin of the Seismological Society, v 83, 619-635.

Grant, L.B. and Sieh, K., 1994, Paleoseismic evidence of clustered earthquakes on the San Andreas fault in the Carrizo Plain, CA.: Journal of Geophysical Research, v. 99, p. 6819-6842.

Grant Ludwig, L. and Akciz, S., 2012, Rupture history of the San Andreas fault in the Carrizo Plain prior to 1300 A.D., Final Technical Report, U.S. Geological Survey National

Earthquake Hazard Reduction Program Award No. G10AP00073.

Grant Ludwig, L., Akciz, S.O., Noriega, G. R., Zielka, O., and Arrowsmith, J R., 2010. Climate-modulated channel incision and rupture history of the San Andreas fault in the Carrizo Plain: Science, v. 327, p. 1117-111.

Gülerce, Z. and Abrahamson, N., 2011, Site-specific design spectra for vertical ground motion: Earthquake Spectra, v. 27, p. 1023-1047.

Hanks, T.C. and Kanamori, H. 1979, A moment magnitude scale: Journal of Geophysical Research, v. 84, p. 2348-2350.a

Hartleb, R., and Wong, I., 2017, Reconnaissance-level fault investigation of Resolution Copper Mining's Near West site, Pinal County, Arizona, unpublished report prepared by Lettis Consultants International.

Houser, B.B., 1994, Geology of the Late Cenozoic Alma Basin, New Mexico and Arizona, New Mexico Geological Society Guidebook 45th Field Conference, p. 121-124.

Johnson, R.A., and Loy, K.L., 1992, Seismic reflection evidence for seismogenic low-angle faulting in southeastern Arizona: Geology, v. 20, p. 597-600.

Keefer, D.I. and Bodily, S.E., 1983, Three-point approximations for continuous random variables: Management Science, v. 26, p. 595-609.

Lienkaemper, J.J., 2001, 1857 slip on the San Andreas fault southeast of Cholame, California: Bulletin of the Seismological Society of America, v. 91, p. 1659-1672.

Lilhanand, K. and Tseng, W.S., 1988, Development and application of realistic earthquake time histories compatible with multiple-damping design spectra: Proceeding of the 9th World Conference on Earthquake Engineering, Tokyo-Kyoto, Japan.

Lindsay, E.H., Smith, G.A., and Haynes, C.V., 1990, Late Cenozoic depositional history and geoarchaeology, San Pedro Valley, Arizona, *in* Gehrels, G.E., and Spencer, J.E., eds., Geologic excursions through the Sonoran Desert region, Arizona and Sonora: Arizona Geological Survey Special Paper 7, p. 9-19.

Lindvall, S.C., Rockwell, T.K., Dawson, T.E., Helms, J.G., and Bowman, K.W., 2002, Evidence for two surface ruptures in the past 500 years on the San Andreas fault at Frazier Mountain, California: Bulletin of the Seismological Society of America, v. 92, p. 2689-2703.

Liu, J., Klinger, K., Sieh, K., and Rubin, C., 2004, Six similar sequential ruptures of the San Andreas fault, Carrizo Plain, California: Geology, v. 32, p. 649-652.

Lockridge, J.S., Fouch, M.J., and Arrowsmith, J.R., 2012, Seismicity within Arizona during the deployment of the EarthScope USArray Transportable Array: Bulletin of the Seismological Society of America, v. 102, p. 1850-1863.

Lund, W.R., 2012, Basin and Range Province Earthquake Working Group II Recommendations to the U.S. Geological Survey National Seismic Hazard Mapping Program for the 2014 Update of the National Seismic Hazard Maps: Utah Geological Survey Open-File Report 591, 17 p.

Machette, M.N., 1998, Contrasts between short- and long-term records of seismicity in the Rio Grande rift – Important implications for seismic hazard assessments in areas of slow extension, *in* W.R. Lund (ed.), Western States Seismic Policy Council Proceedings Volume, Basin and Range Province Seismic Hazards Summit, Utah Geological Survey Miscellaneous Publication 98-2, p. 84-95.

Machette, M.N., Personius, S.F., Kelson, K.I., Haller, K.M., and Dart, R.L., 1998, Map and data for Quaternary faults and folds in New Mexico: U.S. Geological Survey Open-File Report 98-521, 443 p.

Machette, M.N., Personius,F., Menges, C.M., and .Pearthree, P.A., 1986, Map showing Quaternary and Pliocene faults in the Silver City 1° x 2° quadrangle and the Douglas 1° x 2° quadrangle, southeastern Arizona and southwestern New Mexico: U.S. Geological Survey Miscellaneous Field Studies Map MF-1465-C, 12 p. pamphlet, 1 sheet, scale I :250,000.

Mack, G.H., Seager, W.R., and Leeder, M.R., 2003, Synclinal-horst basins: examples from the southern Rio Grande rift and southern transition zone of southwestern New Mexico: Basin Research, v. 15, p. 365-377.

McQuarrie, N., and Wernicke, B.P., 2005, An animated tectonic reconstruction of southwestern North America since 36 Ma: Geosphere, v. 1, p. 147–172.

Menges, C.M. and McFadden, L.D., 1981, Evidence for the latest-Miocene to Pliocene transition from Basin-Range tectonic to post-tectonic landscape evolution in southeastern Arizona: Arizona Geological Society Digest, v. 13, p. 151-160.

Menges, C.M. and Pearthree, P.A., 1983, Map of neotectonic (latest Pliocene-Quaternary) deformation in Arizona: Arizona Bureau of Geology Mineral Technology Open-File Report 83-22, 48 p., scale 1: 500,000.

Menges, C.M. and Pearthree, P.A., 1989, Late Cenozoic tectonism in Arizona and its impact on regional landscape evolution: *in* Geologic Evolution of Arizona, Arizona Geological Society, Digest No. 17, p. 649–680.

Molnar, P., 1979, Earthquake recurrence intervals and plate tectonics: Bulletin of the Seismological Society of America, v. 69, p. 115-133.

Morgan, P., and Swanberg, C.A., 1985, on the Cenozoic uplift and tectonic stability of the Colorado Plateau: Journal of Geodynamics, v. 3, p. 39-63.

Pearthree, P.A., 1998, Quaternary fault data and map of Arizona: Arizona Geological Survey Open-File Report 98-24, 122 p.

Pearthree, P.A., and Calvo, S.S., 1987, The Santa Rita fault zone—Evidence for large magnitude earthquakes with very long recurrence intervals, Basin and Range province of southeastern Arizona: Bulletin of the Seismological Society of America, v. 77, p. 97-116.

Pearthree, P.A., McKittrick, M.A., Jackson, G.A., and Demsey, K.A., 1988, Geologic map of Quaternary and upper Tertiary deposits, Tucson 1° x 2° quadrangle, Arizona: Arizona Geological Survey Open-File Report 88-21, scale 1: 250,000.

Pearthree, P.A., Menges, C.M., and Mayer, L., 1983, Distribution, recurrence, and possible tectonic implications of late Quaternary faulting in Arizona: Arizona Bureau of Geologic Mineral Technical Open-File Report 83-20, 51 p.

Pearthree, P.A., Vincent, K.R., Brazier, R., Fellows, L.D., and Davis, O.K., 1995, Seismic hazard posed by the Sugarloaf fault, central Arizona: Arizona Geological Survey Open-File Report 95-7, 41, p.

Pearthree, P.A., Bull, W.B., and Wallace, T.C., 1990, Geomorphology and Quaternary geology of the Pitaycachi Fault, northeastern Sonora, Mexico: Geologic excursions through the Sonoran Desert Region, Arizona and Sonora, Gehrels, G.E. and Spencer, J.E. eds., University of Arizona Press, pp. 124-135.

Peirce, H.W., 1984, The Mogollon escarpment: Arizona Bureau of Geology and Mineral Technology Fieldnotes, v. 4, p. 8-11.

Petersen, M.D., Frankel, A.D., Harmsen, S.C., Mueller, C.S., Haller, K.M., Wheeler, R.L., Wesson, R.L., Zeng, Y., Boyd, O.S., Perkins, D.M., Luco, N., Field, E.H., Wills, C.J., and Rukstales, K.S., 2008, Documentation for the 2008 update of the United States National Seismic Hazard Maps: U.S. Geological Survey Open-File Report 2008-1128, 61 p.

Petersen, M.D., Frankel, A.D., Harmsen, S.C., Mueller, C.S., Haller, K.M., Wheeler, R.L., Wesson, R.L., Zeng, Y., Boyd, O.S., Perkins, D.M., Luco, N., Field, E.H., Wills, C.J., and Rukstales, K.S., 2008, Documentation for the 2008 update of the United States National Seismic Hazards Maps: U.S. Geological Survey Open-File Report 2008-1128, 61 p.

Piety, L.A. and Anderson, L.W., 1991, The Horseshoe fault--Evidence for prehistoric surface-rupturing earthquakes in central Arizona: Arizona Geology, v. 21, no. 3, p. 1, 4-8.

Runnerstrom, E.E., Grant, L.B., Arrowsmith, J.R., Rhodes, D.D., and Stone, E.M., 2002, Displacement across the Cholame segment of the San Andreas Fault between 1855 and 1896 from cadastral surveys: Bulletin of the Seismological Society of America: v. 92, p. 2,659-2,669.

Scharer, K.M., Weldon, R.J., Gibson, B.C., and Streig, A.R., 2011, Earthquake ages and displacements, Frazier Mountain paleoseismic site, Abstract T51B-2324 presented at 2011 Fall Meeting, AGU, San Francisco, Calif., 5-9 Dec.

Schwartz, D.P. and Coppersmith, K.J., 1984, Fault behavior and characteristic earthquakes--examples from the Wasatch and San Andreas fault zones: Journal of Geophysical Research, v. 89, p. 5681-5698.

Sieh, K.E., 1978, Slip along the San Andreas fault associated with the great 1857 earthquake: Bulletin of the Seismological Society of America, v. 68, p. 1421-1448.

Sieh, K.E. and Jahns, R.H., 1984, Holocene activity of the San Andreas fault at Wallace Creek, California: Geological Society of America Bulletin, v. 95, p. 883-896.

Sims, J.D., 1994, Stream channel offset and abandonment and a 200-year average recurrence interval of earthquakes on the San Andreas fault at Phelan Creek, Carrizo Plain, California, *in* Prentice, C.S., Schwartz, D.P., and Yeats, R.S. (eds.), Proceedings of the workshop on paleoseismology: U.S. Geological Survey Open-File Report 94-568, p. 170-172.

Skotnicki, S.J., Leighty, R.S., and Pearthree, P.A., 1997, Geologic map of the Wildcat Hill quadrangle, Maricopa County, Arizona: Arizona Geological Survey Open-File Report 97-2, 17 p., 1 pl., scale 1: 24,000.

Stepp, J.C., 1972, Analysis of completeness of the earthquake sample in the Puget Sound area and its effect on statistical estimates of earthquake hazard: Proceedings of the International Conference on Microzonation, v. 2, 897-910.

Stirling, M., Rhoades, D., and Berryman, K., 2002, Comparison of earthquake scaling relations derived from data of the instrumental and preinstrumental era: Bulletin of the Seismological Society of America, v. 92, p. 812-830.

Stone, E.M., Grant, L., and Arrowsmith, J.R., 2002, Recent rupture history of the San Andreas Fault southeast of Cholame in the northern Carrizo Plain, California: Bulletin of the Seismological Society of America, v. 92, p. 983-997.

Suter, M., 2008, Structural configuration of the Otates fault (Southern Basin and Range Province) and its rupture in the 3 May 1887 M 7.5 Sonora, Mexico, earthquake: Bulletin of the Seismological Society of America, v. 98, p. 2879-2893.

Suter M., 2015., Rupture of the Pitaycachi Fault in the 1887 Mw 7.5 Sonora, Mexico earthquake (southern Basin-and-Range Province): Rupture kinematics and epicenter inferred from rupture branching patterns Journal of Geophysical Research Solid Earth, v.120, p. 617-641, doi:10.1002/2014JBO11244.

Suter, M. and Contreras, J., 2002, Active tectonics of northeastern Sonora, Mexico (southern Basin and Range Province) and the 3 May 1887 M_W 7.4 earthquake: Bulletin of the Seismological Society of America, v. 92, p. 581-589.

Thomas, P.A., Wong, I.G., and Abrahamson, N., 2010, Verification of probabilistic seismic hazard analysis software programs: PEER Report 2010/106, Pacific Earthquake Engineering Research Center, College of Engineering, University of California, Berkeley, 173 p.

Thomas, P., Wong, I., Zachariasen, J., Olig, S., and Terra, F., 2015, Updated site-specific probabilistic and deterministic seismic hazard analyses, Sierrita Tailings Dam, Green Valley, Arizona: unpublished report prepared for Freeport-McMoran Copper & Gold, Inc. by URS Corporation.

Toppozada, T.R., Branum, D.M., Reichle, M.S., and Hallstrom, C.L., 2002, San Andreas fault zone, California: M>5.5 earthquake history: Bulletin of the Seismological Society of America, v. 92, p. 2555-2601.

Wells, D.L. and Coppersmith, K.J., 1994, New empirical relationships among magnitude, rupture length, rupture width, rupture area, and surface displacement: Bulletin of the Seismological Society of America, v. 84, p. 974-1002.

Wesnousky, S.G., 1986, Earthquakes, Quaternary faults, and seismic hazard in California: Journal Geophysical Research, v. 91, p. 12,587-12,631.

Wesnousky, S.G., 2008, Displacement and geometrical characteristics of earthquake surface ruptures-issues and implications for seismic-hazard analysis and the process of earthquake rupture; Bulletin of the Seismological Society of America, v. 98, p. 1609-1632.

WGCEP (Working Group on California Earthquake Probabilities), 1988, Probabilities of large earthquakes occurring in California on the San Andreas fault: U.S. Geological Survey Open-File Report 88-398, 62 p.

WGCEP (Working Group on California Earthquake Predictions), 1995, Seismic hazards in southern California: probable earthquakes, 1994 to 2024: Bulletin of the Seismological Society of America, v. 95, p. 379-439.

WGCEP (Working Group on California Earthquake Probabilities), 2008, The Uniform California Earthquake Rupture Forecast, Version 2 (UCERF 2), USGS Open-File Report 2007-1437/CGS Special Report 203/SCEC Contribution #1138, Version 1.0.

Wong, I.G. and Humphrey, J.R., 1989, Contemporary seismicity, faulting, and the state of stress in the Colorado Plateau: Geological Society of America Bulletin, v. 101, p. 1127-1146.

Wong, I., Pezzopane, S., and Dober, M., 2008, Site-specific seismic hazard analyses for Miami Tailing Dams, Claypool, Arizona: unpublished report prepared for Freeport-McMoran Copper and Gold Miami Operations.

Wong, I.G., Nemser, E., Dober, M., Olig, S., Bott, J., and Terra, F., Darragh, R., and Silva, W., 2013, Site-specific Seismic hazard analyses for the Resolution Mining Company tailings storage facilities options, Southern Arizona: unpublished report prepared for Resolution Copper Mining.

Wong, I., Terra, F., Olig, S., and Dober, M., 2011, Site-specific seismic hazard evaluation of the Morenci Mine Tailing Dam, Arizona: unpublished report prepared for Freeport-McMoran Copper and Gold Inc.

Wong, I., Dober, M., Olig, S., and Terra, F., 2006, Site-Specific Hazard Evaluation of the Chino Mine Tailing Ponds, New Mexico: unpublished final report prepared for Chino Mines Company, Hurley, New Mexico.

Wong, L, Olig, S., Green, R., Moriwaki, Y., Abrahamson, N., Baures, D., Silva, W., Somervime, P., Davidson, D., Pilz, J., and Dunne, B., 1995, Seismic hazard evaluation of the Magna Tailings Impoundment, *in* W.R. Lund (ed.), Environmental and Engineering Geology of the Wasatch Front Region, Utah Geological Association Publication 24, p. 95-110.

Yeats, R. S., Sieh, K., and Allen, C.R., 1997, The Geology of Earthquakes, Oxford University Press, New York.

Young, J.J., Arrowsmith, JR., Colini, L., Grant, L.B., and Gootee, B., 2002, 3-D excavation and measurement of recent rupture history along the Cholame segment of the San Andreas Fault: Bulletin of the Seismological Society of America, v. 92, p. 2,670-2,688.

Youngs, R.R. and Coppersmith, K.J., 1985, Implications of fault slip rates and earthquake recurrence models to probabilistic seismic hazard estimates: Bulletin of the Seismological Society of America, v. 75, p. 939-964.

Zielke, O., Arrowsmith, J R., Ludwig L G., Akciz, S.O., 2010, Slip in the 1857 and earlier large earthquakes along the Carrizo Plain, San Andreas fault: Science, v. 327, 5969, p. 1119-1122.

Table 1. Fault Parameters[1]

FAULT NO.[2]	FAULT NAME	DISTANCE TO PINAL SCHIST AND GILA CONGLOMERATE SITES (km)	DISTANCE TO SAN MANUEL SITE (km)	RUPTURE MODEL	MAXIMUM RUPTURE LENGTH[3] (km)	MAXIMUM MAGNITUDE[4] (M)	FAULT DIP[5] (degrees)	FAULT TYPE[6]	APPROXIMATE AGE OF YOUNGEST OFFSET	PROBABILITY OF ACTIVITY[7]	SLIP RATE[8] (mm/yr)	COMMENTS
941	Alma Mesa fault	166	166	Independent (1.0)	16	6.3 (0.2) 6.6 (0.6) 6.9 (0.2)	45 E (0.2) 60 E (0.6) 75 E (0.2)	N	< 1.6 Ma	1.0	0.005 (0.5) 0.02 (0.5)	This north-northeast striking normal fault is near the northwestern margin of the Alma basin along the Arizona - New Mexico border (Menges and Pearthree, 1983; Houser, 1994). The Alma Mesa fault is characterized by 10- to 20-m-high fault scarps on deeply dissected Plio-Pleistocene alluvial fan remnants. Our maximum slip rate assumes 20 m of vertical displacement occurred since 1 Ma whereas the minimum rate assumes 10 m occurred since 2 Ma.
	Anderson	154	248	Independent (1.0)	26	6.5 (0.2) 6.8 (0.6) 7.1 (0.2)	35 SW (0.2) 50 SW (0.6) 65 SW (0.2)	N	< 1.6 Ma	1.0	0.001 (0.2) 0.01 (0.6) 0.1 (0.2)	Northwest-striking fault is modified from Pearthree (2013, written communication) and was classified as a potential Quaternary fault in seismic source characterization for Palo Verde Nuclear Generating Station (LCI, 2015). Fault has not yet been included in USGS Quaternary Fault and Fold Database.
2093	Animas Valley faults	216	154	Independent (1.0)	20	6.4 (0.2) 6.7 (0.6) 7.0 (0.2)	45 W (0.2) 60 W (0.6) 75 W (0.2)	N	< 15 ka	1.0	0.005 (0.2) 0.02 (0.6) 0.2 (0.2)	Our characterization here is the same as in our previous study for Chino Mine (Wong *et al.*, 2006). These faults extend along the eastern margin of Animas Valley and the west side of the Pyramid Mountains (Machette *et al.*, 1986). Preferred slip rate is based on observations of 2 to 3 m scarps on late Pleistocene fans (Machette *et al.*, 1998).
	Agua Prieta (MX)	280	190	Independent (1.0)	41	6.7 (0.2) 7.0 (0.6) 7.3 (0.2)	35 E (0.2) 50 E (0.6) 65 E (0.2)	N	< 1.6 Ma	1.0	0.001 (0.2) 0.01 (0.6) 0.1 (0.2)	Fault expressed in bedrock and classified as a potential Quaternary fault in seismic source characterization for Palo Verde Nuclear Generating Station (LCI, 2015). The fault is located in northern Sonora, Mexico and along strike of the Quaternary Pedrogosa fault in southeast Arizona.
Not included in USGS database	Big Burro Mountains fault	189	151	Independent (1.0)	38	6.7 (0.2) 7.0 (0.6) 7.3 (0.2)	45 W (0.2) 60 W (0.6) 75 W (0.2)	N	< 1.6 Ma?	0.7	0.001 (0.5) 0.01 (0.5)	This northwest-striking, southwest-dipping, normal fault along the southwest flank of the Big Burro Mountains is not included in the USGS Quaternary Fault and Fold Database, but we include it as a potential fault source based on mapping of potential Quaternary fault scarps by Machette *et al.* (1986). They estimate tens of meters of slip in Plio-Pleistocene deposits, but little else is known about this poorly understood fault. Based on its poorer geomorphic expression, we assumed a maximum slip rate similar to the preferred rate of the Gold Hill fault zone to the southeast. We assumed 1 to 2 m of slip occurred since ~1 Ma for the minimum rate. We assigned a slightly lower probability of activity of 0.7 because evidence for repeated Quaternary movement is not as strong as other faults in the region that were included by Machette *et al.* (1998) in their Quaternary fault compilation.
951	Big Chino fault	208	295	Independent (1.0)	63	6.9 (0.2) 7.2 (0.6) 7.5 (0.2)	35 SW (0.2) 50 SW (0.6) 65 SW (0.2)	N	<15 ka 10-15 ka	1.0	0.05 (0.2) 0.12 (0.6) 0.3 (0.2)	Slip rates based on 8 m vertical displacement of upper Pleistocene alluvium (80-100 ka): 0.1 – 0.08 mm/yr., and 18 to 25 m vertical displacement of mid Pleistocene (200-400 ka) alluvium: 0.05-0.1 mm/yr (Euge *et al.*, 1992). Maximum value assumes a 3 m event and 10,000 year recurrence interval: 2-0.3 mm/yr. Preferred maximum magnitude based on surface rupture length of 46 km (Pearthree, 1998) and average displacements per event of 1.8 to 2.7 m (Euge *et al.*, 1992).

Table 1. Fault Parameters[1]

FAULT NO.[2]	FAULT NAME	DISTANCE TO PINAL SCHIST AND GILA CONGLOMERATE SITES (km)	DISTANCE TO SAN MANUEL SITE (km)	RUPTURE MODEL	MAXIMUM RUPTURE LENGTH[3] (km)	MAXIMUM MAGNITUDE[4] (M)	FAULT DIP[5] (degrees)	FAULT TYPE[6]	APPROXIMATE AGE OF YOUNGEST OFFSET	PROBABILITY OF ACTIVITY[7]	SLIP RATE[8] (mm/yr)	COMMENTS
	Bootlegger	157	250	Independent (1.0)	32	6.6 (0.2) 6.9 (0.6) 7.2 (0.2)	35 SW (0.2) 50 SW (0.6) 65 SW (0.2)	N	< 1.6 Ma	1.0	0.001 (0.2) 0.01 (0.6) 0.1 (0.2)	Northwest-striking fault is modified from Pearthree (2013, written communication) and was classified as a potential Quaternary fault in seismic source characterization for Palo Verde Nuclear Generating Station (LCI, 2015). Fault has not yet been included in USGS Quaternary Fault and Fold Database.
927	Bunk Robinson	254	167	Independent (1.0)	14	6.3 (0.2) 6.6 (0.6) 6.9 (0.2)	35 W (0.2) 50 W (0.6) 65 W (0.2)	N	<1.6 Ma	1.0	0.001 (0.2) 0.01 (0.6) 0.1 (0.2)	Fault zone consists of four north- to northwest-trending faults on the eastern side of the San Bernardino Valley in southeastern Arizona. Upper Pliocene basalt flows are displaced 20–150 m. Because there is no definitive evidence of middle to late Quaternary faulting, activity of these faults may have been associated with the basaltic eruptions in the late Pliocene or early Quaternary.
937	Cactus Flats faults	125	82	Independent (1.0)	9	6.1 (0.2) 6.4 (0.6) 6.7 (0.2)	50 E (0.2) 65 E (0.6) 80 E (0.2)	N	< 750 ka	0.9	0.001 (0.3) 0.004 (0.4) 0.04 (0.3)	This northwest-striking series of normal faults and fractures in basin-fill and terrace gravels of the Gila River are located in the hanging wall of the Safford fault zone and are unusually straight. Because of this and their relatively short length (< 10 km), we assigned a slightly lower probably of activity of 0.9 as they may be non-tectonic subsidence features or secondary to the Safford fault zone. We assumed slightly steeper dips than typical range-bounding normal faults because of their intrabasin location and very straight traces (Houser, 1994). Preferred slip rate is based on 0.5 m offset since 130 ka, whereas the maximum rate is based on 100 m of offset of a 2.5-Ma volcanic tuff (Machette *et al.*, 1986; 1998). The minimum rate assumes 0.5 m of slip occurred since 500 ka.
933	California Wash fold and faults	174	79	Independent (1.0)	16	6.3 (0.2) 6.6 (0.6) 6.9 (0.2)	45 E (0.2) 60 E (0.6) 75 E (0.2)	N	< 1.6 Ma?	0.6	0.03 (0.2) 0.008 (0.6) 0.003 (0.2)	These short (6 to 8 km long) homoclinal folds and minor faults trend north-northwest along the west side of San Pedro Valley. Middle Pleistocene fan sediments may be deformed but geomorphic expression is very subtle. Plio-Pleistocene basin-fill deposits may be offset by as much as 15 m (Menges and Pearthree, 1983; Lindsay *et al.*, 1990), suggesting comparable preferred slip rates to the Huachuca fault zone. Therefore, we assumed a similar slip rate distribution but assigned a lower probability of activity due to the short length and poor geomorphic expression in Quaternary deposits.
947	Carefree Fault Zone	95	170	Independent (1.0)	11	6.2 (0.2) 6.5 (0.6) 6.8 (0.2)	35 W (0.2) 50 W (0.6) 65 W (0.2)	N	< 750 ka	1.0	0.002 (0.2) 0.01 (0.6) 0.02 (0.2)	Northwest-striking, west side-down normal faults that divide a Precambrian granite pediment from tilted Tertiary volcanic rocks to the west in the McDowell Mountains. Scarps < 3 m high along a contact between the granite bedrock and middle Pleistocene alluvium. Skotnicki *et al.* (1997) interpret middle Pleistocene deposits are faulted but Holocene and late Pleistocene deposits are not displaced. Slip rate is based on < 3 m offset in middle Pleistocene (~300 ka) and older deposits (Pearthree, 1998).
960	Casner Cabin	183	275	Independent (1.0)	10	6.1 (0.2) 6.4 (0.6) 6.7 (0.2)	35 W (0.2) 50 W (0.6) 65 W (0.2)	N	< 750 ka	1.0	0.001 (0.2) 0.01 (0.6) 0.1 (0.2)	This fault zone forms two fairly sharply defined, narrow grabens on Paleozoic bedrock and Pliocene volcanic rocks. Total vertical displacement is at least 40 m. Middle to late Quaternary faulting is likely because a middle Pleistocene alluvial fan in one of the grabens is probably displaced at least 3 m.

Table 1. Fault Parameters[1]

FAULT NO.[2]	FAULT NAME	DISTANCE TO PINAL SCHIST AND GILA CONGLOMERATE SITES (km)	DISTANCE TO SAN MANUEL SITE (km)	RUPTURE MODEL	MAXIMUM RUPTURE LENGTH[3] (km)	MAXIMUM MAGNITUDE[4] (M)	FAULT DIP[5] (degrees)	FAULT TYPE[6]	APPROXIMATE AGE OF YOUNGEST OFFSET	PROBABILITY OF ACTIVITY[7]	SLIP RATE[8] (mm/yr)	COMMENTS
	Chavez Mtn	137	232	Independent (1.0)	40	6.7 (0.2) 7.0 (0.6) 7.3 (0.2)	35 NE (0.2) 50 NE (0.6) 65 NE (0.2)	N	< 1.6 Ma	1.0	0.001 (0.2) 0.01 (0.6) 0.1 (0.2)	The Chavez Mountain fault strikes north-northwest and forms a series of east-facing scarps. Fault is modified from Pearthree (2013, written communication) and was classified as a potential Quaternary fault in seismic source characterization for Palo Verde Nuclear Generating Station (LCI, 2015). Fault has not yet been included in USGS Quaternary Fault and Fold Database.
929	Chiricahua	234	158	Independent (1.0)	29	6.6 (0.2) 6.9 (0.6) 7.2 (0.2)	35 E (0.2) 50 E (0.6) 65 E (0.2)	N	< 750 ka	1.0	0.001 (0.2) 0.01 (0.6) 0.1 (0.2)	This is a fault zone with probable Quaternary activity that extends for about 30 km along the east side of the Chiricahua Mountains in southeasternmost Arizona. The mountain front is steep and fairly linear, however, fault scarps are poorly preserved, are not very high, and are formed only on lower to middle Pleistocene alluvial fans. These relations suggest that this fault has a fairly low middle and late Quaternary slip rate and has not ruptured in the latest Quaternary.
939, 2090, and 2091	Clifton-Rimrock-Pearson Mesa faults	140	114	Linked (0.2)	36 (floating over total length of 67 km)	6.7 (0.2) 7.0 (0.6) 7.3 (0.2)	45 W (0.2) 60 W (0.6) 75 W (0.2)	N	< 130 ka	1.0	0.005 (0.2) 0.02 (0.6) 0.1 (0.2)	These northwest-striking faults were considered as potentially linked because they are all down-to-the-southwest normal faults along the northeastern margin of Duncan Basin (Machette *et al.*, 1998; Pearthree, 1998). Our depiction here includes additional potential Quaternary fault scarps not shown in the USGS database based on mapping by Machette *et al.* (1986).
		151	119	Not linked (0.8) Clifton faults	16	6.3 (0.2) 6.6 (0.6) 6.9 (0.2)		N	< 1.6 Ma		0.003 (0.2) 0.01 (0.6) 0.1 (0.2)	
		172	130	Rimrock fault	6	5.9 (0.2) 6.2 (0.6) 6.5 (0.2)		N			0.005 (0.2) 0.02 (0.6) 0.1 (0.2)	
		176	132	Pearson Mesa fault	8	6.0 (0.2) 6.3 (0.6) 6.6 (0.2)		N			0.003 (0.2) 0.009 (0.6) 0.1 (0.2)	
1014	Conocho	152	208	Independent (1.0)	47	6.8 (0.2) 7.1 (0.6) 7.4 (0.2)	55 NE (0.2) 70 NE (0.6) 85 NE (0.2)	N/SS	< 750 ka	1.0	0.015 (0.2) 0.03 (0.6) 0.06 (0.2)	Northwest-trending, discontinuous system of probable sinistral and oblique-normal slip faults that cuts the northeastern part of the Pliocene-Pleistocene Springerville volcanic field in east-central Arizona. Faults displace Mesozoic bedrock and upper Pliocene to lower Pleistocene basalt flows in a down-to-the-northeast sense. An early Pleistocene cinder cone has been displaced vertically about 30 m by the fault. The faults have probably been active in the middle or late Quaternary, but the age of youngest movement is not well constrained.
1015	Coyote Wash	161	205	Independent (1.0)	42	6.7 (0.2) 7.0 (0.6) 7.3 (0.2)	55 SW (0.2) 70 SW (0.6) 85 SW (0.2)	SS/N	< 750 ka	1.0	0.001 (0.2) 0.01 (0.6) 0.1 (0.2)	Similar to nearby Concho fault, the Coyote Wash fault is a generally northwest-trending, discontinuous system of probable sinistral and oblique-slip faults. The topographic scarp along fault zone evidently is not sharply defined, suggesting faults have probably been active in the middle or late Quaternary, but the age of youngest movement is not well constrained.

Table 1. Fault Parameters[1]

FAULT NO.[2]	FAULT NAME	DISTANCE TO PINAL SCHIST AND GILA CONGLOMERATE SITES (km)	DISTANCE TO SAN MANUEL SITE (km)	RUPTURE MODEL	MAXIMUM RUPTURE LENGTH[3] (km)	MAXIMUM MAGNITUDE[4] (M)	FAULT DIP[5] (degrees)	FAULT TYPE[6]	APPROXIMATE AGE OF YOUNGEST OFFSET	PROBABILITY OF ACTIVITY[7]	SLIP RATE[8] (mm/yr)	COMMENTS
	El Chile	243	162	Independent (1.0)	17	6.3 (0.2) 6.6 (0.6) 6.9 (0.2)	35 E (0.2) 50 E (0.6) 65 E (0.2)	N	< 1.6 Ma	1.0	0.001 (0.2) 0.01 (0.6) 0.1 (0.2)	Fault is located in northern Mexico and expressed in bedrock and classified as a potential Quaternary fault in seismic source characterization for Palo Verde Nuclear Generating Station (LCI, 2015).
	Fronteras	277	183	Independent (1.0)	79	7.0 (0.2) 7.3 (0.6) 7.6 (0.2)	35 W (0.2) 50 W (0.6) 65 W (0.2)	N	< 1.6 Ma	1.0	0.001 (0.2) 0.01 (0.6) 0.1 (0.2)	This normal fault is located in northern Sonora, Mexico and one valley west of the 1887 earthquake rupture of the Pitaycachi fault. Suter and Contreras (2002) considers Quaternary age based on local range front morphology and probable association with seismicity.
2094a and 2094b	Gold Hill fault zone	232	178	Linked (1.0)	24	6.5 (0.2) 6.8 (0.6) 7.1 (0.2)	45 W (0.2) 60 W (0.6) 75 W (0.2)	N	< 130 ka	1.0	0.002 (0.2) 0.01 (0.6) 0.09 (0.2)	Our characterization for this fault zone is from Wong *et al.* (2006). This normal fault bounds the southwestern flank of the Big Burro Mountains. We assumed a linked rupture model for the northern (2094a) and southern (2094b) sections based on their short individual lengths and kinematic compatibility. Reconnaissance scarp studies found evidence of repeated Quaternary activity with scarps 6 to 8.5 m high on older alluvial fan surfaces (Machette *et al.*, 1986). Preferred slip rate based on 2.9 m of surface offset measured on surfaces estimated to be 200 to 500 ka (Machete *et al.*, 1998).
2095	Gray Ranch	261	188	Independent (1.0)	20	6.4 (0.2) 6.7 (0.6) 7.0 (0.2)	45 E (0.2) 60 E (0.6) 75 E (0.2)	N	< 15 ka	1.0	0.004 (0.2) 0.04 (0.6) 0.4 (0.2)	The Gray Ranch fault zone is marked by three en echelon, discontinuous, east-facing, south-trending scarps along the eastern flank of a south-central part of the Peloncillo Mountains, an elongate range that straddles the Arizona/New Mexico state boundary. The scarps record evidence of multiple faulting events during or before the middle Pleistocene and at least one event in the late Pleistocene (Vincent and Krider, 1997).
946	Horseshoe Fault Zone	94	180	Independent (1.0)	21	6.4 (0.2) 6.7 (0.6) 7.0 (0.2)	35 NE (0.2) 50 NE (0.6) 65 NE (0.2)	N	< 15 ka	1.0	0.01 (0.3) 0.04 (0.6) 0.1 (0.1)	Nearly perpendicular normal faults along the western and southern margins of the Horseshoe Basin, an asymmetric graben in the upland region between the Mazatzal Mountains and Humboldt Mountain. Trenches, scarp analyses and mapping indicate latest Pleistocene and Holocene faulting along the entire zone and two or more episodes of faulting since 300 ka. Scarp analyses, soil development, topographic relations, and fault trench results indicate a slip rate of about 0.04 ± 0.03 mm/yr; displacements of about 1.5 to 2 m, and recurrence intervals of approximately 100 kyr (Pearthree, 1998). Piety and Anderson (1991) estimate the paleoearthquakes were magnitude 6.5 to 7. Fault dip is generalized as NE, a combination of E on the northern section and N on southern section. Slip rate is based on < 5 ± 2.5 m of vertical displacement in the past 150 kyr (northern section) and < 2 m of vertical displacement in the past 200 to 300 kyr on the southern section (Pearthree 1998). (~2 to 7.5m/150yr = 0.03 ± 0.02 mm/yr) (2m/200 to 300 kyr = 0.04 ± 0.03 mm/yr).

Table 1. Fault Parameters[1]

FAULT NO.[2]	FAULT NAME	DISTANCE TO PINAL SCHIST AND GILA CONGLOMERATE SITES (km)	DISTANCE TO SAN MANUEL SITE (km)	RUPTURE MODEL	MAXIMUM RUPTURE LENGTH[3] (km)	MAXIMUM MAGNITUDE[4] (M)	FAULT DIP[5] (degrees)	FAULT TYPE[6]	APPROXIMATE AGE OF YOUNGEST OFFSET	PROBABILITY OF ACTIVITY[7]	SLIP RATE[8] (mm/yr)	COMMENTS
2100 and 2102	Hot Spring and Walnut Springs faults	311	294	Linked (1.0)	44	6.8 (0.2) 7.1 (0.6) 7.4 (0.2)	35 W (0.2) 50 W (0.6) 65 W (0.2)	N	< 1.6 Ma	1.0	0.004 (0.2) 0.02 (0.6) 0.06 (0.2)	These normal faults bound the margin between the Engle Basin to the west and the Caballo block to the east. We linked these faults because they overlap considerably and are kinematically compatible with each other, and show similar geomorphic expression and age of activity. However, little is known about either of them. Although the Hot Spring fault offsets 2 to 3 Ma basalts by as much as 90 m (Machette, 1987), it does not appear to offset Rio Grande terrace deposits older than 150 ka (Foley *et al.*, 1988), suggesting that rates of activity decreased since mid-Quaternary time. Significant (but unquantified) offsets of the Palomas Formation also supports early Pleistocene activity along both faults (Machette *et al.*, 1998). Our maximum rate assumes 90 m of offset occurred since 2 Ma and our preferred rate allows for as much as 2 m of undetected slip since 150 ka, whereas the minimum rate assumes only 2 m of slip occurred since 700 ka.
932	Huachuca fault zone	218	123	Independent (1.0)	25	6.5 (0.2) 6.8 (0.6) 7.1 (0.2)	45 E (0.2) 60 E (0.6) 75 E (0.2)	N	130 to 750 ka	1.0	0.03 (0.2) 0.008 (0.6) 0.003 (0.2)	This north-striking, east-dipping, normal fault zone parallels the Huachuca Mountains, but is 3 to 8 km east of the embayed range front. It is characterized by 2- to 3-m-high scarps on lower and middle Pleistocene fan deposits (Demsey and Pearthree, 1994). Preferred slip rate assumes 3 m of vertical slip occurred since 440 ka; maximum rate assumes 3 m occurred since 130 ka, and minimum rates assume only 2 m occurred since 750 ka.
935	Little Rincon Mountains fault	128	36	Independent (1.0)	17	6.3 (0.2) 6.6 (0.6) 6.9 (0.2)	45 E (0.2) 60 E (0.6) 75 E (0.2)	N	< 1.6 Ma?	0.9	0.009 (0.5) 0.06 (0.5)	Quaternary movement is suspected on two short sections of this fault that defines the western margin of the San Pedro structural trough east of the Rincon Mountains. Fairly sharp 40-m-high scarps on basin deposits of unknown age (Plio-Pleistocene?) suggests Quaternary activity (Pearthree *et al.*, 1988). Our maximum rate assumes 40 m of offset occurred since early Pleistocene (750 ka) whereas our minimum rate assumes 40 m of offset occurred since early Pliocene (~5 Ma).
2013, 2012, and 2011	Mockingbird Hill fault zone and Mogollon fault	170	164	Linked (0.5)	72	7.0 (0.2) 7.3 (0.6) 7.6 (0.2)	45 W (0.2) 60 W (0.6) 75 W (0.2)	N	< 750 ka	1.0	0.02 (0.2) 0.08 (0.6) 0.7 (0.2)	Our characterization for these fault is from Wong *et al.* (2006). These normal faults are assumed to be linked due to their adjacent, nearly continuous, along-strike position, kinematic compatibility along the eastern margin of the Mangas graben, and individual short lengths. Preferred slip rate based on 110 m of offset of Clum Mine pediment gravels, which are believed to be Plio-Pleistocene (assumed ~1.6 Ma).
		199	180	Independent (0.5) Mockingbird Hill-Mogollon faults	22	6.5 (0.2) 6.8 (0.6) 7.1 (0.2)	45 W (0.2) 60 W (0.6) 75 W (0.2)	N	< 1.6 Ma	1.0	0.02 (0.2) 0.08 (0.6) 0.7 (0.2)	
		187	184	Unnamed faults east of Alma	12	6.2 (0.2) 6.5 (0.6) 6.8 (0.2)	55 W (0.2) 70 W (0.6) 85 W (0.2)	N	< 1.6 Ma	1.0	0.003 (0.5) 0.02 (0.5)	These north-striking normal faults along the western flank of the Mogollon Mountains are characterized by lineaments and possible scarps on high level alluvial surfaces formed on the Plio-Pleistocene basin fill of the Gila Conglomerate (Ratte, 1981). Our maximum rate assumes as much as 10 m of offset occurred since 500 ka, whereas our minimum rate assumes 5 m of offset occurred since 1.6 Ma.

Table 1. Fault Parameters[1]

FAULT NO.[2]	FAULT NAME	DISTANCE TO PINAL SCHIST AND GILA CONGLOMERATE SITES (km)	DISTANCE TO SAN MANUEL SITE (km)	RUPTURE MODEL	MAXIMUM RUPTURE LENGTH[3] (km)	MAXIMUM MAGNITUDE[4] (M)	FAULT DIP[5] (degrees)	FAULT TYPE[6]	APPROXIMATE AGE OF YOUNGEST OFFSET	PROBABILITY OF ACTIVITY[7]	SLIP RATE[8] (mm/yr)	COMMENTS
979	Mormon Lake	166	261	Independent (1.0)	15	6.3 (0.2) 6.6 (0.6) 6.9 (0.2)	45 W (0.2) 60 W (0.6) 75 W (0.2)	N	< 1.6 Ma	0.5	0.001 (0.2) 0.01 (0.6) 0.2 (0.2)	Over 60 m of displacement on this northwest-trending normal fault zone have produced steep and linear, west-facing escarpment that bounds the east side of topographic low containing Mormon Lake (Menges and Pearthree, 1983). No definitive offset of Quaternary units has been documented.
931	North Swisshelm	215	129	Independent (1.0)	25	6.5 (0.2) 6.8 (0.6) 7.1 (0.2)	35 NE (0.2) 50 NE (0.6) 65 NE (0.2)	N	< 1.6 Ma	1.0	0.001 (0.2) 0.01 (0.6) 0.1 (0.2)	The fault forms a fairly short, but high and and locally steep, northwest-trending scarp formed on late Cenozoic alluvium on the northeast side of the Swisshelm Mountains. Probable Quaternary age, but no evidence of activity since early Pleistocene (Duke, 1979).
	Oak Creek North	194	189	Independent (1.0)	17	6.3 (0.2) 6.6 (0.6) 6.9 (0.2)	35 E (0.2) 50 E (0.6) 65 E (0.2)	N	< 1.6 Ma	1.0	0.0025 (0.2) 0.025 (0.6) 0.25 (0.2)	The fault is a major north- to northeast-striking east-side-down normal fault bounding the west side of Oak Creek Canyon and extending north to the southern flank of the San Francisco Mountains. Unfaulted Pliocene rocks preclude Quaternary activity on southern two-thirds of fault, however, northern portion of fault displaces lower Pleistocene (1.0 – 1.6 Ma) volcanic rocks by about 25 m.
928	Pedregosa	246	160	Independent (1.0)	27	6.5 (0.2) 6.8 (0.6) 7.1 (0.2)	35 E (0.2) 50 E (0.6) 65 E (0.2)	N	< 750 ka	1.0	0.001 (0.2) 0.01 (0.6) 0.1 (0.2)	Fault forms discontinuous north to northeast-trending 5- to 15-m-high scarps on early to middle Pleistocene fans on the northeast side of the Pedrogosa Mountains, but a younger basalt flow crosses the fault and is not displaced. This implies fault was last active in the early to middle Pleistocene.
982	Phone Booth	197	291	Independent (1.0)	11	6.2 (0.2) 6.5 (0.6) 6.8 (0.2)	35 NE (0.2) 50 NE (0.6) 65 NE (0.2)	N	< 1.6 Ma	1.0	0.0005 (0.2) 0.005 (0.6) 0.05 (0.2)	This zone of faults forms a narrow graben and horst in volcanic rocks of the San Francisco field. Total surface displacement on Miocene and Pliocene volcanic rocks is about 30 m (Pearthree, 1996). The moderately sharp geomorphic expression suggest possible Quaternary activity.
126	Pitaycachi fault zone	281	191	Independent (1.0)	102	7.1 (0.2) 7.4 (0.6) 7.7 (0.2)	35 W (0.2) 50 W (0.6) 65 W (0.2)	N	1887	1.0	0.01 (0.25) 0.02 (0.5) 0.1 (0.25)	Rupture of this complex north-striking fault zone along the western edge of the Sierra Madre Occidental Plateau was responsible for the ~**M** 7.5 1887 Sonora, Mexico earthquake, the largest normal-slip crustal event to have occurred historically in the southern Basin and Range (Suter, 2006; 2015), if not the world (Yeats *et al*., 1997). Suter (2015) reports a maximum net slip of 5.2 m, a surface rupture length of 101.8 km, and an average surface offset of 2.60 m. Although this zone includes multiple faults that may behave as independent segments (for example, Otates, Teras and Pitaycahi), for simplicity and because of its great distance to the site, we only characterized it as a single independent fault source, which is supported by the 102 km-long 1887 rupture that included portions of all three main segments (Suter, 2015). Late Cenozoic net slip rate estimates range from 0.03 to 0.08 mm/yr along the fault zone, which appears slightly higher than Quaternary estimates of ~0.02 mm/yr (Suter, 2015), based on offsets of 9 to 13 m of early Pleistocene alluvial surfaces (Bull and Pearthree, 1988; Pearthree *et al*., 1990). Absolute age constraints are lacking so we judged a wider distribution of weights may better account for the large uncertainties.

Table 1. Fault Parameters[1]

FAULT NO.[2]	FAULT NAME	DISTANCE TO PINAL SCHIST AND GILA CONGLOMERATE SITES (km)	DISTANCE TO SAN MANUEL SITE (km)	RUPTURE MODEL	MAXIMUM RUPTURE LENGTH[3] (km)	MAXIMUM MAGNITUDE[4] (M)	FAULT DIP[5] (degrees)	FAULT TYPE[6]	APPROXIMATE AGE OF YOUNGEST OFFSET	PROBABILITY OF ACTIVITY[7]	SLIP RATE[8] (mm/yr)	COMMENTS
949	Prescott Valley grabens	198	283	Independent (1.0)	9	6.1 (0.2) 6.4 (0.6) 6.7 (0.2)	60 W (0.2) 90 (0.4) 60 E (0.4)	N	<750 ka	1.0	0.01 (0.3) 0.06 (0.4) 0.15 (0.3)	Upper Pleistocene deposits may be faulted. Slip rate is based on 4 m displacement in 70-110 kyr, and < 11 m displacement in 110 to 700 kyr (Pearthree, 1998). Crustal dip uncertain but steeper and east dips favored given linear trace geometry and location along the western margin of a basin (Pearthree, 1998).
2087a and 2087b	Red Hills fault	315	189	Linked (1.0)	14	6.3 (0.2) 6.6 (0.6) 6.9 (0.2)	35 W (0.2) 50 W (0.6) 65 W (0.2)	N	< 130 ka	1.0	0.01 (0.2) 0.04 (0.6) 0.2 (0.2)	This normal fault bounds the eastern margin of Palomas Basin and has significant structural relief. It merges with the Caballo fault to the north and abuts the Derry Hills fault to the south. We assumed the northern (2087a) and southern (2087b) sections of Machette *et al.* (1998) were linked due to their individual short lengths, continuous along-strike geometry, and kinematic compatibility. We assumed the Red Hills fault behaves independently from the Caballo fault because the former does not appear to have ruptured 1 or 2 times during the Holocene like the Caballo fault. Prominent scarps were observed on late Pleistocene surfaces (Seager *et al*., 1982) and Machette *et al.* (1998) categorized the slip rate as <0.2 mm/yr based on 3 to 5 m scarps on these surfaces. Our preferred rate assumes 4 m of vertical slip occurred since 130 ka. Our maximum rate assumes 5 m of slip occurred since 30 ka, whereas our minimum rate assumes 3 m of slip occurred since 250 ka.
	Rock House South	186	280	Independent (1.0)	26	6.5 (0.2) 6.8 (0.6) 7.1 (0.2)	35 NE (0.2) 50 NE (0.6) 65 NE (0.2)	N	< 1.6 Ma	1.0	0.001 (0.2) 0.01 (0.6) 0.1 (0.2)	Renamed fault from one of the Leupp faults, a group of northwest-trending normal faults are at the easternmost edge of and beyond the Pliocene-Quaternary San Francisco volcanic field in north-central Arizona. These faults cut Paleozoic and Mesozoic bedrock, locally middle Pleistocene basalt, and Quaternary alluvium.
936a and 936b	Safford fault zone (northern and southern sections)	128	78	Linked (1.0)	31	6.6 (0.2) 6.9 (0.6) 7.2 (0.2)	45 E (0.2) 60 E (0.6) 75 E (0.2)	N	< 15 ka	1.0	0.005 (0.2) 0.015 (0.6) 0.1 (0.2)	This northwest-striking, northeast-dipping normal fault extends along the base of the Pinaleno Mountains and is characterized by fault scarps showing recurrent Quaternary movement (Menges and Pearthree, 1983; Machette *et al.*, 1986). We linked the northern and southern sections because of their individual short lengths, similar scarp morphology and age of youngest movement. Our preferred slip rate is based on 5 to 10 m of vertical displacement on middle and late Quaternary deposits (Machette *et al.*, 1986) assumed to be ~500 ka. Maximum and minimum rate assumed to be similar to the Rimrock fault (2090).
943	Sand Tank	171	193	Independent (1.0)	23	6.5 (0.2) 6.8 (0.6) 7.1 (0.2)	35 NW (0.2) 50 NW (0.6) 65 NW (0.2)	N	< 130 ka	1.0	0.001 (0.2) 0.01 (0.6) 0.03 (0.2)	The fault forms a short (~3 km) , low (<2 m) fault scarp trending north to northwest in Pleistocene alluvium along the western piedmont of the Sand Tank Mountains. The length of this fault source is based on subtle air photo lineaments that extend farther north and southwest with no discernable offset on Pleistocene fan surfaces. Trenching by Demsey and Pearthree (1990) strongly suggest only one surface rupture in the past 70-200 ka and that this late Pleistocene earthquake produced 1.5 to 2 m of vertical displacement.

Table 1. Fault Parameters[1]

FAULT NO.[2]	FAULT NAME	DISTANCE TO PINAL SCHIST AND GILA CONGLOMERATE SITES (km)	DISTANCE TO SAN MANUEL SITE (km)	RUPTURE MODEL	MAXIMUM RUPTURE LENGTH[3] (km)	MAXIMUM MAGNITUDE[4] (M)	FAULT DIP[5] (degrees)	FAULT TYPE[6]	APPROXIMATE AGE OF YOUNGEST OFFSET	PROBABILITY OF ACTIVITY[7]	SLIP RATE[8] (mm/yr)	COMMENTS
934	Santa Rita fault zone	159	70	Independent (1.0)	52	6.8 (0.2) 7.1 (0.6) 7.4 (0.2)	30 W (0.2) 50 W (0.6) 65 W (0.2)	N	< 130 ka	1.0	0.08 (0.2) 0.025 (0.6) 0.008 (0.2)	This fault is characterized by discontinuous late Quaternary scarps that trend north to northeast along the base of the Santa Rita Mountains. A trench near Madera Canyon exposed late Pleistocene alluvium displaced ~2 m and middle Pleistocene alluvium displaced ~3.5 m (Pearthree and Calvo, 1987). This is generally consistent with scarp studies that indicate 3-m-scarps on late Pleistocene alluvial fans and terraces, whereas scarps are as high as 5 m on late-middle Pleistocene alluvium (~200 to 300 ka) (Pearthree and Calvo, 1987). Our preferred slip rate of 0.025 mm/yr is based on 2 to 3 m of late Pleistocene slip, and 3 to 5 m of slip since 200 to 300 ka. Our minimum rate of 0.008 mm/yr assumes only 3 m of slip occurred since ~500 ka and our maximum is about 3 times our preferred rate. This addresses uncertainties in rates given possible temporal clustering, the lack of absolute age constraints, and the limited recurrence information. We assumed shallower dips than typical basin and range normal faults based on interpretation of seismic-reflection data (e.g., Johnson and Loy, 1992). However, we did not assume dips as shallow as 20° as suggested by Johnson and Loy (1992) based on arguments against such shallow dips for earthquake ruptures discussed by Wong *et al.* (1995).
945	Sugarloaf Fault Zone	62	144	Independent (1.0)	8	6.0 (0.2) 6.3 (0.6) 6.6 (0.2)	35 NE (0.2) 50 NE (0.6) 65 NE (0.2)	N	< 130 ka	1.0	0.005 (0.3) 0.02 (0.6) 0.05 (0.1)	Northwest-striking normal fault that forms an asymmetric graben along the western flank of the Mazatzal Mountains. East-facing scarps are low but sharp and as much as 5 m high between granite bedrock and basin-fill deposits. Natural exposures and two trenches revealed late and latest Pleistocene deposits are offset, but middle Pleistocene to Holocene deposits are not faulted. Slip rate is based on < 1 m vertical displacement in the past 50 to 100 kyr Pearthree (1998).
2097	Unnamed faults west of the Pyramid Mountains	217	152	Independent (1.0)	16	6.3 (0.2) 6.6 (0.6) 6.9 (0.2)	35 W (0.2) 50 W (0.6) 35 W (0.2)	N	< 130 ka	0.9	0.009 (0.2) 0.03 (0.6) 0.17 (0.2)	These poorly-studied normal faults bound the western flank of the Pyramid Mountains, and are subparallel to the Animas Valley faults (2093), but have more subdued scarps. Based on this and because these faults may be associated with the Animas Valley faults (Machette *et al.*, 1998), we assumed similar slip rates to the Animas Valley faults, but a slightly lower probability of activity.
948	Verde	150	240	Independent (1.0)	8	6.0 (0.2) 6.3 (0.6) 6.6 (0.2)	60 E (0.3) 75 E (0.4) 90 (0.3)	N	< 130 ka	1.0	0.001 (0.2) 0.02 (0.6) 0.2 (0.2)	The Verde fault zone is the master, steeply northwest-dipping fault on the southwestern margin of the Verde Valley, which is a large, asymmetric, southwest-tilted graben in the Basin and Range province near the margin of the Colorado Plateaus. The fault forms a high, relatively linear, steep, northeast-facing mountain front. Morphologic analysis of alluvial fan scarp profiles suggests an early to middle Holocene time of youngest movement (Pearthree et al., 1983); however, if the steep slope elements of these scarps are due to local erosion, then the youngest faulting may be late Pleistocene (Euge et al., 1992).
1016	Vernon	141	196	Independent (1.0)	59	6.9 (0.2) 7.2 (0.6) 7.5 (0.2)	55 NE (0.2) 70 NE (0.6) 85 NE (0.2)	SS/N	< 750 ka	1.0	0.001 (0.2) 0.01 (0.6) 0.1 (0.2)	This fault zone is a generally northwest-trending, probable sinistral and oblique-slip system of faults that cuts through the middle of the Pliocene-Pleistocene Springerville volcanic field in east-central Arizona. Basalts as young as Pleistocene are deformed by the fault zone.

Table 1. Fault Parameters[1]

FAULT NO.[2]	FAULT NAME	DISTANCE TO PINAL SCHIST AND GILA CONGLOMERATE SITES (km)	DISTANCE TO SAN MANUEL SITE (km)	RUPTURE MODEL	MAXIMUM RUPTURE LENGTH[3] (km)	MAXIMUM MAGNITUDE[4] (M)	FAULT DIP[5] (degrees)	FAULT TYPE[6]	APPROXIMATE AGE OF YOUNGEST OFFSET	PROBABILITY OF ACTIVITY[7]	SLIP RATE[8] (mm/yr)	COMMENTS
2092	Washburn Ranch	236	167	Independent (1.0)	12	6.2 (0.2) 6.5 (0.6) 6.8 (0.2)	35 E (0.2) 50 E (0.6) 65 E (0.2)	N	< 15 ka	1.0	0.001 (0.2) 0.01 (0.6) 0.1 (0.2)	This zone of en echelon faults bound the western margin of the Animas Valley and eastern margin of the Peloncillo Mountains, an elongate range that straddles the Arizona/New Mexico state boundary. The fault has fresh scarps that appear to be Holocene in age on the basis of their morphology.
940	Whitlock Wash Fault	78	7	Independent (1.0)	23	6.5 (0.2) 6.8 (0.6) 7.1 (0.2)	60 W (0.2) 75 W (0.6) 90 (0.2)	N	< 1.6 Ma	0.9	0.001 (0.2) 0.01 (0.6) 0.1 (0.2)	Discontinuous north- to northwesrt-striking, W-down normal faults along the eastern side of San Pedro Valley. Quaternary activity is suspected based on a prominent escarpment and faulting in Pliocene basin-fill deposits. No evidence of Quaternary movement has been found. Mapping on the southern zone revealed lower to middle Quaternary deposits that are not faulted. Probability of activity is assumed to be 0.9, as evidence for Quaternary activity is equivocal (Pearthree, 1998). The slip rate is unknown, but probably < 0.02 mm/yr (Pearthree1998).

[1] Faults within 200 km of the site. Parameters for the more distant southern California faults, including the San Andreas fault system, are shown in Table 2.
[2] Fault numbers, nomenclature, geometry, and ages from U.S. Geological Survey Quaternary Faults and Fold Database of the United States (http://earthquake.usgs.gov/regional/qfaults/) unless noted otherwise.
[3] End to end straight line distance rounded to the nearest km.
[4] Preferred values estimated using the empirical relationships of Wells and Coppersmith (1994), for all fault types, Stirling *et al.* (2002) censored all fault types, and Wesnousky (2008) all fault types based on maximum surface rupture length.
[5] Dips are averages for the seismogenic crust.
[6] (SS) strike slip, (R) reverse, (N) normal,
[7] Probability of activity considers the likelihood that a fault is an independent seismogenic structure capable of generating earthquakes within the modern stress field.
[8] Rates are average net slip rates. Recurrence models used in the analysis were: characteristic (weighted 0.2), maximum magnitude (weighted 0.2), and truncated exponential (weighted 0.2). b-value for faults was mean b-value for SBR seismic source zone.

Table 2a. Southern California and Baja California Fault Source Parameters Included in the Analyses

Fault Name fm2.1 (0.5) [1] fm 2.2 (0.5)	P(a)[2]	Rupture Length (km)	Slip Rate (mm/yr)	SR unc.[3]	Aseismic Slip Factor[4]	Paleoseismic Recurrence Interval (yrs)	Sense of Slip[5]	Downdip Width (km)	Width unc.	Rupture Top (km)	Rupture Bottom (km)	Dip (degrees)	Dip Direction	Preferred Mmax ± 0.3[6]
San Andreas Fault Zone [segmented (0.9)]														
San Andreas-1906 rupture	1.0	473.0	24.0	3.0	0	300	rl-ss	13.0	2	0	13.0	90		7.9
San Andreas Parkfield	1.0	36.4	34.0	5.0	0	24.5	rl-ss	10.2	2	0	10.2	90		6.7
San Andreas-Cholame	1.0	62.5	34.0	5.0	0	155	rl-ss	12.0	2	0	12.0	90		7.0
San Andreas-Carrizo	1.0	59.0	34.0	3.0	0	175	rl-ss	15.1	2	0	15.1	90		7.1
San Andreas-Big Bend	1.0	49.7	34.0	3.0	0	175	rl-ss	15.1	2	0	15.1	90		7.0
San Andreas-Mojave N	1.0	36.9	27.0	7.0	0	155	rl-ss	15.1	2	0	15.1	90		6.8
San Andreas-Mojave S	1.0	97.6	29.0	7.0	0	130	rl-ss	13.1	2	0	13.1	90		7.3
San Andreas-San Bernardino N	1.0	35.3	22.0	6.0	0	175	rl-ss	12.8	2	0	12.8	90		6.8
San Andreas-San Bernardino S	1.0	43.4	16.0	6.0	0	200	rl-ss	12.8	2	0	12.8	90		6.9
San Andreas-San Gorgonio Pass/Garnet Hill	1.0	55.9	10.0	6.0	0	225	rl-ss	19.3	2	0	16.4	58	N	7.0
San Andreas-Coachella	1.0	69.4	20.0	5.0	0	212	rl-ss	11.1	2	0	11.1	90		7.1
Rupture Scenarios (see SoSAF Table 2b)														
San Jacinto - Imperial Fault Zone [segmented (0.9)]														
Imperial	1.0	45.8	20.0	5.0	0	—	rl-ss	14.7	2	0	14.6	82	N	6.9
Superstition Hills	1.0	36.2	4.0	2.0	0	—	rl-ss	12.6	2	0	12.6	90		6.8
Superstition Mountain	1.0	26.3	5.0	3.0	0	395	rl-ss	12.4	2	0	12.4	90		6.6
San Jacinto-Borrego	1.0	34.2	4.0	2.0	0	130	rl-ss	13.1	2	0	13.1	90		6.7
San Jacinto-Coyote Creek	1.0	42.9	4.0	2.0	0	375	rl-ss	15.9	2	0	15.9	90		6.9
San Jacinto-Clark	1.0	46.8	14.0	6.0	0	240	rl-ss	16.8	2	0	16.8	90		7.0
San Jacinto-Anza	1.0	46.1	18.0	6.0	0	240	rl-ss	16.8	2	0	16.8	90		7.0
San Jacinto-Anza stepover	1.0	24.2	9.0	4.0	0	—	rl-ss	16.8	2	0	16.8	90		6.6
San Jacinto-SJV stepover	1.0	24.2	9.0	4.0	0	—	rl-ss	16.8	2	0	16.8	90		6.6
San Jacinto- San Jacinto Valley	1.0	18.5	18.0	6.0	0	—	rl-ss	18.5	2	0	18.5	90		6.5
San Jacinto-San Bernardino	1.0	45.1	6.0	4.0	0	200	rl-ss	16.1	2	0	16.1	90		6.9
Rupture Scenarios (see Table 2c)														
Cerro Prieto[7] (Scenario A-0.6, Scenario B-0.4)	1.0	See Below[8]	20[9]	See below[9]	0.0	—	rl-ss	13.3	2	0	13.3	90		7.1[10] (-0.3, +0.5)

[1] "fm2.1" and "fm2.2" refer to two alternative fault models used in the calculations, weighted equally. Refer to WGCEP (2008) for discussion.

[2] Probability of activity considers the likelihood that a fault is an independent seismogenic structure capable of generating earthquakes within the modern stress field.

[3] Uncertainty in slip rate value. Single number implies slip rates are modeled with slip rate value in "Slip Rate" column ± value in "SR unc.", with weightings of 0.2, 0.6, 0.2.

[4] Aseismic slip factor (ASF) is used to account for some fraction of aseismic slip due to fault creep by decreasing the effective coseismic rupture area (multiply fault area by 1-ASF to determine effective rupture area). A totally locked fault will have an ASF of 0 and a fully creeping fault will have an ASF of 1.0.

[5] (ss) strike slip, (r) reverse, (n) normal, (rl) rt. lateral, (ll) left lateral, (o) oblique

[6] Mmax obtained either from historical data or calculated from empirical magnitude-area (M-A) and/or magnitude-length (M-L) relationships. For strike-slip faults we used the average of Wells and Coppersmith (1994) M-L and Hanks and Bakun (2002) M-A relationships; for others, we used the average of Wells and Coppersmith (1994) M-L and M-A relationships.

[7] Added to UCERF2 model for this study. Cerro Prieto has been added to UCERF3. Two scenarios included for the northern endpoint: Scenario A (weighted 0.6) at Cerro Prieto Volcano, in Mexico; Scenario B (weighted 0.4) ≈45 km northwest of Cerro Prieto Volcano, in U.S. (after Magistrale, 2002).

[8] Characteristic rupture (see footnote 11) allowed to float over entire fault length (138 km for Scenario A and 183 km for Scenario B).

[9] Slip rate distribution used for the Cerro Prieto fault: 0.15 mm/yr (weighted 0.25), 0.20 mm/yr (weighted 0.35), 0.35 mm/yr (weighted 0.25), and 0.40 mm/yr (weighted 0.15). No fault-specific slip rate data are available for the Cerro Prieto fault. However, it may be the principal plate-bounding structure at this latitude, with slip from the Imperial fault being transferred to the Cerro Prieto fault (T. Rockwell, citied in Table B1 of UCERF3). Therefore, we assumed a broad range of slip rates similar to that in UCERF3 for the Imperial fault, 15 to 40 mm/yr, and slightly preferred 20 mm/yr based on the limited paleoseismic data available for the Imperial fault (5 m of slip over a recurrence interval of 250 yrs; Thomas and Rockwell, 1996).

[10] Preferred magnitude based on estimated size of the 1915 and 1934 earthquakes (Biehler *et al*., 1964), although little is documented about the extent of previous ruptures. Upper bound magnitude is slightly larger, allowing for more uncertainty and the entire fault to rupture.

Table 2b. Maximum Magnitudes and Rupture Rates for the Southern San Andreas Fault*

	Rupture Name (segments involved)	Area (km^2)	Ells-B Mag	H&B Mag	A-Priori Rate	Ells-B Rate	H&B Rate	Comments
	Weight				**0.5**	**0.25**	**0.25**	
1	PK	78	6.09	5.87	3.46E-02	2.49E-02	5.26E-02	Rupture area is reduced from fault by 0.79 aseismic factor
2	CH	750.2	7.08	6.9	5.00E-05	5.21E-05	5.46E-05	
3	CC	891.2	7.15	7	3.00E-04	1.60E-04	5.74E-05	
4	BB	751	7.08	6.9	3.00E-04	5.68E-04	5.26E-04	
5	NM	556.5	6.95	6.73	2.00E-04	1.05E-04	1.44E-04	
6	SM	1279	7.31	7.21	5.00E-04	6.45E-04	6.78E-04	
7	NSB	451.9	6.86	6.64	7.00E-04	7.12E-04	6.64E-04	
8	SSB	555.5	6.94	6.73	5.00E-05	5.10E-05	5.17E-05	
9	BG	843	7.13	6.97	5.00E-04	1.88E-04	1.35E-05	
10	CO	693.4	7.04	6.86	2.50E-03	6.70E-03	1.21E-02	Rupture area is reduced from fault by 0.1 aseismic factor
11	PK+CH	828.2	7.12	6.96	1.60E-03	4.36E-03	7.01E-03	
12	CH+CC	1641.4	7.42	7.36	3.00E-04	2.39E-04	2.15E-04	
13	CC+BB	1642.2	7.42	7.36	0	5.02E-06	5.07E-06	
14	BB+NM	1307.5	7.32	7.23	0	1.01E-06	1.01E-06	
15	NM+SM	1835.4	7.46	7.42	7.00E-04	4.95E-06	5.04E-06	
16	SM+NSB	1730.9	7.44	7.39	6.00E-04	8.79E-04	8.90E-04	
17	NSB+SSB	1007.4	7.2	7.07	8.00E-04	1.05E-03	1.22E-03	
18	SSB+BG	1398.5	7.35	7.26	9.00E-04	5.03E-06	4.95E-06	
19	BG+CO	1536.4	7.39	7.32	7.00E-04	2.83E-04	4.10E-04	
20	PK+CH+CC	1719.4	7.44	7.38	7.00E-04	4.26E-04	4.19E-04	
21	CH+CC+BB	2392.4	7.58	7.58	0	9.94E-07	9.93E-07	
22	CC+BB+NM	2198.7	7.54	7.53	0	1.00E-06	1.01E-06	
23	BB+NM+SM	2586.4	7.61	7.62	2.50E-04	1.88E-04	2.67E-04	
24	NM+SM+NSB	2287.4	7.56	7.55	1.00E-04	7.24E-05	6.69E-05	
25	SM+NSB+SSB	2286.4	7.56	7.55	4.00E-04	6.05E-04	7.55E-04	
26	NSB+SSB+BG	1850.4	7.47	7.43	4.00E-04	2.22E-04	3.05E-05	
27	SSB+BG+CO	2091.9	7.52	7.5	4.00E-04	2.23E-04	2.48E-04	
28	PK+CH+CC+BB	2470.4	7.59	7.59	4.00E-04	8.20E-04	8.34E-04	
29	CH+CC+BB+NM	2948.8	7.67	7.7	0	9.91E-07	9.99E-07	
30	CC+BB+NM+SM	3477.7	7.74	7.79	4.00E-04	1.95E-04	4.99E-06	
31	BB+NM+SM+NSB	3038.4	7.68	7.71	0	9.95E-07	1.00E-06	
32	NM+SM+NSB+SSB	2842.9	7.65	7.68	2.00E-04	1.04E-04	1.02E-04	
33	SM+NSB+SSB+BG	3129.4	7.7	7.73	3.00E-04	2.92E-04	1.97E-04	
34	NSB+SSB+BG+CO	2543.8	7.61	7.61	4.00E-04	2.23E-04	2.17E-04	
35	PK+CH+CC+BB+NM	3026.9	7.68	7.71	7.00E-04	1.54E-03	1.66E-03	
36	CH+CC+BB+NM+SM	4227.8	7.83	7.9	5.00E-04	4.16E-04	2.67E-04	
37	CC+BB+NM+SM+NSB	3929.6	7.79	7.86	1.00E-04	8.64E-05	5.55E-05	

*** From Table 3, Appendix G, WGCEP (2008)**

Table 2b. Maximum Magnitudes and Rupture Rates for the Southern San Andreas Fault*

	Rupture Name (segments involved)	Area (km^2)	Ells-B Mag	H&B Mag	A-Priori Rate	Ells-B Rate	H&B Rate	Comments
	Weight				**0.5**	**0.25**	**0.25**	
38	BB+NM+SM+NSB+SSB	3593.9	7.76	7.81	5.00E-05	4.92E-05	5.42E-05	
39	NM+SM+NSB+SSB+BG	3685.9	7.77	7.83	1.00E-04	6.19E-05	3.29E-05	
40	SM+NSB+SSB+BG+CO	3822.8	7.78	7.85	4.00E-04	3.58E-04	4.16E-04	
41	PK+CH+CC+BB+NM+SM	4305.9	7.83	7.92	2.00E-03	1.04E-03	6.43E-04	
42	CH+CC+BB+NM+SM+NSB	4679.8	7.87	7.96	0	9.91E-07	9.89E-07	
43	CC+BB+NM+SM+NSB+SSB	4485.1	7.85	7.94	1.00E-04	9.04E-05	6.76E-05	
44	BB+NM+SM+NSB+SSB+BG	4436.9	7.85	7.93	0	1.01E-06	1.01E-06	
45	NM+SM+NSB+SSB+BG+CO	4379.2	7.84	7.93	1.00E-04	6.01E-05	3.90E-05	
46	PK+CH+CC+BB+NM+SM+NSB	4757.8	7.88	7.97	5.00E-04	4.21E-04	3.49E-04	
47	CH+CC+BB+NM+SM+NSB+SSB	5235.3	7.92	8.03	5.00E-05	5.00E-05	5.09E-05	
48	CC+BB+NM+SM+NSB+SSB+BG	5328.1	7.93	8.04	5.00E-05	4.44E-05	3.00E-05	
49	BB+NM+SM+NSB+SSB+BG+CO	5130.2	7.91	8.02	5.00E-05	4.50E-05	4.70E-05	
50	PK+CH+CC+BB+NM+SM+NSB+SSB	5313.3	7.93	8.04	1.00E-04	1.00E-04	1.09E-04	
51	CH+CC+BB+NM+SM+NSB+SSB+BG	6078.2	7.98	8.12	0	9.95E-07	1.01E-06	
52	CC+BB+NM+SM+NSB+SSB+BG+CO	6021.5	7.98	8.11	1.00E-05	9.66E-06	9.24E-06	
53	PK+CH+CC+BB+NM+SM+NSB+SSB+BG	6156.3	7.99	8.12	5.00E-05	4.65E-05	4.09E-05	
54	CH+CC+BB+NM+SM+NSB+SSB+BG+CO	6771.6	8.03	8.18	0	1.01E-06	9.93E-07	
55	PK+CH+CC+BB+NM+SM+NSB+SSB+BG+CO	6849.7	8.04	8.18	1.00E-04	8.29E-05	6.59E-05	
Total					*5.42E-02*	*4.88E-02*	*8.37E-02*	

PK Parkfield
CH Cholame
CC Carrizo
BB Big Bend
NM Mojave North
SM Mojave South
NSB San Bernardino North
SSB San Bernardino South
BG San Gorgonio Pass-Garnet Hill (aka Banning-Garnet Hill)
CO Coachella

*** From Table 3, Appendix G, WGCEP (2008)**

Table 2c. Maximum Magnitudes and Rupture Rates for the San Jacinto Fault*

	Rupture Name (segments involved)	Area (km^2)	Ells-B Mag	H&B Mag	A-Priori Rate	Ells-B Rate	H&B Rate	Comments
	Weight				**0.5**	**0.25**	**0.25**	
1	SBV	725.7	7.06	6.88	2.31E-03	4.39E-04	4.42E-04	
2	SJV (SJV+SJV stepover sections)	686.7	7.04	6.85	2.43E-03	4.50E-04	4.49E-04	
3	A (A+A stepover sections)	1193.9	7.28	7.17	0	8.83E-05	8.82E-05	
4	C	786.1	7.1	6.93	0	8.87E-05	8.98E-05	
5	CC	681.5	7.03	6.85	8.89E-04	4.50E-04	4.48E-04	
6	B	403.6	6.81	6.59	4.82E-03	4.45E-04	4.43E-04	Rupture area is reduced from fault by 0.1 aseismic factor
7	SM	325.8	6.71	6.49	1.09E-03	1.50E-03	4.01E-03	Rupture area is reduced from fault by 0.1 aseismic factor
8	SBV+SJV	1412.4	7.35	7.27	1.32E-03	4.49E-04	4.41E-04	
9	SJV+A	1880.6	7.47	7.44	0	4.41E-04	4.50E-04	
10	A+C	1980.1	7.5	7.47	3.15E-03	1.21E-03	1.16E-03	
11	A+CC	1875.4	7.47	7.43	0	8.82E-05	9.00E-05	
12	CC+B	1085.1	7.24	7.12	8.89E-04	4.50E-04	4.47E-04	
13	B+SM	729.4	7.06	6.89	1.09E-03	4.40E-04	4.43E-04	
14	SBV+SJV+A	2606.4	7.62	7.62	0	4.47E-04	4.48E-04	
15	SJV+A+C	2666.8	7.63	7.64	0	4.48E-04	4.51E-04	
16	SJV+A+CC	2562.2	7.61	7.61	0	8.91E-05	8.93E-05	
17	A+CC+B	2279.1	7.56	7.55	0	9.02E-05	8.95E-05	
18	CC+B+SM	1411	7.35	7.27	8.89E-04	4.48E-04	4.40E-04	
19	SBV+SJV+A+C	3392.5	7.73	7.78	1.05E-03	4.49E-04	4.41E-04	
20	SBV+SJV+A+CC	3287.9	7.72	7.76	0	8.94E-05	9.03E-05	
21	SJV+A+CC+B	2965.8	7.67	7.7	0	8.82E-05	8.89E-05	
22	A+CC+B+SM	2604.9	7.62	7.62	0	8.93E-05	8.96E-05	
23	SBV+SJV+A+CC+B	3691.5	7.77	7.83	0	8.80E-05	8.97E-05	
24	SJV+A+CC+B+SM	3291.6	7.72	7.76	0	8.94E-05	9.03E-05	
25	SBV+SJV+A+CC+B+SM	4017.3	7.8	7.88	0	8.90E-05	8.82E-05	
Total					*1.99E-02*	*9.04E-03*	*1.15E-02*	

SBV San Bernardino Valley
SJV San Jacinto Valley
A Anza
C Clark
CC Coyote Creek
B Borrego Mountain
SM Superstition Mountain
Note: Does not include Imperial or Superstition Hills faults

*** From Table 3, Appendix G, WGCEP (2008)**

Table 3. Completeness Estimates and Number of Earthquakes in Each Magnitude Interval

Magnitude Range (M)	Equivalent Time of Completeness (yr)	Number of Earthquakes
3.0 – 3.5	36	40
> 3.5 – 4.0	57	29
> 4.0 – 4.5	77	14
> 4.5 – 5.0	77	4
> 5.0 – 5.5	137	11
> 5.5	137	1

Table 4. Recurrence Parameters for the SBR Background Zone

Realization	b-value	N (M ≥ 5)	Weight
1	0.68	0.0762	0.125
2	0.64	0.0948	0.125
3	0.75	0.0581	0.125
4	0.78	0.0604	0.125
5	0.70	0.0844	0.125
6	0.84	0.0418	0.125
7	0.76	0.0507	0.125
8	0.73	0.0611	0.125

Table 5
Mean UHS

(a) Pinal Schist and Gila Conglomerate Sites

Period (sec)	Spectral Acceleration (g)			
	1,000-Year Return Period	2,500-Year Return Period	4,750-Year Return Period	10,000-Year Return Period
0.01	0.042	0.076	0.107	0.15
0.03	0.049	0.090	0.13	0.20
0.05	0.062	0.12	0.17	0.26
0.10	0.089	0.17	0.25	0.38
0.15	0.098	0.18	0.27	0.41
0.20	0.095	0.18	0.26	0.39
0.25	0.087	0.16	0.23	0.35
0.30	0.078	0.14	0.20	0.30
0.40	0.064	0.110	0.16	0.23
0.50	0.057	0.092	0.13	0.19
0.75	0.043	0.067	0.090	0.13
1.00	0.032	0.050	0.065	0.090
2.00	0.023	0.033	0.043	0.058
3.00	0.017	0.025	0.032	0.042
4.00	0.012	0.017	0.021	0.027
5.00	0.0094	0.013	0.016	0.020
7.50	0.0069	0.010	0.013	0.016
10.0	0.0053	0.0076	0.010	0.013

(b) Rhyolite and Diabase Sites

Period (sec)	Spectral Acceleration (g)			
	1,000-Year Return Period	2,500-Year Return Period	4,750-Year Return Period	10,000-Year Return Period
0.01	0.032	0.059	0.085	0.12
0.03	0.039	0.074	0.109	0.16
0.05	0.053	0.100	0.15	0.22
0.10	0.072	0.14	0.21	0.31
0.15	0.073	0.14	0.20	0.31
0.20	0.067	0.12	0.18	0.27
0.25	0.058	0.106	0.15	0.23
0.30	0.051	0.091	0.13	0.20
0.40	0.040	0.069	0.099	0.15
0.50	0.034	0.056	0.079	0.11
0.75	0.026	0.040	0.054	0.076
1.00	0.020	0.029	0.039	0.054
2.00	0.015	0.021	0.027	0.036
3.00	0.012	0.017	0.021	0.028
4.00	0.0089	0.013	0.016	0.020
5.00	0.0068	0.010	0.013	0.016
7.50	0.0057	0.0083	0.011	0.013
10.0	0.0046	0.0066	0.0089	0.011

Table 6
Controlling Earthquakes

(a) Pinal Schist and Gila Conglomerate Sites

Distance (km)	PGA				1.0 Sec SA			
	M*[1]	D*[1]	M-bar[2]	D-bar[2]	M*[1]	D*[1]	M-bar[2]	D-bar[2]
1,000-Year Return Period								
All	5.1	25	-	-	7.3	350	-	-
< 200	-	-	5.7	44	-	-	6.0	53
> 200	-	-	7.1	258	-	-	7.4	388
2,500-Year Return Period								
All	5.1	15	-	-	7.3	350	-	-
< 200	-	-	5.7	33	-	-	6.0	40
> 200	-	-	7.1	239	-	-	7.5	395
4,750-Year Return Period								
All	5.1	15	-	-	6.1	15	-	-
< 200	-	-	5.7	27	-	-	6.0	33
> 200	-	-	7.2	231	-	-	7.6	399
10,000-Year Return Period								
All	5.5	15	-	-	6.1	15	-	-
< 200	-	-	5.7	23	-	-	6.1	26
> 200	-	-	7.2	226	-	-	7.7	404

[1] Modal magnitude and distance are based on full hazard results for all magnitudes and distances.
[2] Mean magnitudes and distances are computed for hazard from events at distances less than and greater than 200 km due to the bimodal nature of the hazard. Hazard from events at less than 200 km are from background seismicity and local faults. Hazard from events greater than 200 km are from faults in Southern California and Northern Mexico.

(c) Rhyolite and Diabase Sites

Distance (km)	PGA				1.0 Sec SA			
	M*[1]	D*[1]	M-bar[2]	D-bar[2]	M*[1]	D*[1]	M-bar[2]	D-bar[2]
1,000-Year Return Period								
All	5.1	35	-	-	7.3	350	-	-
< 200	-	-	5.7	52	-	-	6.0	51
> 200	-	-	7.1	264	-	-	7.4	388
2,500-Year Return Period								
All	5.3	25	-	-	7.3	350	-	-
< 200	-	-	5.7	38	-	-	6.0	40
> 200	-	-	7.1	242	-	-	7.5	394
4,750-Year Return Period								
All	5.3	25	-	-	6.1	15	-	-
< 200	-	-	5.7	32	-	-	6.0	33
> 200	-	-	7.2	233	-	-	7.6	399
10,000-Year Return Period								
All	5.3	15	-	-	6.1	15	-	-
< 200	-	-	5.7	26	-	-	6.1	26
> 200	-	-	7.2	227	-	-	7.7	404

[1] Modal magnitude and distance are based on full hazard results for all magnitudes and distances.
[2] Mean magnitudes and distances are computed for hazard from events at distances less than and greater than 200 km due to the bimodal nature of the hazard. Hazard from events at less than 200 km are from background seismicity and local faults. Hazard from events greater than 200 km are from faults in Southern California and Northern Mexico.

Table 7
CMS Conditioned to 10,000-Year Return Period UHS
(a) Pinal Schist and Gila Conglomerate Sites

Period (sec)	T* = 0.2 sec Horizontal	T* = 1.5 sec Horizontal
0.01	0.15	0.12
0.02	0.16	0.13
0.03	0.17	0.14
0.05	0.22	0.17
0.075	0.28	0.21
0.10	0.32	0.23
0.15	0.38	0.27
0.20	0.39	0.28
0.25	0.33	0.27
0.30	0.28	0.24
0.40	0.21	0.20
0.50	0.16	0.17
0.75	0.093	0.13
1.00	0.060	0.090
1.50	0.030	0.058
2.00	0.018	0.037
3.00	0.0083	0.018
4.00	0.0048	0.011
5.00	0.0031	0.0072
7.50	0.0012	0.0029
10.00	0.0006	0.0015

(b) Rhyolite and Diabase Sites

Period (sec)	T* = 0.2 sec	T* = 1.5 sec
	Horizontal	Horizontal
0.01	0.12	0.11
0.02	0.13	0.11
0.03	0.14	0.12
0.05	0.19	0.16
0.075	0.24	0.20
0.10	0.27	0.21
0.15	0.29	0.23
0.20	0.27	0.22
0.25	0.22	0.20
0.30	0.18	0.17
0.40	0.13	0.14
0.50	0.099	0.11
0.75	0.057	0.076
1.00	0.036	0.054
1.50	0.019	0.036
2.00	0.012	0.024
3.00	0.0057	0.012
4.00	0.0034	0.0074
5.00	0.0022	0.0050
7.50	0.0009	0.0020
10.00	0.0005	0.0011

Table 8
Properties of Seed Time Histories

Record Sequence Number	Year	Earthquake Name	Station Name	Mag	ClstD (km)	V_S30 (m/s)	Comp	PGA (g)	PGV (cm/s)	PGD (cm)	AI (m/sec)	5-95% Dur(sec)
238	1980	Mammoth Lakes-03	Long Valley Dam (L Abut)	5.9	18.1	537	090	0.08	5.98	2.37	0.05	12.80
318	1981	Westmorland	Superstition Mtn Camera	5.9	19.4	363	045	0.08	3.92	1.82	0.04	11.13
2622	1999	Chi-Chi, Taiwan-03	TCU071	6.2	16.4	625	E	0.19	13.37	3.67	0.33	8.88
4125	2004	Parkfield-02	Parkfield-Gold Hill 6W	6.0	15.8	232	360	0.10	4.96	2.28	0.08	12.29
4472	2009	L'Aquila, Italy	Celano	6.3	21.4	613	XTE	0.08	4.90	3.12	0.04	6.63
8110	2011	Christchurch, New Zealand	MQZ	6.2	16.1	650	N	0.10	6.41	3.90	0.08	10.00
8126	2011	Christchurch, New Zealand	ROLC	6.2	24.3	296	S61W	0.18	8.39	5.11	0.13	11.84

Mag moment magnitude
ClstD closest distance
Comp component
PGA peak horizontal ground acceleration
PGV peak horizontal ground velocity
PGD peak horizontal ground displacement
AI Arias intensity
Dur duration

Table 9
Properties of Spectrally-Matched Time Histories

(a) Pinal Schist and Gila Conglomerate Sites

Record Sequence Number	Year	Earthquake Name	Station Name	Mag	ClstD (km)	V_S30 (m/s)	Comp	PGA (g)	PGV (cm/s)	PGD (cm)	AI (m/sec)	5-95% Dur(sec)
238	1980	Mammoth Lakes-03	Long Valley Dam (L Abut)	5.9	18.1	537	090	0.16	9.90	4.11	0.22	11.80
318	1981	Westmorland	Superstition Mtn Camera	5.9	19.4	363	045	0.16	10.04	3.83	0.22	11.67
2622	1999	Chi-Chi, Taiwan-03	TCU071	6.2	16.4	625	E	0.16	8.30	3.33	0.19	9.79
4125	2004	Parkfield-02	Parkfield-Gold Hill 6W	6.0	15.8	232	360	0.14	12.25	4.61	0.24	11.62
4472	2009	L'Aquila, Italy	Celano	6.3	21.4	613	XTE	0.15	12.78	6.31	0.16	8.13
8110	2011	Christchurch, New Zealand	MQZ	6.2	16.1	650	N	0.15	14.56	9.90	0.24	10.21
8126	2011	Christchurch, New Zealand	ROLC	6.2	24.3	296	S61W	0.16	6.44	2.27	0.13	10.73

(b) Rhyolite and Diabase Sites

Record Sequence Number	Year	Earthquake Name	Station Name	Mag	ClstD (km)	V_S30 (m/s)	Comp	PGA (g)	PGV (cm/s)	PGD (cm)	AI (m/sec)	5-95% Dur(sec)
238	1980	Mammoth Lakes-03	Long Valley Dam (L Abut)	5.9	18.1	537	090	0.13	7.75	3.49	0.12	13.26
318	1981	Westmorland	Superstition Mtn Camera	5.9	19.4	363	045	0.12	7.15	3.59	0.11	12.19
2622	1999	Chi-Chi, Taiwan-03	TCU071	6.2	16.4	625	E	0.13	7.85	3.04	0.11	10.10
4125	2004	Parkfield-02	Parkfield-Gold Hill 6W	6.0	15.8	232	360	0.10	9.63	3.91	0.17	13.21
4472	2009	L'Aquila, Italy	Celano	6.3	21.4	613	XTE	0.12	7.05	3.45	0.08	8.29
8110	2011	Christchurch, New Zealand	MQZ	6.2	16.1	650	N	0.13	9.59	3.83	0.12	10.41
8126	2011	Christchurch, New Zealand	ROLC	6.2	24.3	296	S61W	0.13	4.98	2.32	0.06	10.97

Mag	moment magnitude
ClstD	closest distance
Comp	component
PGA	peak horizontal ground acceleration
PGV	peak horizontal ground velocity
PGD	peak horizontal ground displacement
AI	Arias intensity
Dur	duration

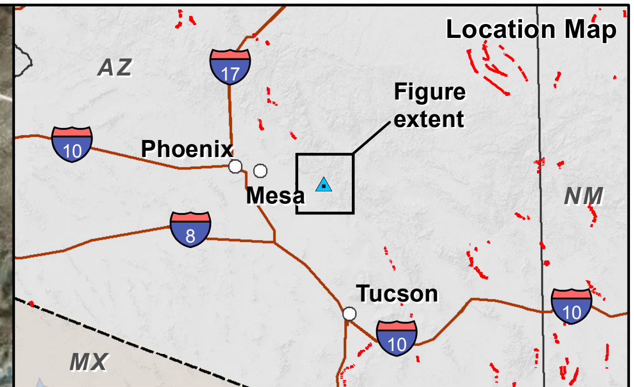

EXPLANATION

Site location

USGS fault; solid where certain, dashed where approximate, dotted where concealed (USGS, 2010)

Source:
Aerial imagery from ESRI

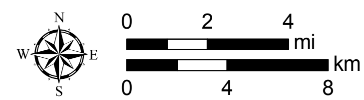

Map projection and scale: NAD 1983 UTM Zone 12N, 1:300,000

Site Location Map

RESOLUTION COPPER, NEAR WEST SITE

LCI Lettis Consultants International, Inc. | Figure 1

File path: S:\12511\Figures\Figure_01.mxd; Date: 08/30/2017; User: ase, LCI; Rev.1

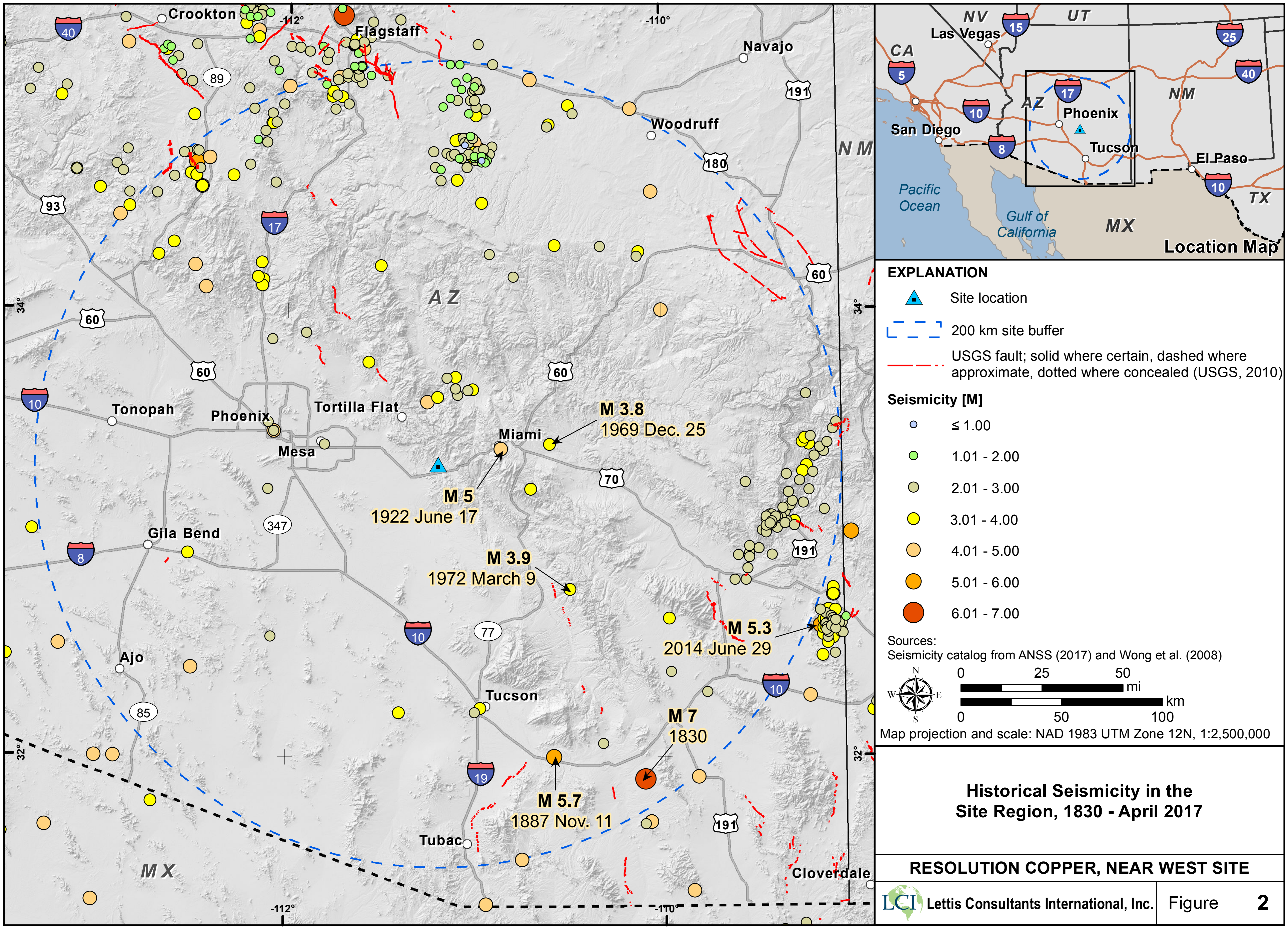

Historical Seismicity in the Site Region, 1830 - April 2017

RESOLUTION COPPER, NEAR WEST SITE

LCI Lettis Consultants International, Inc. | Figure 2

File path: S:\1251\Figures\Figure_02.mxd; Date: 10/04/2017; User: ase, LCI; Rev.1

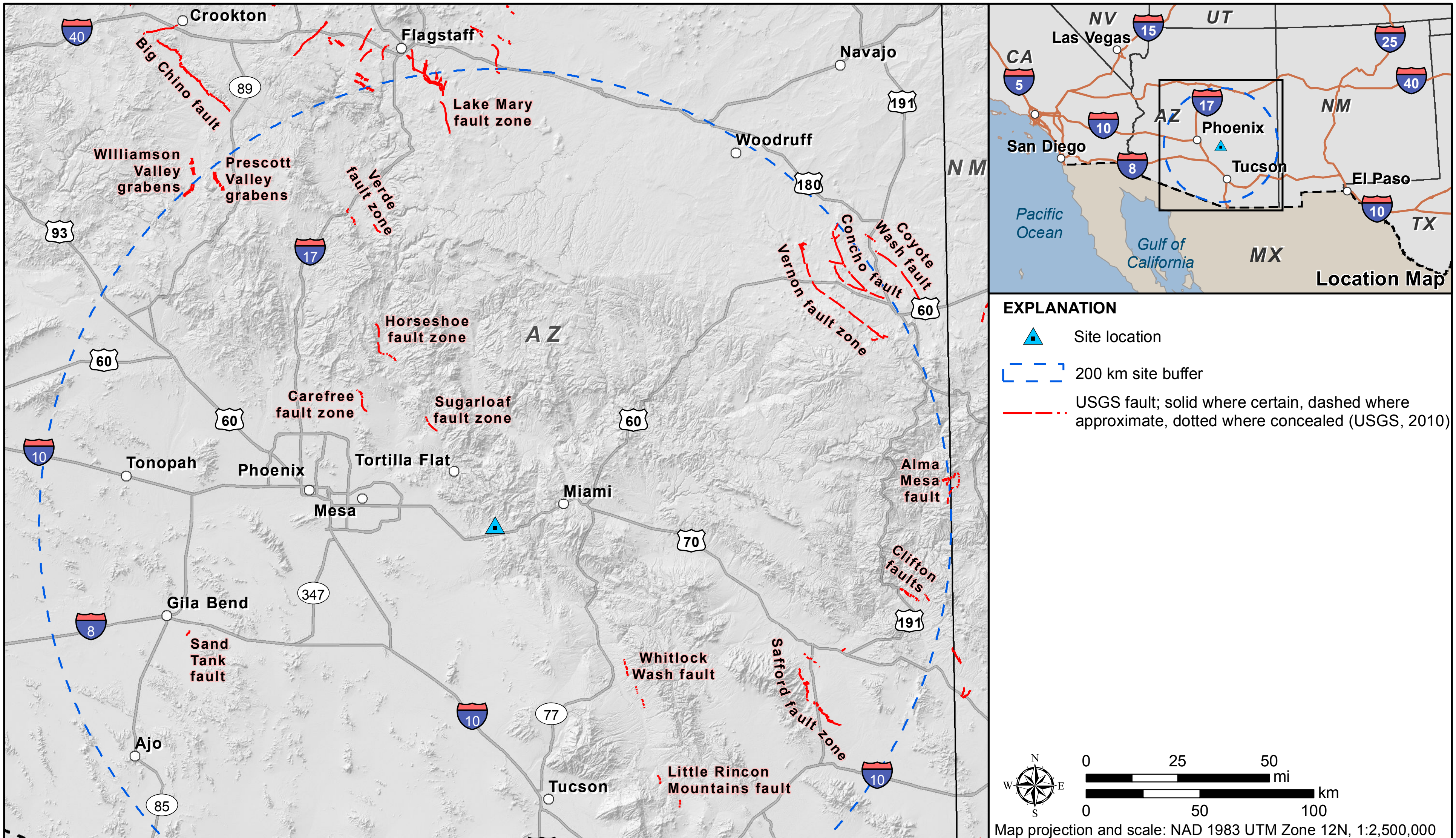

Quaternary Faults in the Site Region

RESOLUTION COPPER, NEAR WEST SITE

Lettis Consultants International, Inc. | Figure 3

File path: S:\1251\Figures\Figure_03.mxd; Date: 08/31/2017; User: ase, LCI; Rev.1

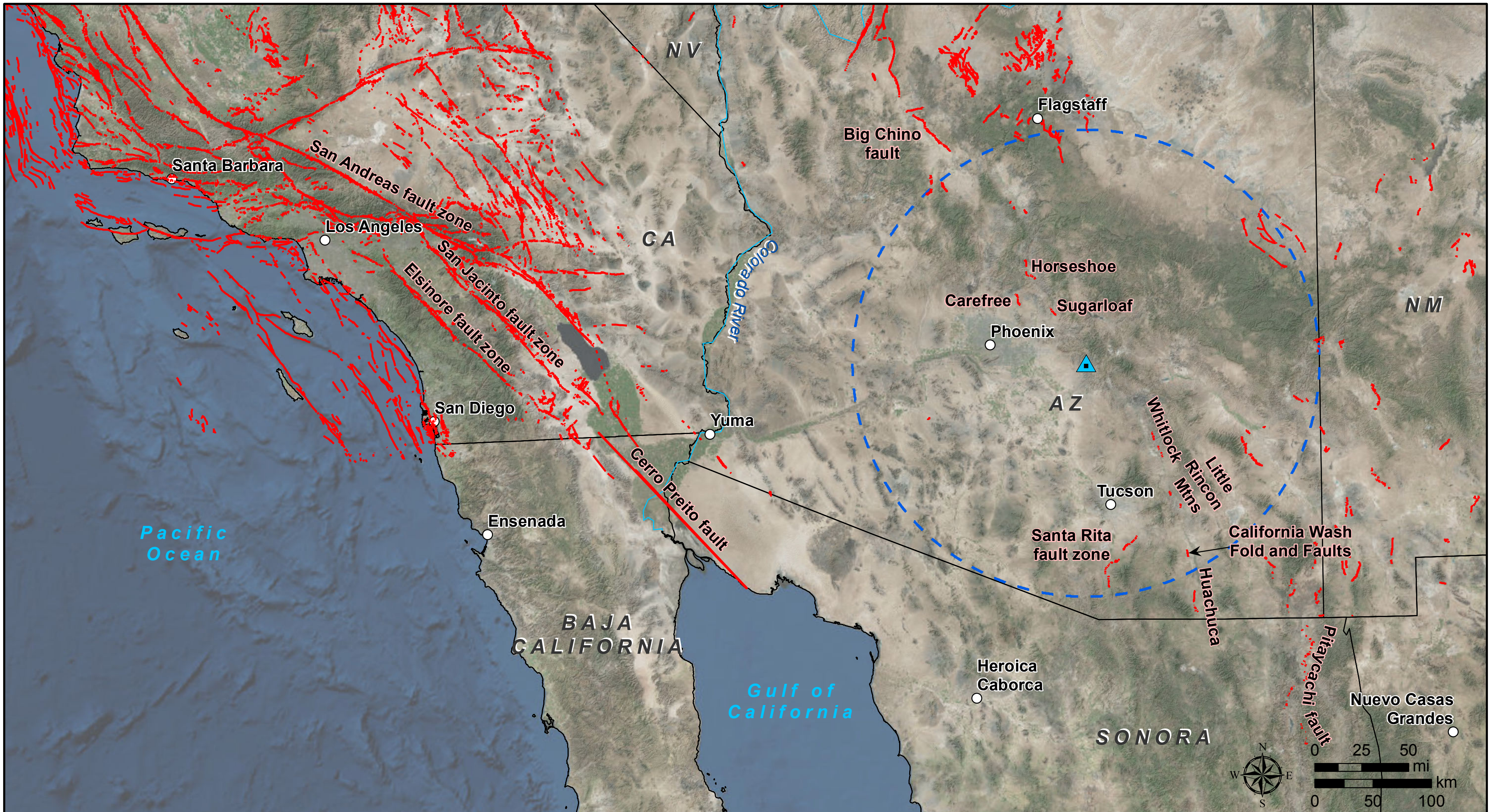

EXPLANATION

Site location

200 km site buffer

USGS fault; solid where certain, dashed where approximate, dotted where concealed (USGS, 2010)

Note:
- USGS fault data does not extend south of the US border

Sources:
- Cerro Prieto trace from UCER3 (Field et al., 2013)
- Aerial imagery from ESRI

Map projection and scale: NAD 1983 UTM Zone 12N, 1:5,000,000

Regional Faults

RESOLUTION COPPER, NEAR WEST SITE

Lettis Consultants International, Inc. | Figure 4

File path: S:\1251\Figures\Figure_04.mxd; Date: 10/20/2017; User: ase, LCI; Rev.1

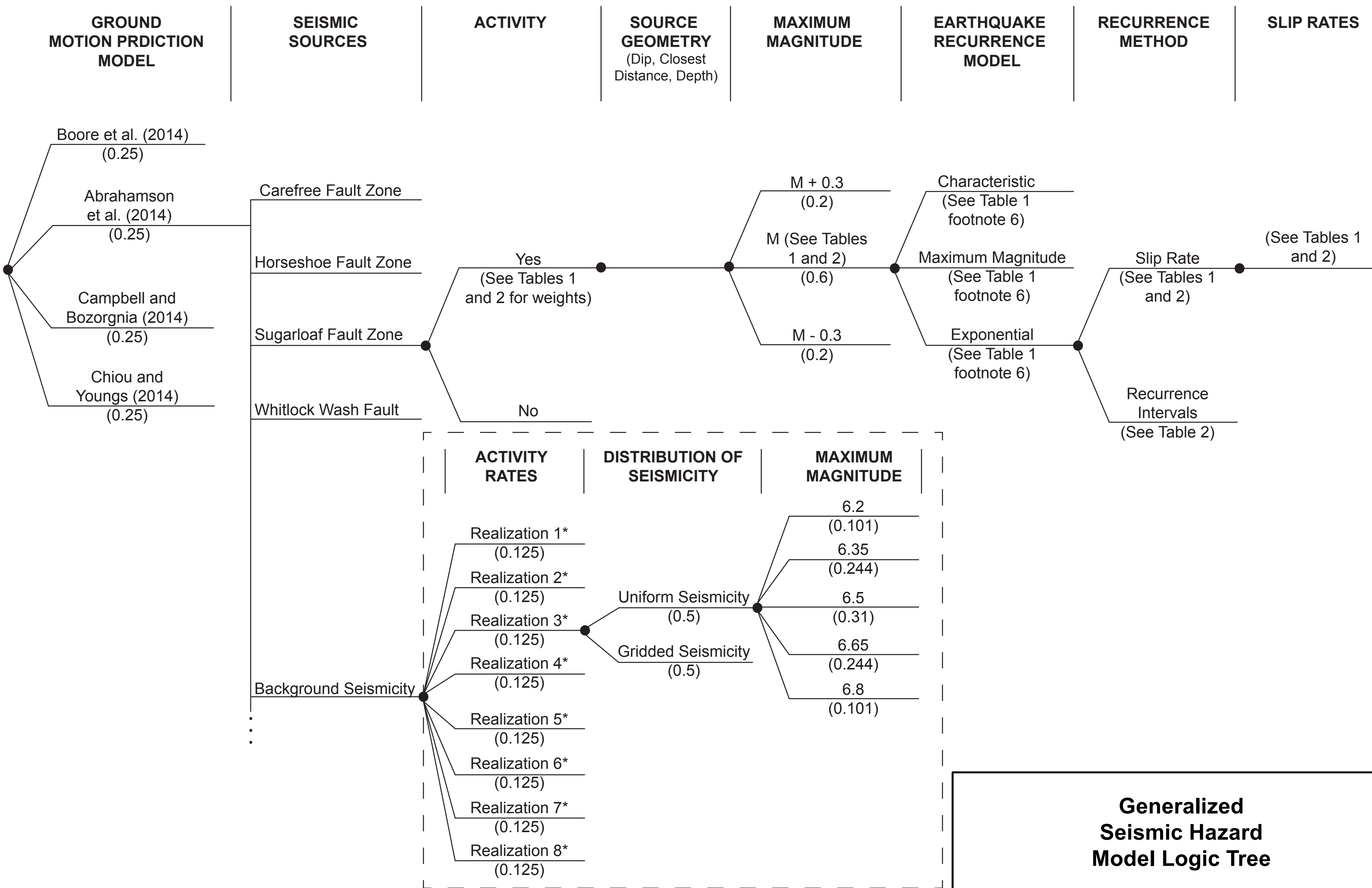

* See Table 4.

Generalized Seismic Hazard Model Logic Tree

RESOLUTION COPPER, NEAR WEST SITE

Lettis Consultants International, Inc.

Figure **5**

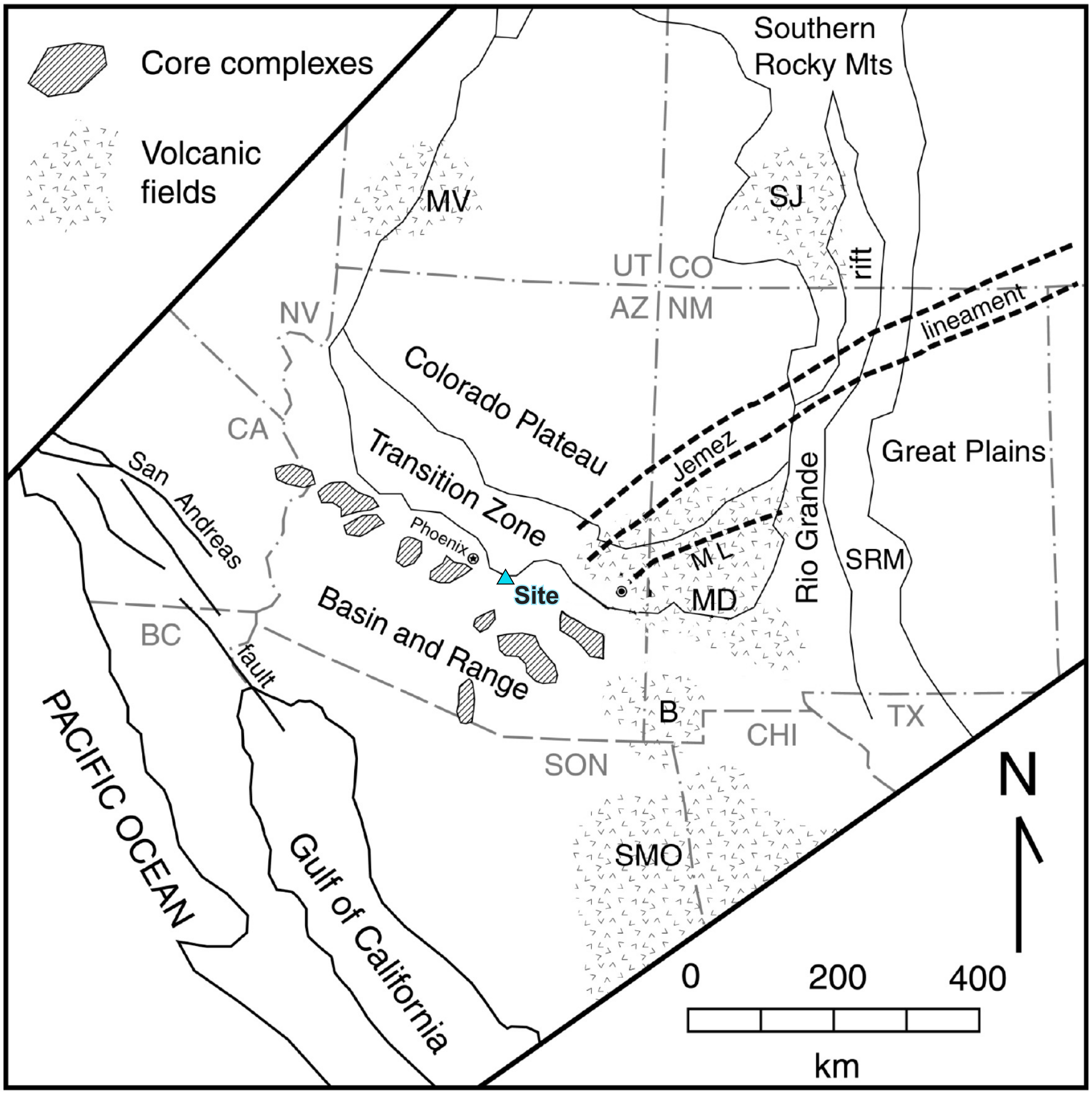

EXPLANATION

▲ Site location

Source: Figure modified from Drewes et al. (1985) and Wong et al. (2013)

Seismotectonic Setting

RESOLUTION COPPER, NEAR WEST SITE

Lettis Consultants International, Inc. | Figure **6**

File path: S:\1251\Figures\Figure_06.ai; Date: 08/31/2017; User: Åse Mitchell, LCI; Rev.1

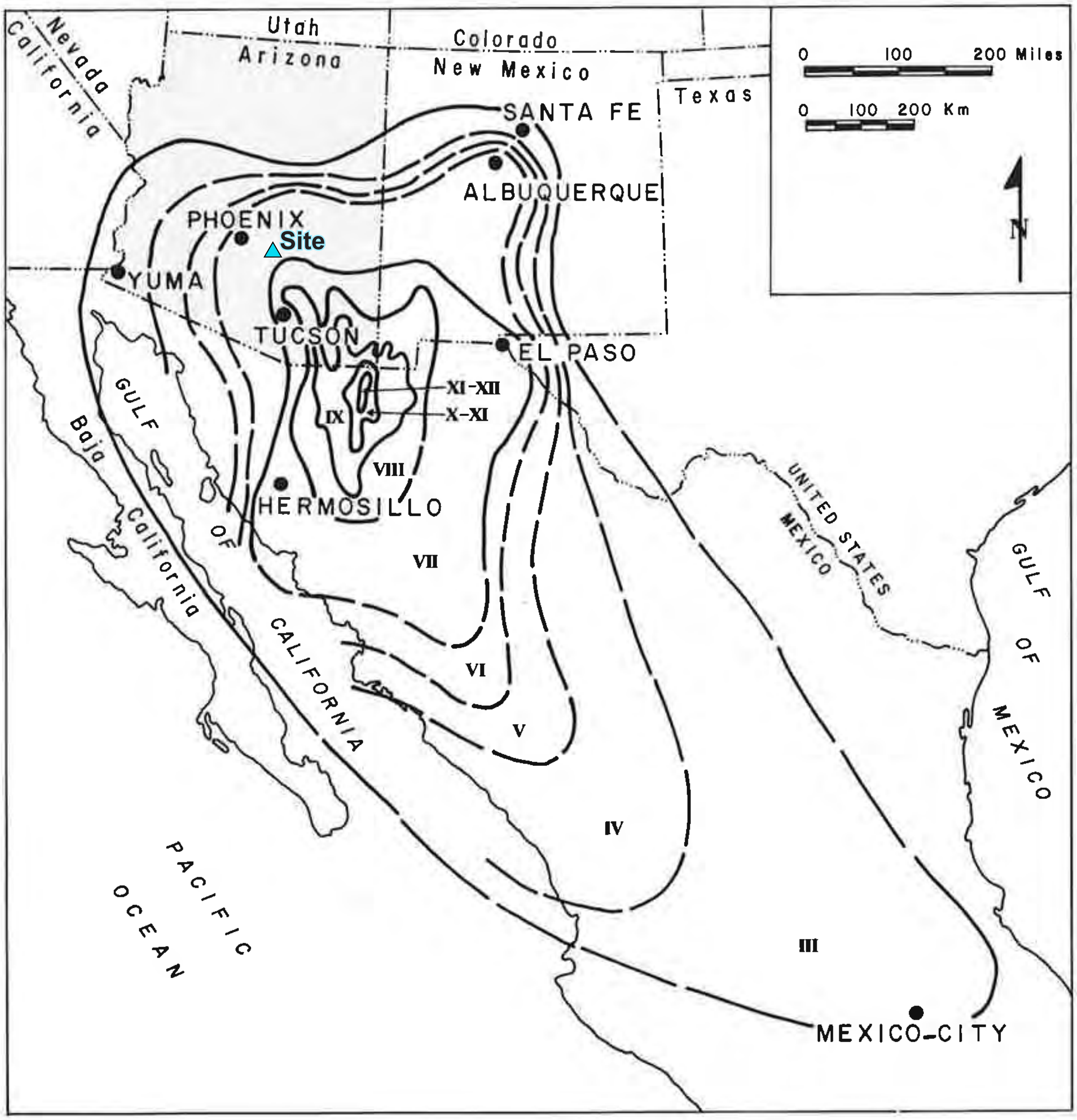

EXPLANATION

△ Site location

Source: Figure modified from DuBois et al. (1982)

Isoseismal Map of 3 May 1887 M 7.4 Sonora, Mexico Earthquake

RESOLUTION COPPER, NEAR WEST SITE

Lettis Consultants International, Inc. | Figure **7**

File path: S:\1251\Figures\Figure_07.ai; Date: 08/31/2017; User: Åse Mitchell, LCI; Rev.1

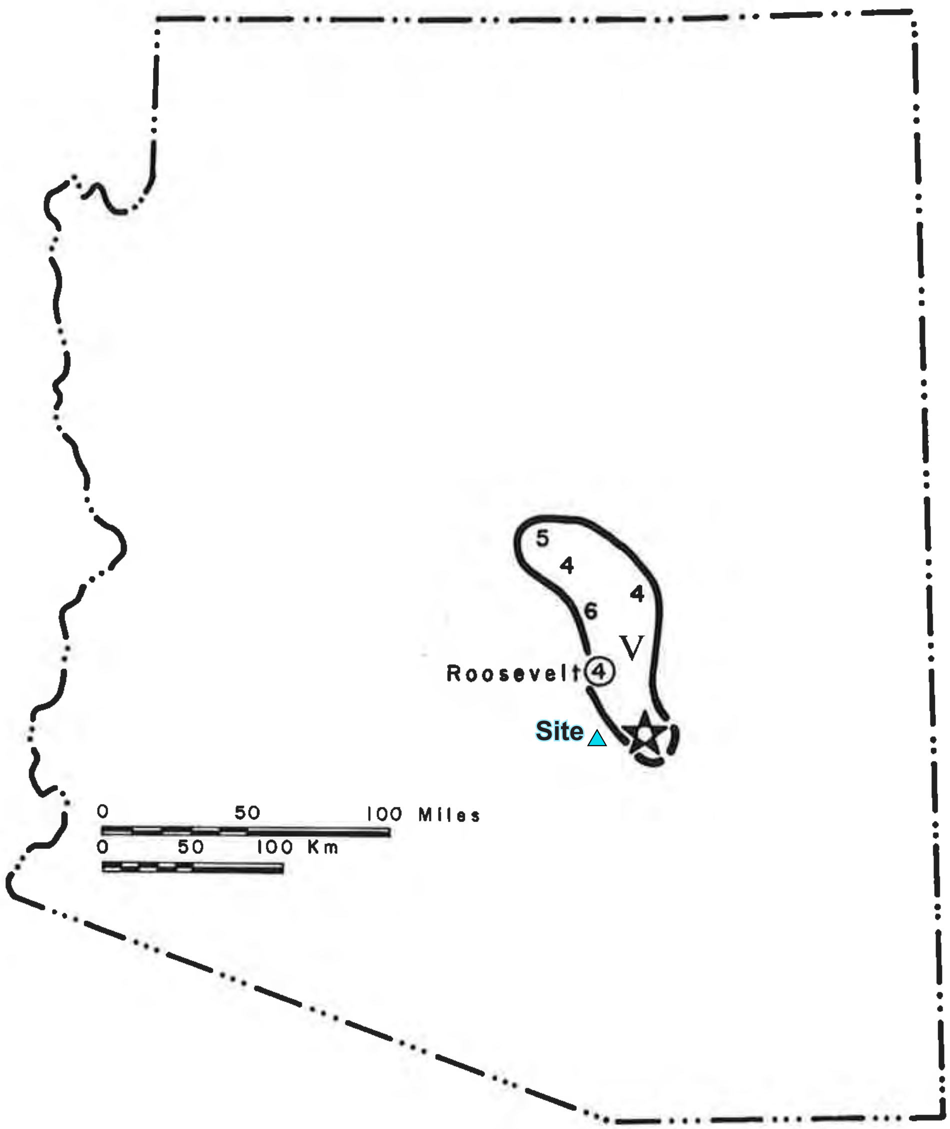

EXPLANATION

△ Site location

Source: Figure modified from DuBois et al. (1982)

File path: S:\1251\Figures\Figure_08.ai; Date: 08/31/2017; User: Åse Mitchell, LCI; Rev.1

Isoseismal Map of the 17 June 1922 Miami, Arizona, Earthquake

RESOLUTION COPPER, NEAR WEST SITE		
Lettis Consultants International, Inc.	Figure	**8**

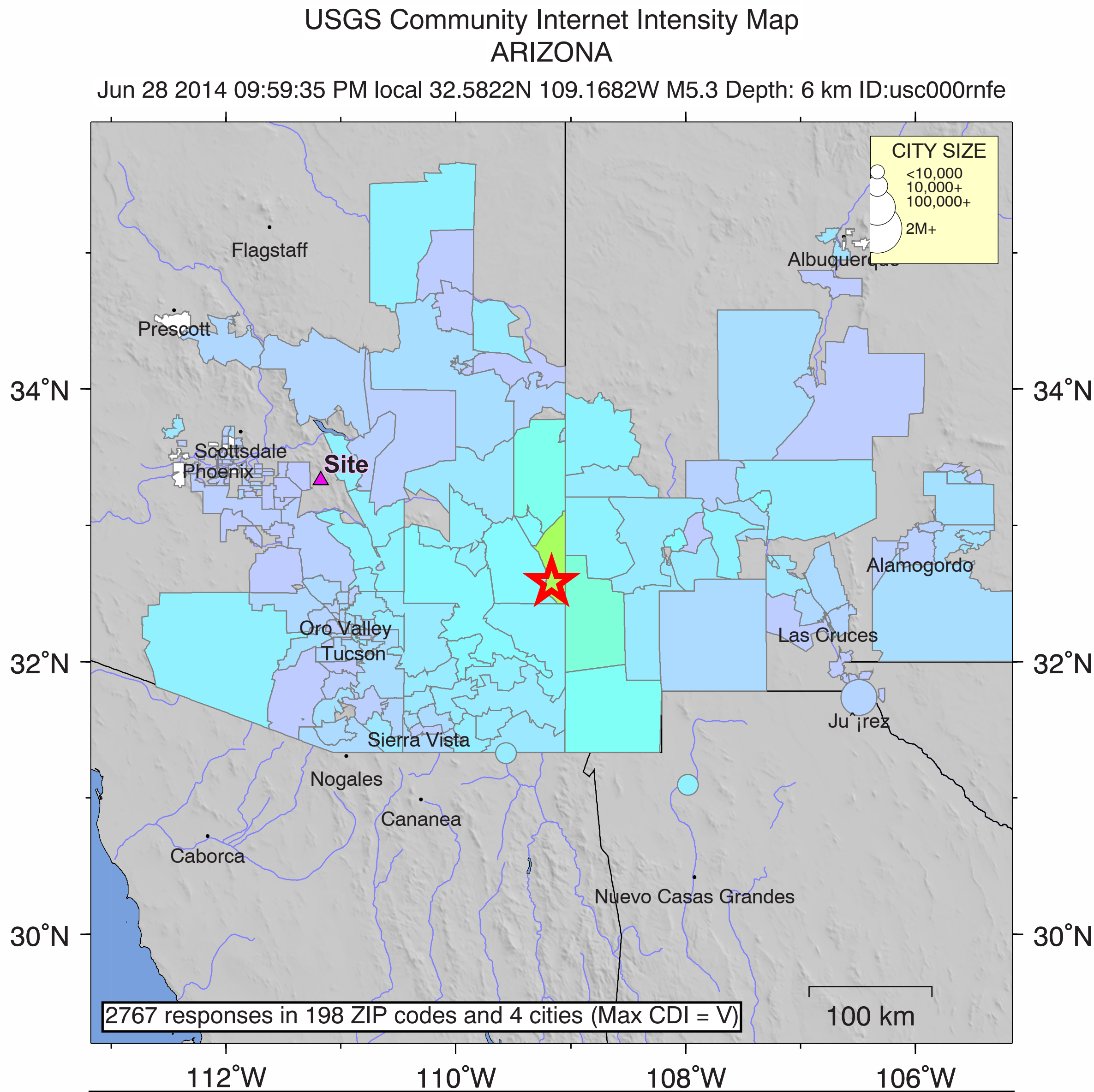

INTENSITY	I	II-III	IV	V	VI	VII	VIII	IX	X+
SHAKING	Not felt	Weak	Light	Moderate	Strong	Very strong	Severe	Violent	Extreme
DAMAGE	none	none	none	Very light	Light	Moderate	Moderate/Heavy	Heavy	V. Heavy

Processed: Fri Jan 22 03:18:23 2016

EXPLANATION

▲ Site location

☆ Earthquake epicenter

Source: Figure modified from USGS (2014)

Did You Feel It Map for the 28 June 2014 M 5.2 Southeastern Arizona Earthquake

RESOLUTION COPPER, NEAR WEST SITE

Lettis Consultants International, Inc. | Figure 9

File path: S:\1251\Figures\Figure_09.ai; Date: 08/31/2017; User: Åse Mitchell, LCI; Rev.1

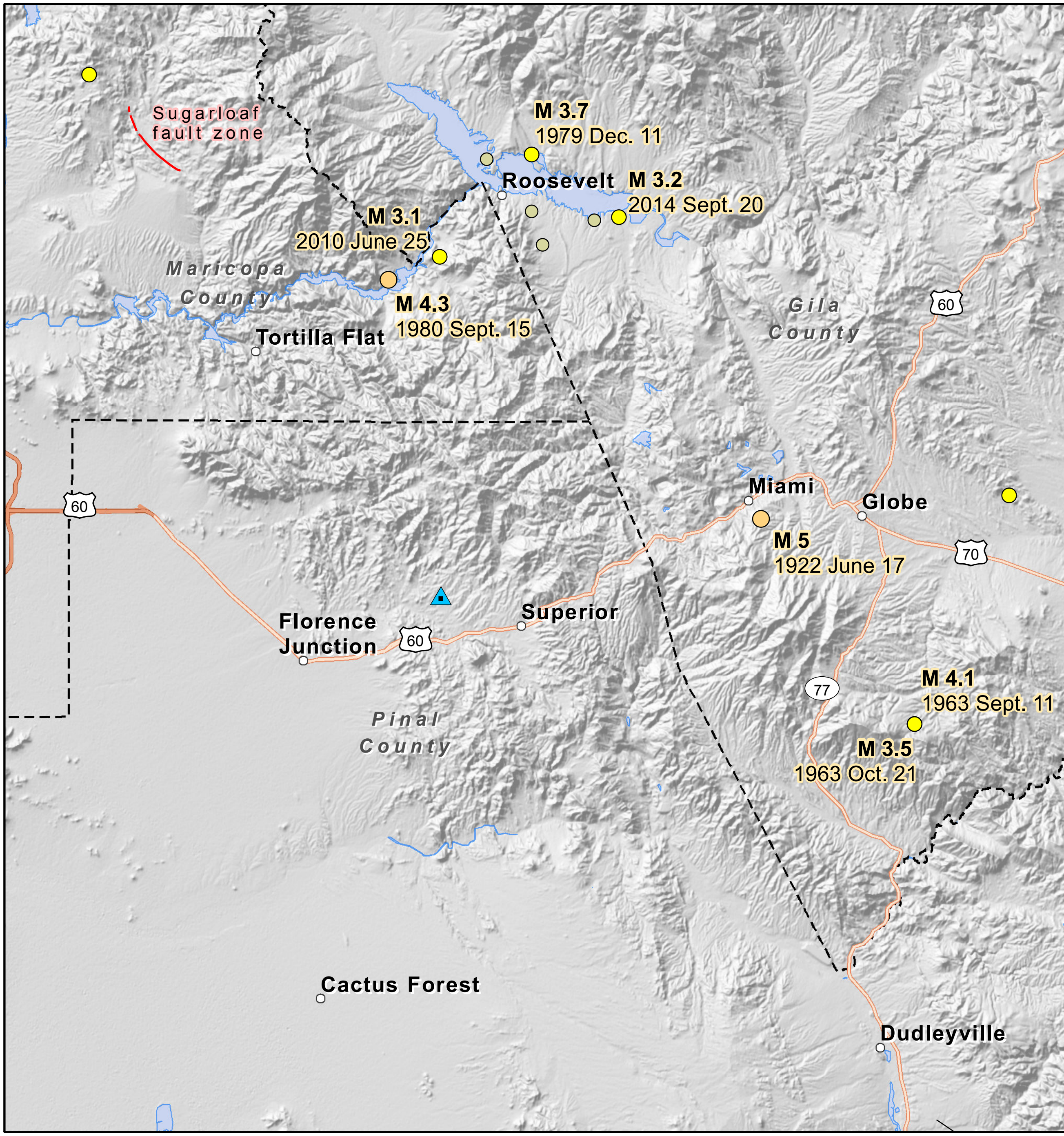

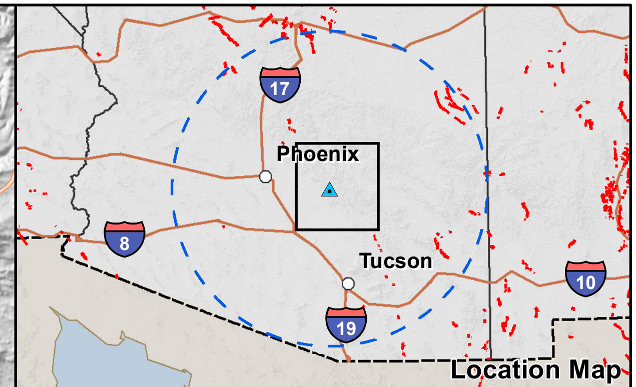

EXPLANATION

Site location

200 km site buffer

USGS fault; solid where certain, dashed where approximate, dotted where concealed (USGS, 2010)

Seismicity [M]

2.01 - 3.00

3.01 - 4.00

4.01 - 5.00

Sources:
Seismicity catalog from ANSS (2017) and Wong et al. (2008)

0 10 20 mi

0 10 20 km

Map projection and scale: NAD 1983 UTM Zone 12N, 1:600,000

Local Historical Earthquakes, 1830 - April 2017

RESOLUTION COPPER, NEAR WEST SITE

Lettis Consultants International, Inc. | Figure **10**

File path: S:\1251\Figures\Figure_10.mxd; Date: 10/19/2017; User: nora, LCI; Rev.1

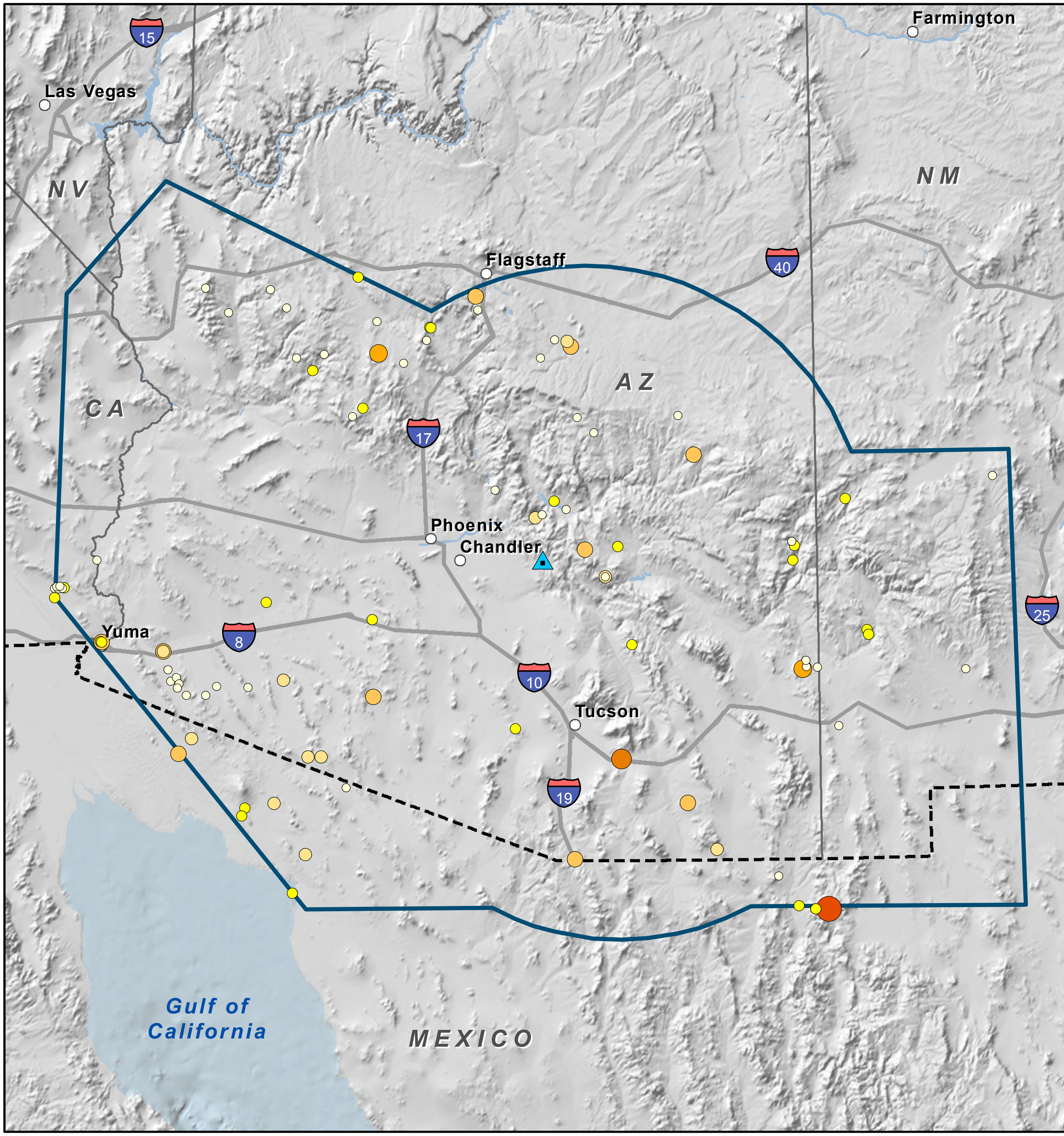

EXPLANATION

Site location

SBR zone

Seismicity [M]

- 3.0 - 3.5
- 3.5 - 4.0
- 4.0 - 4.5
- 4.5 - 5.0
- 5.0 - 5.5
- 5.5 - 6.0
- 6.0 - 6.5
- 6.5 - 7.0

Sources:
Seismicity catalog from ANSS (2017) and Wong et al. (2008)

N S E W

0 25 50 mi

0 50 100 km

Map projection and scale: NAD 1983 UTM Zone 12N, 1:4,500,000

Independent Earthquakes, 1830 - April 2017, in the SBR Seismic Source Zone (M ≥ 3.0)

RESOLUTION COPPER, NEAR WEST SITE

LCI Lettis Consultants International, Inc. | Figure **11**

File path: S:\1251\Figures\Figure_11.mxd; Date: 09/01/2017; User: ase, LCI; Rev.1

EXPLANATION

Magnitude bin:	Completeness:
3.0 - 3.5	3.0 - 3.5
3.5 - 4.0	3.5 - 4.0
4.0 - 4.5	4.0 - 5.0
4.5 - 5.0	≥ 5.0
5.0 - 5.5	
5.5 - 6.0	
6.0 - 6.5	
6.5 - 7.0	

Stepp Plot for the SBR Seismic Source Zone

RESOLUTION COPPER, NEAR WEST SITE

Lettis Consultants International, Inc.

Figure **12**

File path: S:\1251\Figures\Figure_12.ai; Date: 08/31/2017; User: Åse Mitchell, LCI; Rev.1

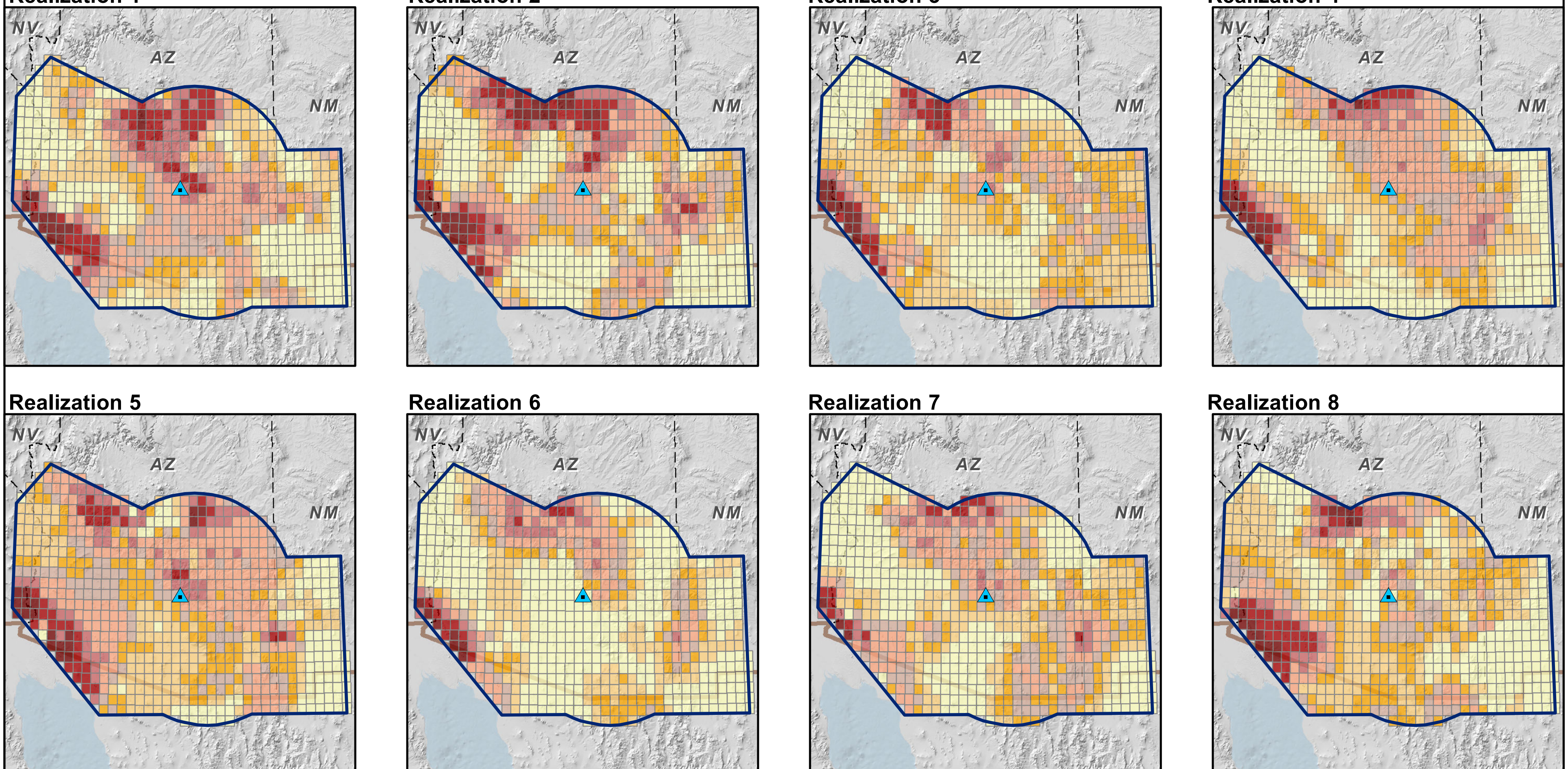

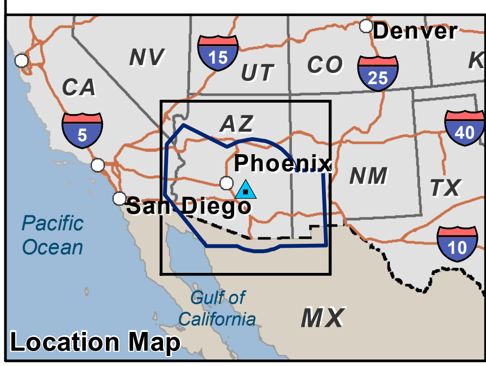

EXPLANATION

Site location

Gridded seismicity data:

SBR zone

Rate

$\leq 2.5\times10^{-5}$	1.01×10^{-4} - 2.0×10^{-4}
2.6×10^{-5} - 5.0×10^{-5}	2.01×10^{-4} - 3.00×10^{-4}
5.10×10^{-5} - 7.50×10^{-5}	3.01×10^{-4} - 5.00×10^{-4}
7.6×10^{-5} - 1.0×10^{-4}	$\geq 5.01\times10^{-4}$

N S E W

0 100 200 mi

0 100 200 km

Map projection and scale: NAD 1983 UTM Zone 12N, 1:13,000,000

Gridded Seismicity for the SBR Seismic Source Zone

RESOLUTION COPPER, NEAR WEST SITE

LCI Lettis Consultants International, Inc.

Figure **13**

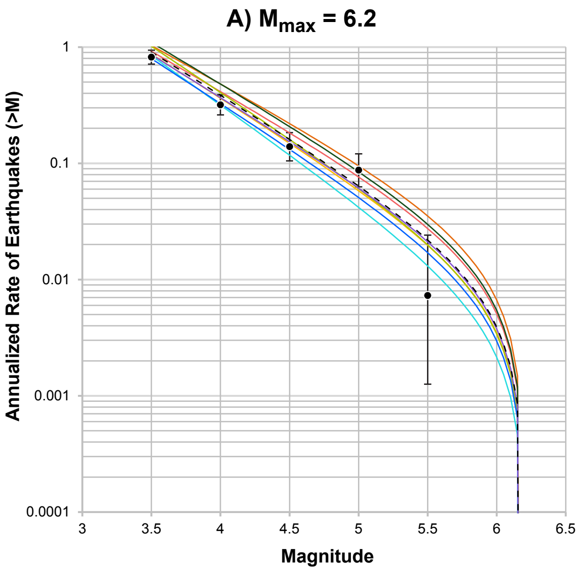

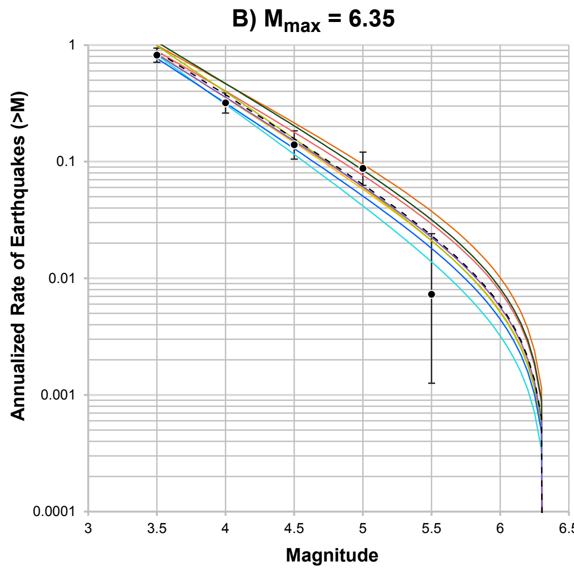

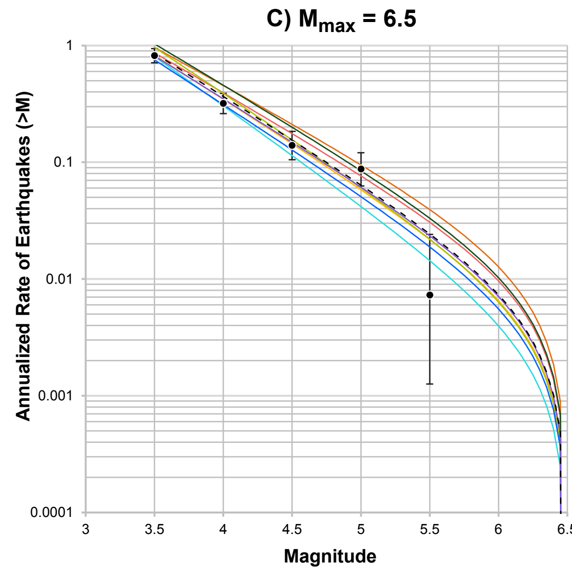

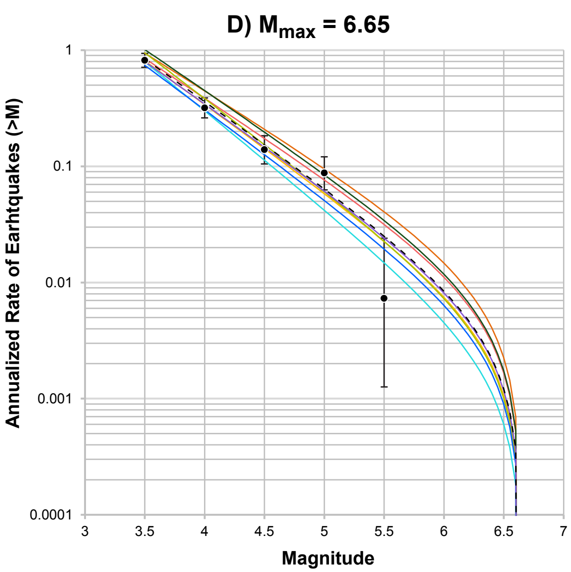

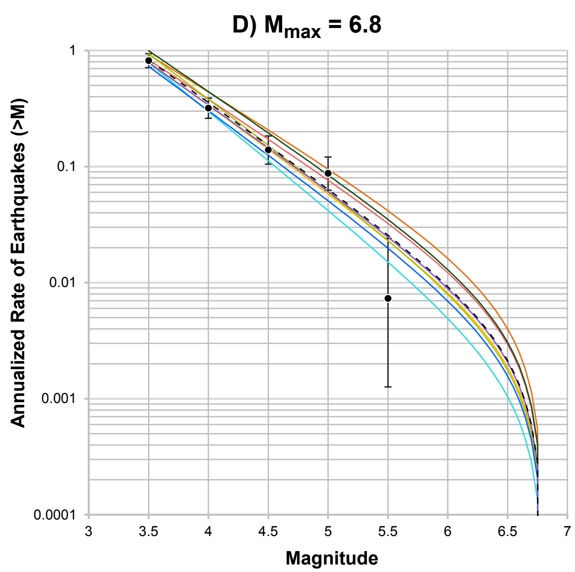

EXPLANATION

Cumulative earthquake rate

Mean result

Realization:

1, 2, 3, 4, 5, 6, 7, 8

Note: Error bars on cumulative earthquake rate represent two standard deviations.

Earthquake Recurrence of the SBR Seismic Source Zone

RESOLUTION COPPER, NEAR WEST SITE

Lettis Consultants International, Inc. | Figure **14**

File path: S:\1251\Figures\Figure_14.ai; 11/16/2017; User: Åse, LCI; Rev.1

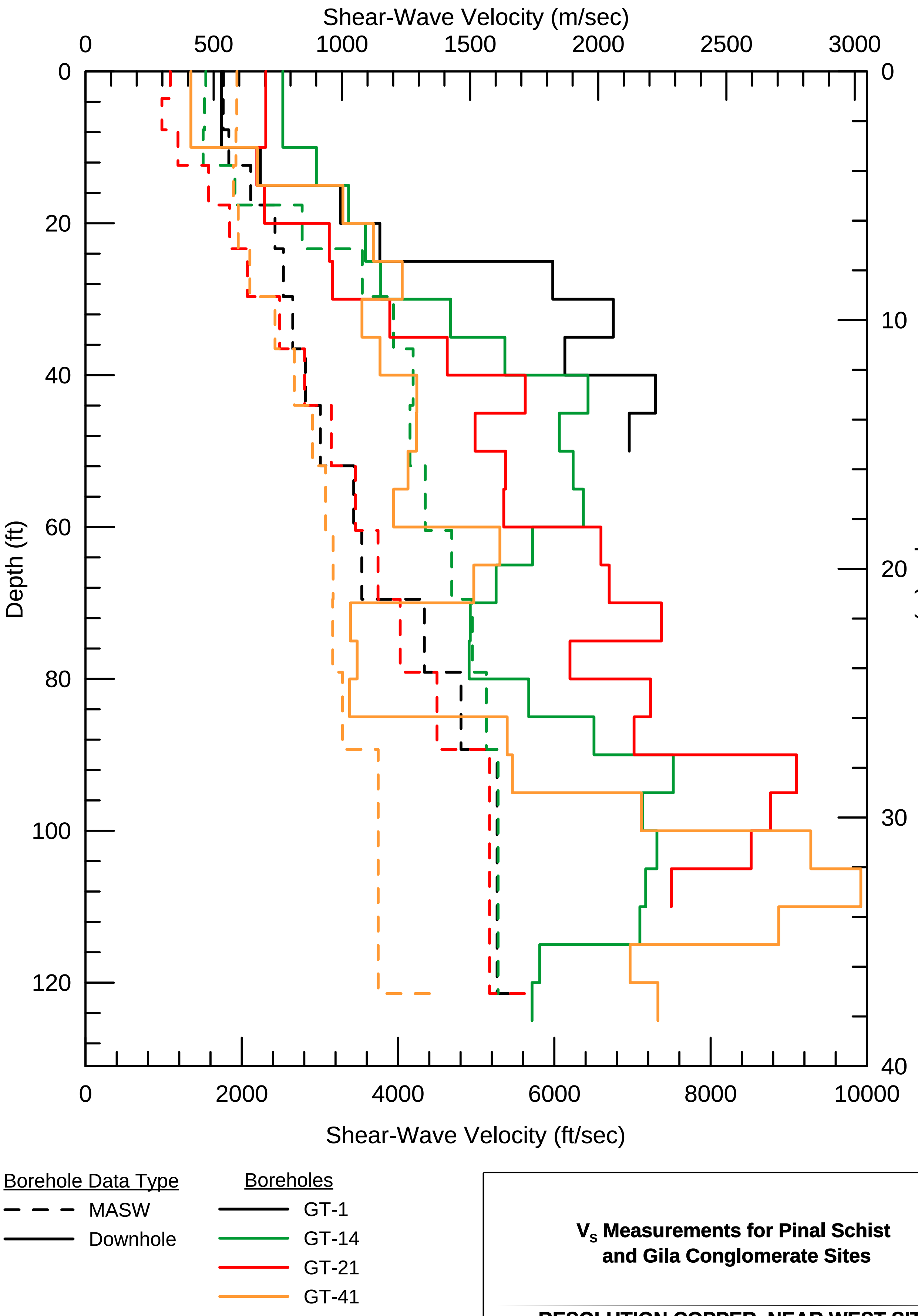

V_s Measurements for Pinal Schist and Gila Conglomerate Sites

RESOLUTION COPPER, NEAR WEST SITE

Lettis Consultants International, Inc.

Figure 15a

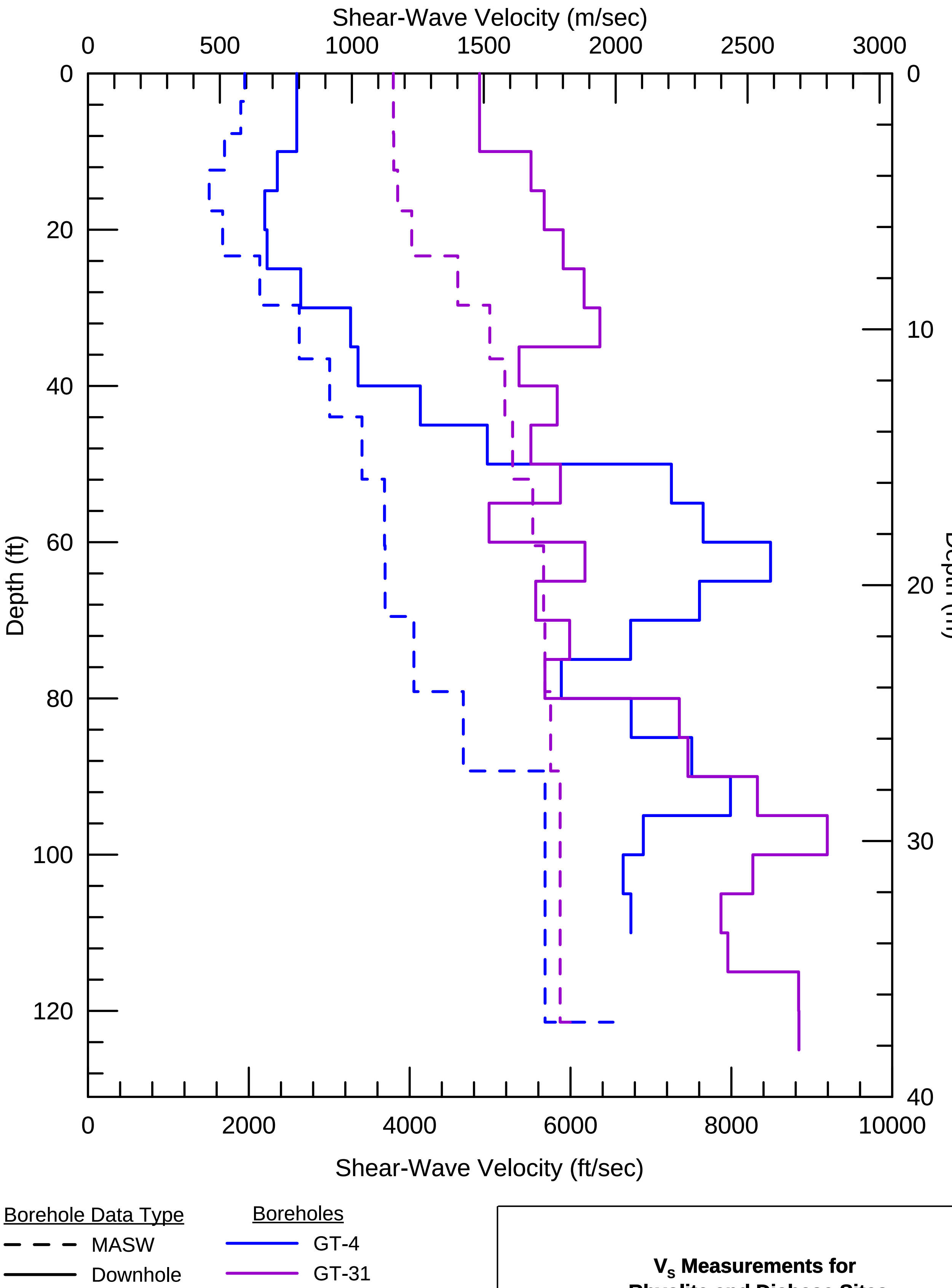

V_S Measurements for Rhyolite and Diabase Sites

RESOLUTION COPPER, NEAR WEST SITE

Lettis Consultants International, Inc.

Figure 15b

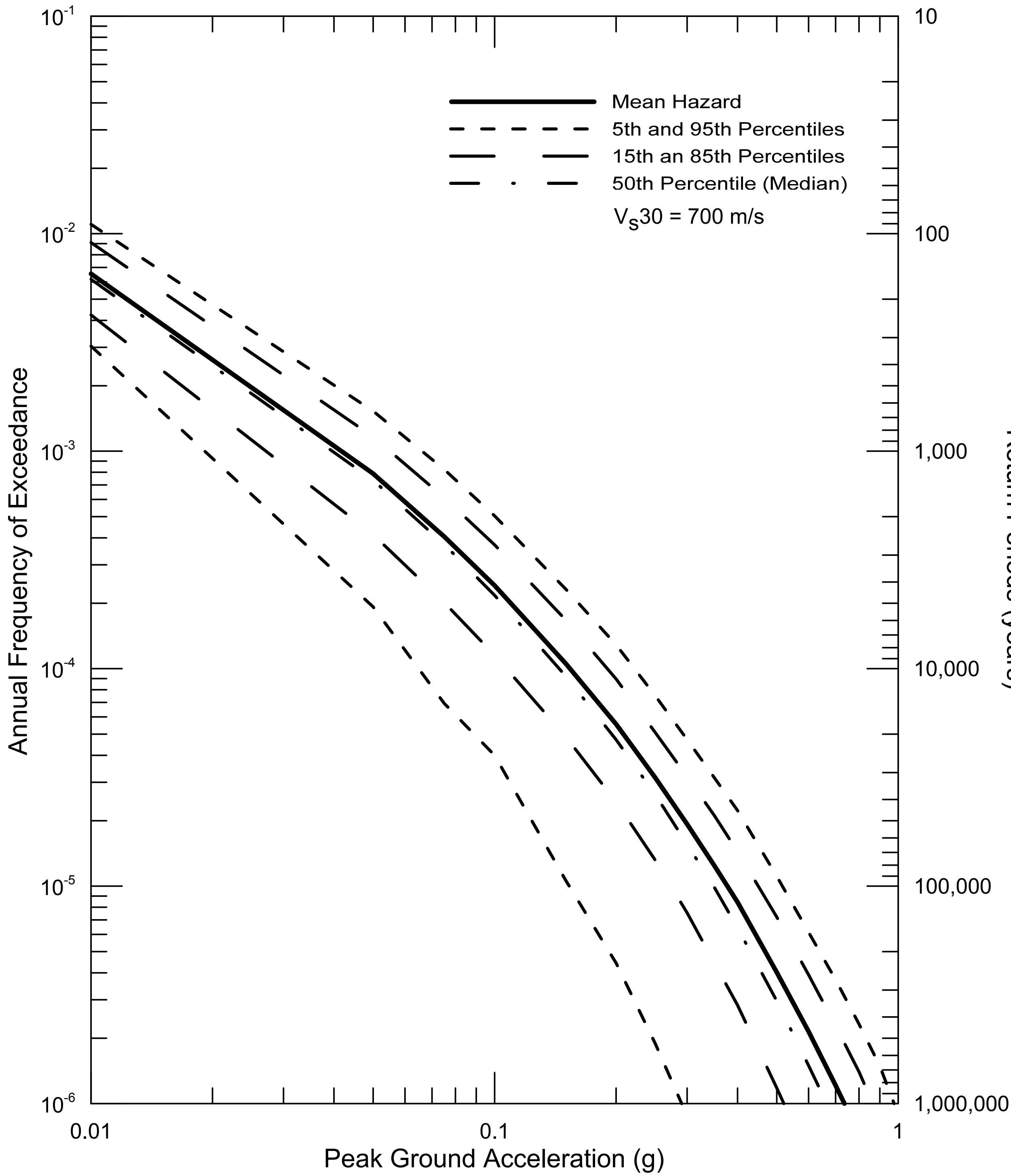

Seismic Hazard Curves
for Peak Horizontal Acceleration
for Pinal Schist and Gila Conglomerate Sites

RESOLUTION COPPER, NEAR WEST SITE

LCI **Lettis Consultants International, Inc.** **Figure 16**

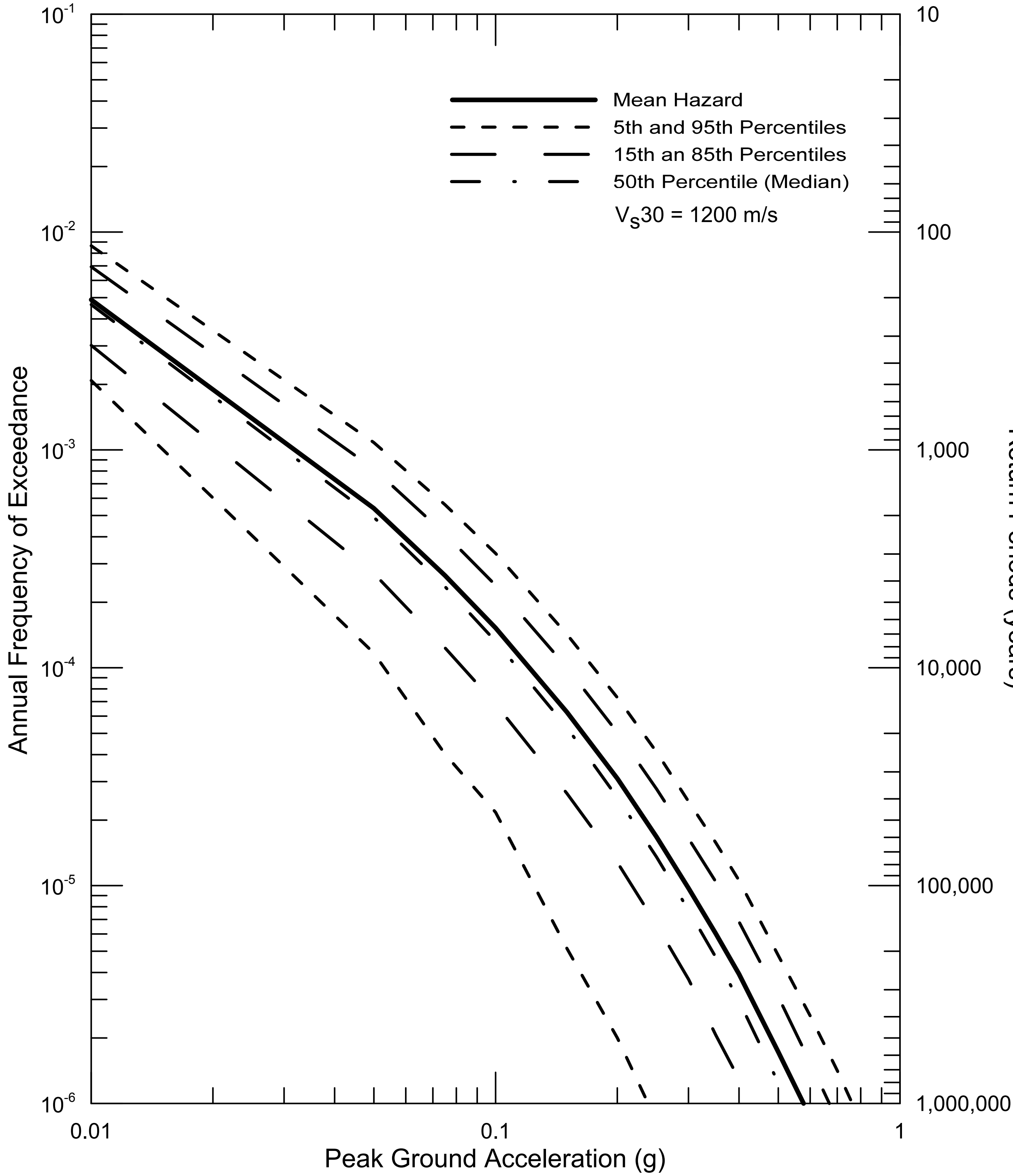

Seismic Hazard Curves for Peak Horizontal Acceleration for Rhyolite and Diabase Sites

RESOLUTION COPPER, NEAR WEST SITE

Lettis Consultants International, Inc.

Figure 17

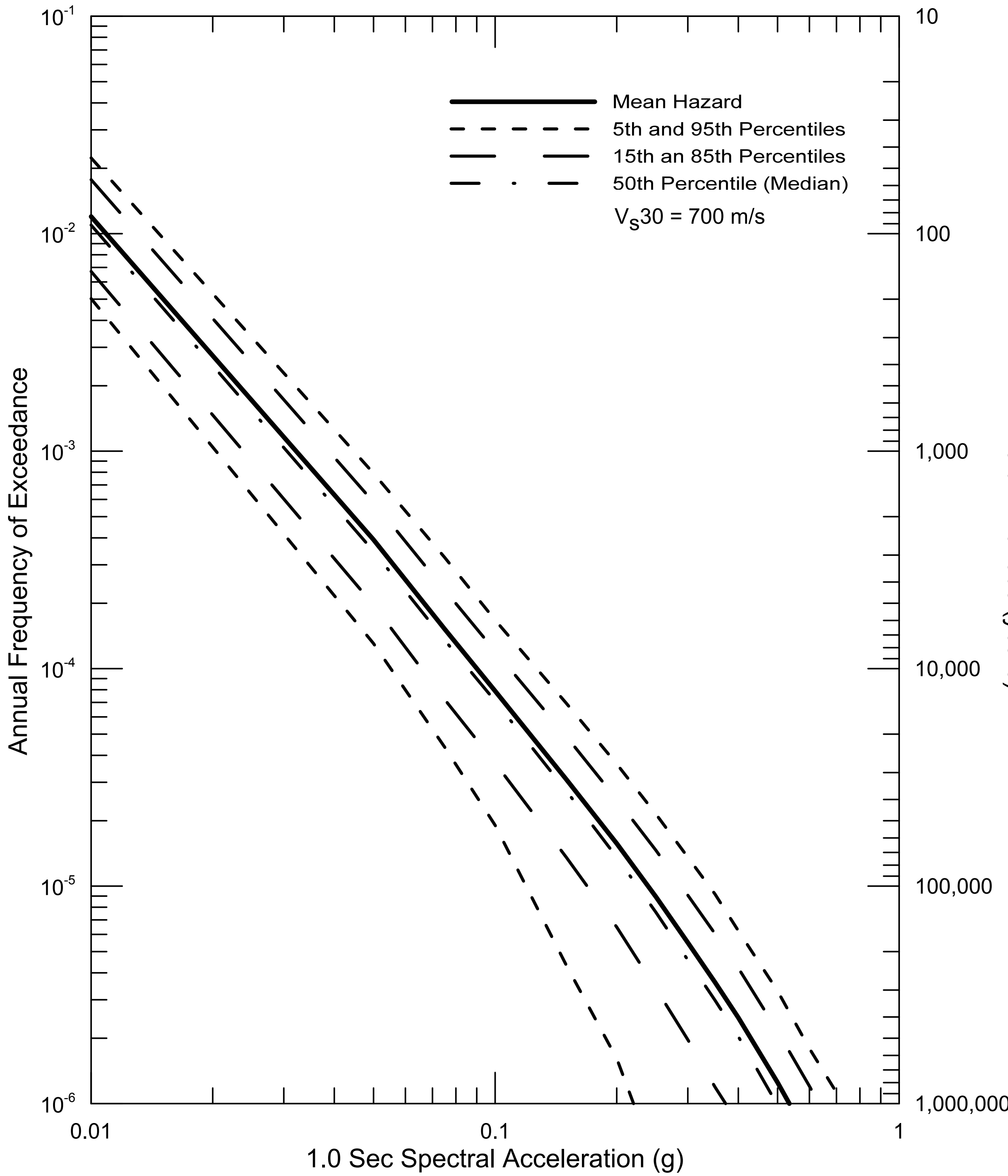

Seismic Hazard Curves
for 1.0 Sec Horizontal Spectral Acceleration
for Pinal Schist and Gila Conglomerate Sites

RESOLUTION COPPER, NEAR WEST SITE

LCI **Lettis Consultants International, Inc.** **Figure 18**

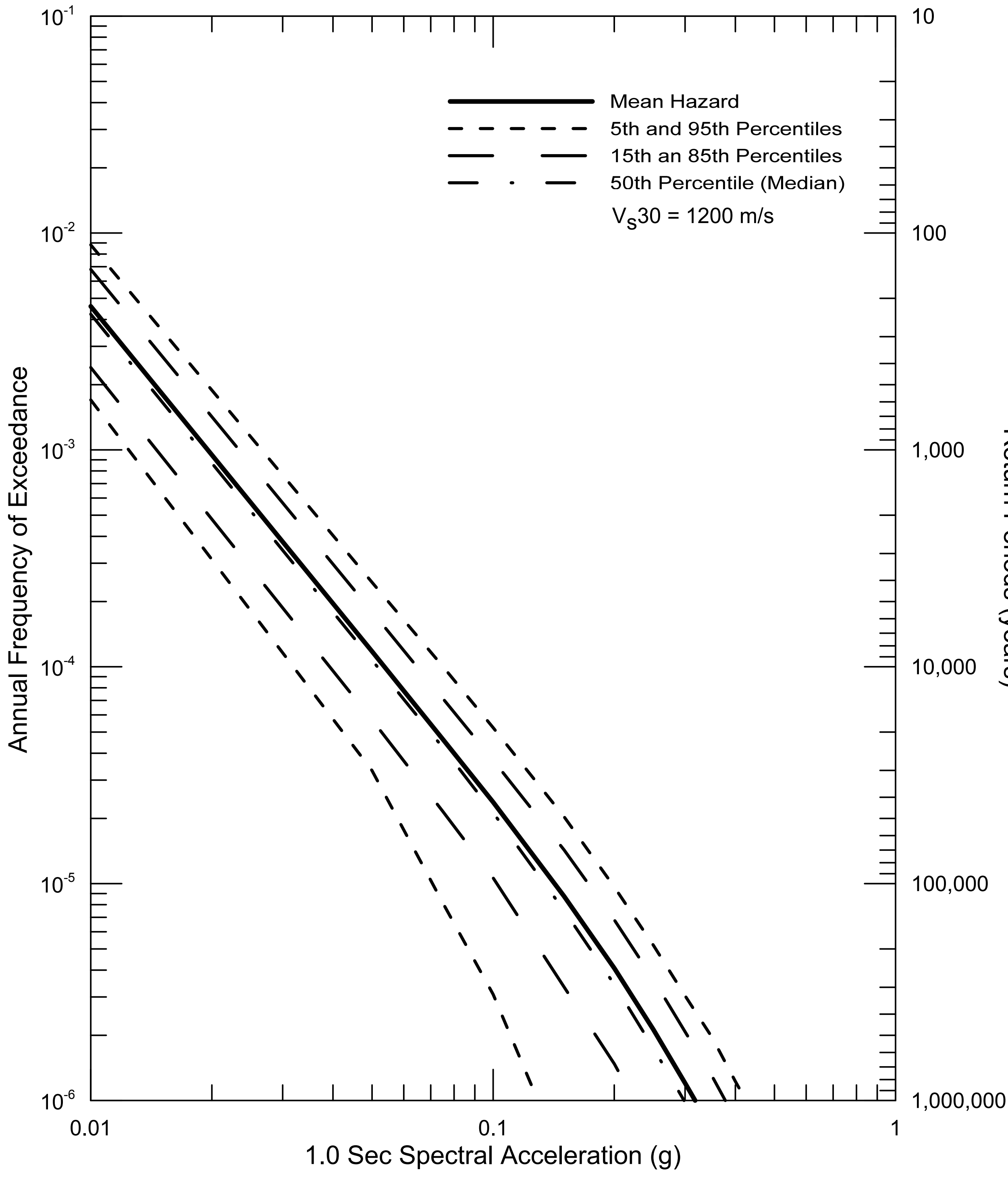

Seismic Hazard Curves
for 1.0 Sec Horizontal Spectral Acceleration
for Rhyolite and Diabase Sites

RESOLUTION COPPER, NEAR WEST SITE

Lettis Consultants International, Inc. | **Figure 19**

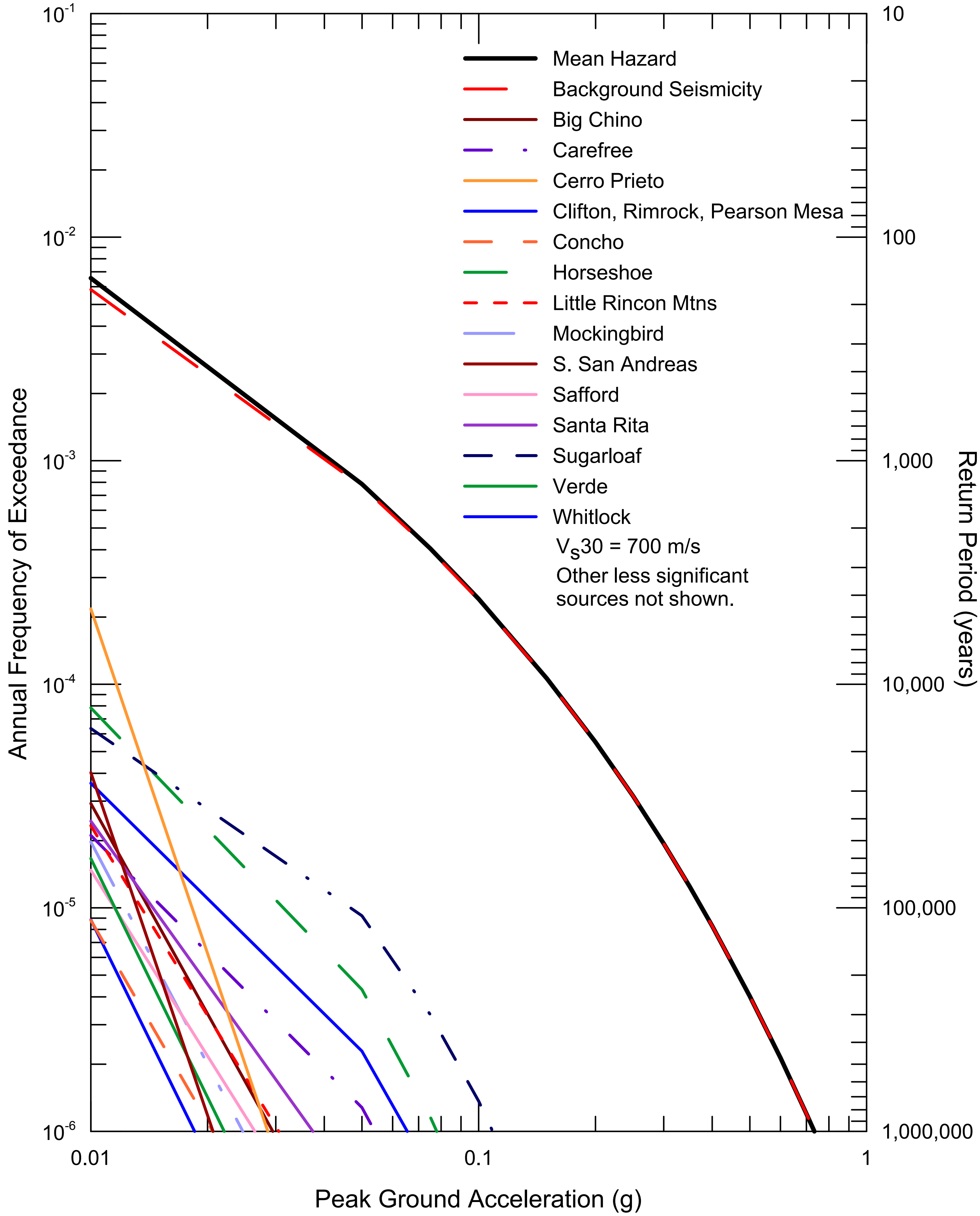

Seismic Source Contributions for Mean Peak Horizontal Acceleration Hazard for Pinal Schist and Gila Conglomerate Sites

RESOLUTION COPPER, NEAR WEST SITE

Lettis Consultants International, Inc. | **Figure 20**

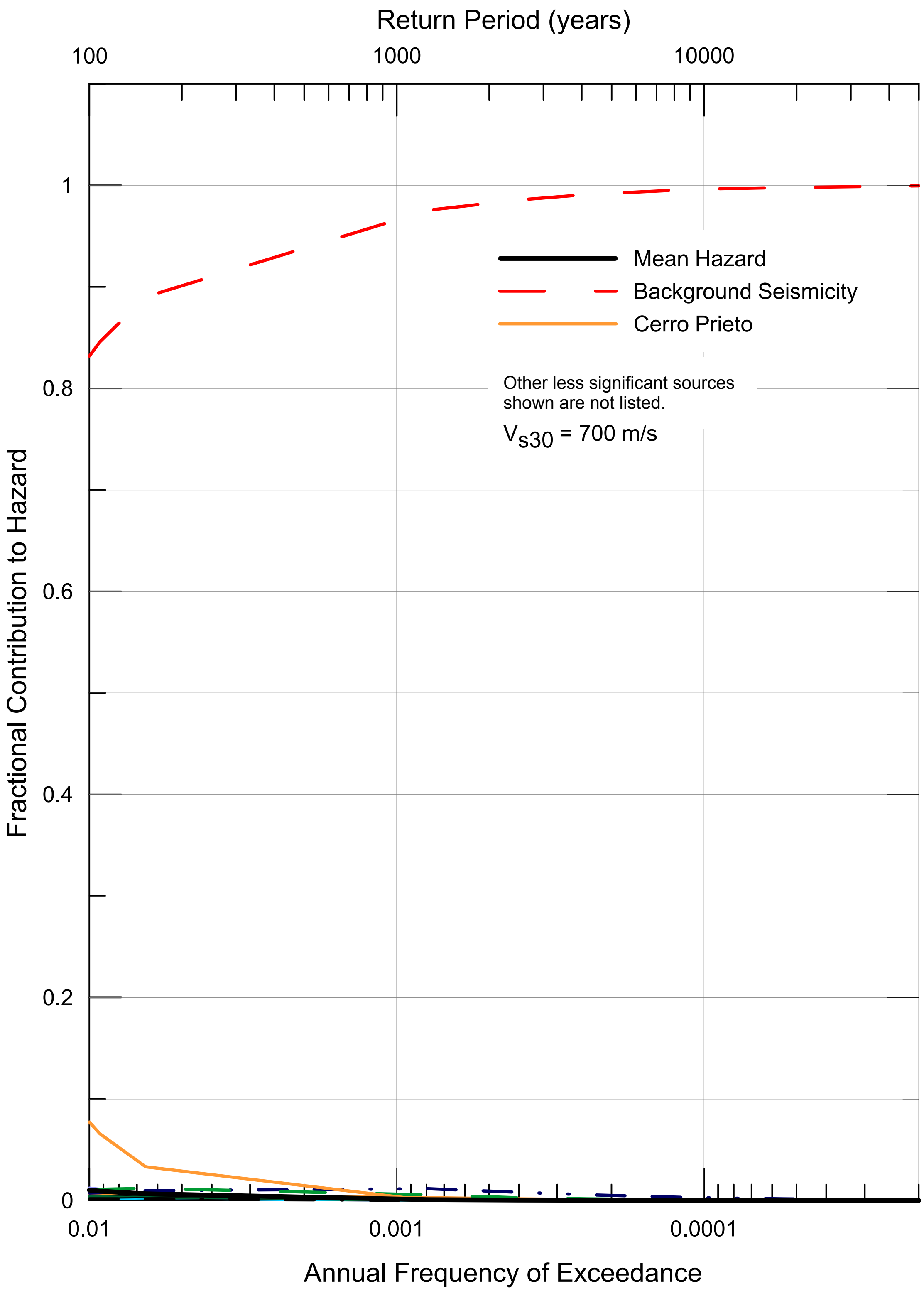

Seismic Source Fractional Contributions for Mean Peak Horizontal Acceleration Hazard for Pinal Schist and Gila Conglomerate Sites

RESOLUTION COPPER, NEAR WEST SITE

Lettis Consultants International, Inc.

Figure 21

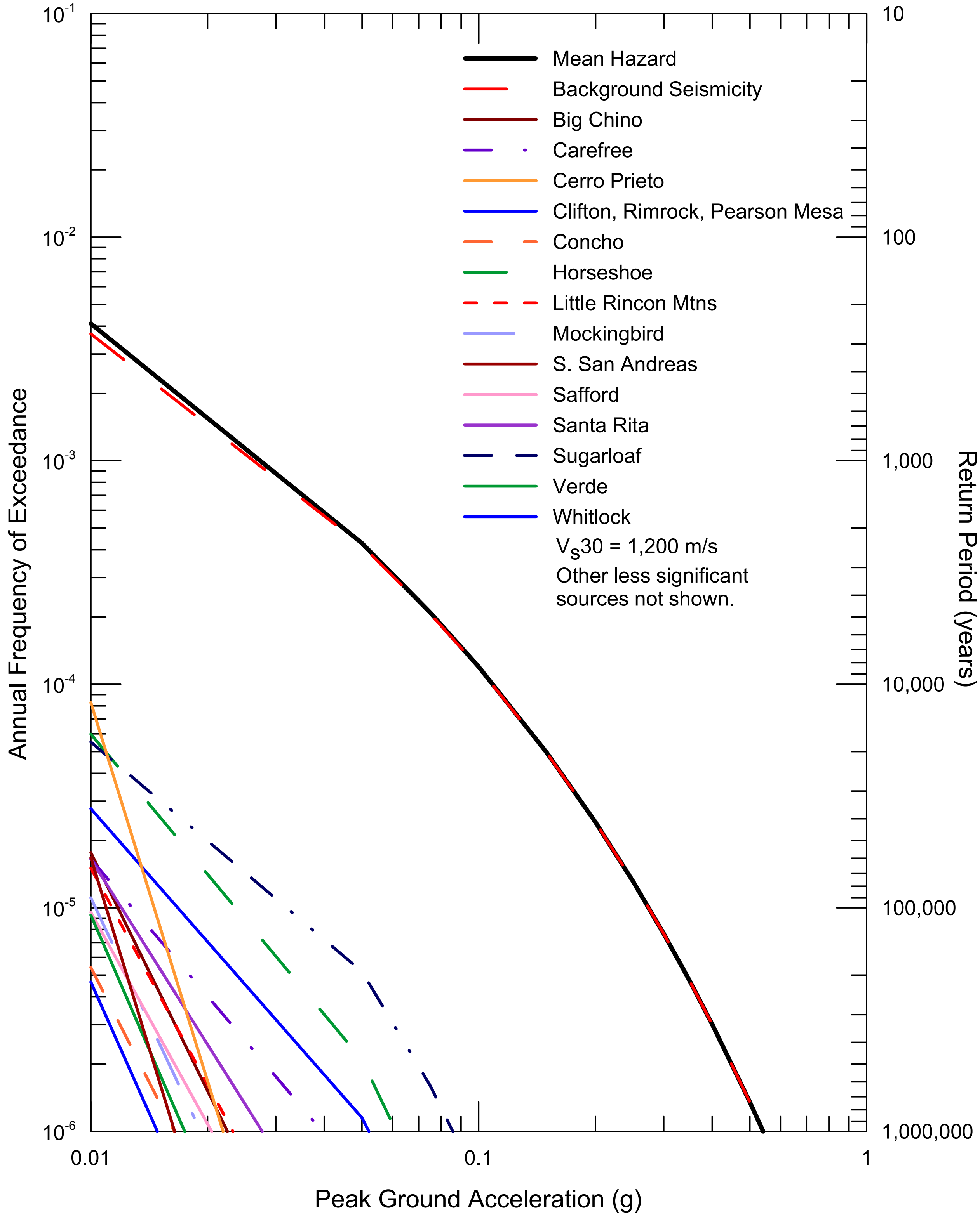

Seismic Source Contributions for Mean Peak Horizontal Acceleration Hazard for Rhyolite and Diabase Sites

RESOLUTION COPPER, NEAR WEST SITE

Lettis Consultants International, Inc. | **Figure 22**

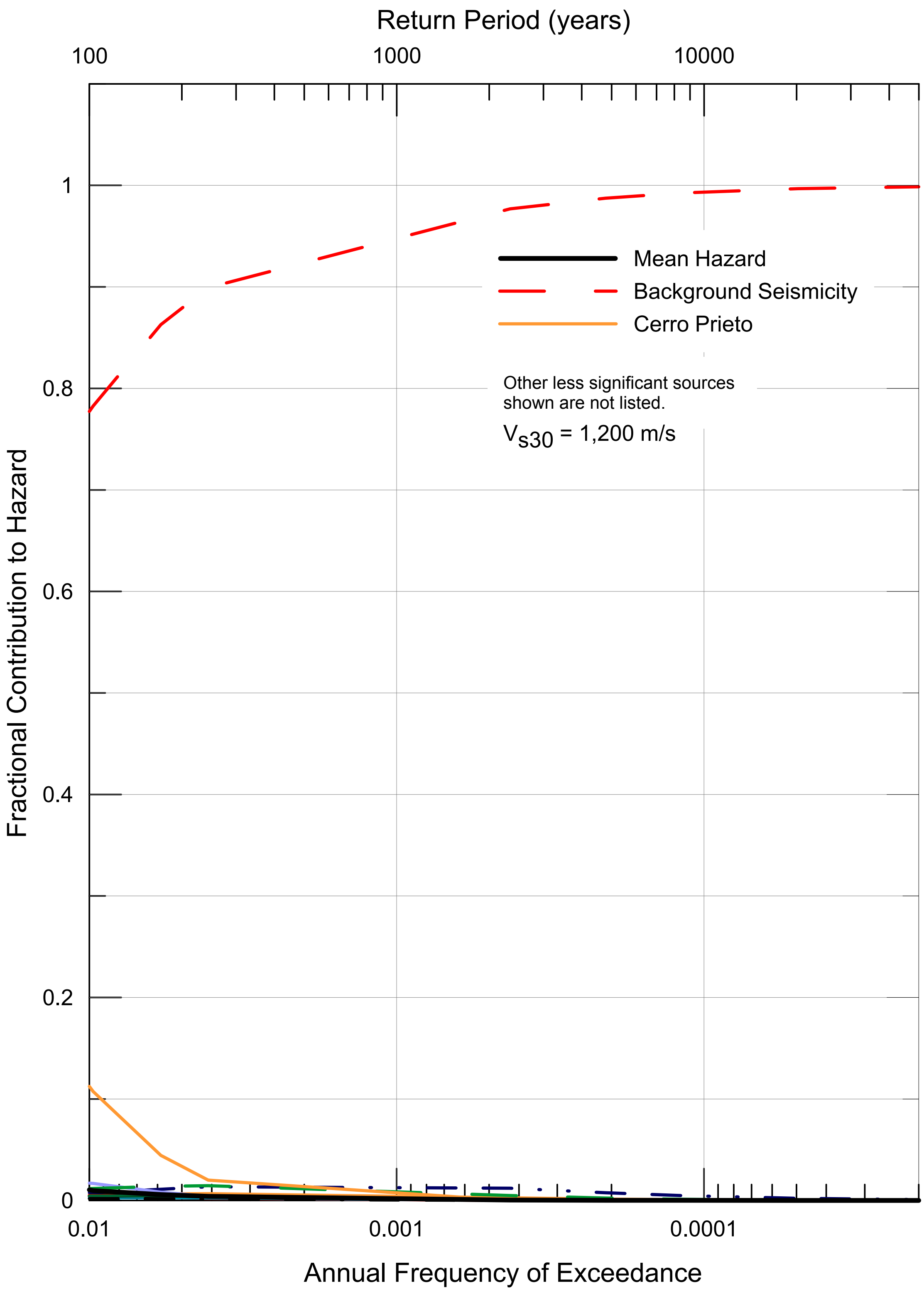

Seismic Source Fractional Contributions for Mean Peak Horizontal Acceleration Hazard for Rhyolite and Diabase Sites

RESOLUTION COPPER, NEAR WEST SITE

Lettis Consultants International, Inc.

Figure 23

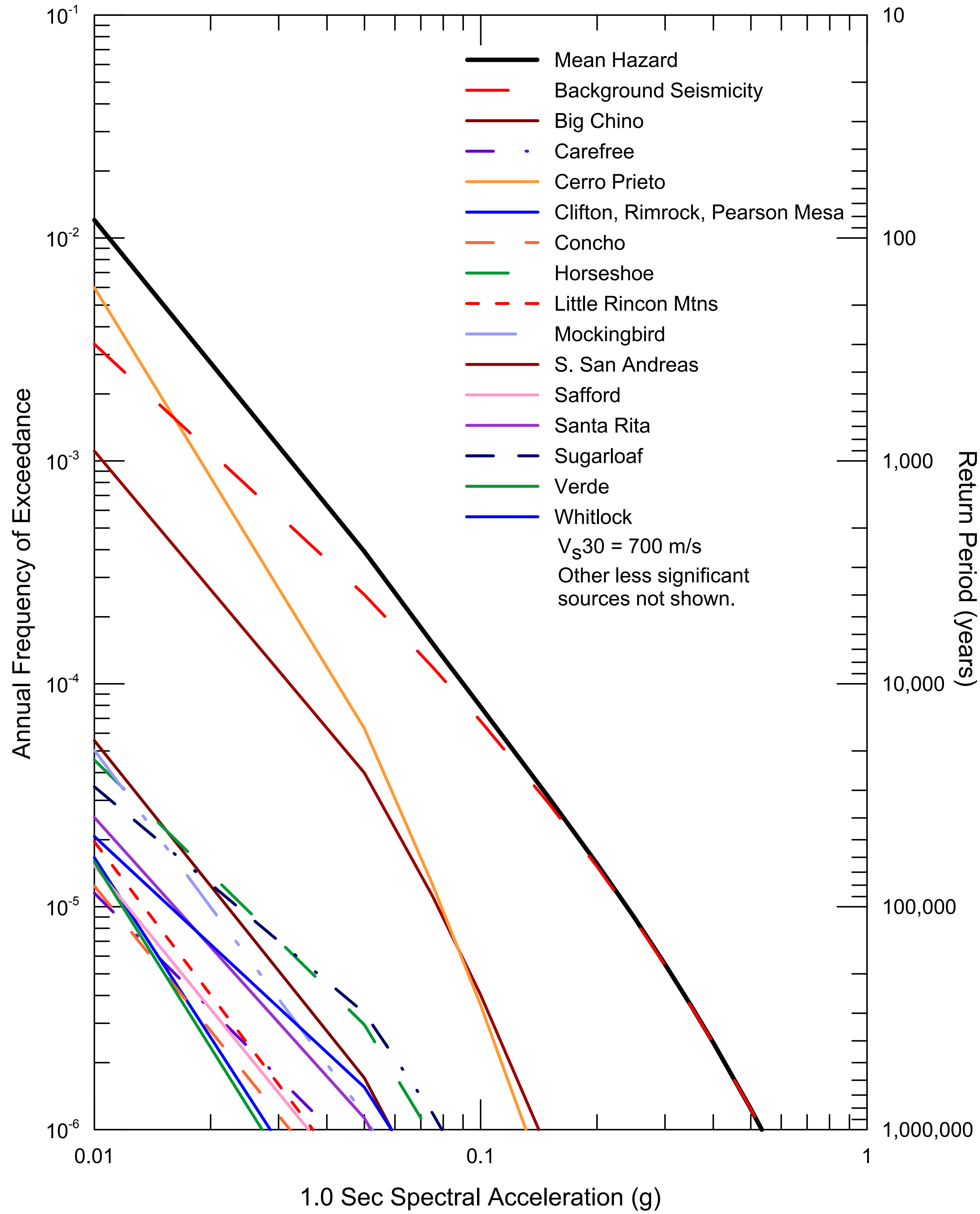

Seismic Source Contributions for Mean 1.0 Sec Horizontal Spectral Acceleration Hazard for Pinal Schist and Gila Conglomerate Sites

RESOLUTION COPPER, NEAR WEST SITE

Lettis Consultants International, Inc.

Figure 24

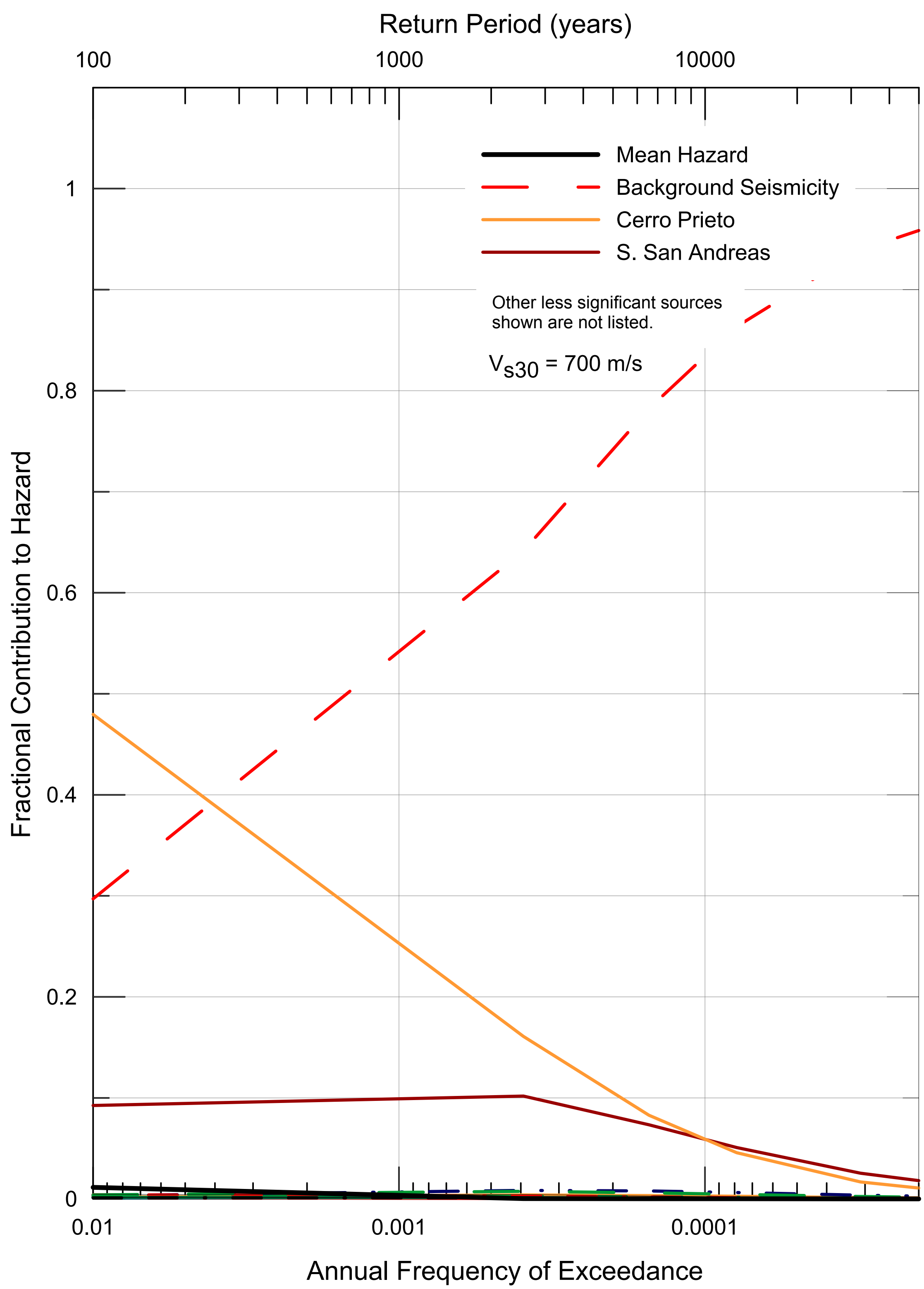

Seismic Source Fractional Contributions for Mean 1.0 Sec Spectral Horizontal Acceleration Hazard for Pinal Schist and Gila Conglomerate Sites

RESOLUTION COPPER, NEAR WEST SITE

Lettis Consultants International, Inc.

Figure 25

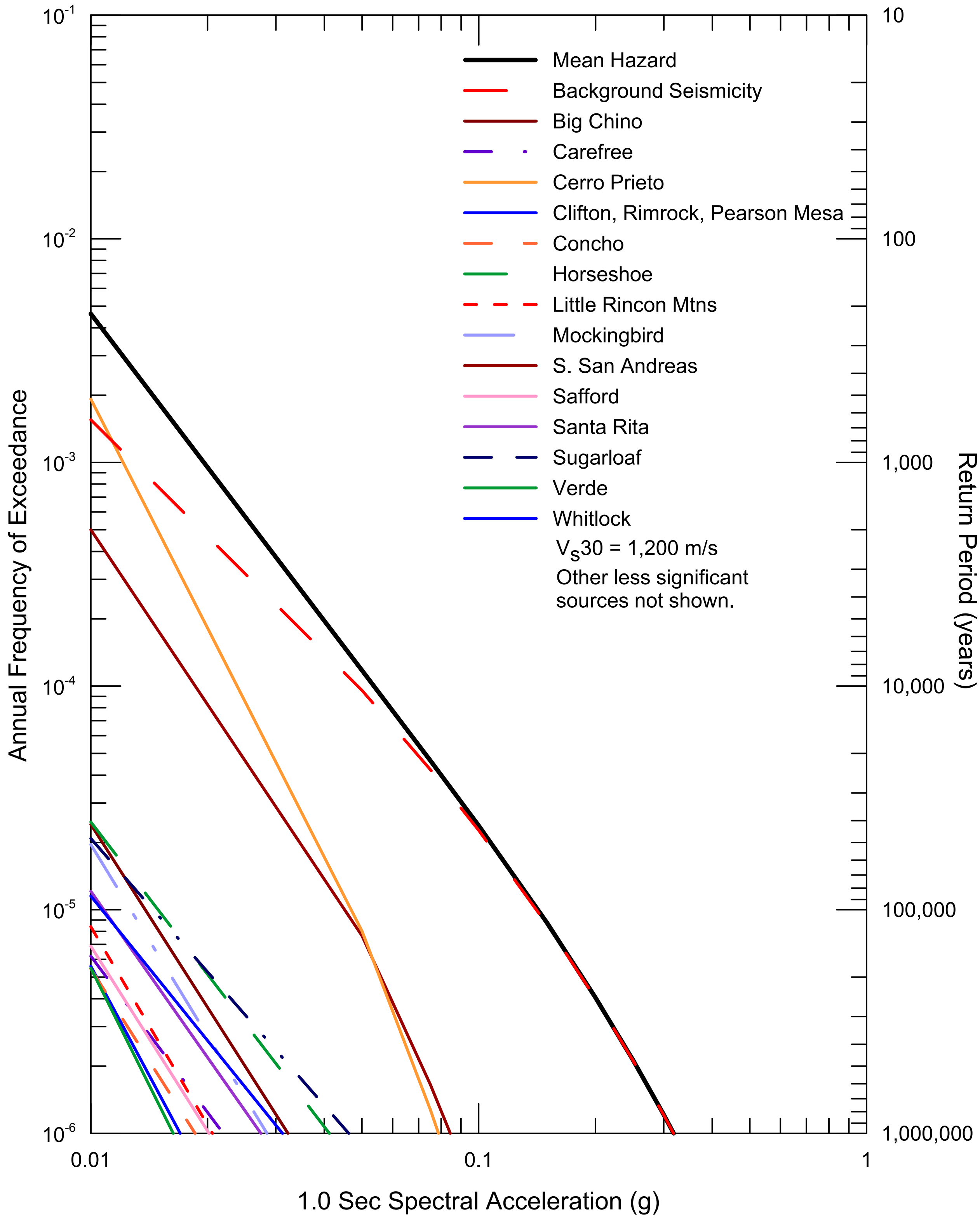

Seismic Source Contributions for Mean 1.0 Sec Horizontal Spectral Acceleration Hazard for Rhyolite and Diabase Sites

RESOLUTION COPPER, NEAR WEST SITE

Lettis Consultants International, Inc.

Figure 26

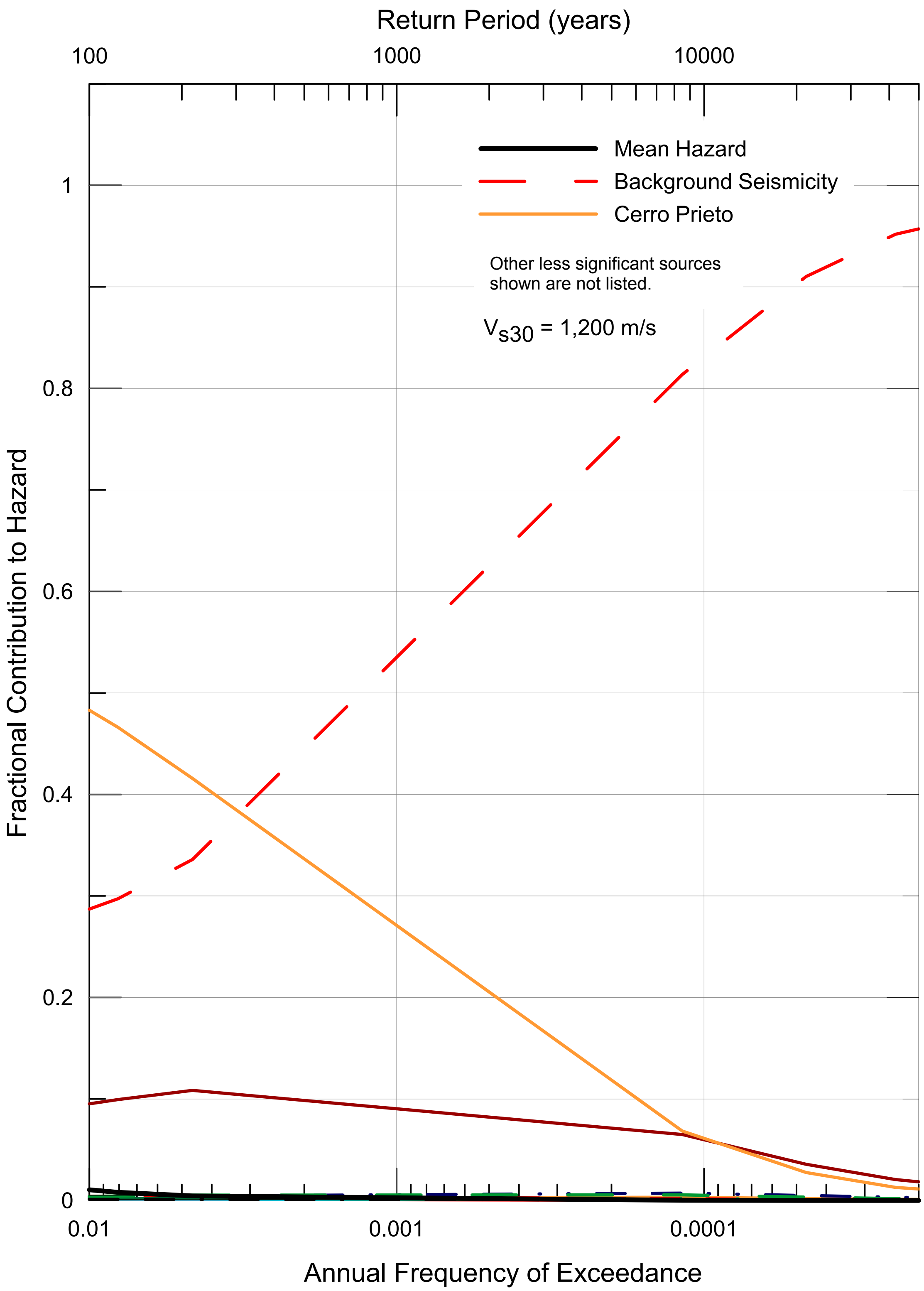

Seismic Source Fractional Contributions for Mean 1.0 Sec Spectral Horizontal Acceleration Hazard for Rhyolite and Diabase Sites

RESOLUTION COPPER, NEAR WEST SITE

Lettis Consultants International, Inc.

Figure 27

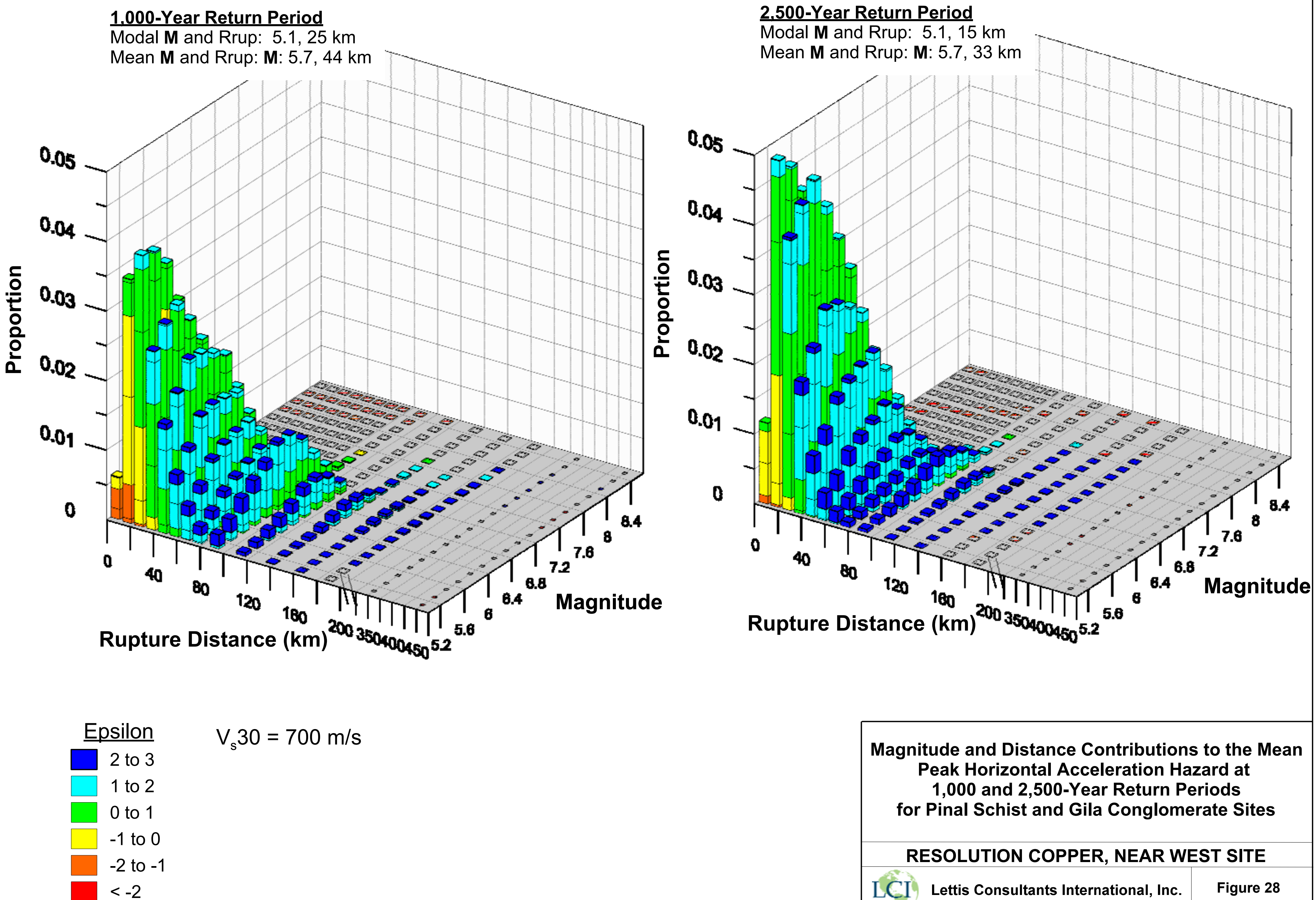

Magnitude and Distance Contributions to the Mean Peak Horizontal Acceleration Hazard at 1,000 and 2,500-Year Return Periods for Pinal Schist and Gila Conglomerate Sites

RESOLUTION COPPER, NEAR WEST SITE

Lettis Consultants International, Inc.

Figure 28

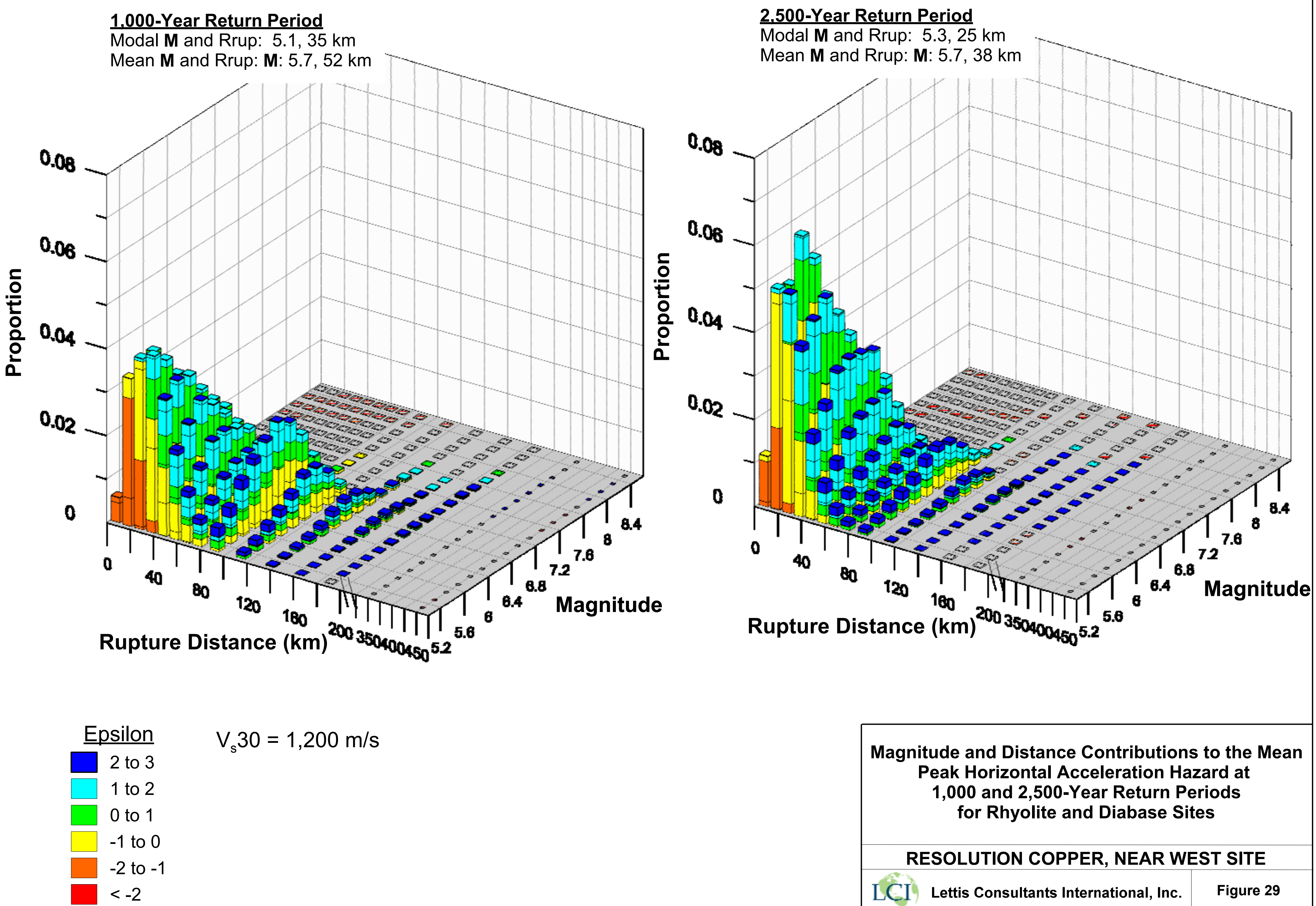

V_s30 = 1,200 m/s

Magnitude and Distance Contributions to the Mean Peak Horizontal Acceleration Hazard at 1,000 and 2,500-Year Return Periods for Rhyolite and Diabase Sites

RESOLUTION COPPER, NEAR WEST SITE

Lettis Consultants International, Inc. | **Figure 29**

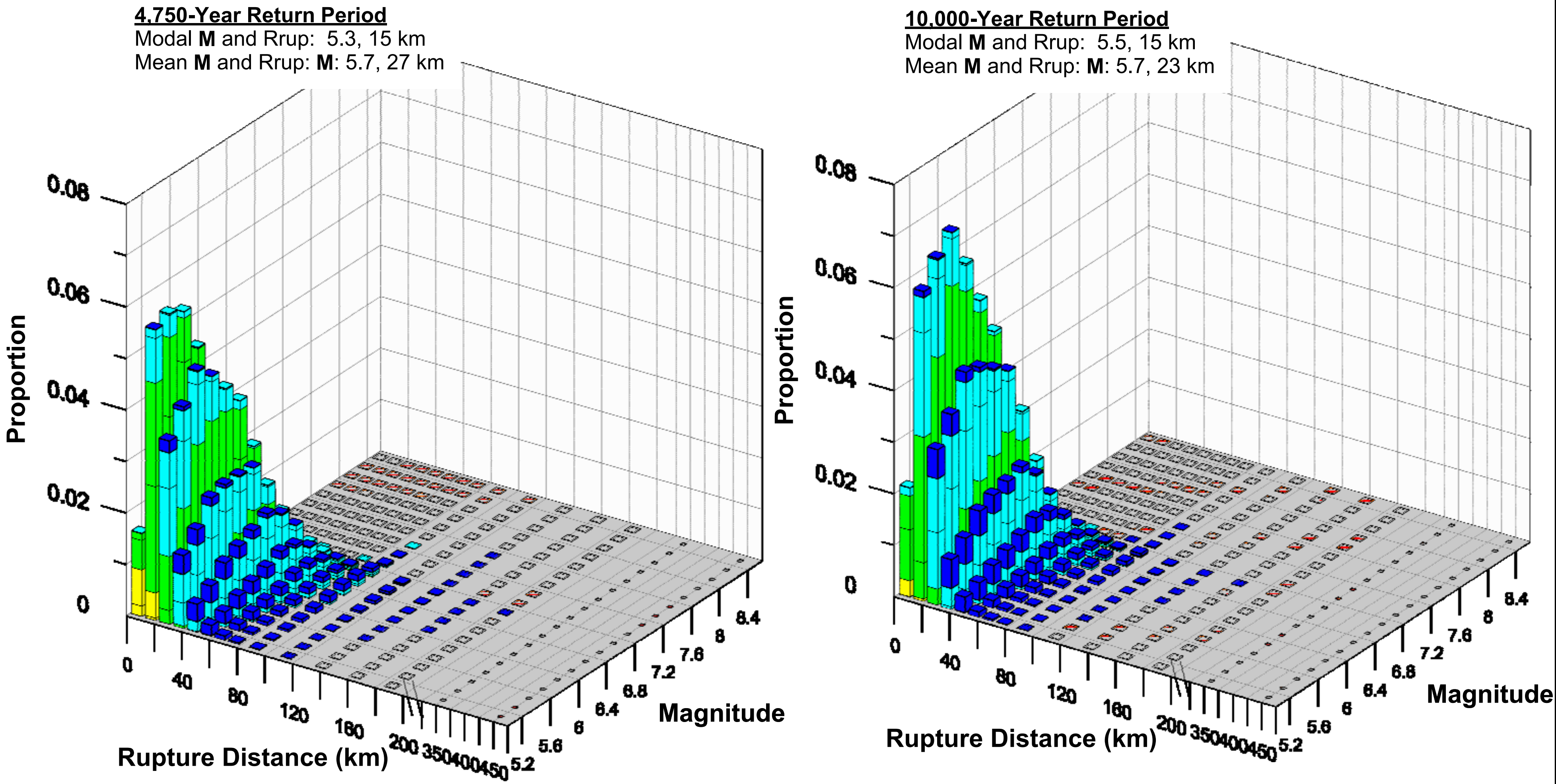

Epsilon

- 2 to 3
- 1 to 2
- 0 to 1
- -1 to 0
- -2 to -1
- < -2

V_s30 = 700 m/s

Magnitude and Distance Contributions to the Mean Peak Horizontal Spectral Hazard at 4,750 and 10,000-Year Return Periods for Pinal Schist and Gila Conglomerate Sites

RESOLUTION COPPER, NEAR WEST SITE

Lettis Consultants International, Inc. | **Figure 30**

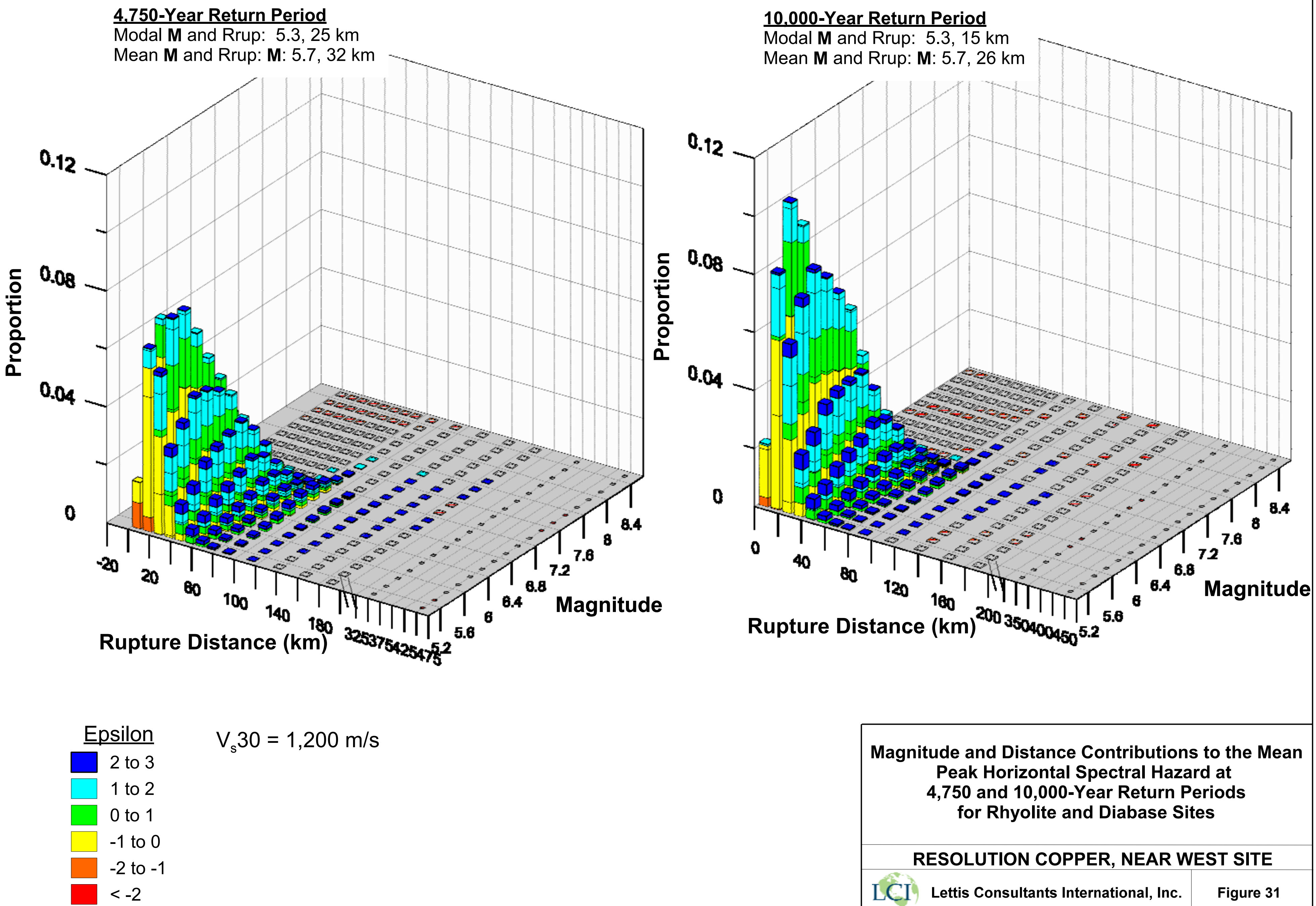

Magnitude and Distance Contributions to the Mean Peak Horizontal Spectral Hazard at 4,750 and 10,000-Year Return Periods for Rhyolite and Diabase Sites

RESOLUTION COPPER, NEAR WEST SITE

Lettis Consultants International, Inc.	Figure 31

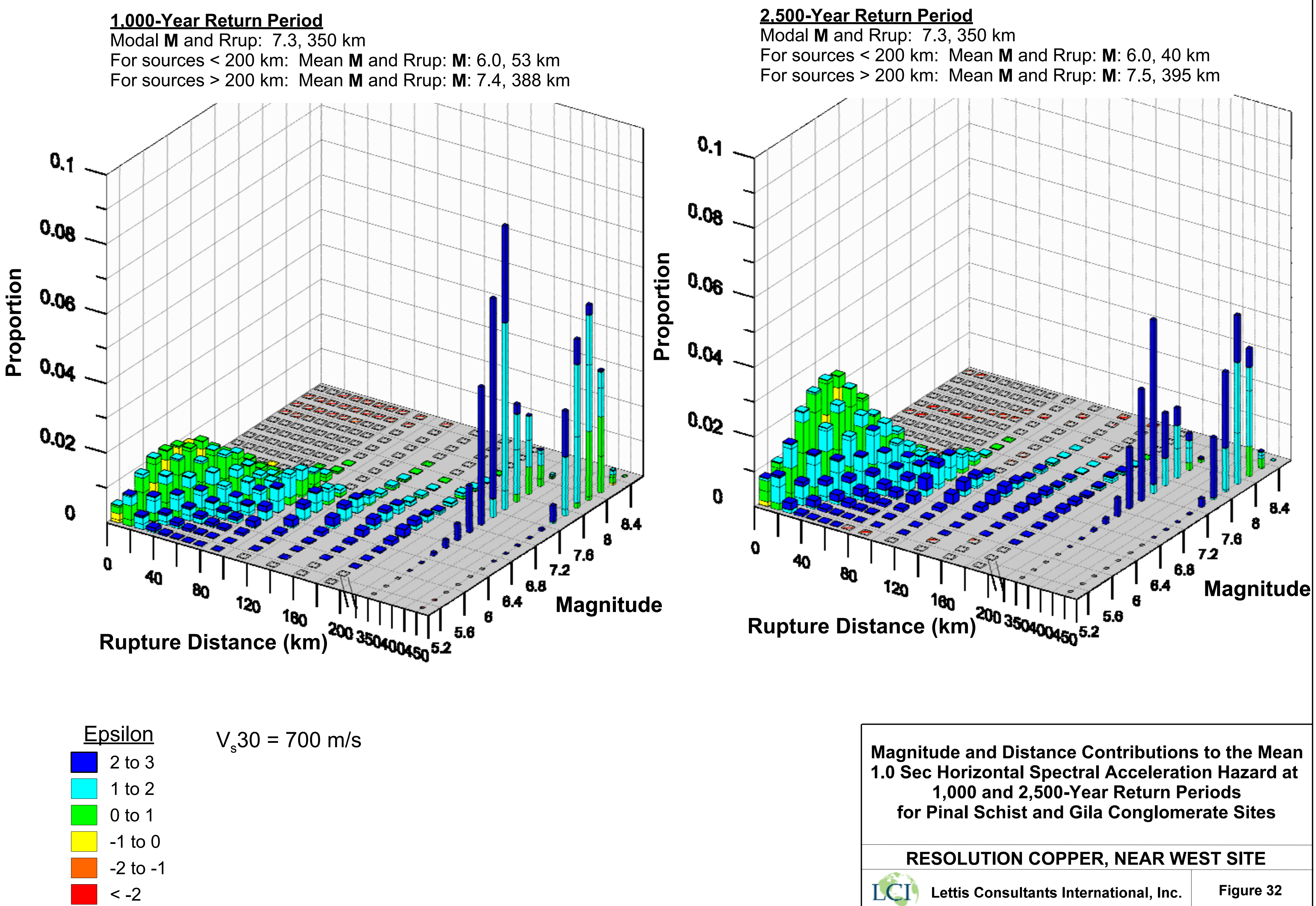

Magnitude and Distance Contributions to the Mean 1.0 Sec Horizontal Spectral Acceleration Hazard at 1,000 and 2,500-Year Return Periods for Pinal Schist and Gila Conglomerate Sites

RESOLUTION COPPER, NEAR WEST SITE

Lettis Consultants International, Inc.

Figure 32

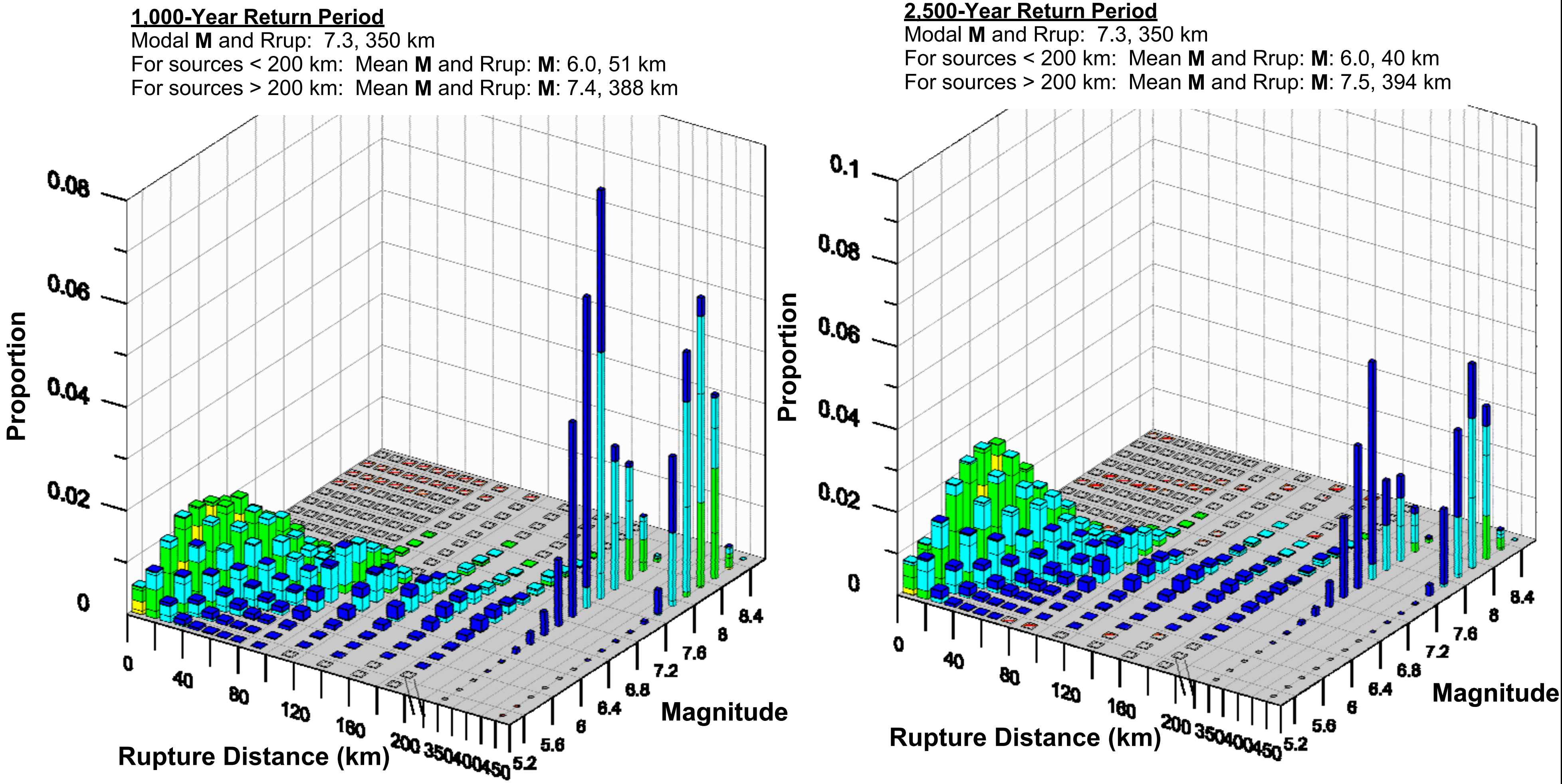

V_s30 = 1,200 m/s

Magnitude and Distance Contributions to the Mean 1.0 Sec Horizontal Spectral Acceleration Hazard at 1,000 and 2,500-Year Return Periods for Rhyolite and Diabase Sites

RESOLUTION COPPER, NEAR WEST SITE

Lettis Consultants International, Inc. | Figure 33

4,750-Year Return Period
Modal **M** and Rrup: 6.1, 15 km
For sources < 200 km: Mean **M** and Rrup: **M**: 6.0, 33 km
For sources > 200 km: Mean **M** and Rrup: **M**: 7.6, 399 km

10,000-Year Return Period
Modal **M** and Rrup: 6.1, 15 km
For sources < 200 km: Mean **M** and Rrup: **M**: 6.1, 26 km
For sources > 200 km: Mean **M** and Rrup: **M**: 7.7, 404 km

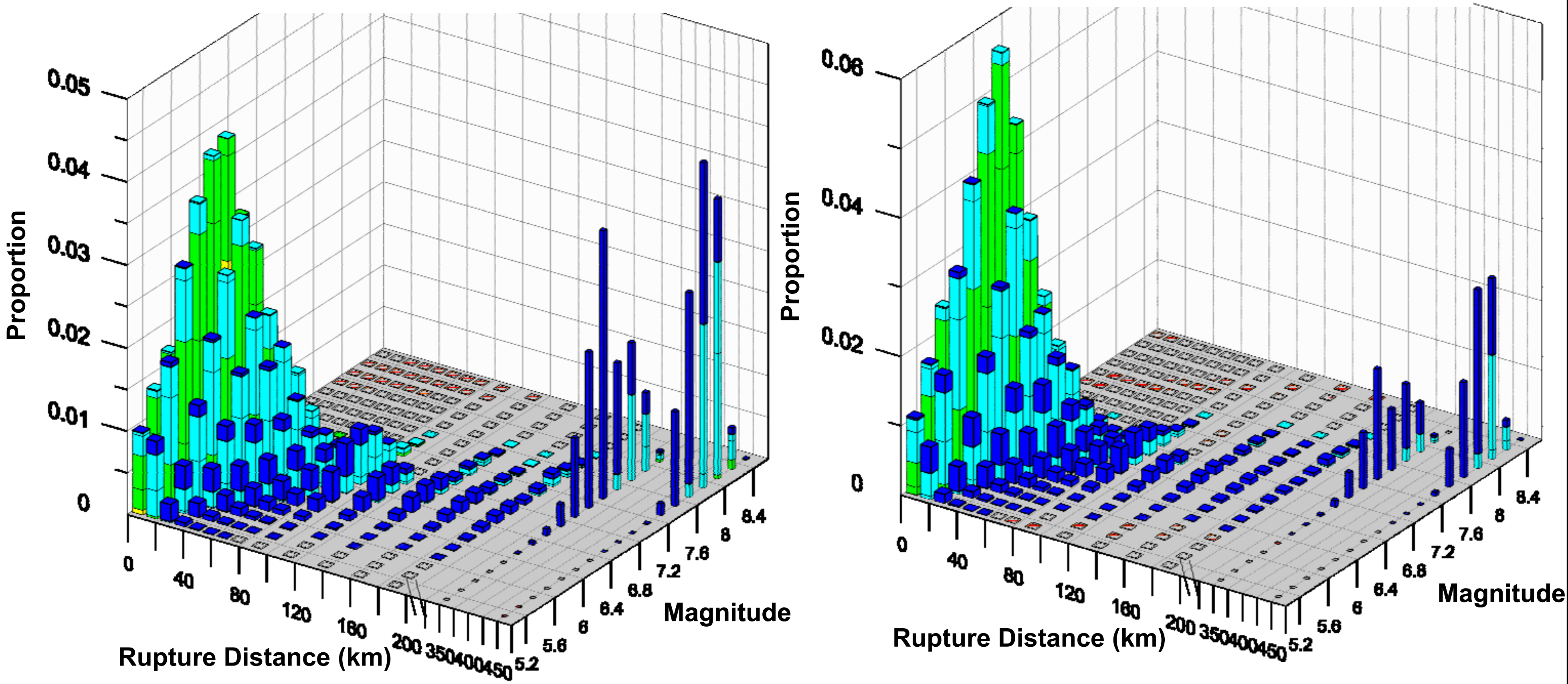

Epsilon

- 2 to 3
- 1 to 2
- 0 to 1
- -1 to 0
- -2 to -1
- < -2

V_s30 = 700 m/s

Magnitude and Distance Contributions to the Mean 1.0 Sec Horizontal Spectral Acceleration Hazard at 4,750 and 10,000-Year Return Periods for Pinal Schist and Gila Conglomerate Sites

RESOLUTION COPPER, NEAR WEST SITE

LCI Lettis Consultants International, Inc. | **Figure 34**

4,750-Year Return Period
Modal **M** and Rrup: 6.1, 15 km
For sources < 200 km: Mean **M** and Rrup: **M**: 6.0, 33 km
For sources > 200 km: Mean **M** and Rrup: **M**: 7.6, 399 km

10,000-Year Return Period
Modal **M** and Rrup: 6.1, 15 km
For sources < 200 km: Mean **M** and Rrup: **M**: 6.1, 26 km
For sources > 200 km: Mean **M** and Rrup: **M**: 7.7, 404 km

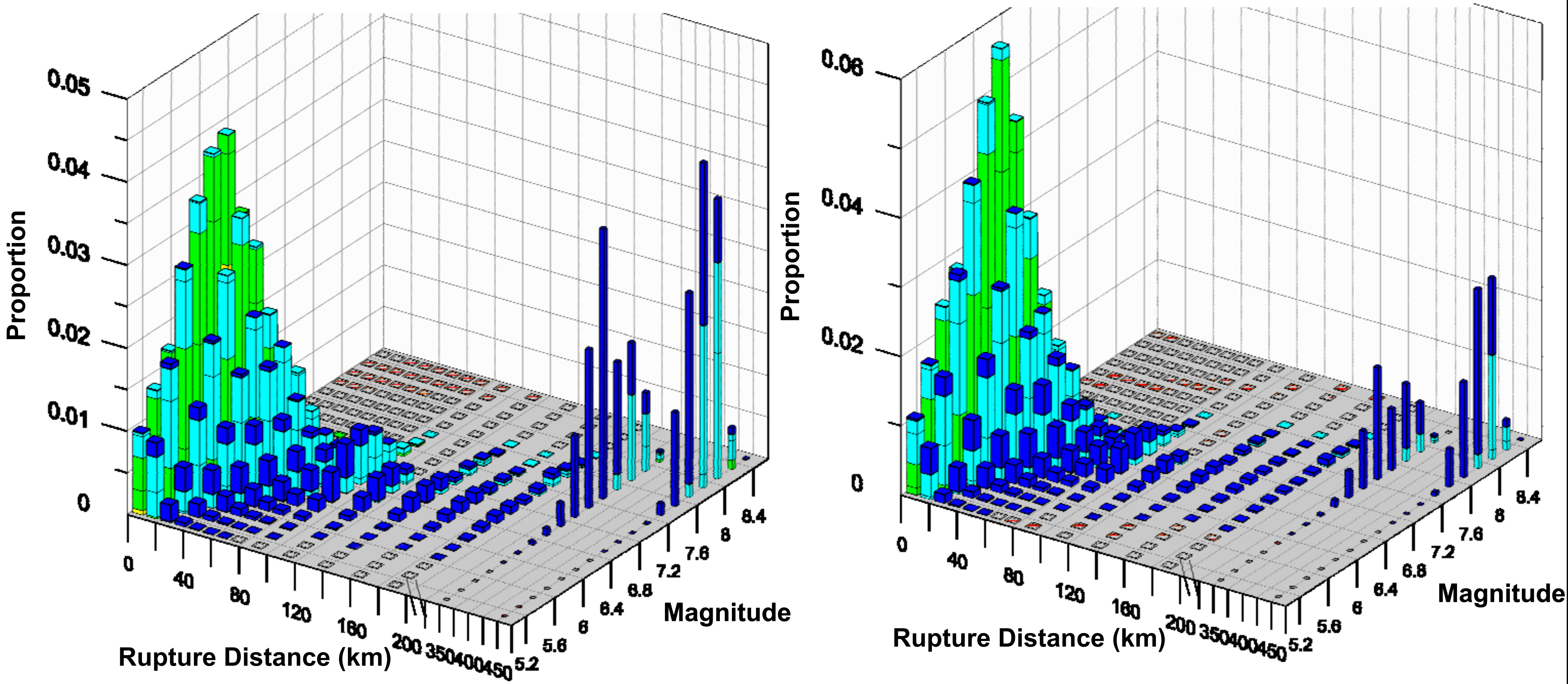

Epsilon
- 2 to 3
- 1 to 2
- 0 to 1
- -1 to 0
- -2 to -1
- < -2

V_s30 = 1,200 m/s

Magnitude and Distance Contributions to the Mean 1.0 Sec Horizontal Spectral Acceleration Hazard at 4,750 and 10,000-Year Return Periods for Rhyolite and Diabase Sites

RESOLUTION COPPER, NEAR WEST SITE

Lettis Consultants International, Inc. | Figure 35

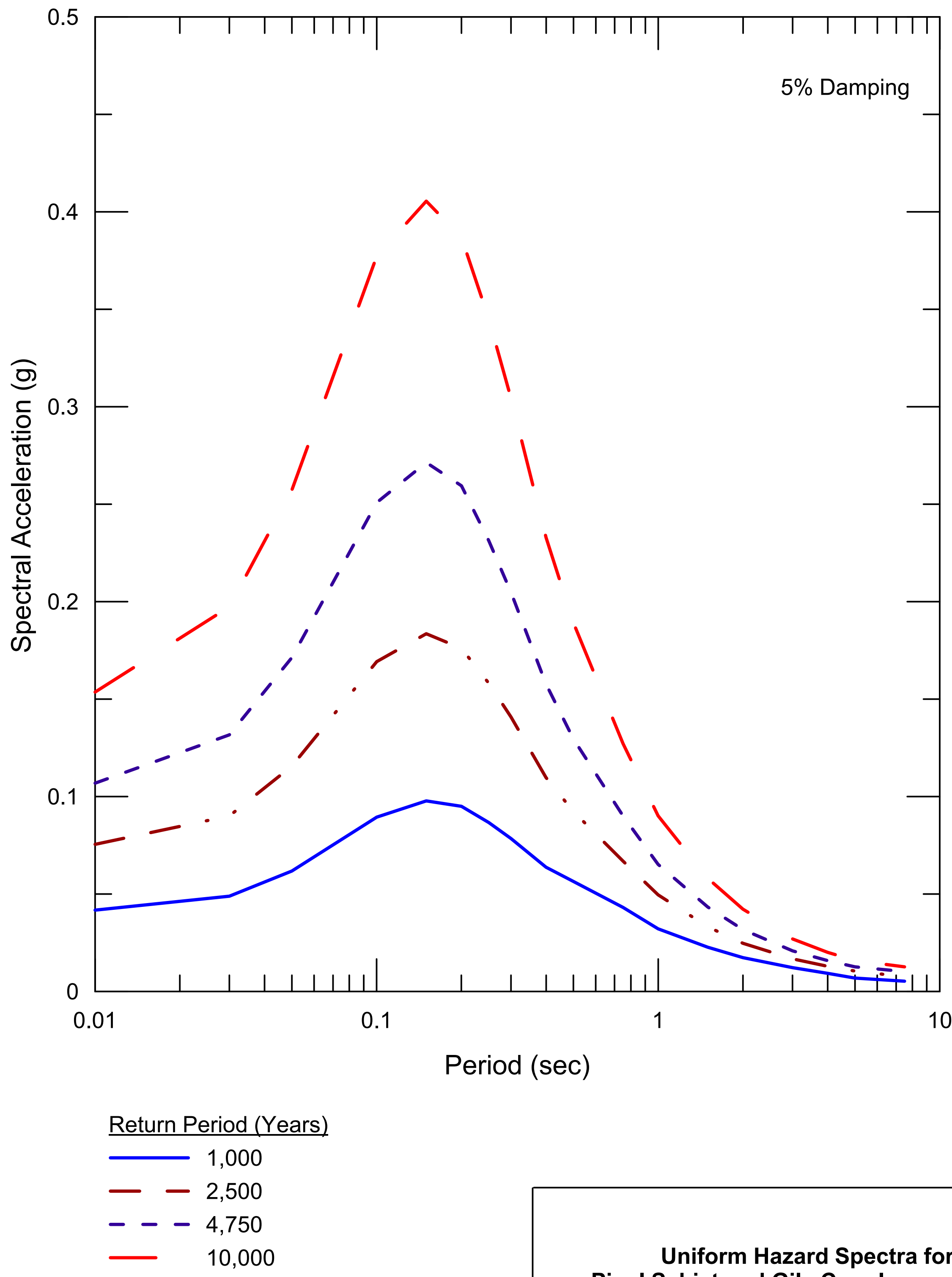

Uniform Hazard Spectra for
Pinal Schist and Gila Conglomerate Sites

RESOLUTION COPPER, NEAR WEST SITE

Lettis Consultants International, Inc. | **Figure 36**

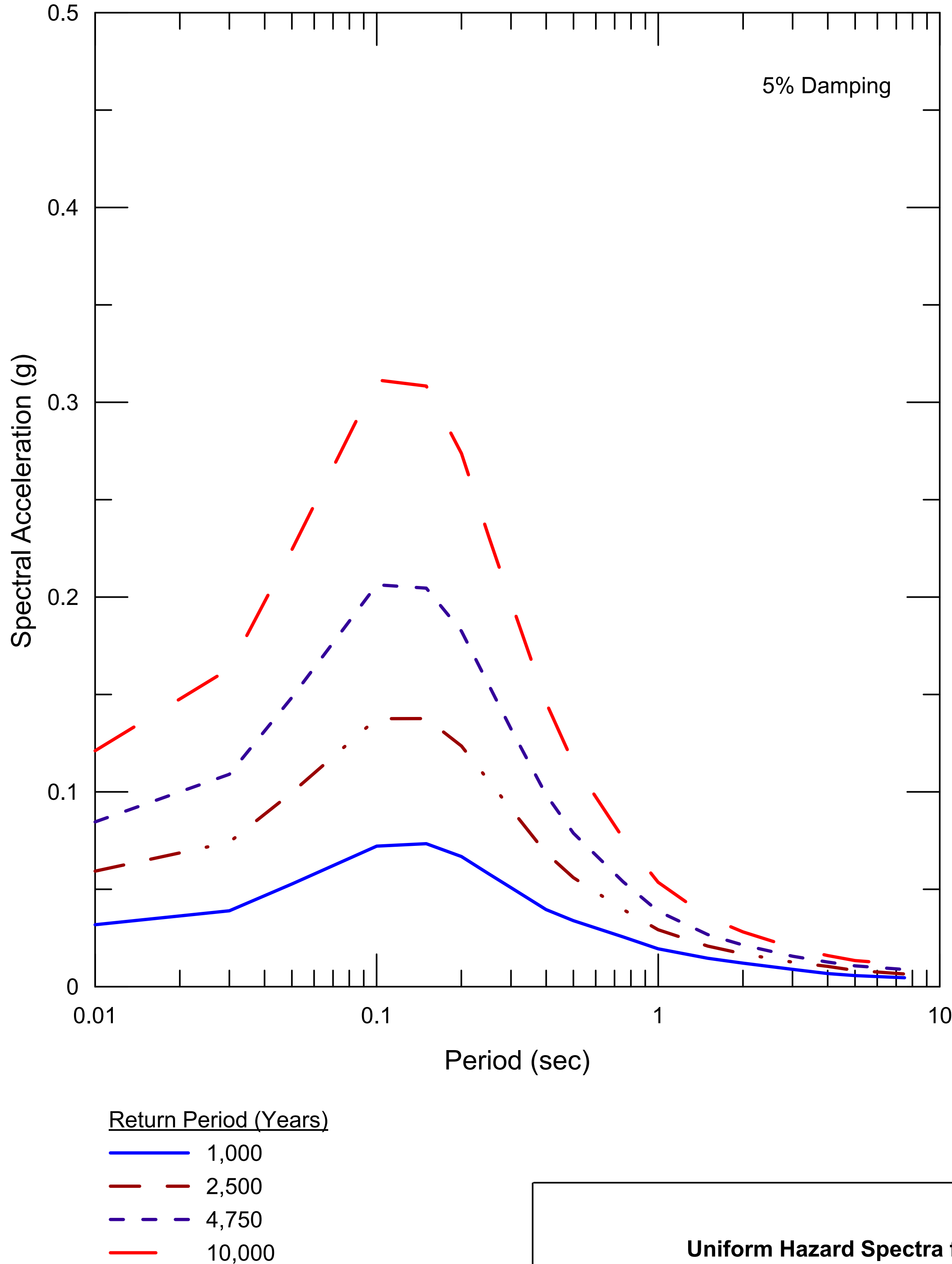

Uniform Hazard Spectra for Rhyolite and Diabase Sites

RESOLUTION COPPER, NEAR WEST SITE

Lettis Consultants International, Inc. | **Figure 37**

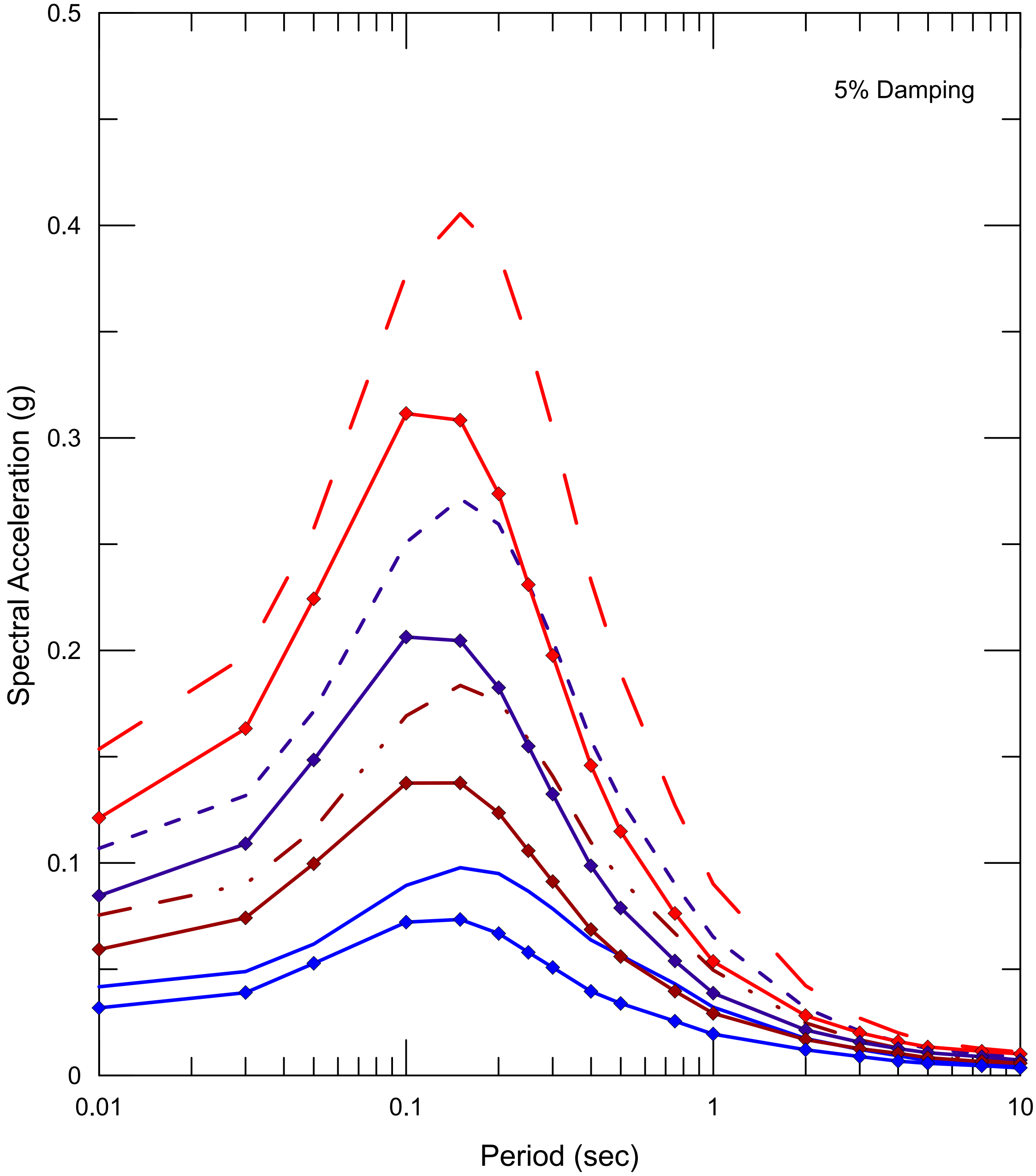

Pinal Schist and Gila Conglomerate
Return Period (Years)

1,000
2,500
4,750
10,000

Rhyolite and Diabase
Return Period (Years)

1,000
2,500
4,750
10,000

Comparison of Uniform Hazard Spectra for Pinal Schist and Gila Conglomerate and Rhyolite and Diabase Sites

RESOLUTION COPPER, NEAR WEST SITE

Lettis Consultants International, Inc. | **Figure 38**

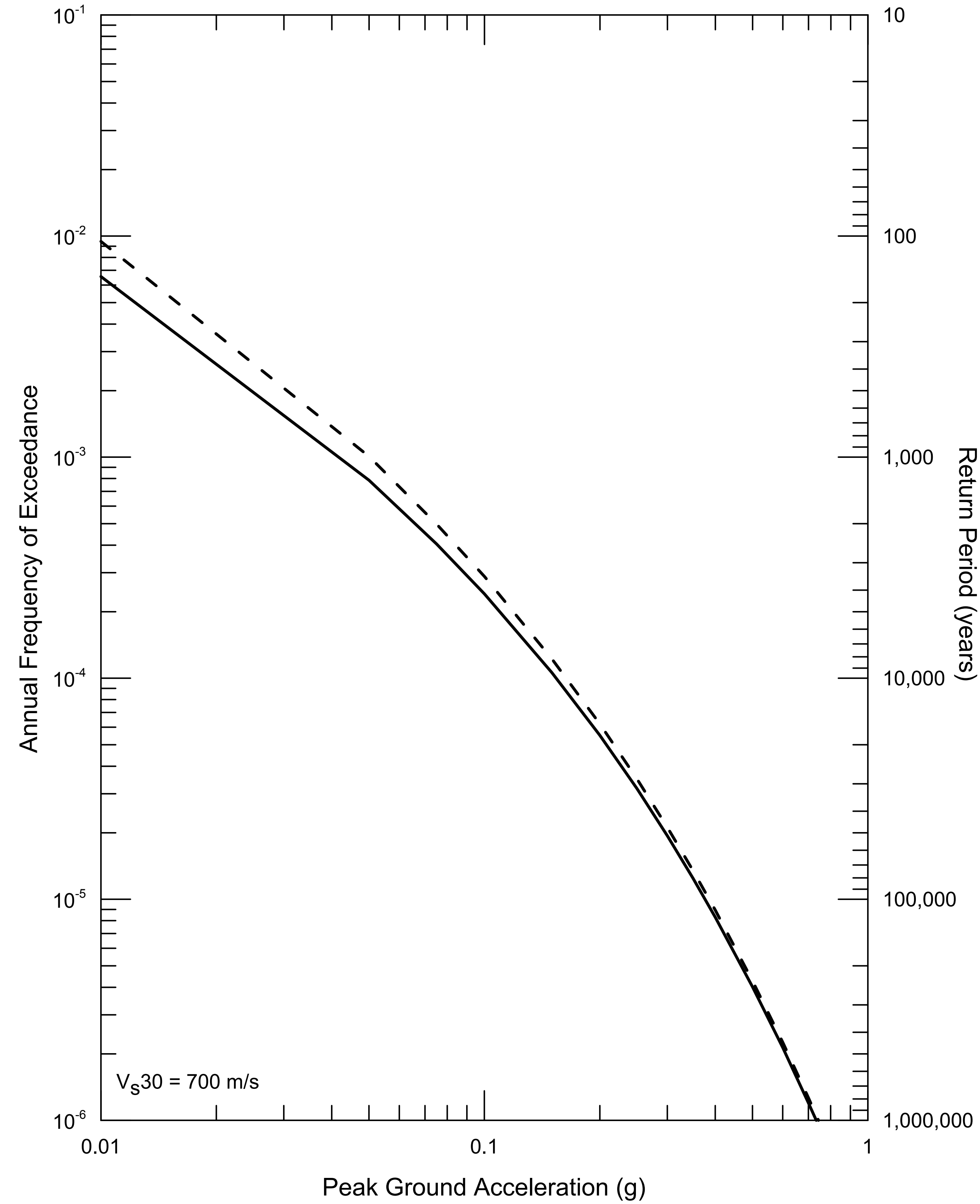

Mean Peak Horizontal Acceleration Hazard for Pinal Schist and Gila Conglomerate Sites, Mmin = 5 and 4

RESOLUTION COPPER, NEAR WEST SITE

Lettis Consultants International, Inc.

Figure 39

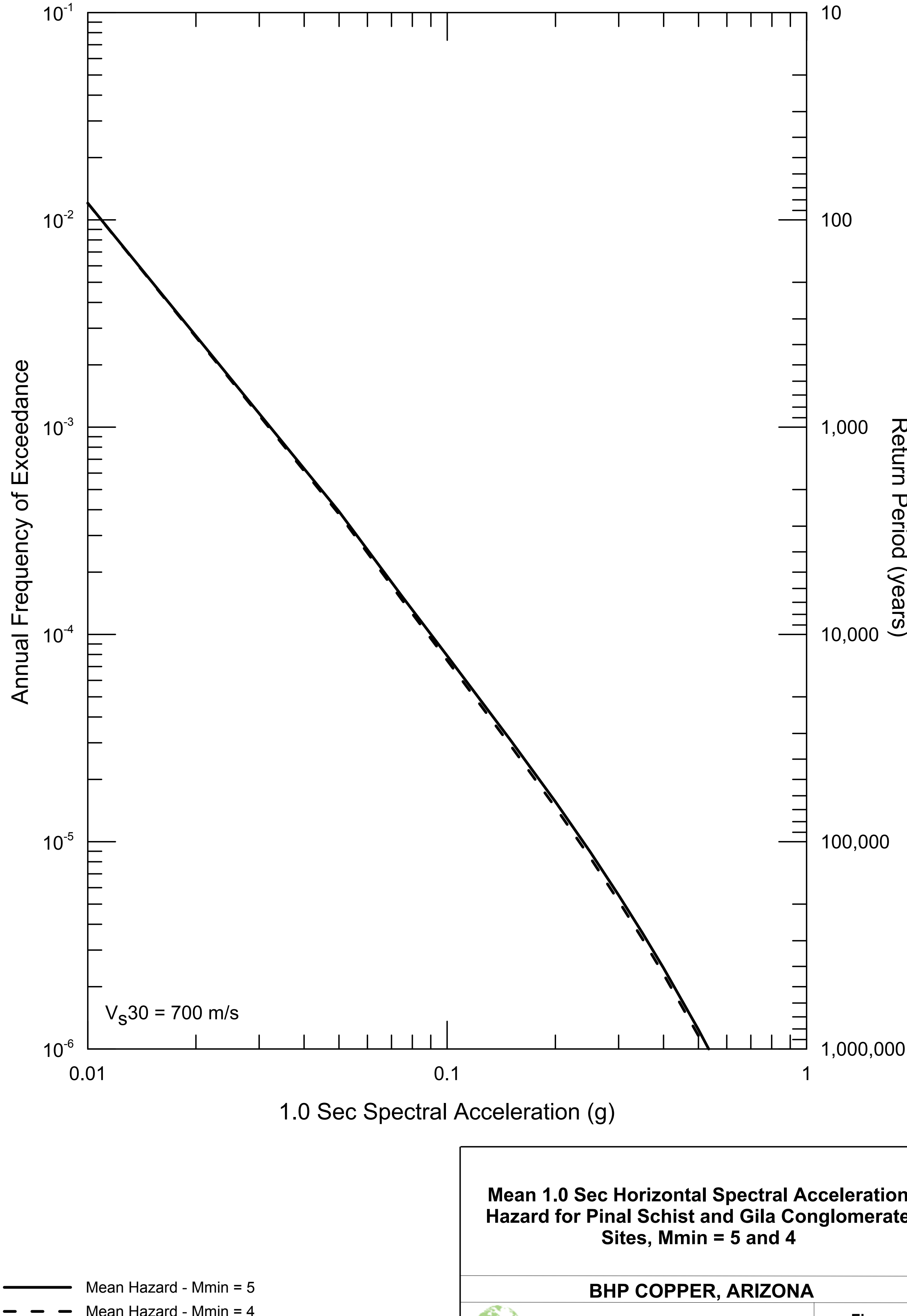

Mean 1.0 Sec Horizontal Spectral Acceleration Hazard for Pinal Schist and Gila Conglomerate Sites, Mmin = 5 and 4

BHP COPPER, ARIZONA

Lettis Consultants International, Inc.	**Figure 40**

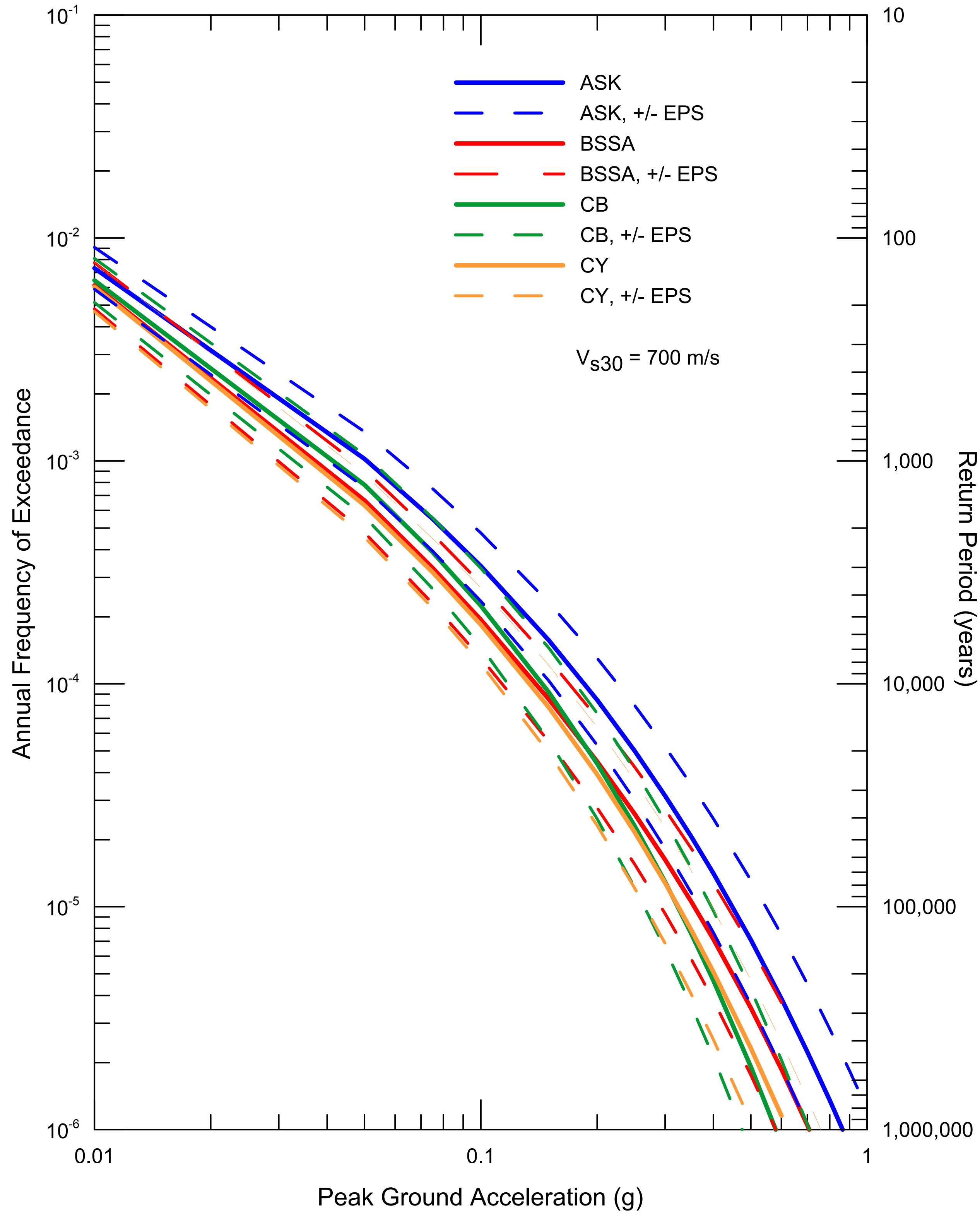

Sensitivity of Mean Peak Horizontal Acceleration Hazard from Crustal Sources to GMMs for Pinal Schist and Gila Conglomerate Sites

RESOLUTION COPPER, NEAR WEST SITE

Lettis Consultants International, Inc. | **Figure 41**

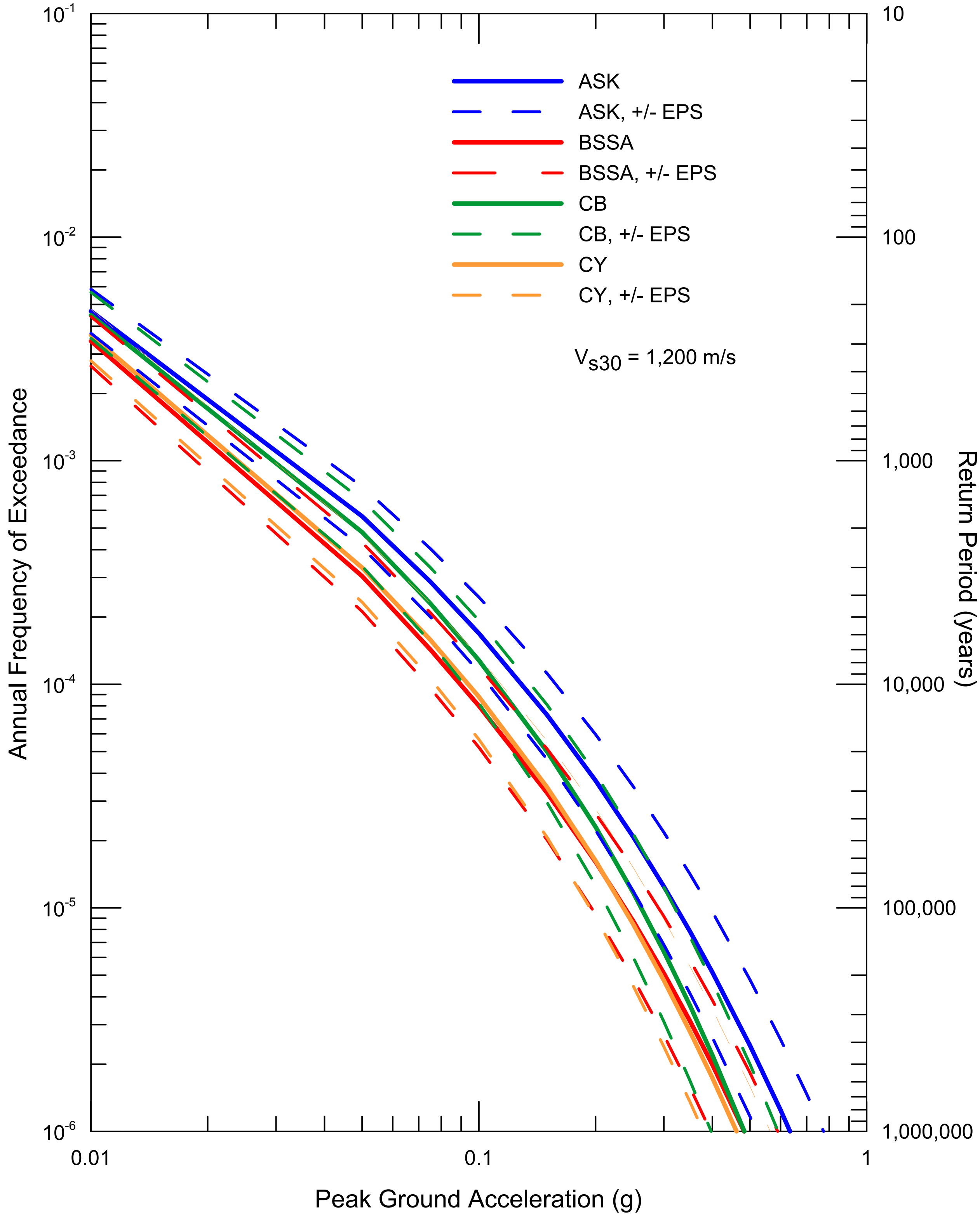

Sensitivity of Mean Peak Horizontal Acceleration Hazard from Crustal Sources to GMMs for Rhyolite and Diabase Sites

RESOLUTION COPPER, NEAR WEST SITE

Lettis Consultants International, Inc. | **Figure 42**

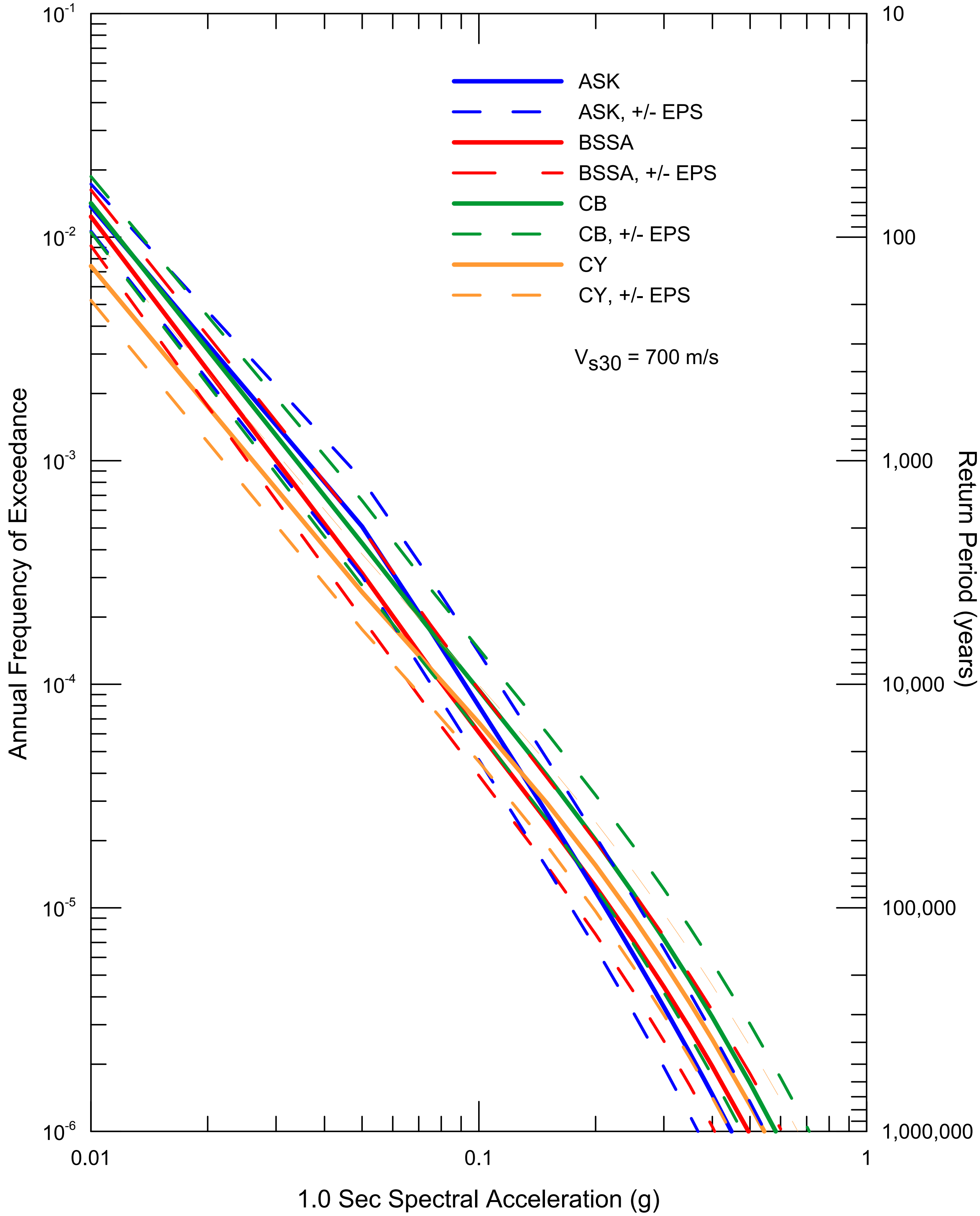

Sensitivity of Mean 1.0 Sec Horizontal Spectral Acceleration Hazard from Crustal Sources to GMMs for Pinal Schist and Gila Conglomerate Sites

RESOLUTION COPPER, NEAR WEST SITE

Lettis Consultants International, Inc.

Figure 43

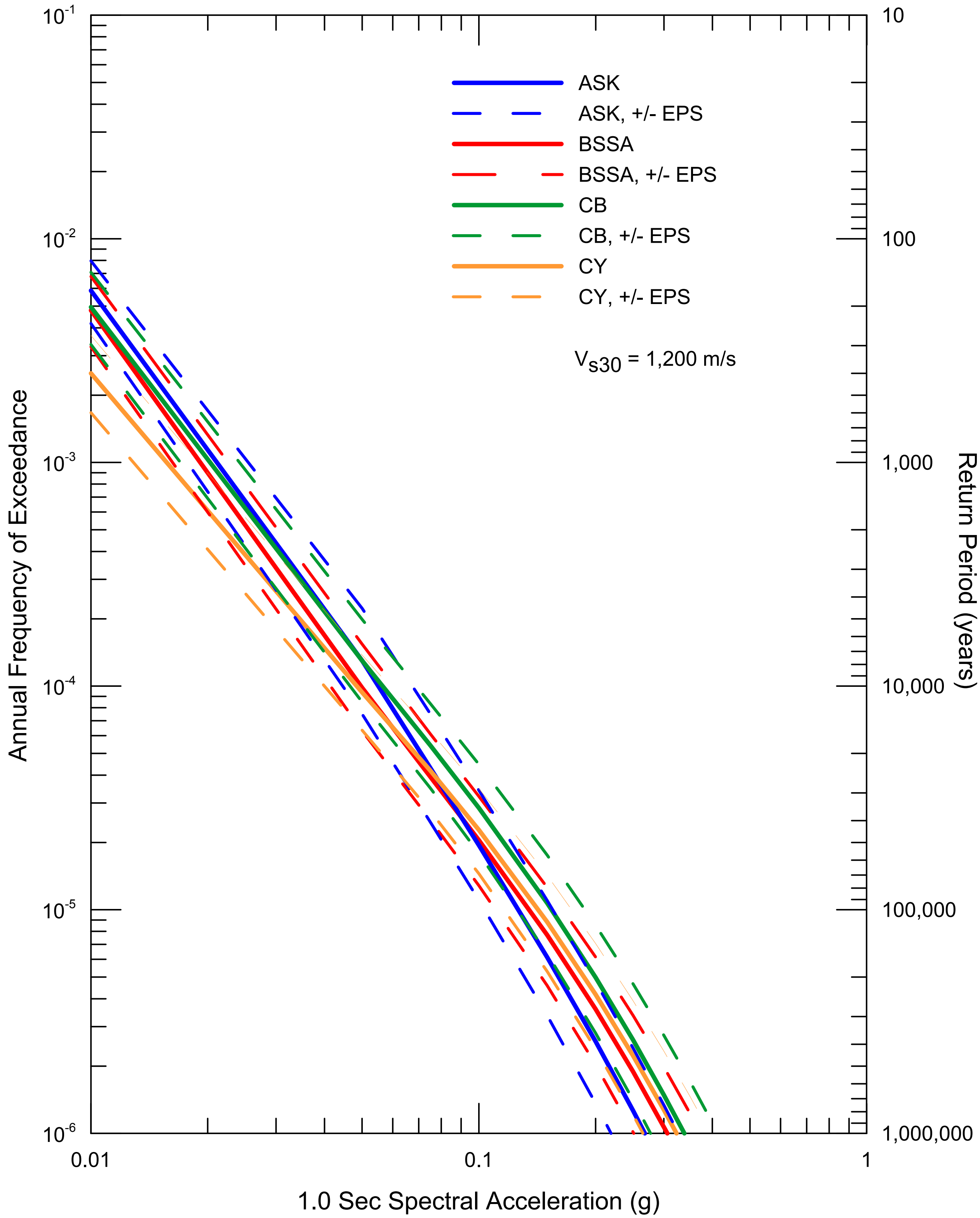

Sensitivity of Mean 1.0 Sec Horizontal Spectral Acceleration Hazard from Crustal Sources to GMMs for Rhyolite and Diabase Sites

RESOLUTION COPPER, NEAR WEST SITE

Lettis Consultants International, Inc. | **Figure 44**

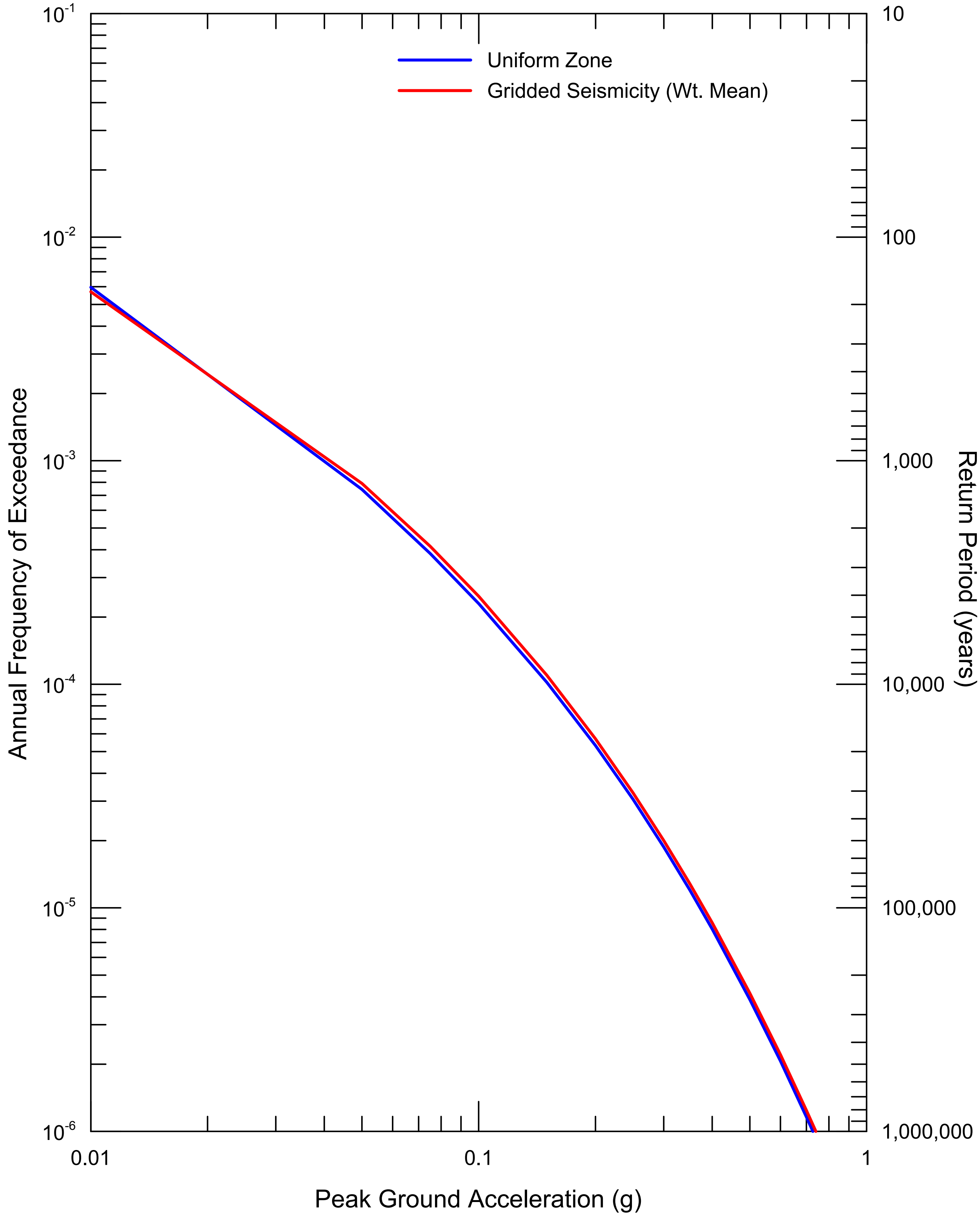

V_S30 = 700 m/s

Hazard Curves shown represent hazard with end branch weights of 1.0 (e.g. 100% SBR Uniform Background Seismicity)

Sensitivity of Mean Peak Horizontal Acceleration Hazard to Gridded and Uniform Background Seismicity for Pinal Schist and Gila Conglomerate Sites

RESOLUTION COPPER, NEAR WEST SITE

Lettis Consultants International, Inc. **Figure 45**

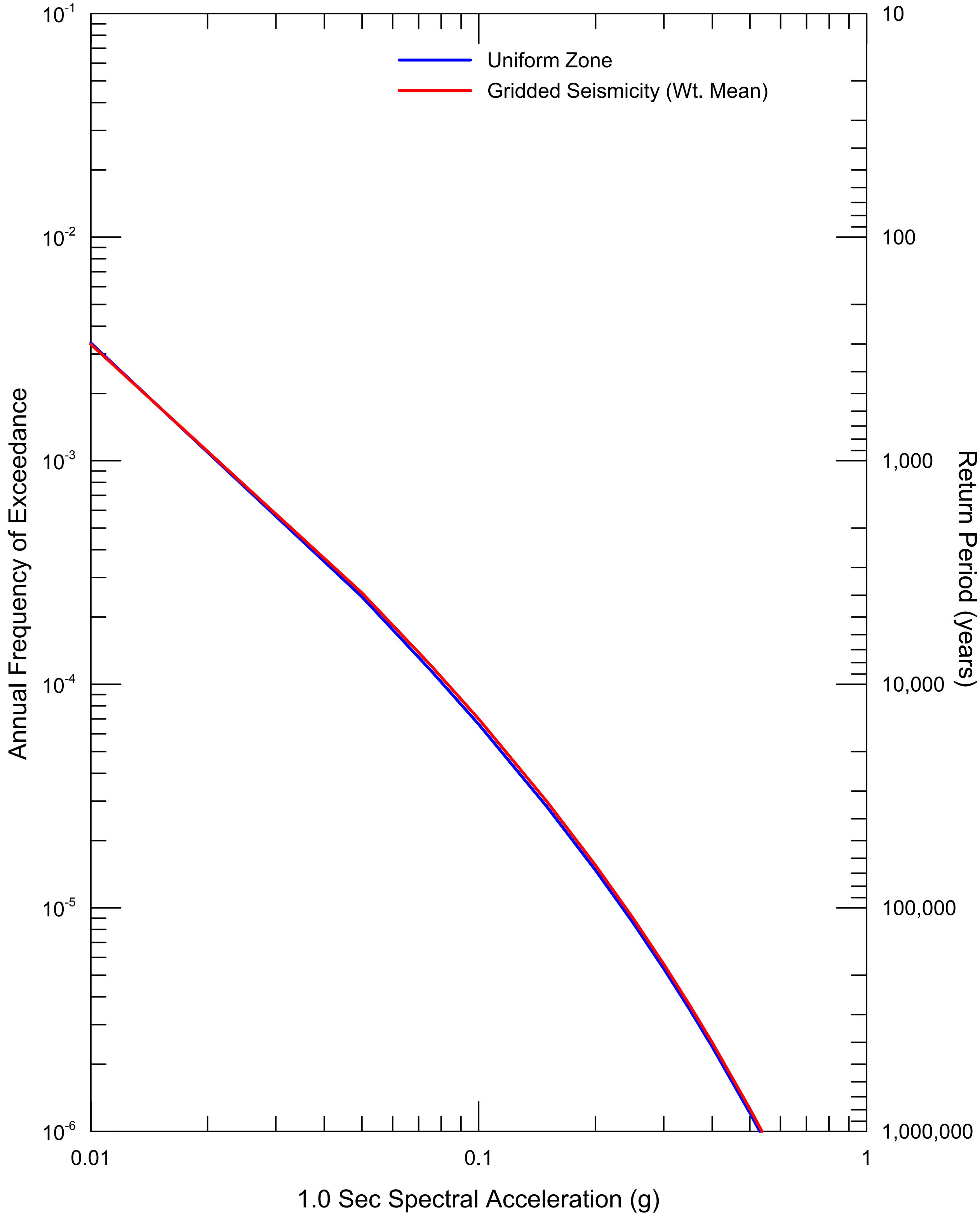

V_S30 = 700 m/s

Hazard Curves shown represent hazard
with end branch weights of 1.0
(e.g. 100% SBR Uniform Background Seismicity)

Sensitivity of Mean 1.0 Sec Horizontal Spectral Acceleration Hazard to Gridded and Uniform Background Seismicity for Pinal Schist and Gila Conglomerate Sites

RESOLUTION COPPER, NEAR WEST SITE

Lettis Consultants International, Inc. | **Figure 46**

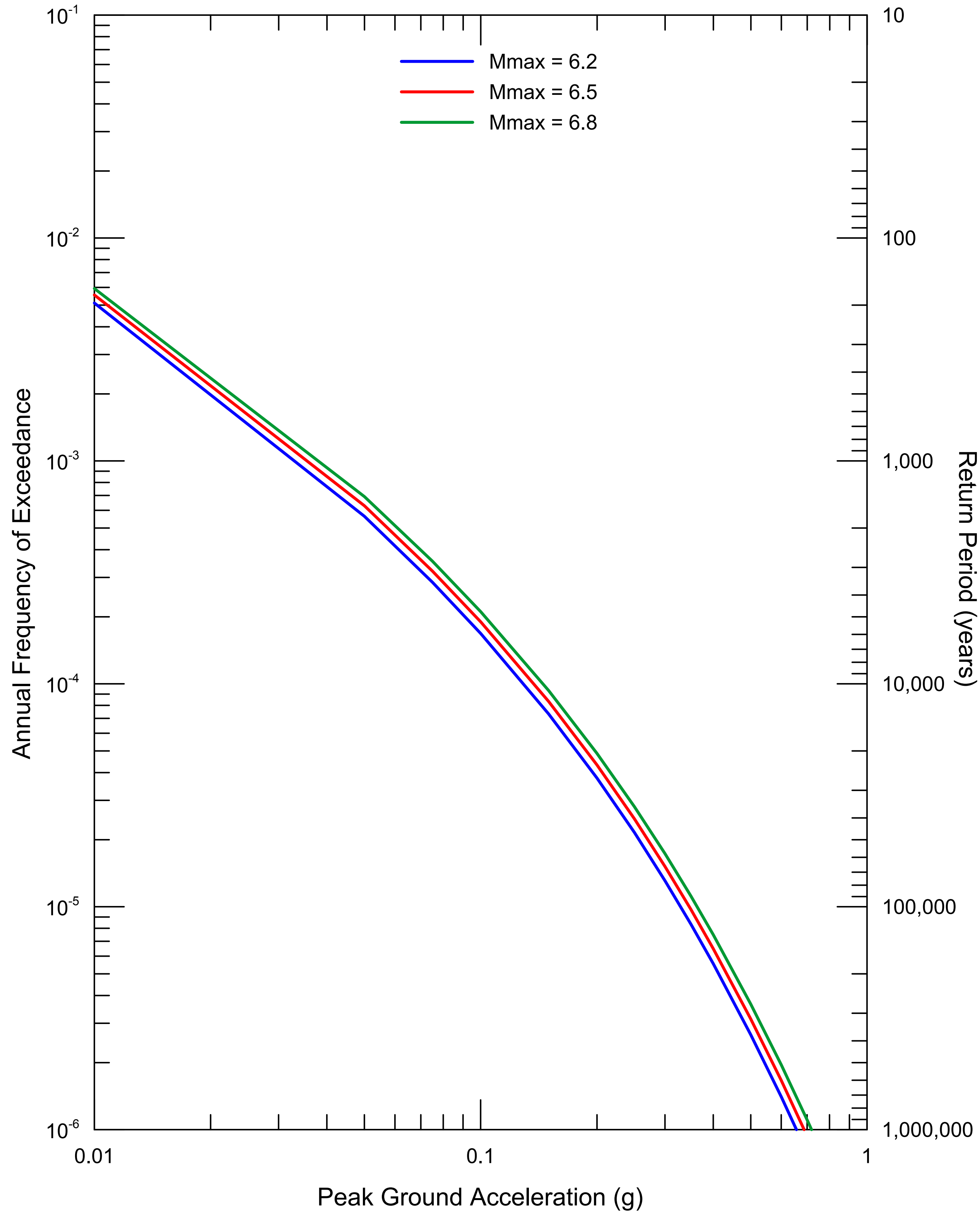

V_S30 = 700 m/s

Hazard Curves shown represent hazard
with end branch weights of 1.0
(e.g. 100% SBR Background Seismicity Mmax = 6.2)

Sensitivity of Mean Peak Horizontal Acceleration Hazard to Mmax for Background Seismicity for Pinal Schist and Gila Conglomerate Sites

RESOLUTION COPPER, NEAR WEST SITE

Lettis Consultants International, Inc.

Figure 47

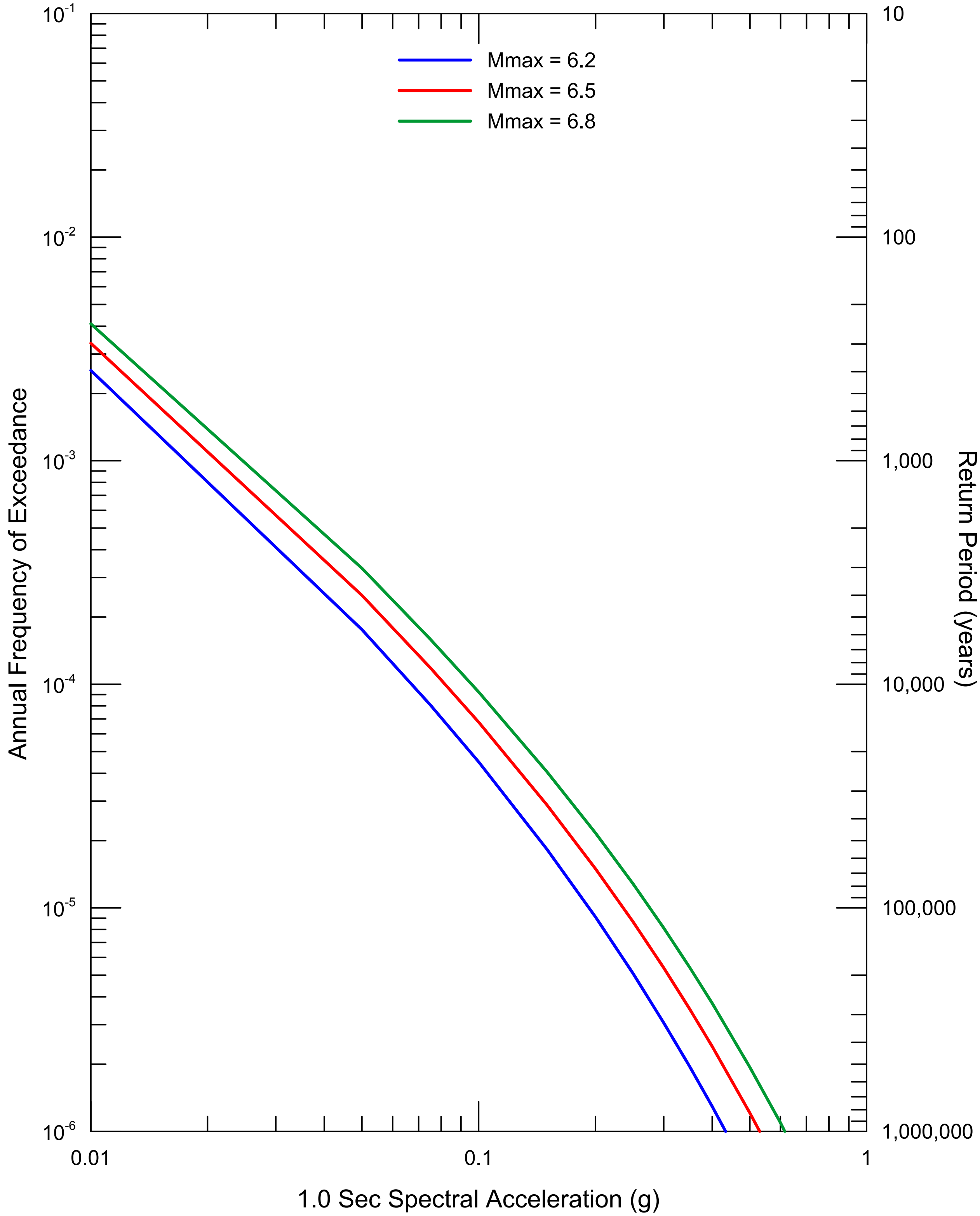

V_S30 = 700 m/s

Hazard Curves shown represent hazard with end branch weights of 1.0 (e.g. 100% SBR Background Seismicity Mmax = 6.2)

Sensitivity of Mean 1.0 Sec Horizontal Spectral Acceleration Hazard to Mmax for Background Seismicity for Pinal Schist and Gila Conglomerate Sites

RESOLUTION COPPER, NEAR WEST SITE

Lettis Consultants International, Inc.

Figure 48

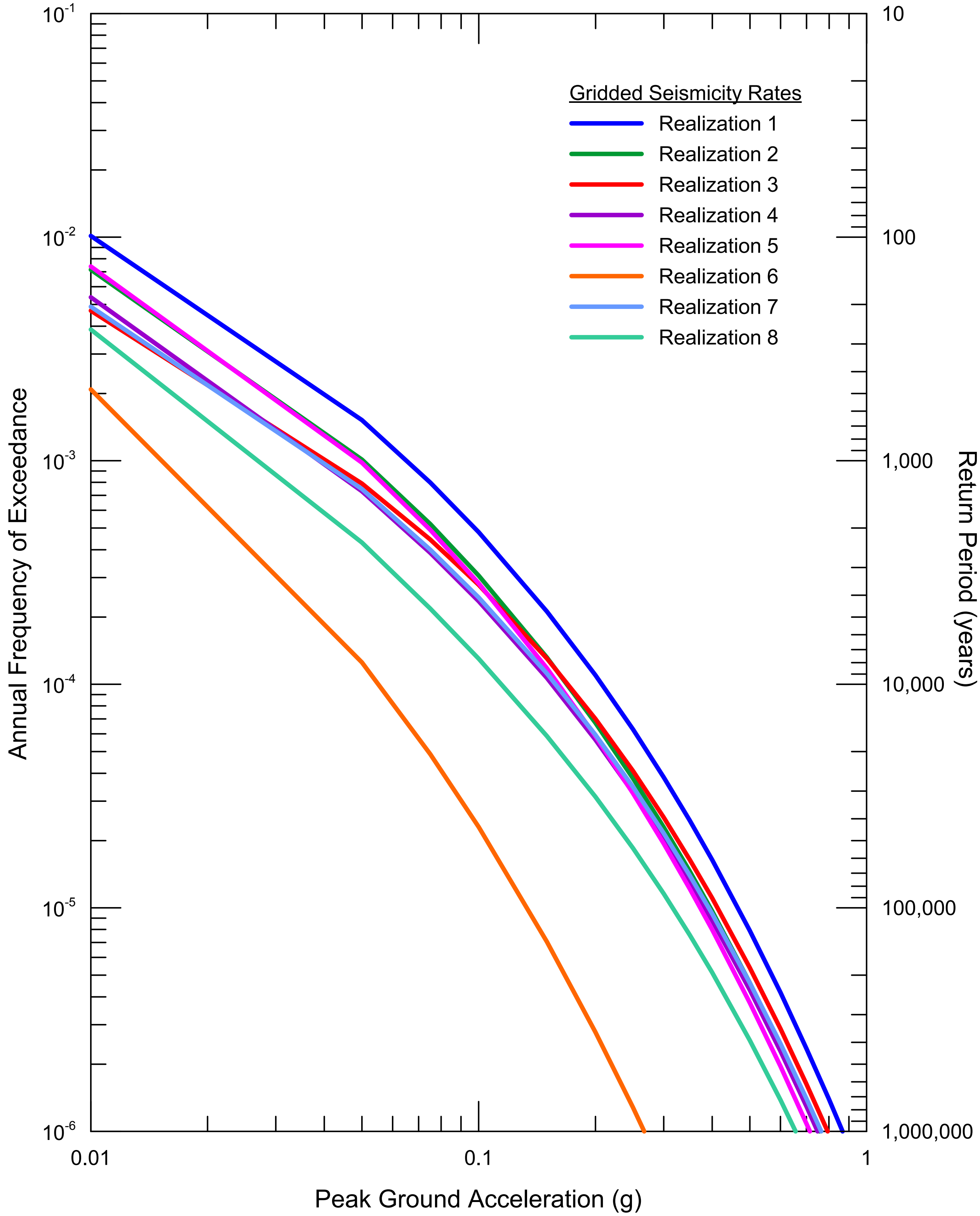

V_S30 = 700 m/s

Hazard Curves shown represent hazard
with end branch weights of 1.0
(e.g. 100% Gridded Seismicity Realization 1)

Sensitivity of Mean Peak Horizontal Acceleration Hazard to Gridded Seismicity Rate Realizations for Pinal Schist and Gila Conglomerate Sites

RESOLUTION COPPER, NEAR WEST SITE

Lettis Consultants International, Inc.	**Figure 49**

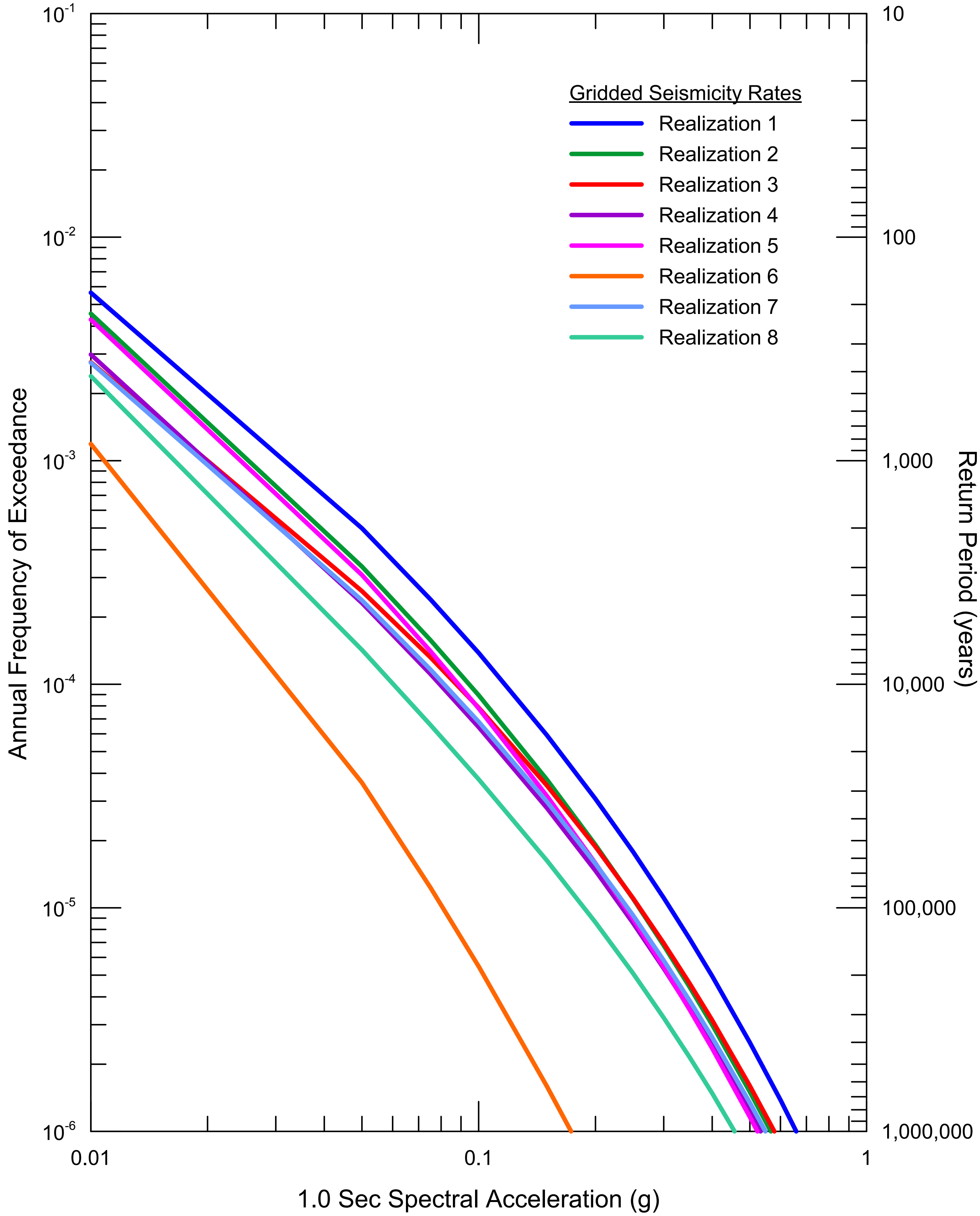

V_S30 = 700 m/s

Hazard Curves shown represent hazard
with end branch weights of 1.0
(e.g. 100% Gridded Seismicity Realization 1)

Sensitivity of Mean 1.0 Sec Horizontal Spectral Acceleration Hazard to Gridded Seismicity Rate Realizations for Pinal Schist and Gila Conglomerate Sites

RESOLUTION COPPER, NEAR WEST SITE

Lettis Consultants International, Inc. | **Figure 50**

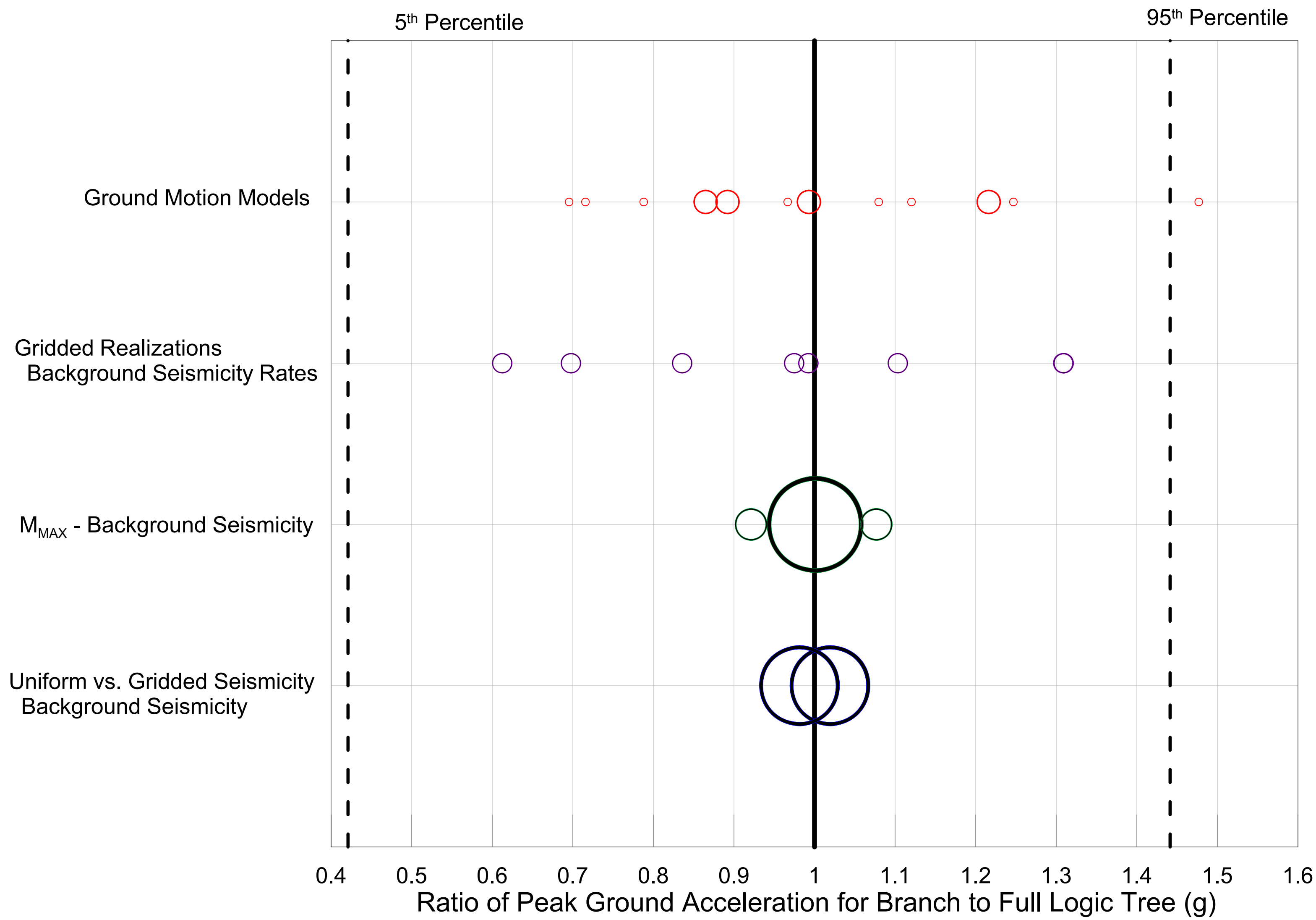

V_S30 = 700 m/sec

Symbol size proportional to logic tree branch weight.

Tornado Plot for Peak Ground Acceleration at 10,000-Year Return Period for Pinal Schist and Gila Conglomerate Sites

RESOLUTION COPPER, NEAR WEST SITE

Lettis Consultants International, Inc.

Figure 51

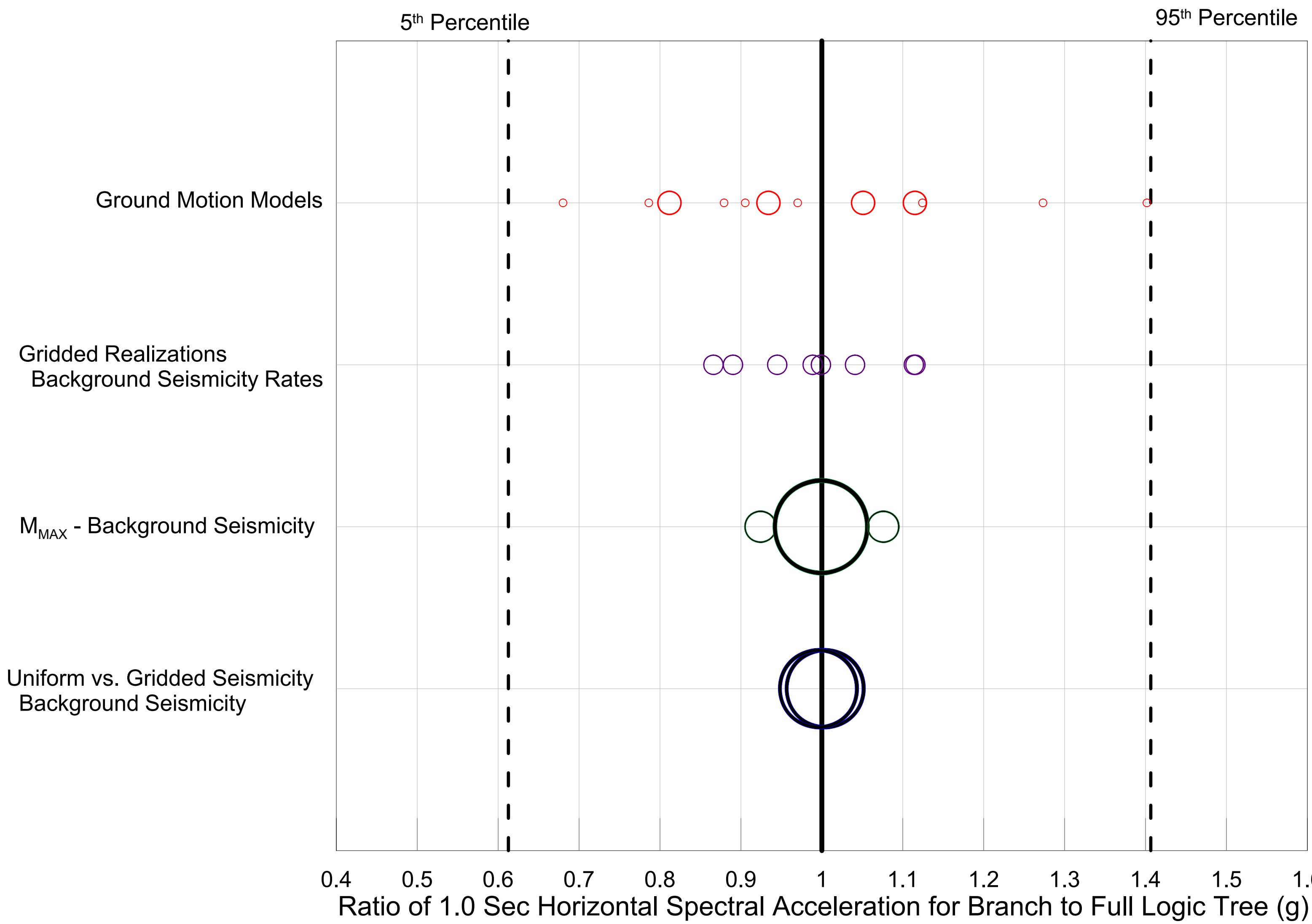

V_S30 = 700 m/sec

Symbol size proportional to logic tree branch weight.

Tornado Plot for 1.0 Sec Horizontal Spectral Acceleration at 10,000-Year Return Period for Pinal Schist and Gila Conglomerate Sites

RESOLUTION COPPER, NEAR WEST SITE

Lettis Consultants International, Inc. **Figure 52**

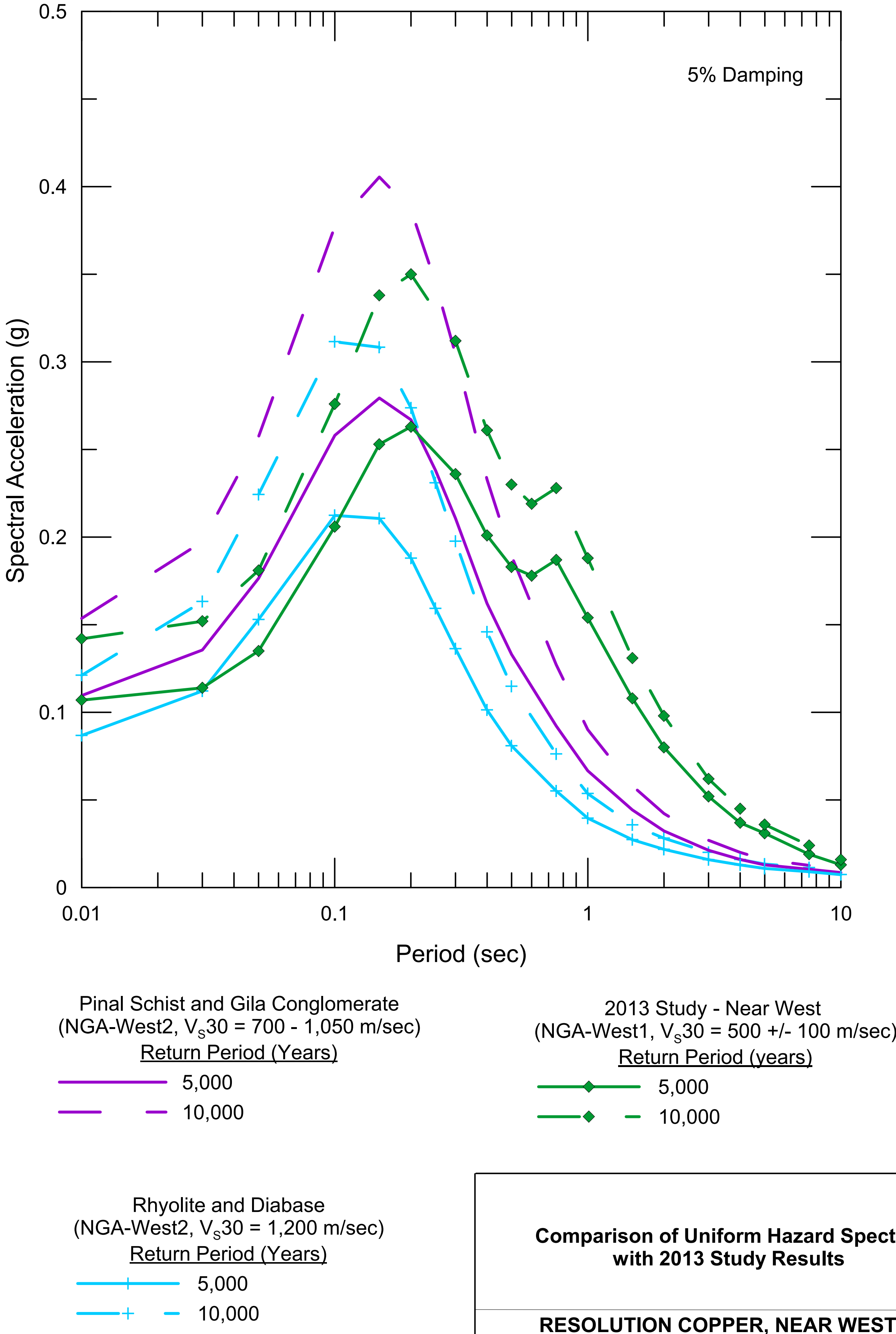

Comparison of Uniform Hazard Spectra with 2013 Study Results

RESOLUTION COPPER, NEAR WEST SITE

Lettis Consultants International, Inc. | **Figure 53**

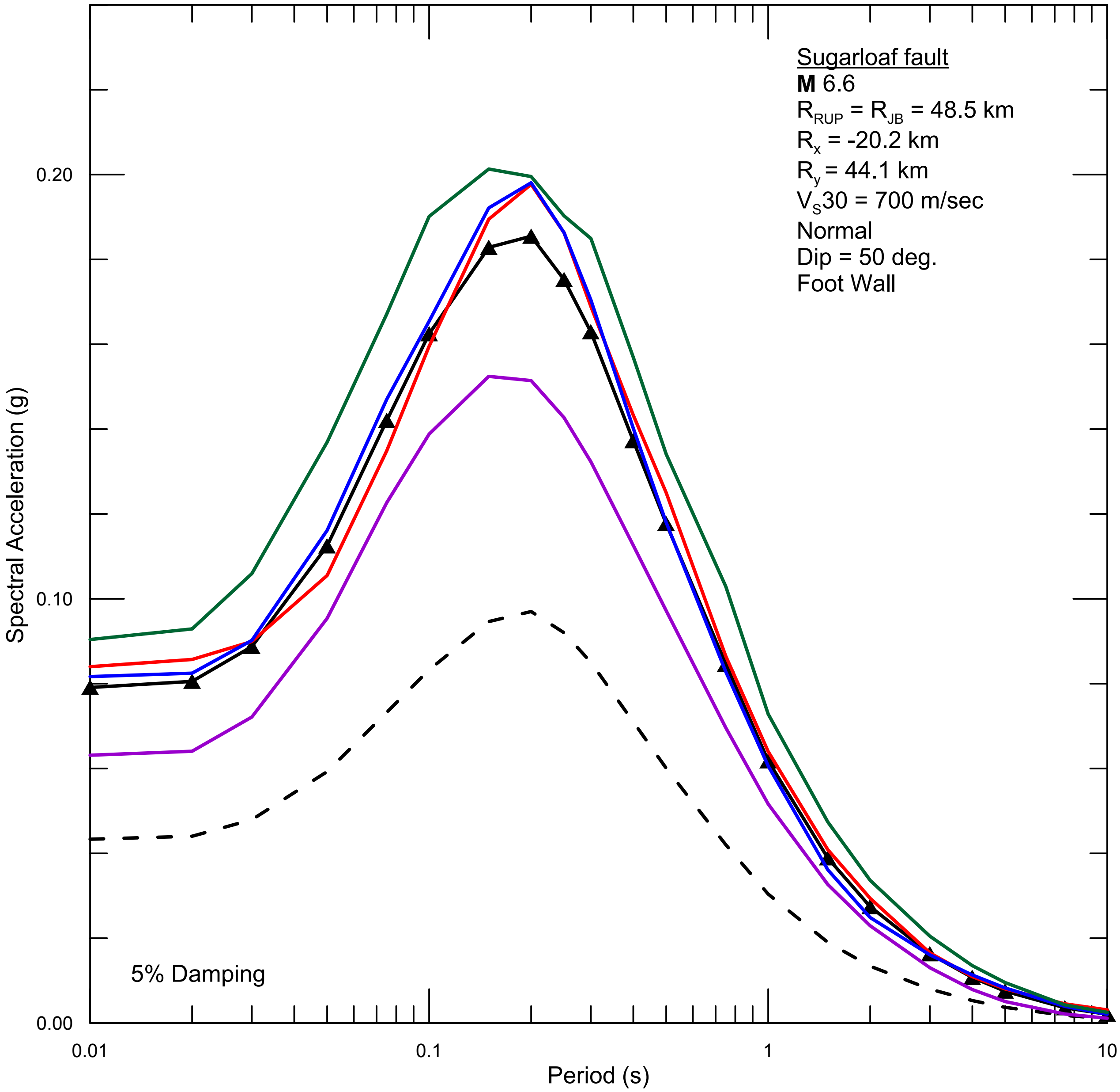

Geometric Mean

Median

84th Percentile

84th Percentile Ground Motion Models

Abrahamson *et al.* (2016)

Boore *et al.* (2016)

Campbell and Bozorgnia (2016)

Chiou and Youngs (2016)

Sensitivity of 84th Percentile Deterministic Spectrum for M 6.6 Sugarloaf Event to Ground Motion Models (V_S30 = 700 m/sec) for Pinal Schist and Gila Conglomerate Sites

RESOLUTION COPPER, NEAR WEST SITE

Lettis Consultants International, Inc.

Figure 54

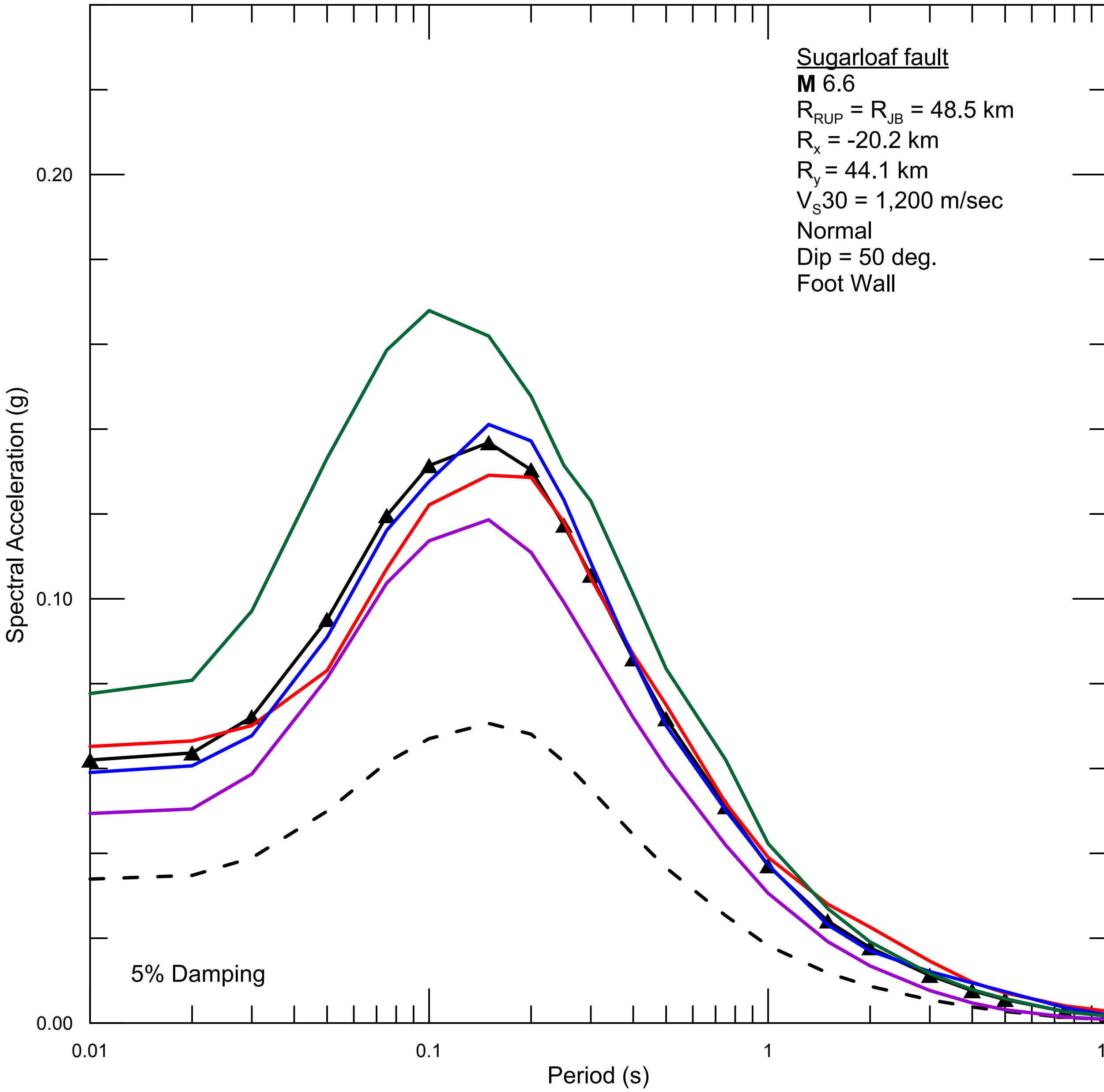

Geometric Mean

Median

84th Percentile

84th Percentile Ground Motion Models

Abrahamson *et al.* (2016)

Boore *et al.* (2016)

Campbell and Bozorgnia (2016)

Chiou and Youngs (2016)

Sensitivity of 84th Percentile Deterministic Spectrum for M 6.6 Sugarloaf Event to Ground Motion Models (V_S30 = 1,200 m/sec) for Rhyolite and Diabase Sites

RESOLUTION COPPER, NEAR WEST SITE

Lettis Consultants International, Inc.

Figure 55

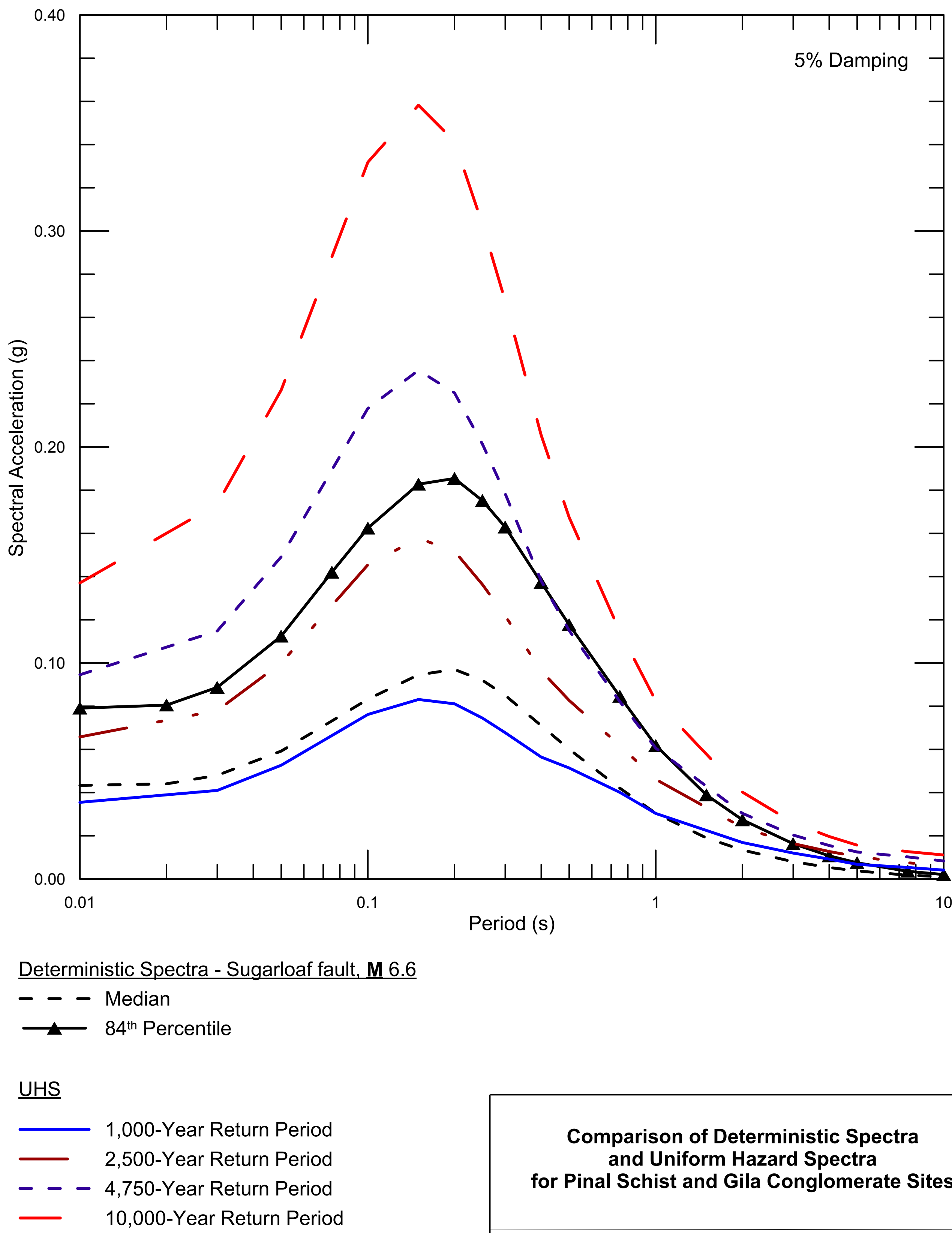

Comparison of Deterministic Spectra and Uniform Hazard Spectra for Pinal Schist and Gila Conglomerate Sites

RESOLUTION COPPER, NEAR WEST SITE

Lettis Consultants International, Inc.

Figure 56

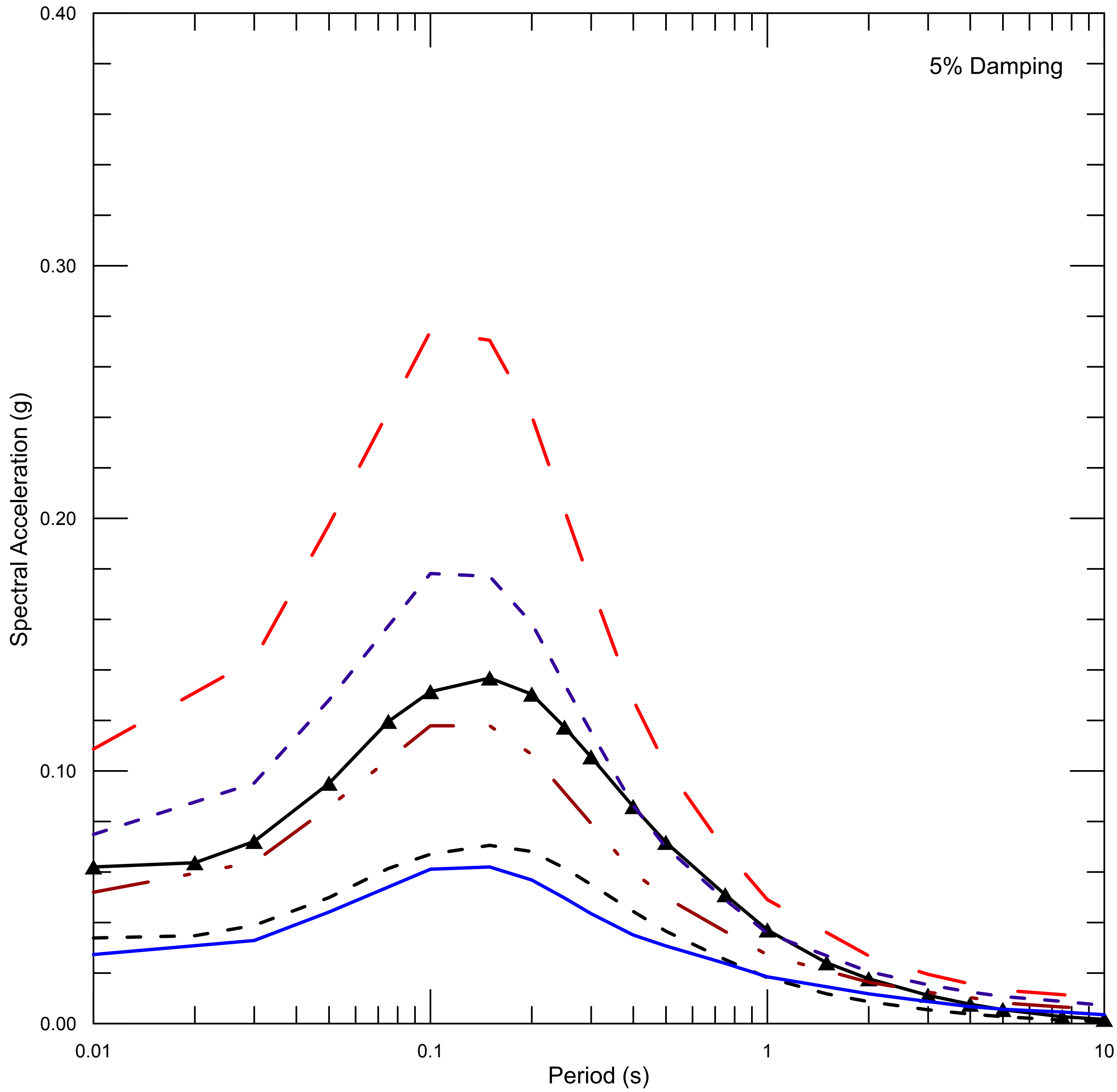

Deterministic Spectra - Sugarloaf fault, **M** 6.6

Median

84th Percentile

UHS

1,000-Year Return Period

2,500-Year Return Period

4,750-Year Return Period

10,000-Year Return Period

Comparison of Deterministic Spectra and Uniform Hazard Spectra for Rhyolite and Diabase Sites

RESOLUTION COPPER, NEAR WEST SITE

Lettis Consultants International, Inc.

Figure 57

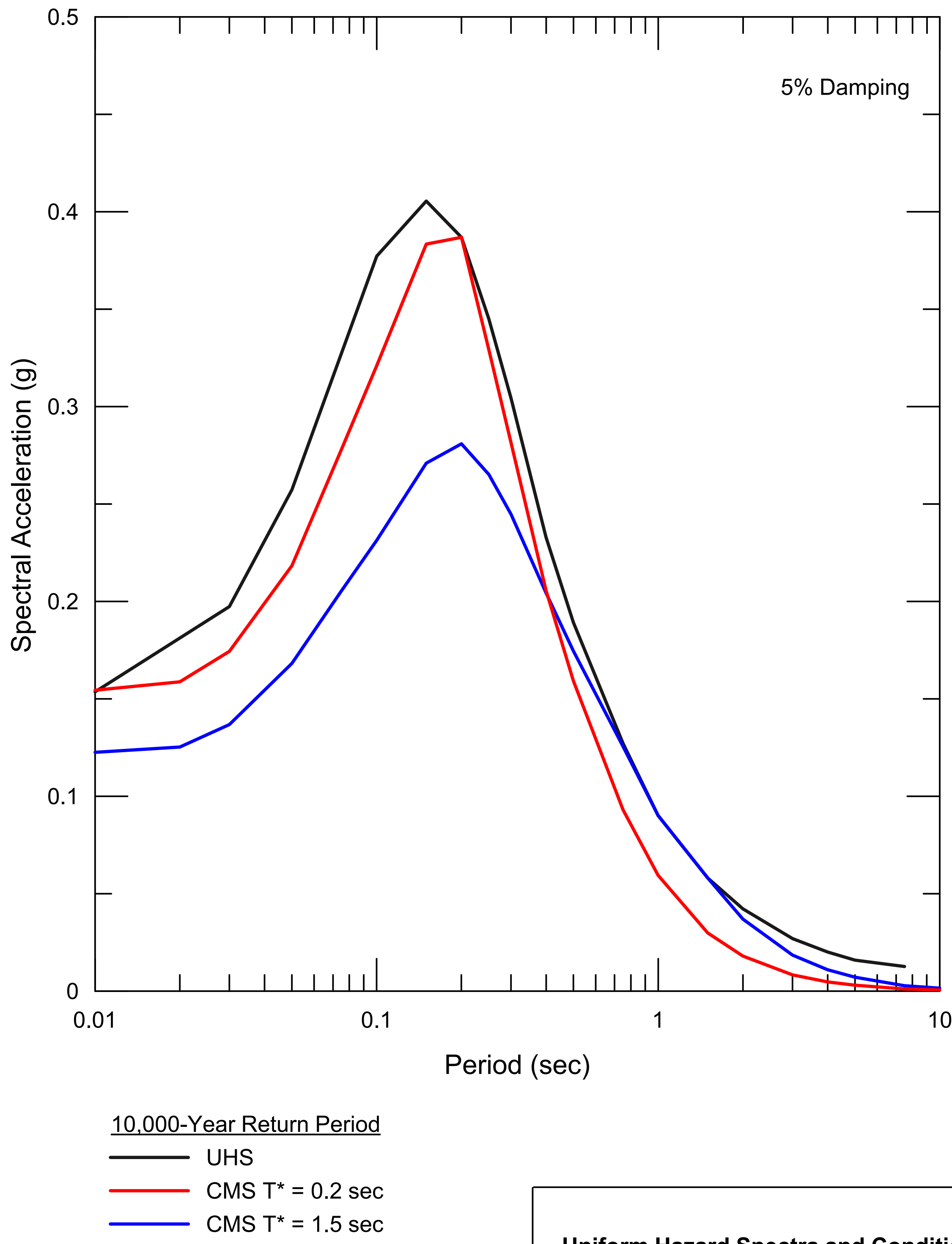

Uniform Hazard Spectra and Conditional Mean Spectra at the 10,000-Year Return Period for Pinal Schist and Gila Conglomerate Sites

RESOLUTION COPPER, NEAR WEST SITE

Lettis Consultants International, Inc. | **Figure 58**

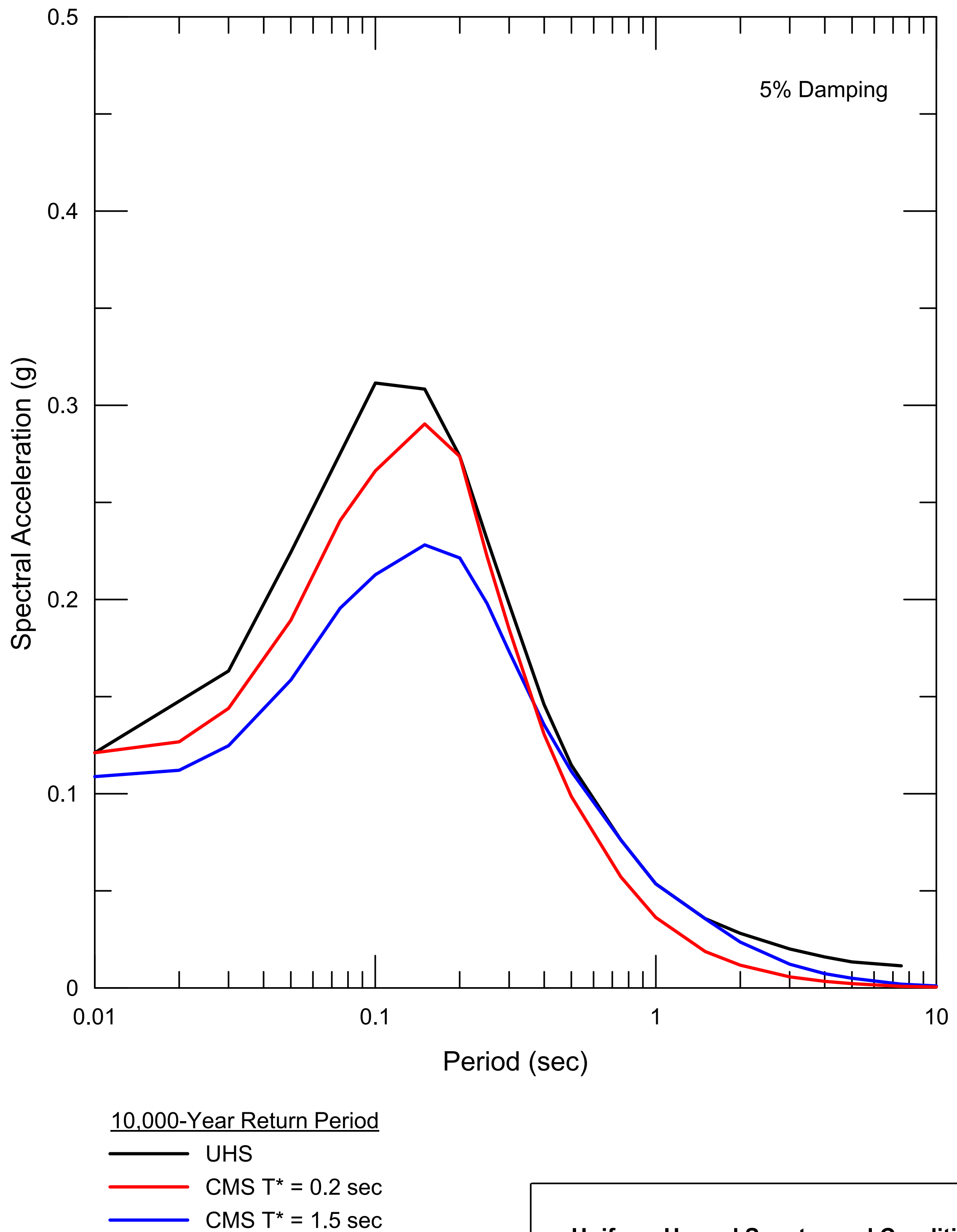

Uniform Hazard Spectra and Conditional Mean Spectra at the 10,000-Year Return Period for Rhyolite and Diabase Sites

RESOLUTION COPPER, NEAR WEST SITE

Lettis Consultants International, Inc. | **Figure 59**

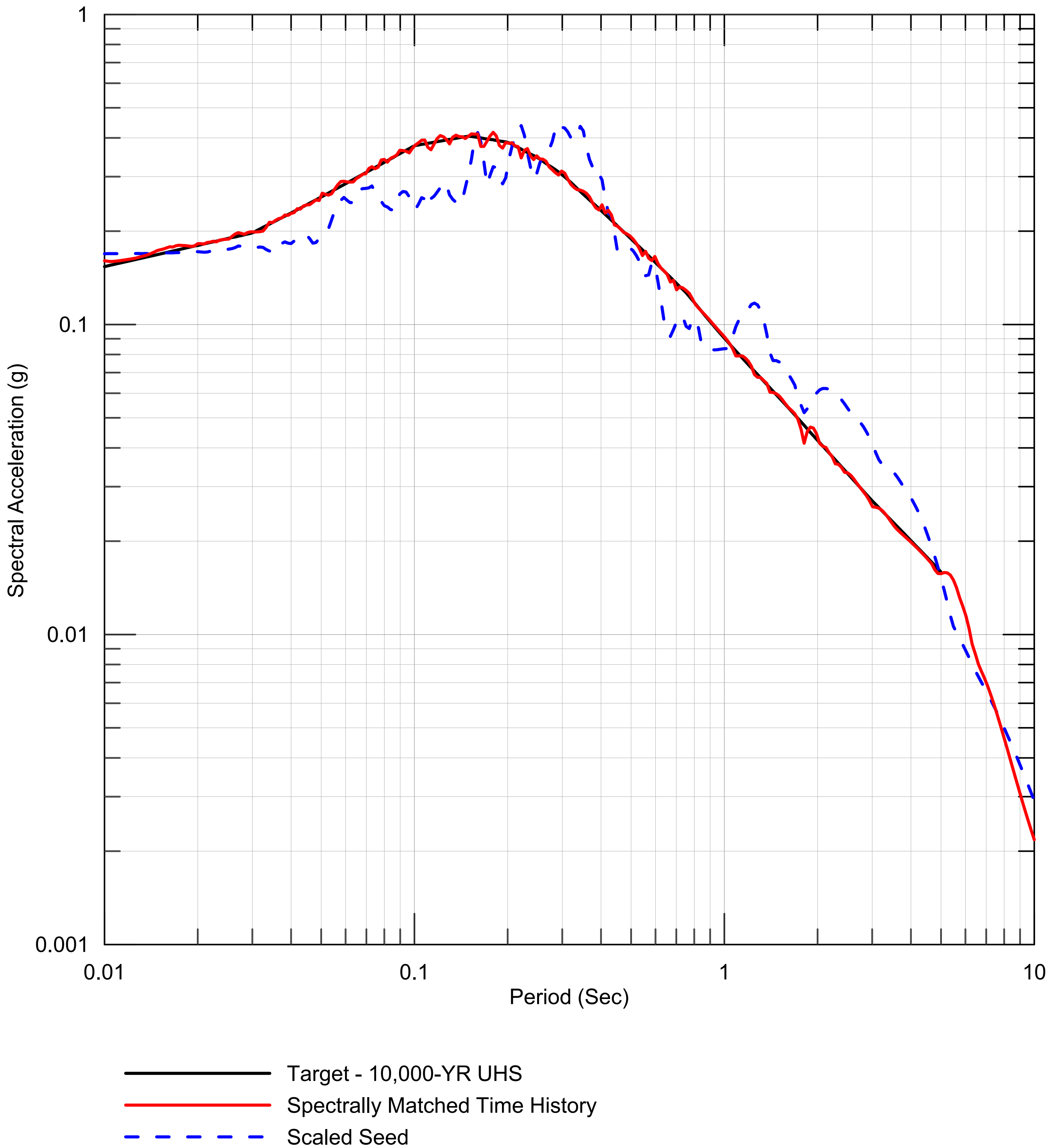

SEED: PEER RSN 238

Response Spectra for Time History Spectrally-Matched to 10,000-Year Return Period Horizontal UHS, Pinal Schist and Gila Conglomerate Sites 1980 Mammoth Lakes-03 - Long Valley Dam (L Abut) (090)

RESOLUTION COPPER, NEAR WEST SITE

Lettis Consultants International, Inc.

Figure 60

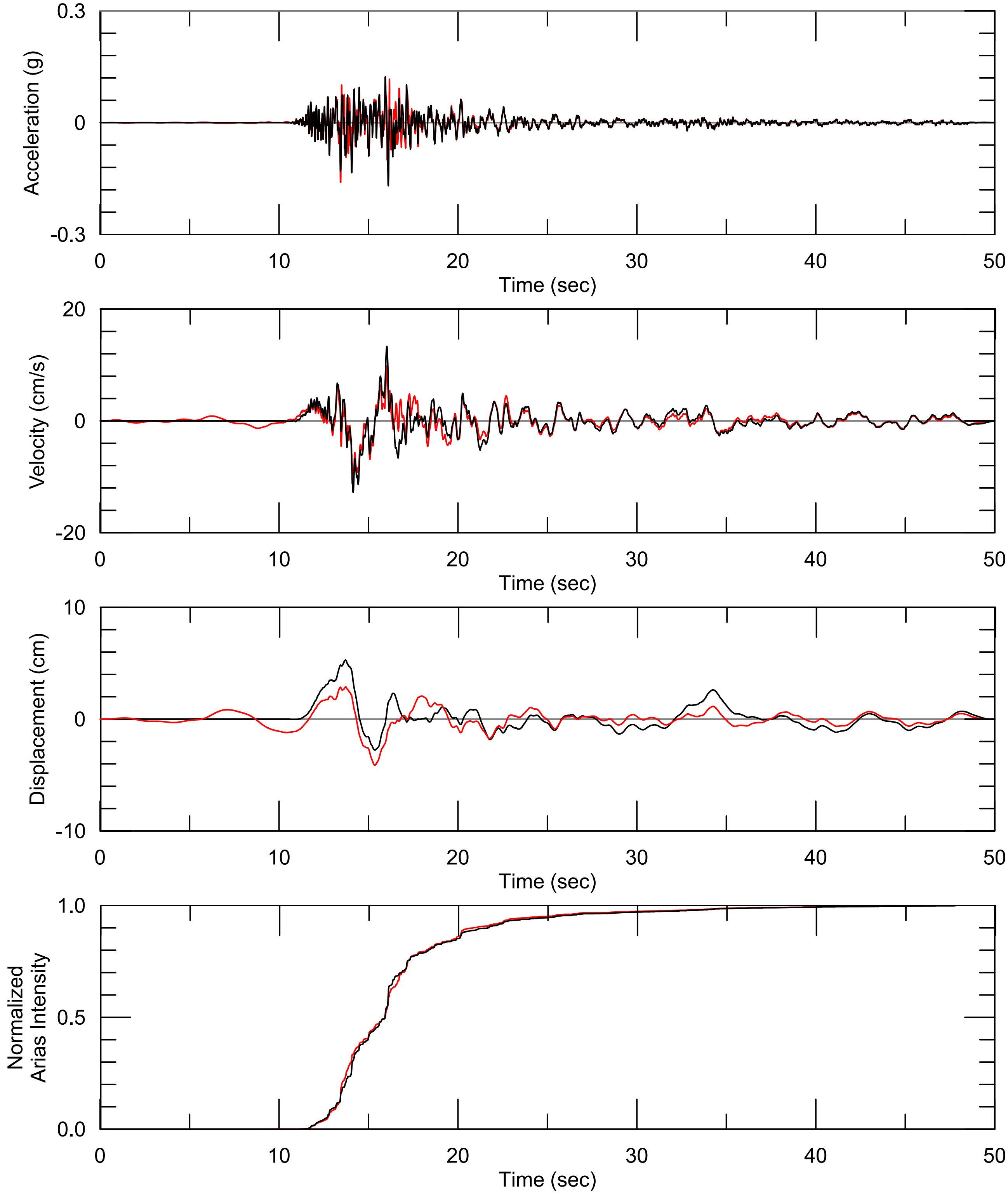

Spectrally Matched Motion

Scaled Seed Time History

Time History Spectrally-Matched to
10,000-Year Return Period Horizontal UHS,
Pinal Schist and Gila Conglomerate Sites
1980 Mammoth Lakes-03 - Long Valley Dam (L Abut) (090)

RESOLUTION COPPER, NEAR WEST SITE

Lettis Consultants International, Inc.

Figure 61

SEED: PEER RSN 238

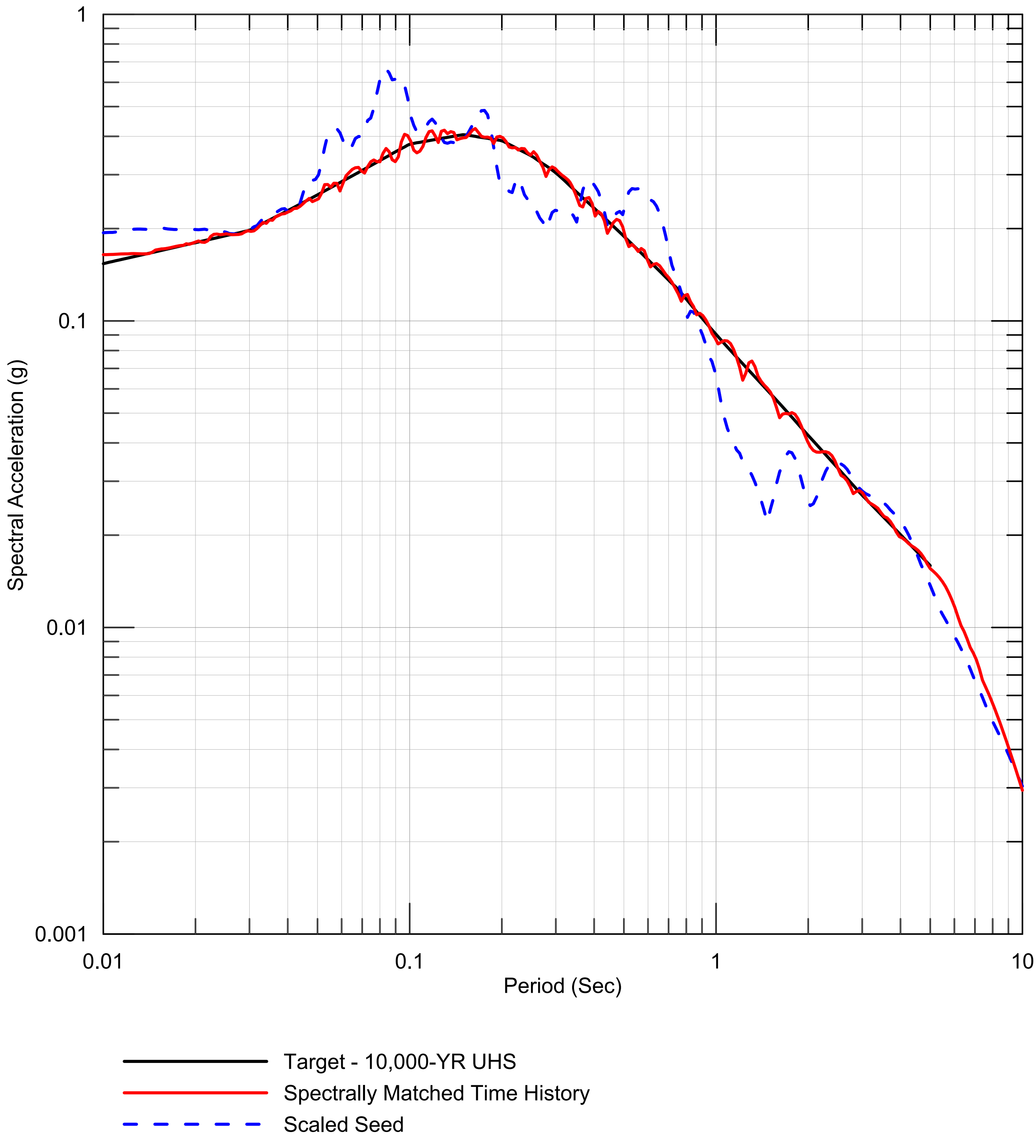

SEED: PEER RSN 318

Response Spectra for Time History Spectrally-Matched to 10,000-Year Return Period Horizontal UHS, Pinal Schist and Gila Conglomerate Sites 1981 Westmorland - Superstition Mtn Camera (045)

RESOLUTION COPPER, NEAR WEST SITE

Lettis Consultants International, Inc.

Figure 62

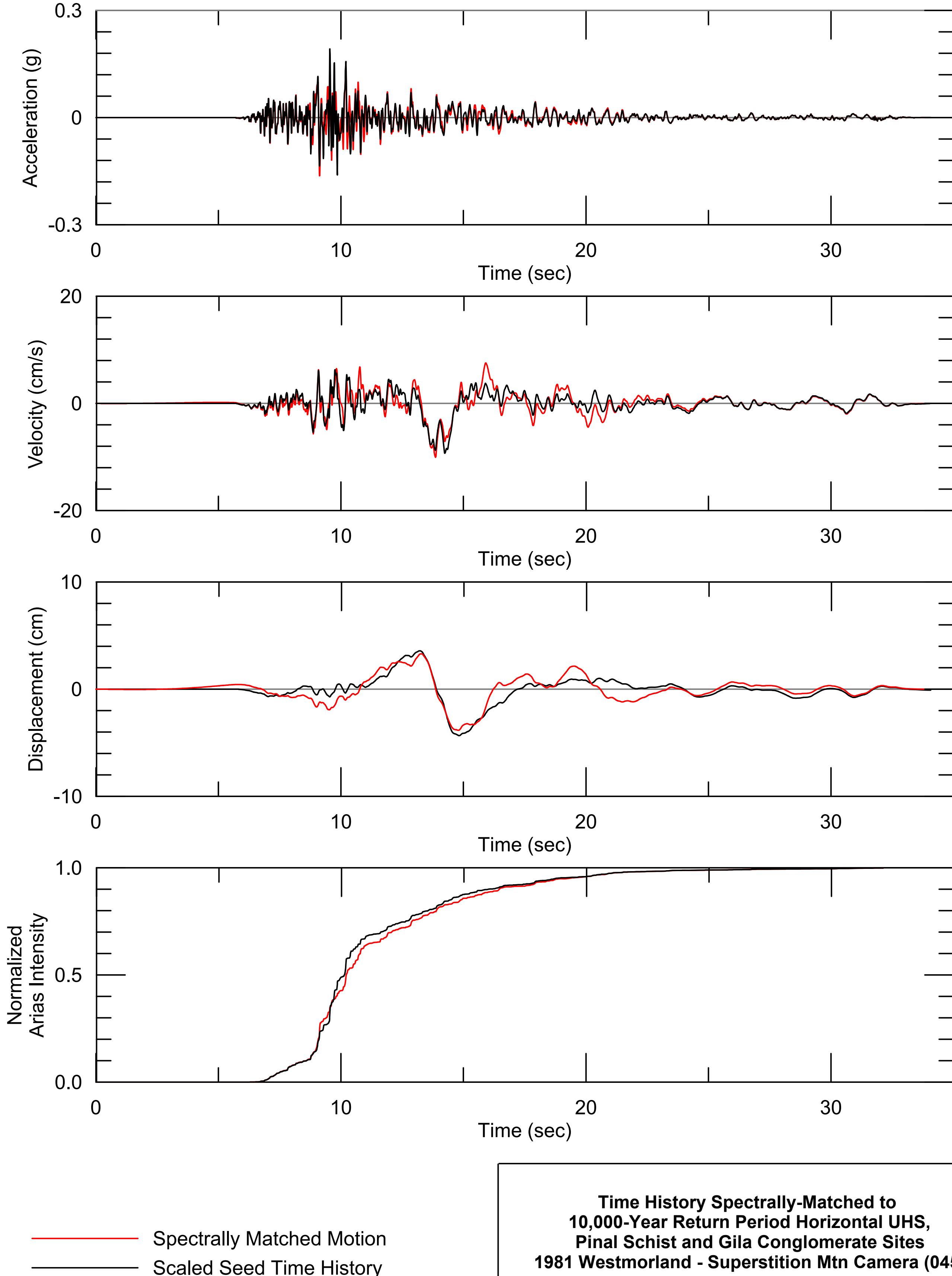

SEED: PEER RSN 318

Time History Spectrally-Matched to 10,000-Year Return Period Horizontal UHS, Pinal Schist and Gila Conglomerate Sites 1981 Westmorland - Superstition Mtn Camera (045)

RESOLUTION COPPER, NEAR WEST SITE

Lettis Consultants International, Inc.

Figure 63

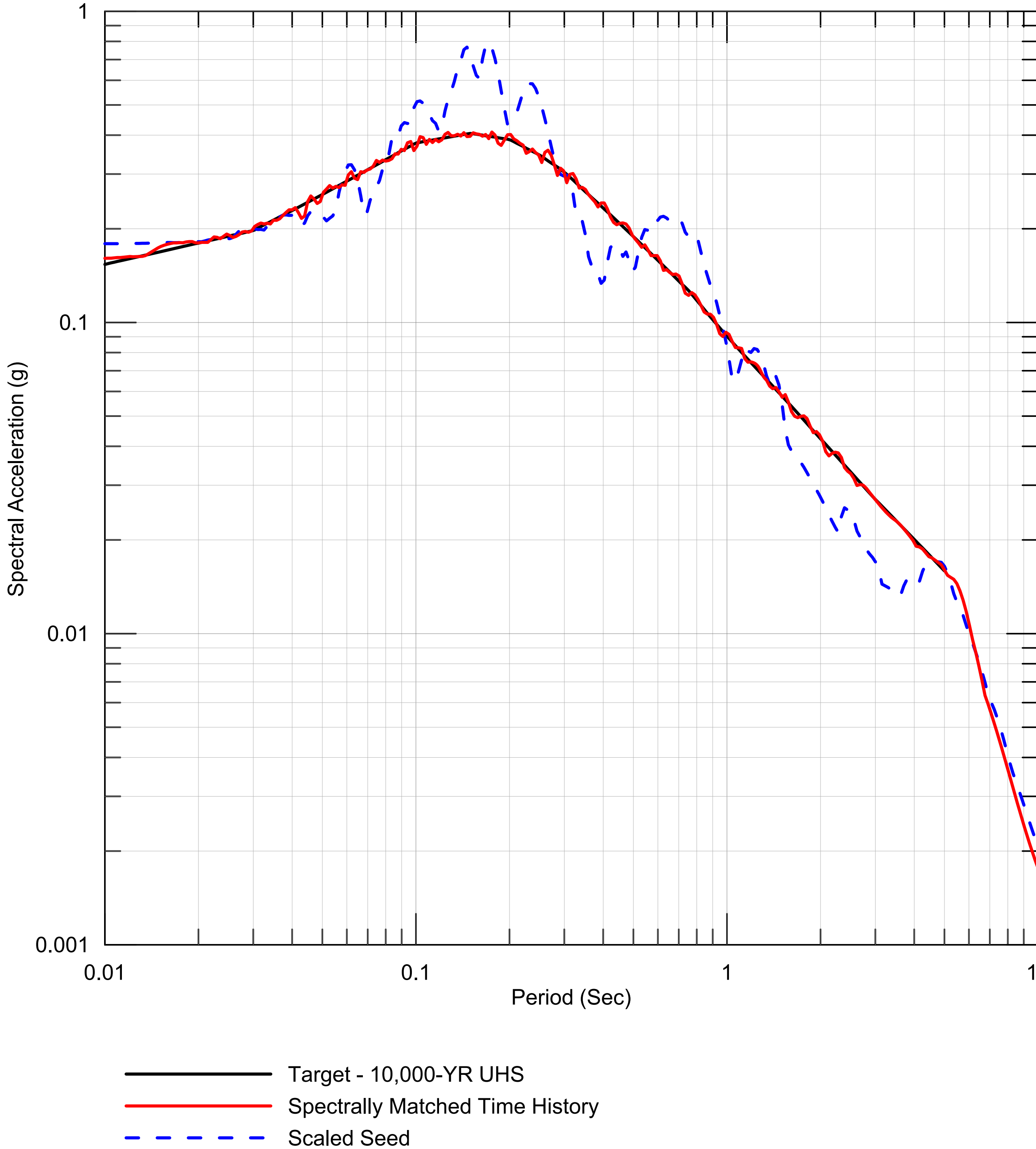

Response Spectra for Time History Spectrally-Matched to 10,000-Year Return Period Horizontal UHS, Pinal Schist and Gila Conglomerate Sites 1999 Chi-Chi,Taiwan-04 - TCU071 (E)

RESOLUTION COPPER, NEAR WEST SITE

Lettis Consultants International, Inc.

Figure 64

SEED: PEER RSN 2622

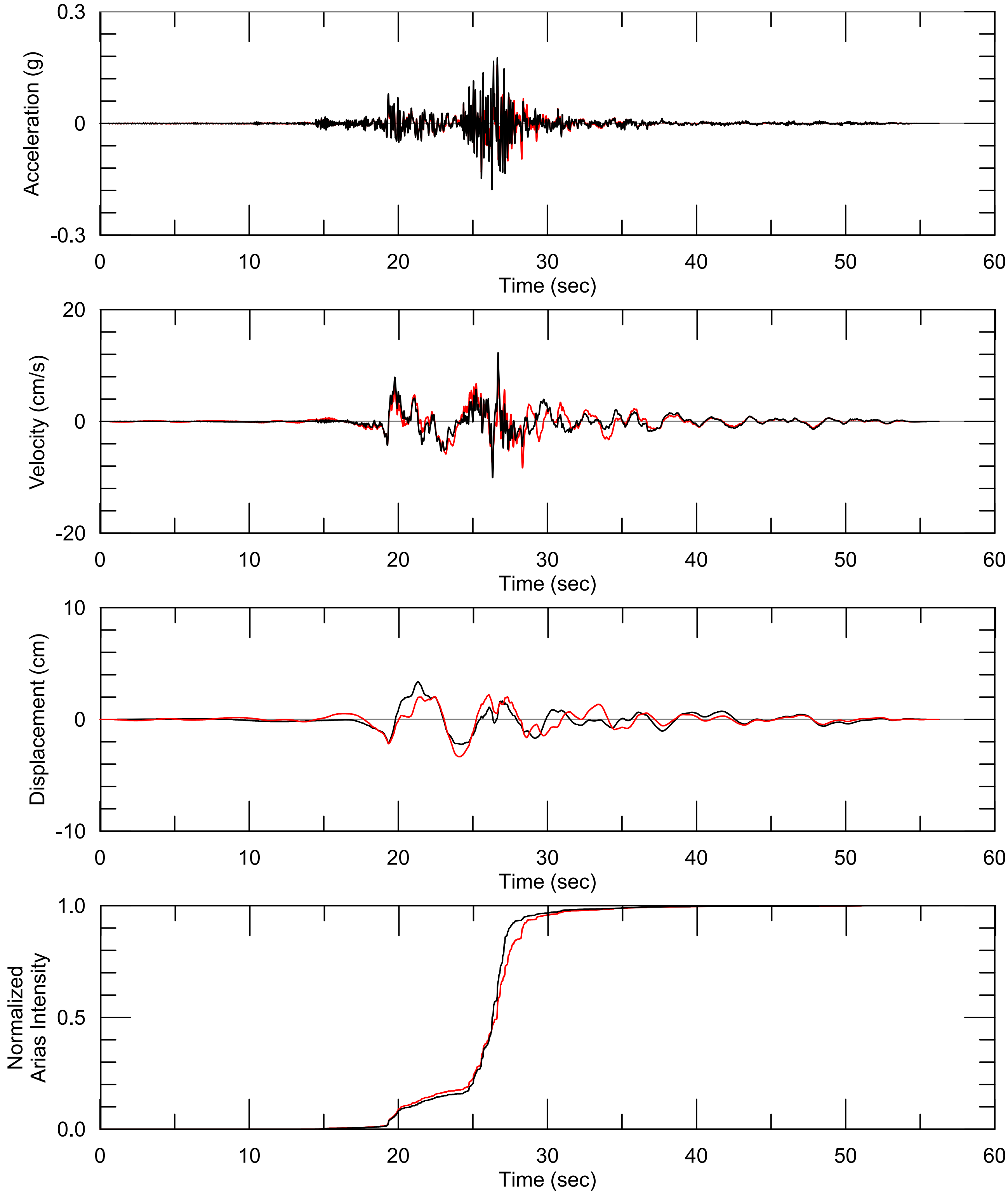

Spectrally Matched Motion
Scaled Seed Time History

SEED: PEER RSN 2622

Time History Spectrally-Matched to
10,000-Year Return Period Horizontal UHS,
Pinal Schist and Gila Conglomerate Sites
1999 Chi-Chi,Taiwan-04 - TCU071 (E)

RESOLUTION COPPER, NEAR WEST SITE

Lettis Consultants International, Inc.

Figure
65

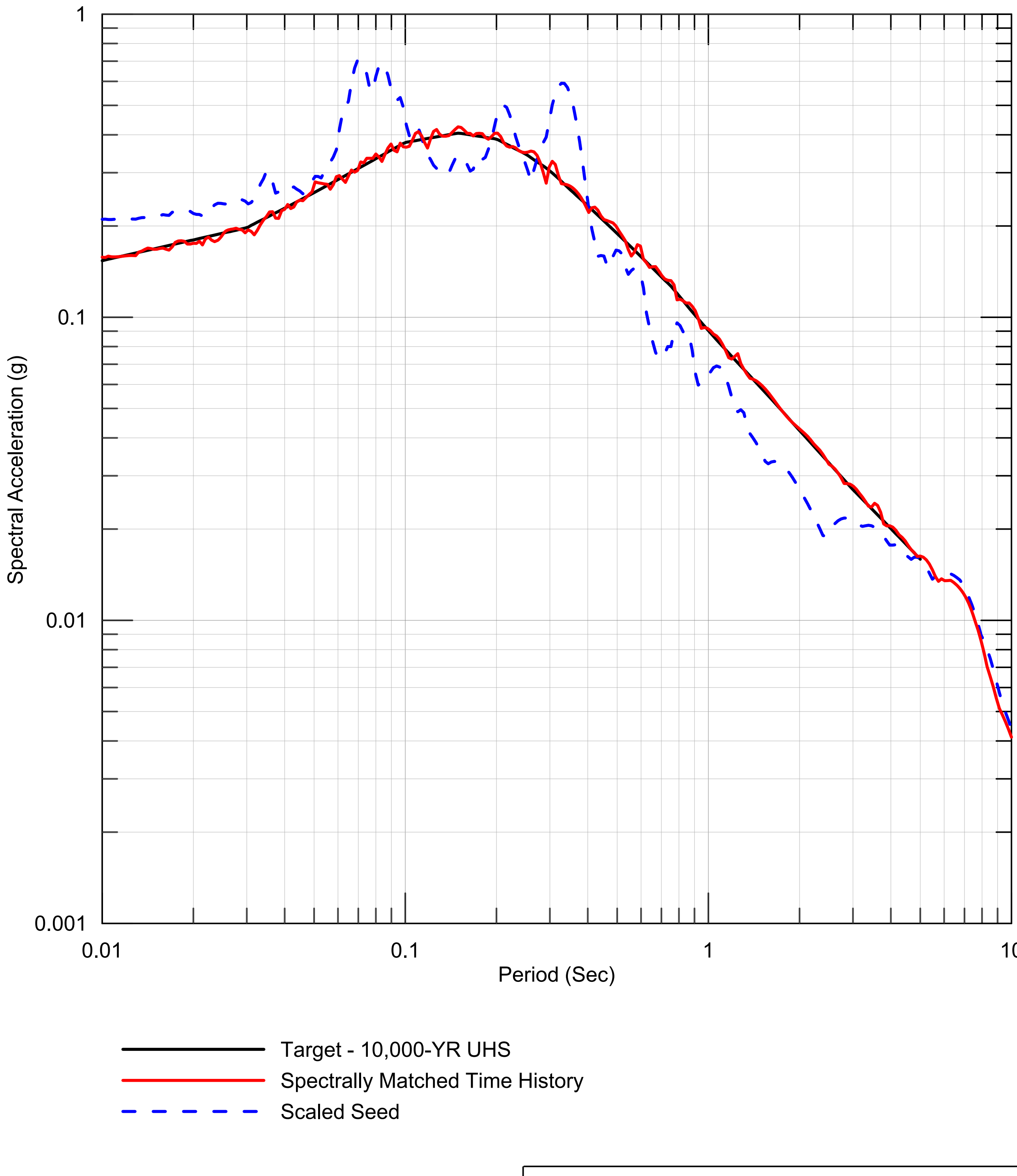

SEED: PEER RSN 4125

Response Spectra for Time History Spectrally-Matched to 10,000-Year Return Period Horizontal UHS, Pinal Schist and Gila Conglomerate Sites 2004 Parkfield-02 - Parkfield-Gold Hill 6W (360)

RESOLUTION COPPER, NEAR WEST SITE

Lettis Consultants International, Inc.

Figure 66

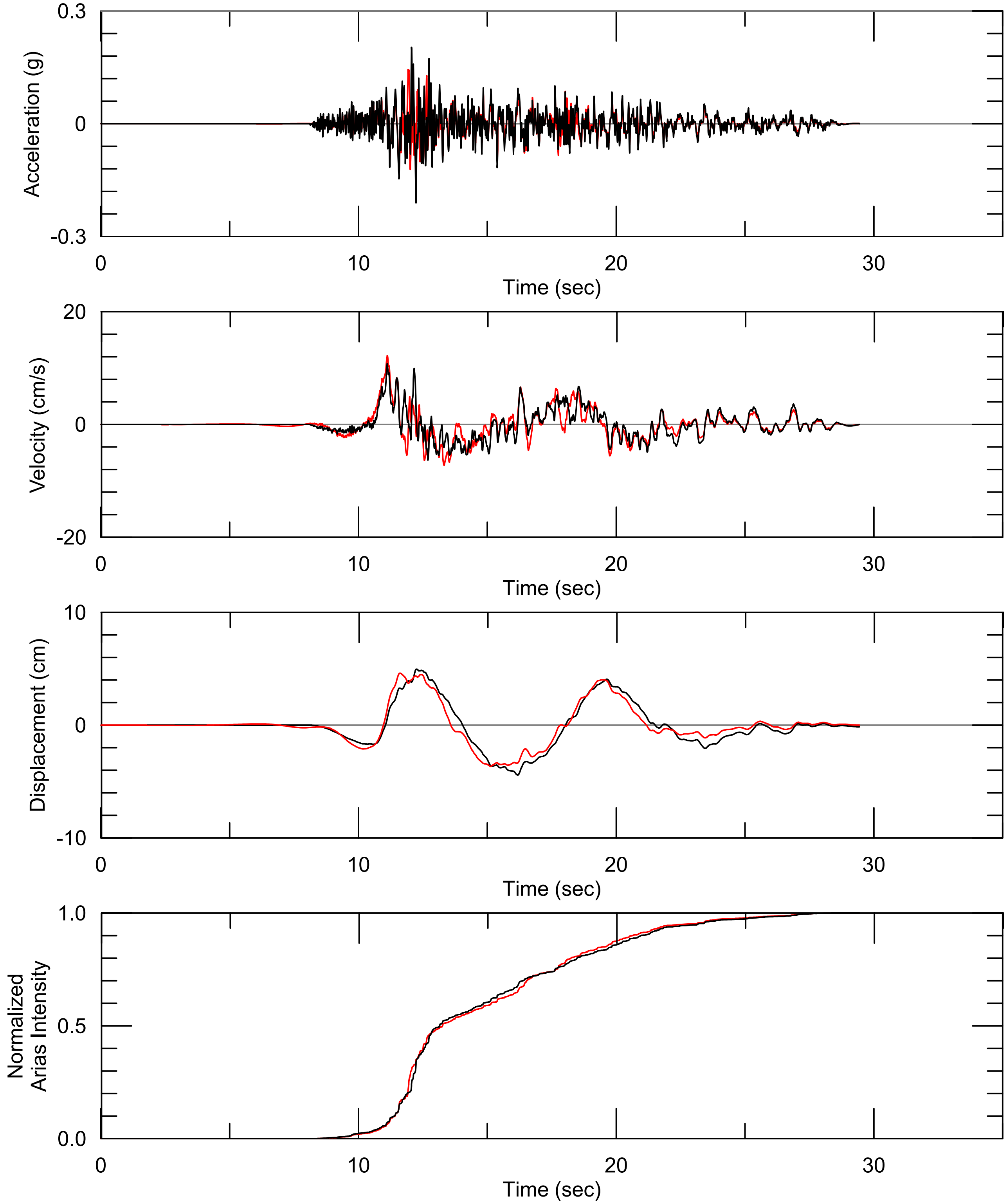

SEED: PEER RSN 4125

Time History Spectrally-Matched to 10,000-Year Return Period Horizontal UHS, Pinal Schist and Gila Conglomerate Sites 2004 Parkfield-02 - Parkfield-Gold Hill 6W (360)

RESOLUTION COPPER, NEAR WEST SITE

Lettis Consultants International, Inc.

Figure 67

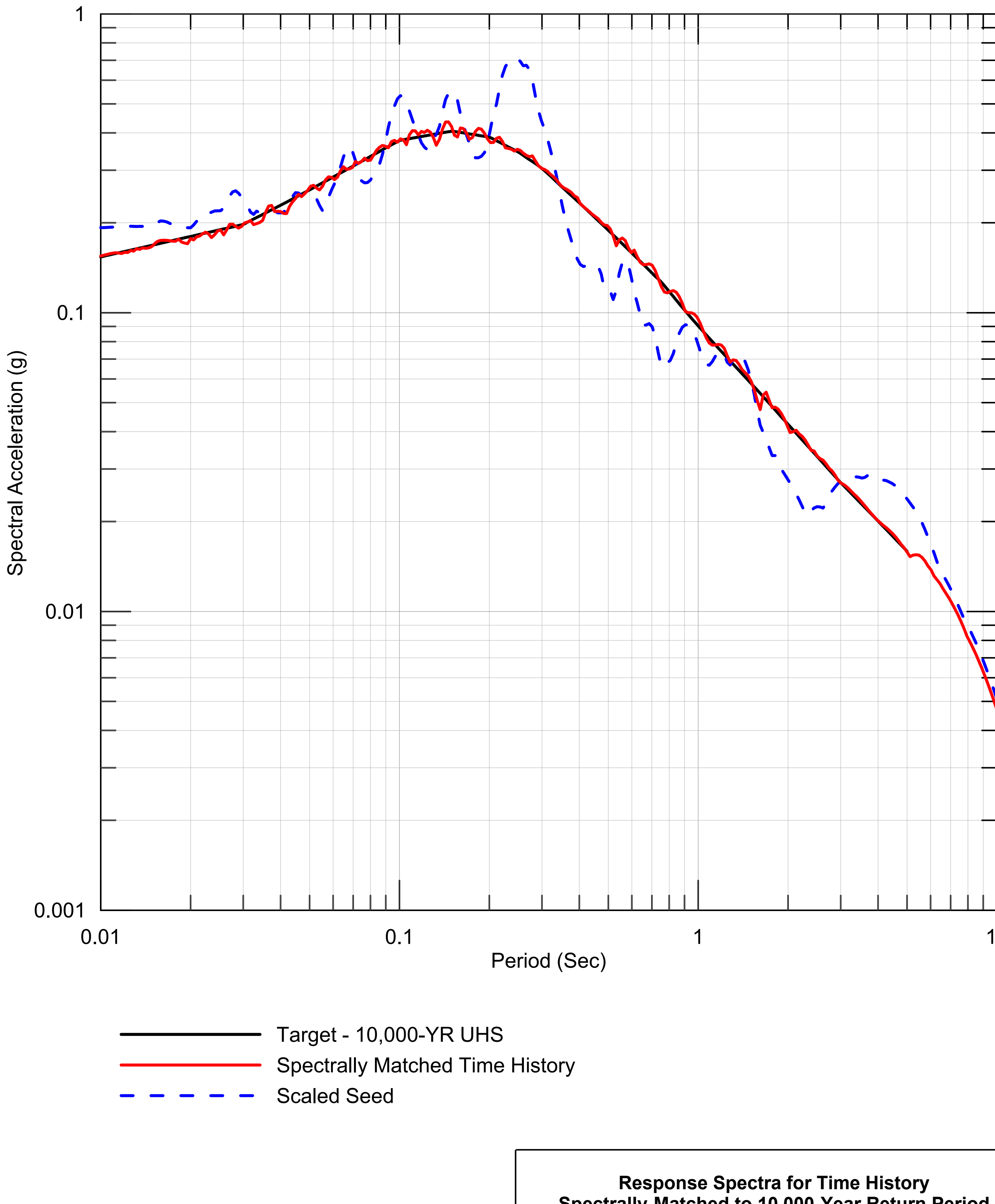

SEED: PEER RSN 4472

Response Spectra for Time History Spectrally-Matched to 10,000-Year Return Period Horizontal UHS, Pinal Schist and Gila Conglomerate Sites 2009 L'Aquila, Italy - Celano (XTE)

RESOLUTION COPPER, NEAR WEST SITE

Lettis Consultants International, Inc.

Figure 68

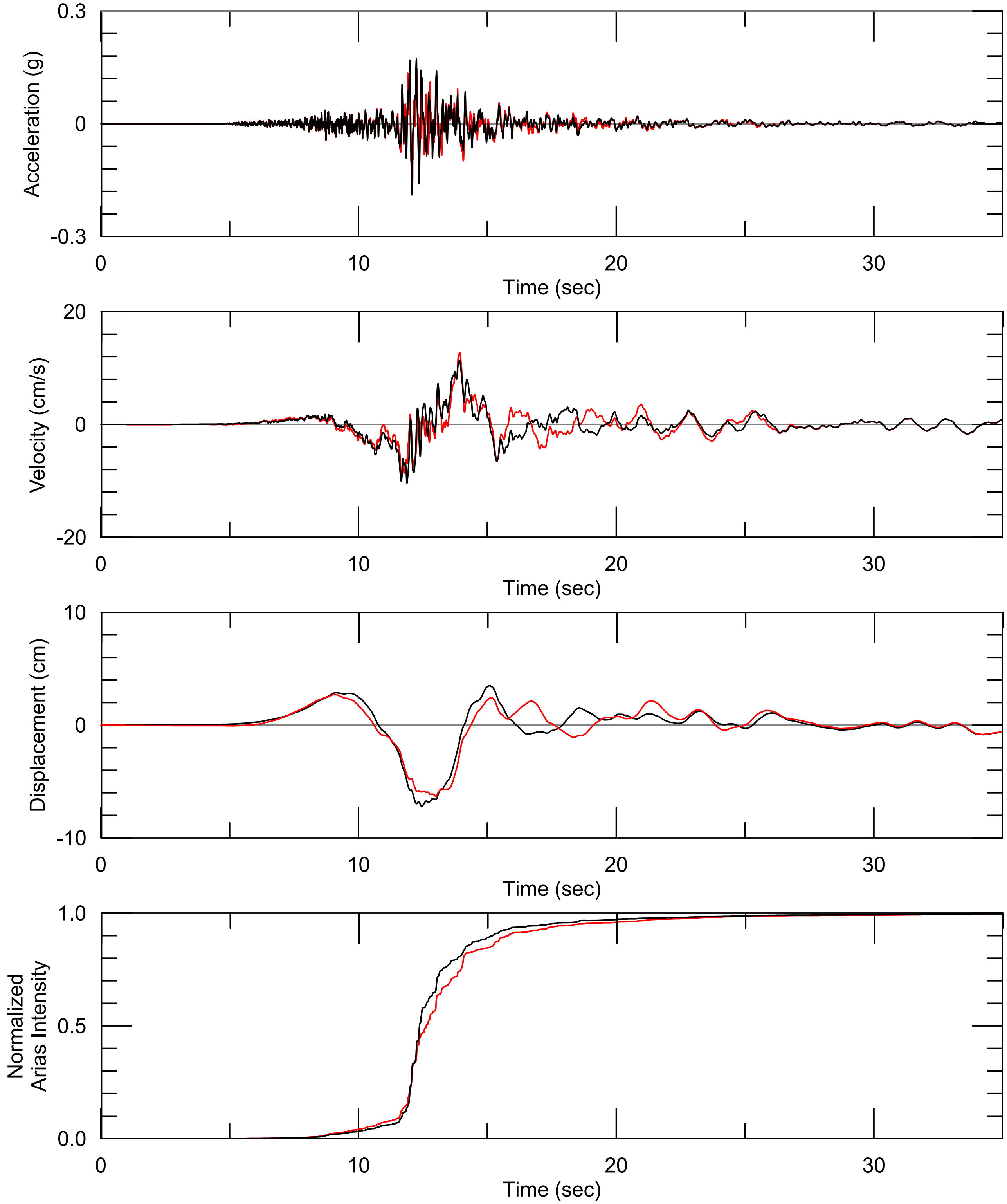

Spectrally Matched Motion

Scaled Seed Time History

SEED: PEER RSN 4472

Time History Spectrally-Matched to 10,000-Year Return Period Horizontal UHS, Pinal Schist and Gila Conglomerate Sites 2009 L'Aquila, Italy - Celano (XTE)

RESOLUTION COPPER, NEAR WEST SITE

Lettis Consultants International, Inc.

Figure 69

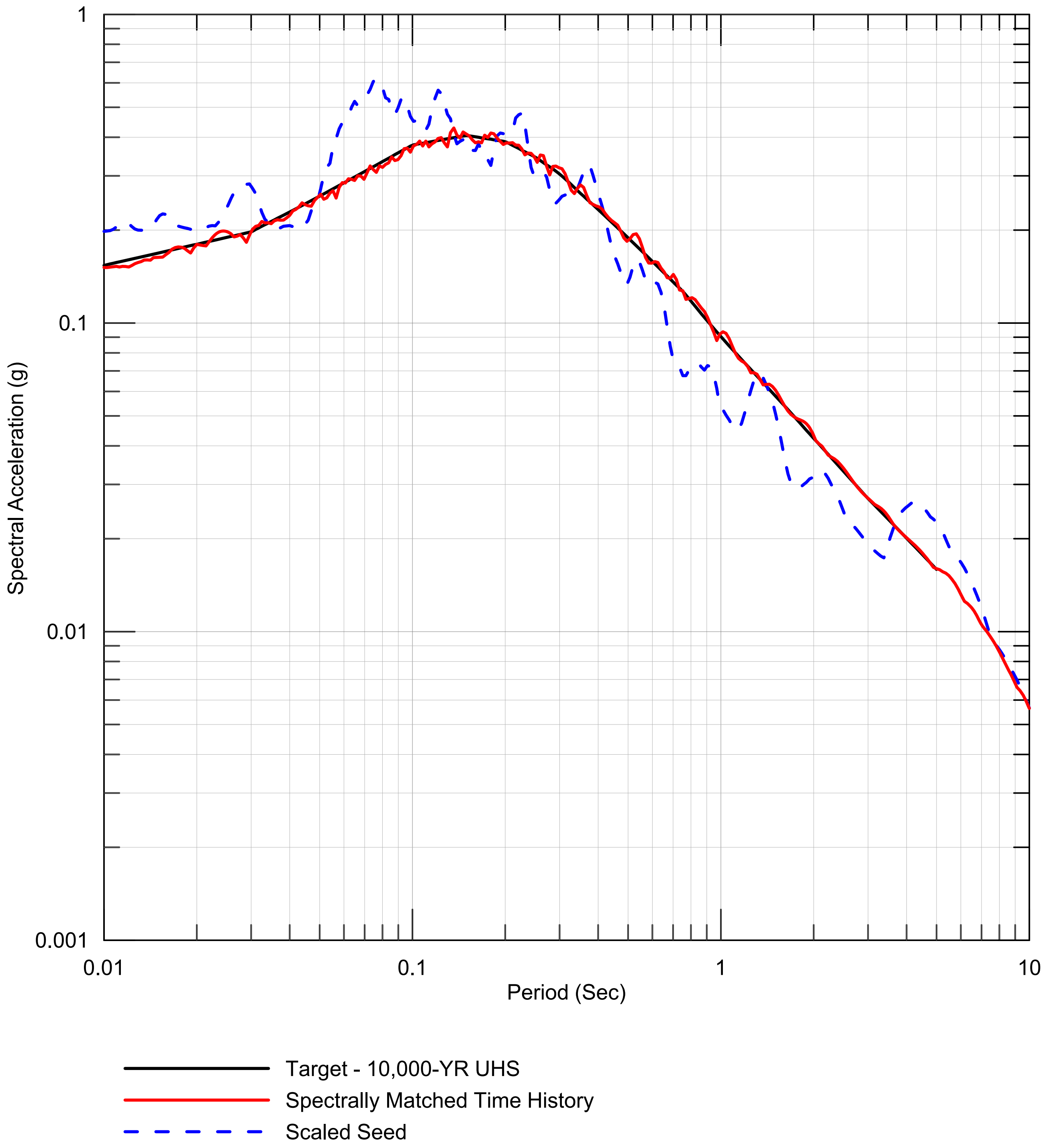

SEED: PEER RSN 8110

Response Spectra for Time History Spectrally-Matched to 10,000-Year Return Period Horizontal UHS, Pinal Schist and Gila Conglomerate Sites 2011 Christchurch, New Zealand - MQZ (N)

RESOLUTION COPPER, NEAR WEST SITE

Lettis Consultants International, Inc.

Figure 70

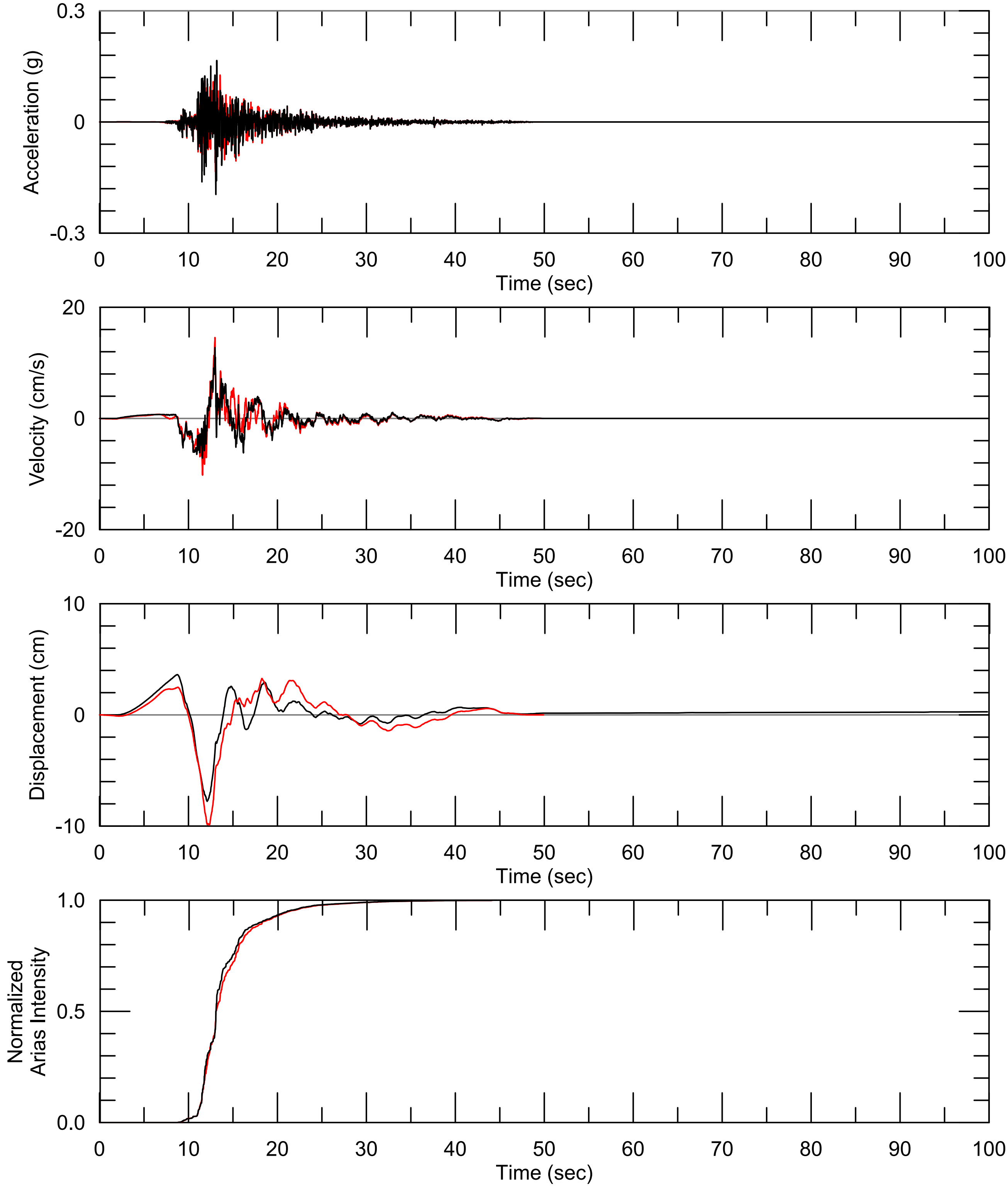

Spectrally Matched Motion
Scaled Seed Time History

SEED: PEER RSN 8110

Time History Spectrally-Matched to 10,000-Year Return Period Horizontal UHS, Pinal Schist and Gila Conglomerate Sites 2011 Christchurch, New Zealand - MQZ (N)

RESOLUTION COPPER, NEAR WEST SITE

Lettis Consultants International, Inc.

Figure 71

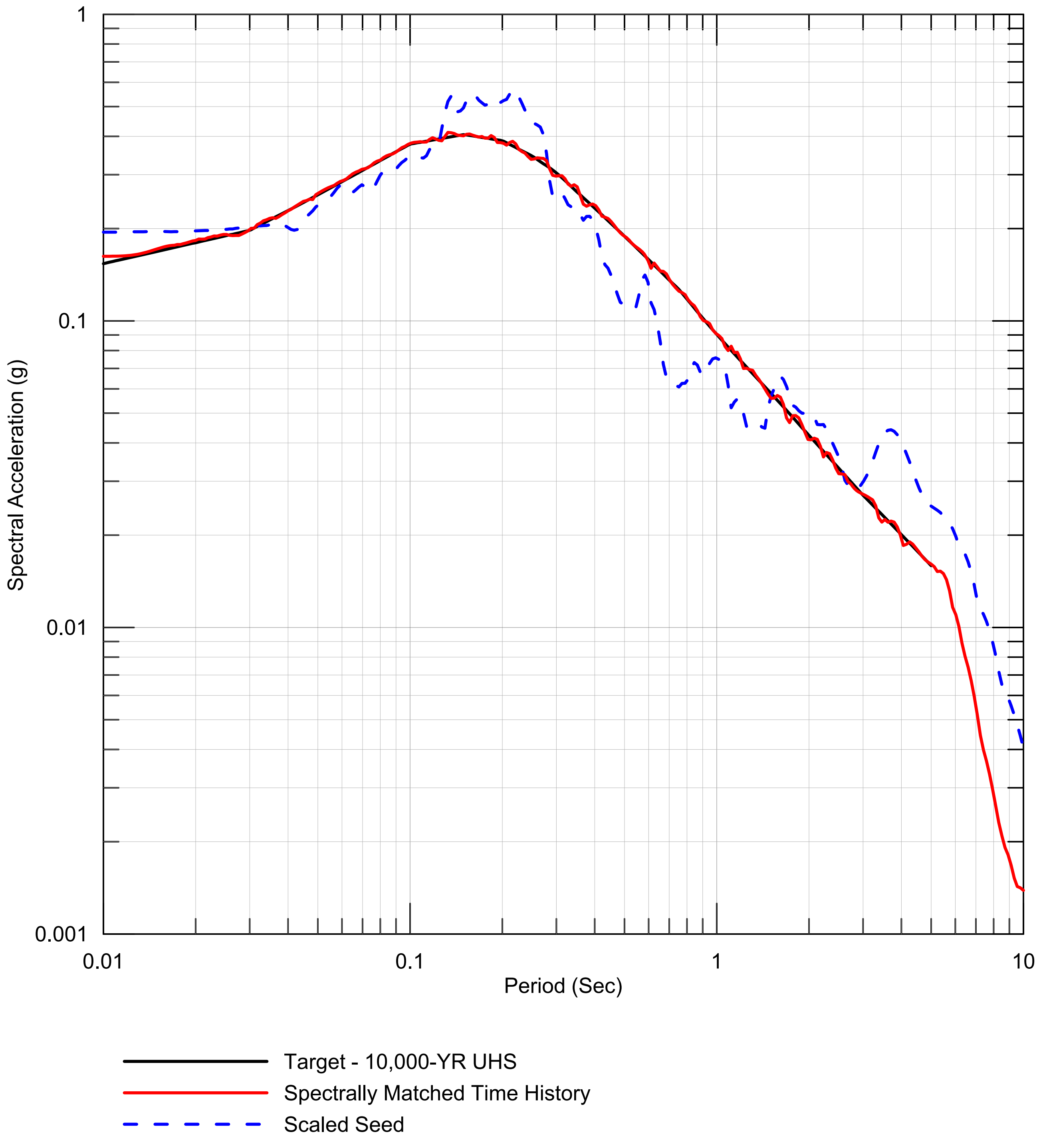

Response Spectra for Time History Spectrally-Matched to 10,000-Year Return Period Horizontal UHS, Pinal Schist and Gila Conglomerate Sites 2011 Christchurch, New Zealand - ROLC (61W)

RESOLUTION COPPER, NEAR WEST SITE

Lettis Consultants International, Inc.

Figure 72

SEED: PEER RSN 8126

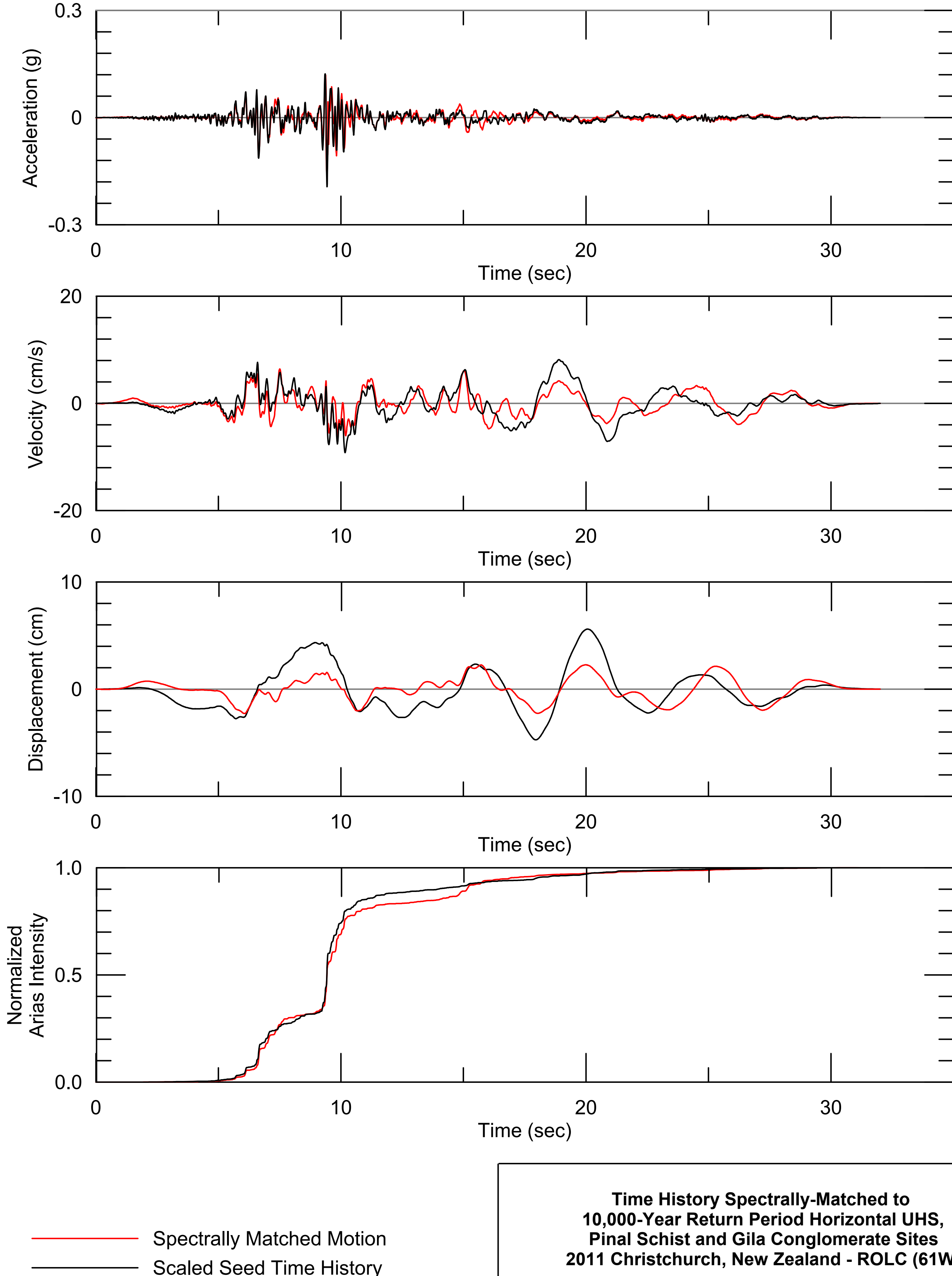

SEED: PEER RSN 8126

Time History Spectrally-Matched to 10,000-Year Return Period Horizontal UHS, Pinal Schist and Gila Conglomerate Sites 2011 Christchurch, New Zealand - ROLC (61W)

RESOLUTION COPPER, NEAR WEST SITE

Lettis Consultants International, Inc.

Figure 73

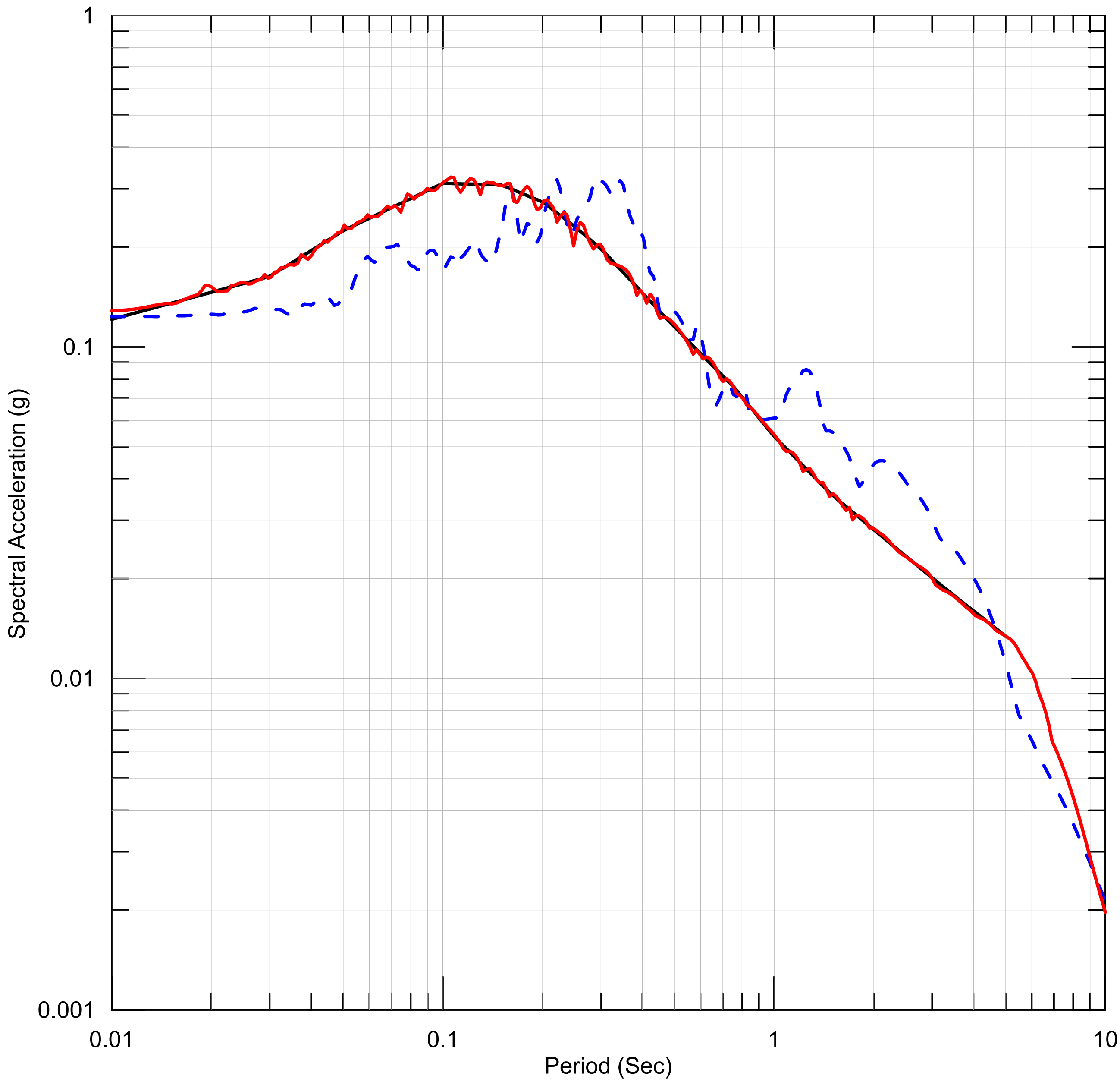

Target - 10,000-YR UHS
Spectrally Matched Time History
Scaled Seed

SEED: PEER RSN 238

Response Spectra for Time History Spectrally-Matched to 10,000-Year Return Period Horizontal UHS, Rhyolite and Diabase Sites 1980 Mammoth Lakes-03 - Long Valley Dam (L Abut) (090)

RESOLUTION COPPER, NEAR WEST SITE

Lettis Consultants International, Inc.

Figure 74

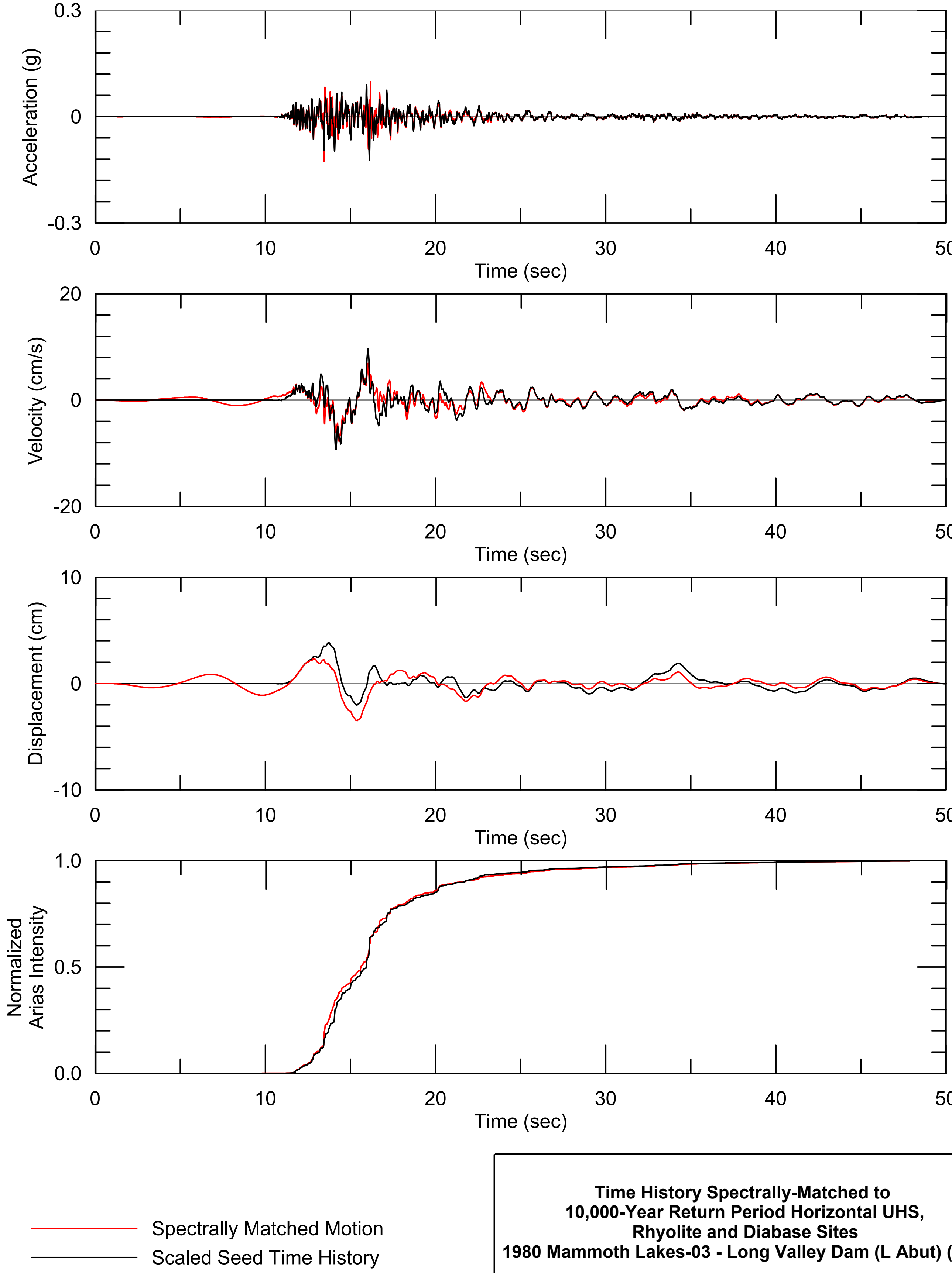

SEED: PEER RSN 238

Time History Spectrally-Matched to
10,000-Year Return Period Horizontal UHS,
Rhyolite and Diabase Sites
1980 Mammoth Lakes-03 - Long Valley Dam (L Abut) (090)

RESOLUTION COPPER, NEAR WEST SITE

Lettis Consultants International, Inc.

Figure 75

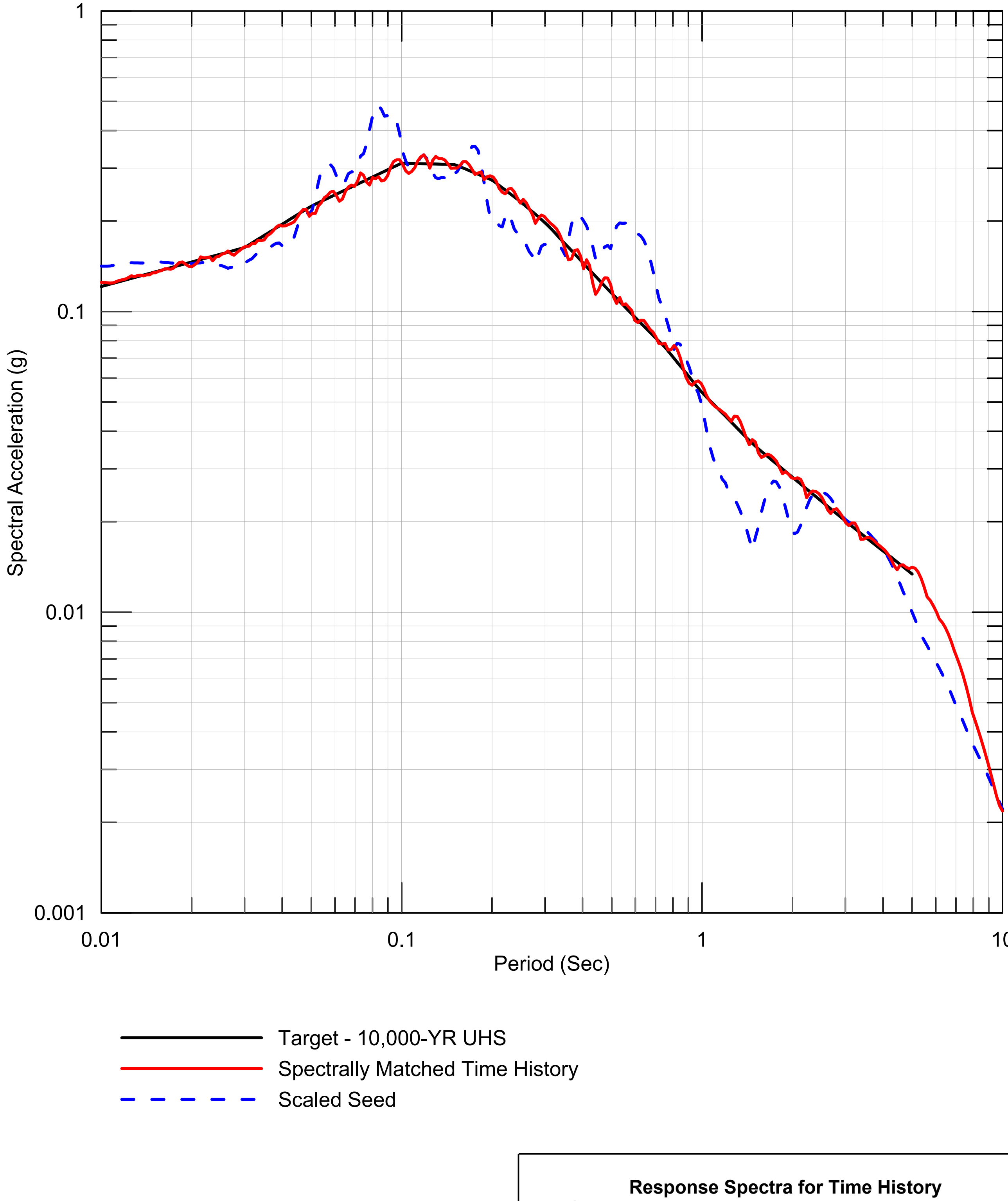

Response Spectra for Time History Spectrally-Matched to 10,000-Year Return Period Horizontal UHS, Rhyolite and Diabase Sites 1981 Westmorland - Superstition Mtn Camera (045)

RESOLUTION COPPER, NEAR WEST SITE

SEED: PEER RSN 318

Lettis Consultants International, Inc.

Figure 76

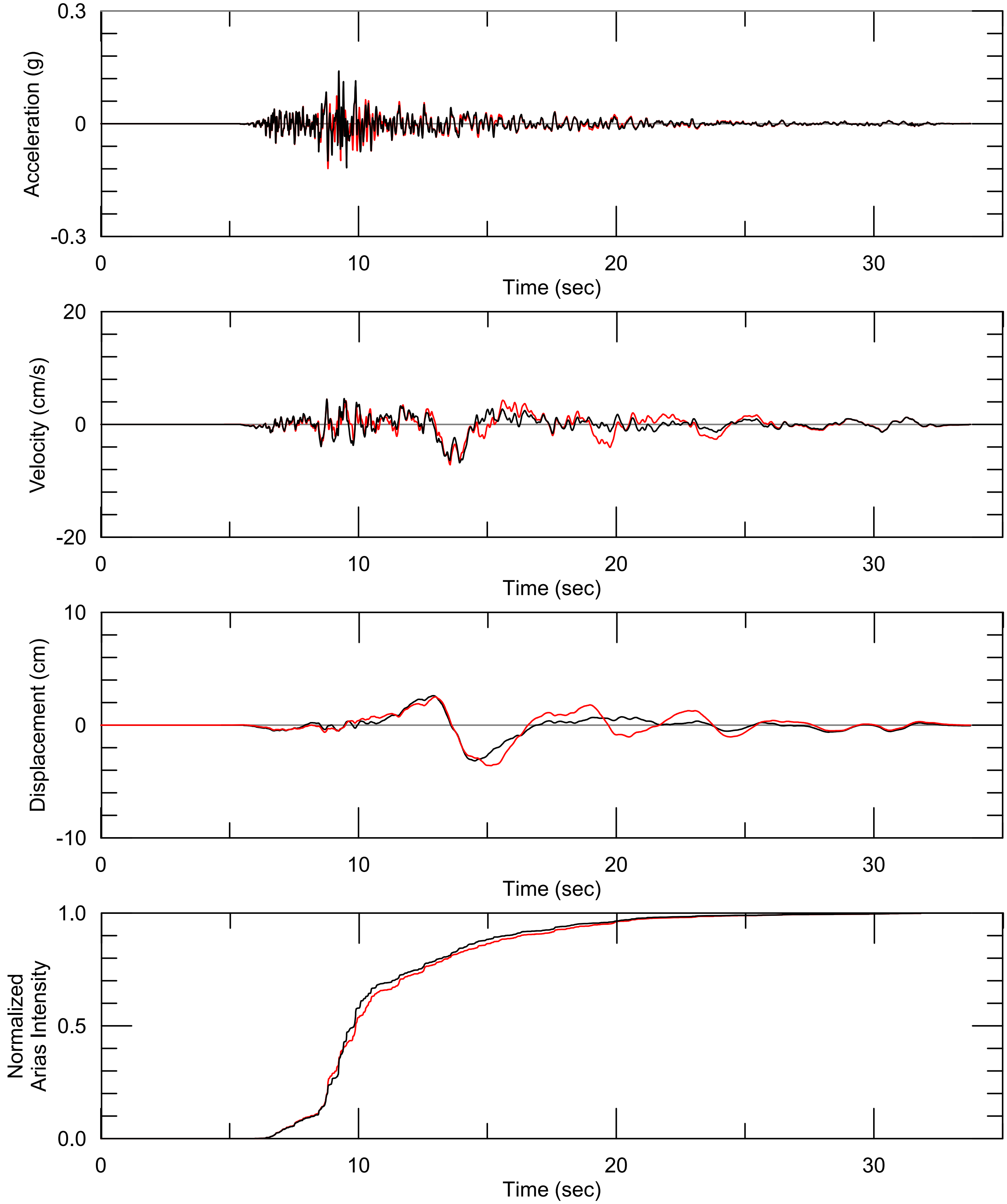

Spectrally Matched Motion
Scaled Seed Time History

SEED: PEER RSN 318

Time History Spectrally-Matched to 10,000-Year Return Period Horizontal UHS, Rhyolite and Diabase Sites 1981 Westmorland - Superstition Mtn Camera (045)

RESOLUTION COPPER, NEAR WEST SITE

Lettis Consultants International, Inc.

Figure 77

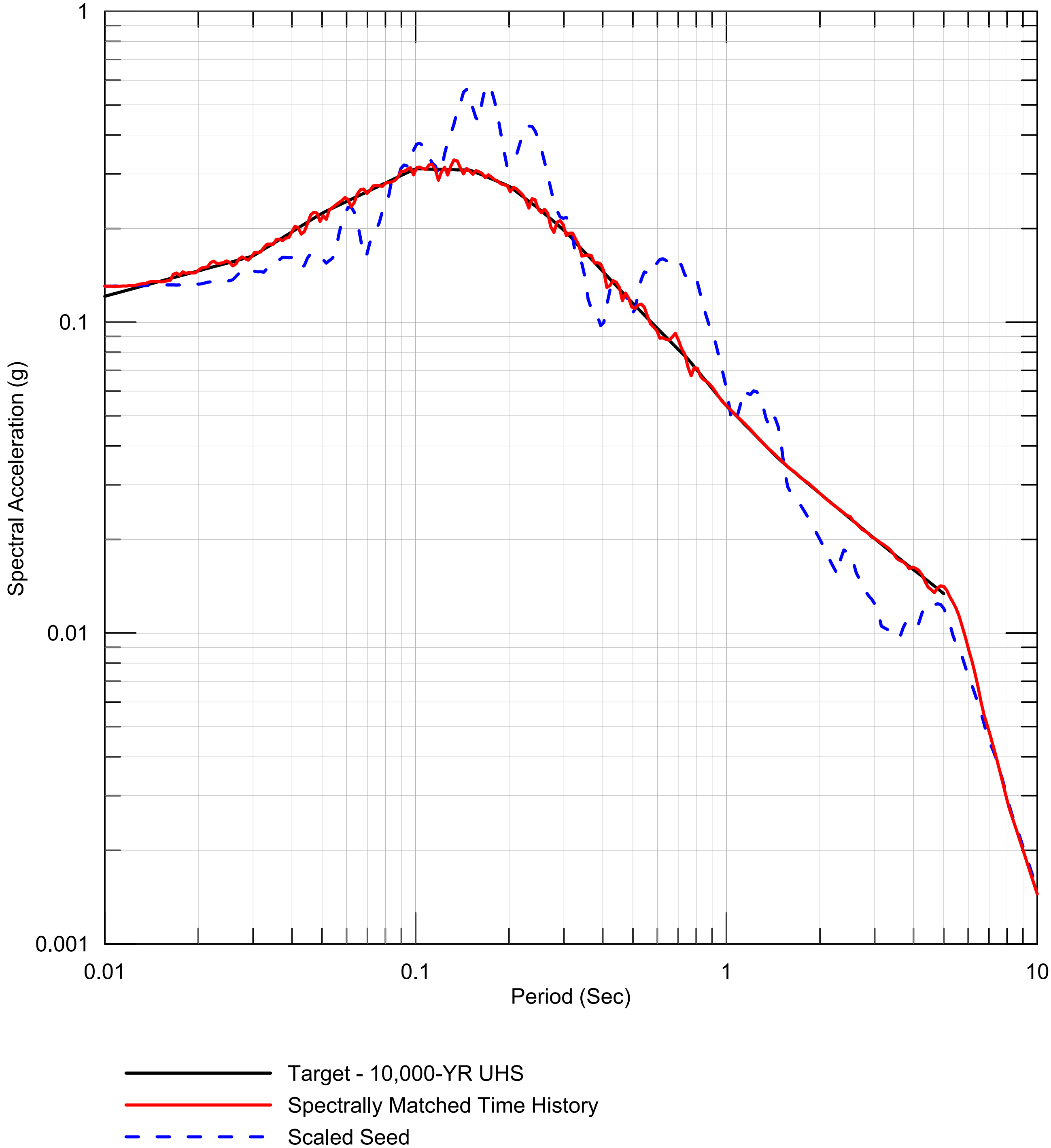

SEED: PEER RSN 2622

Response Spectra for Time History Spectrally-Matched to 10,000-Year Return Period Horizontal UHS, Rhyolite and Diabase Sites 1999 Chi-Chi,Taiwan-04 - TCU071 (E)

RESOLUTION COPPER, NEAR WEST SITE

LCI **Lettis Consultants International, Inc.**

Figure 78

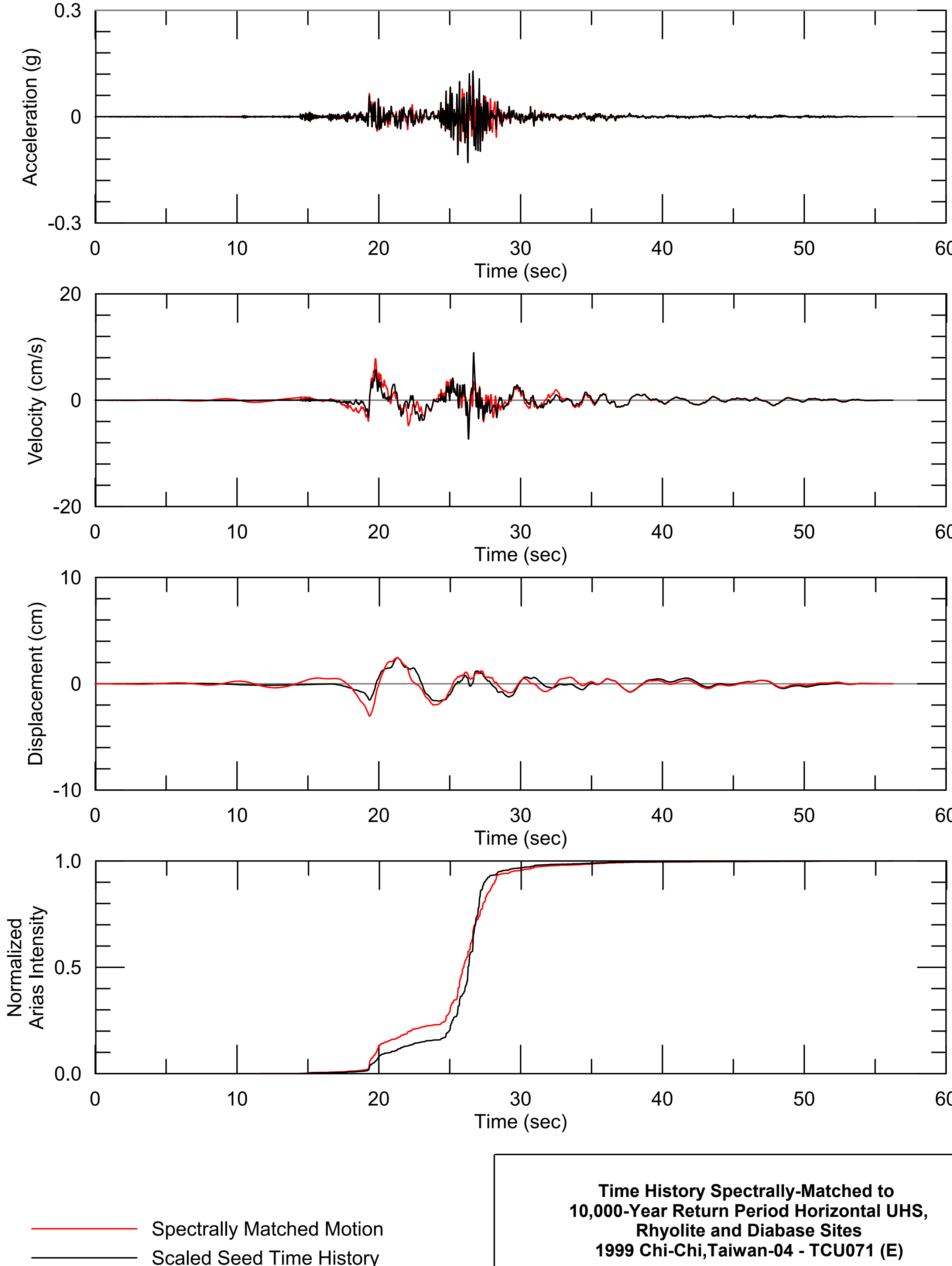

SEED: PEER RSN 2622

Time History Spectrally-Matched to 10,000-Year Return Period Horizontal UHS, Rhyolite and Diabase Sites 1999 Chi-Chi,Taiwan-04 - TCU071 (E)

RESOLUTION COPPER, NEAR WEST SITE

Lettis Consultants International, Inc.

Figure 79

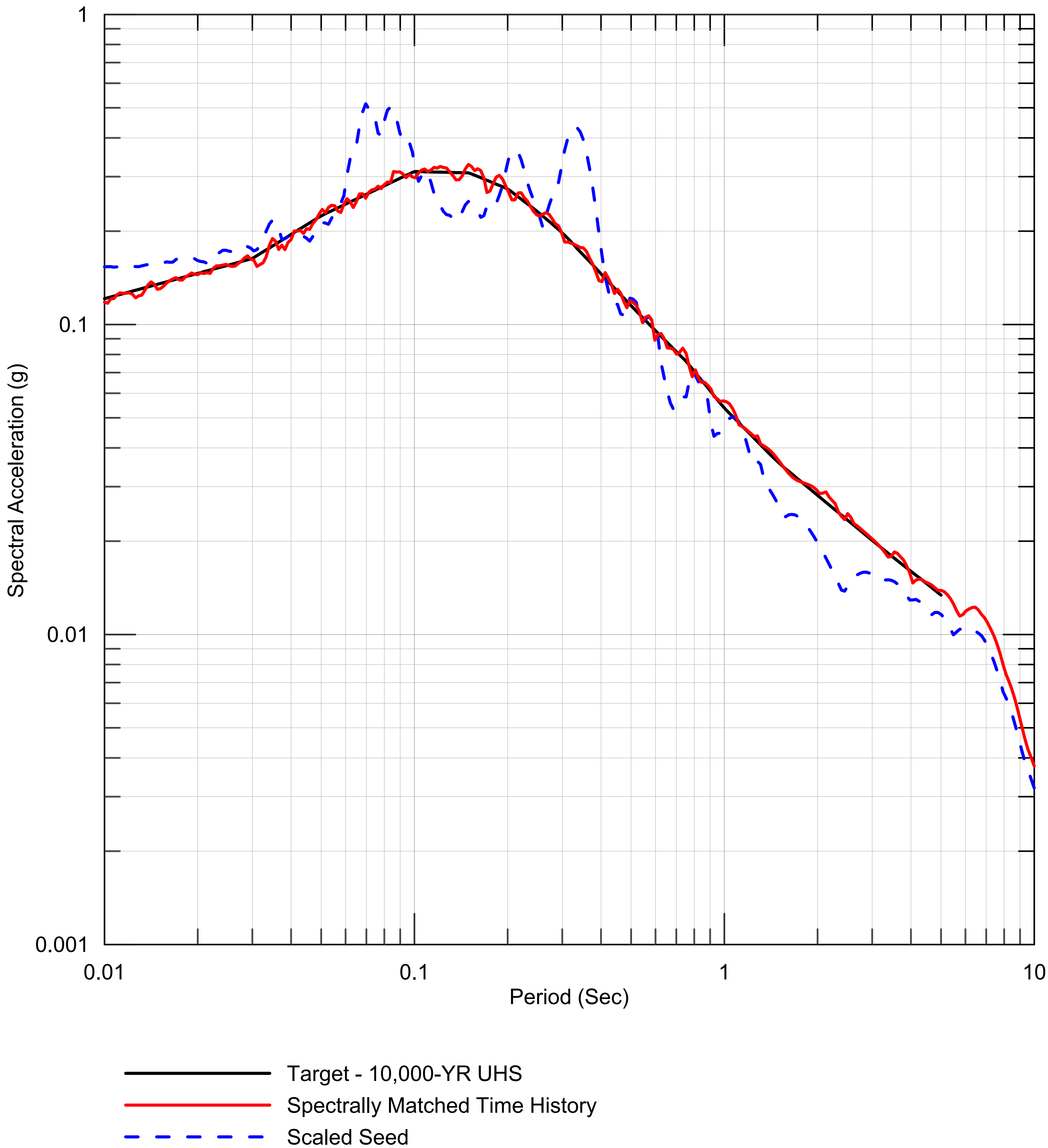

SEED: PEER RSN 4125

Response Spectra for Time History Spectrally-Matched to 10,000-Year Return Period Horizontal UHS, Rhyolite and Diabase Sites 2004 Parkfield-02 - Parkfield-Gold Hill 6W (360)

RESOLUTION COPPER, NEAR WEST SITE

Lettis Consultants International, Inc.

Figure 80

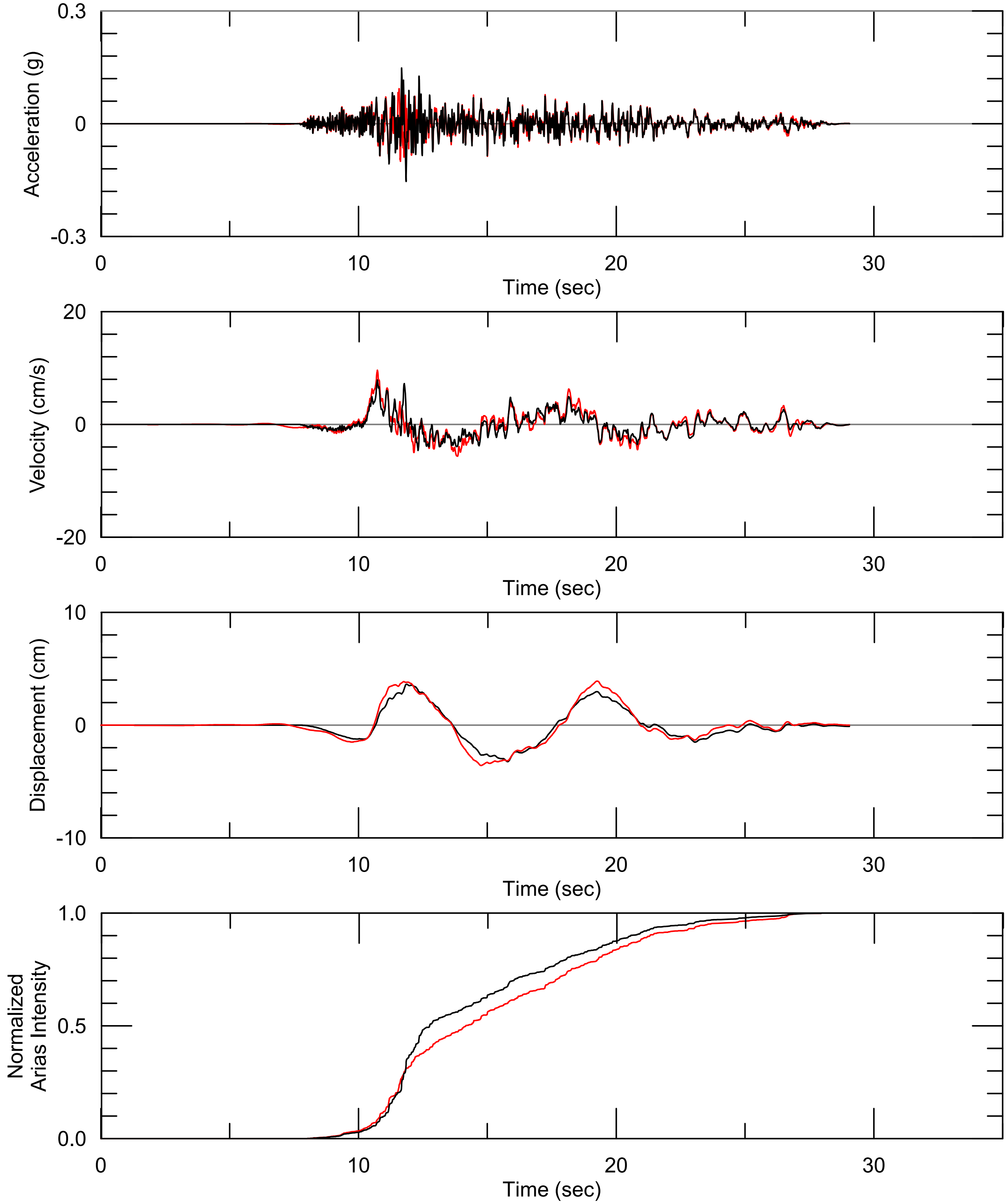

Spectrally Matched Motion
Scaled Seed Time History

SEED: PEER RSN 4125

Time History Spectrally-Matched to 10,000-Year Return Period Horizontal UHS, Rhyolite and Diabase Sites 2004 Parkfield-02 - Parkfield-Gold Hill 6W (360)

RESOLUTION COPPER, NEAR WEST SITE

Lettis Consultants International, Inc.

Figure 81

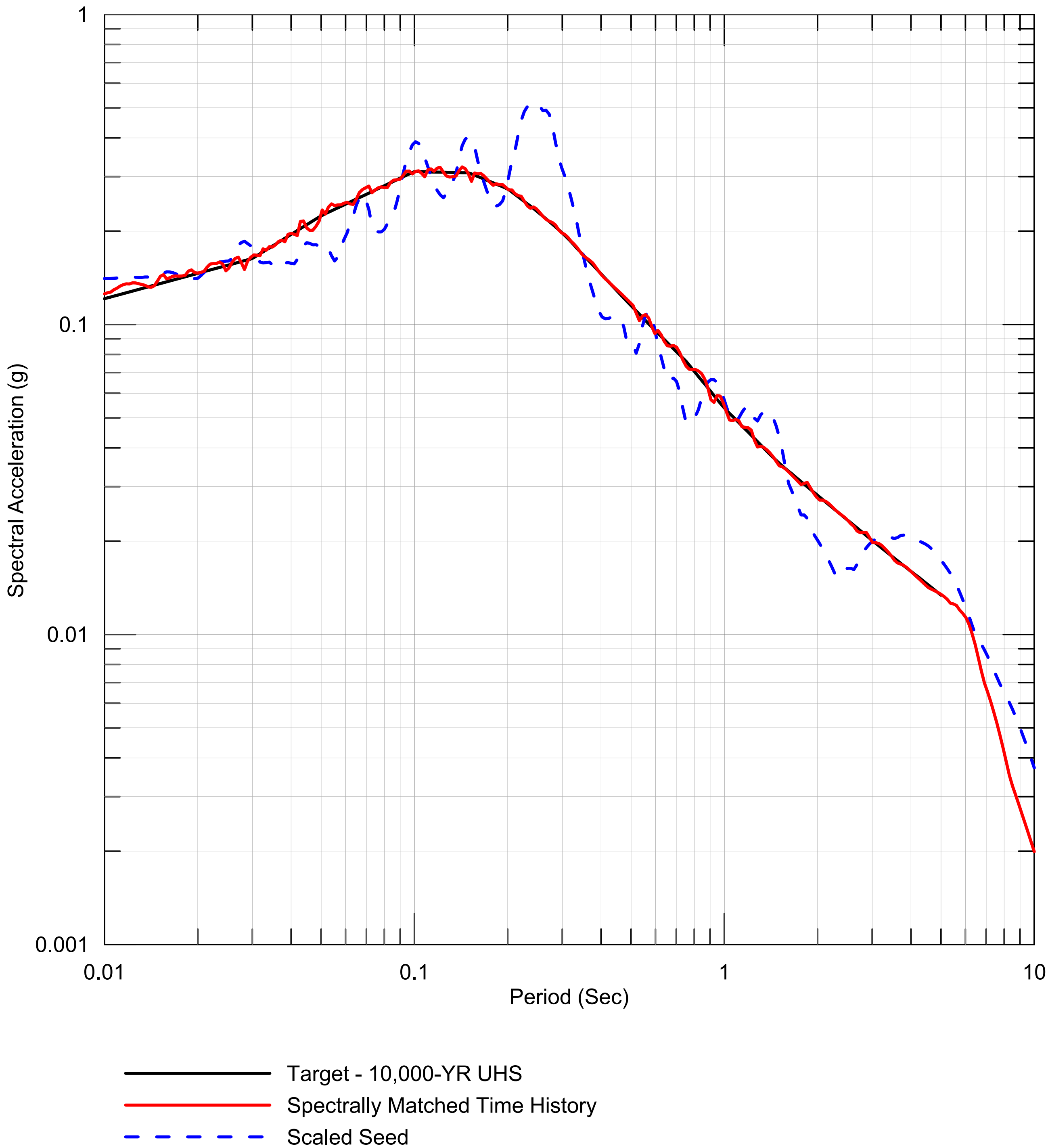

Response Spectra for Time History Spectrally-Matched to 10,000-Year Return Period Horizontal UHS, Rhyolite and Diabase Sites 2009 L'Aquila, Italy - Celano (XTE)

RESOLUTION COPPER, NEAR WEST SITE

Lettis Consultants International, Inc.

Figure 82

SEED: PEER RSN 4472

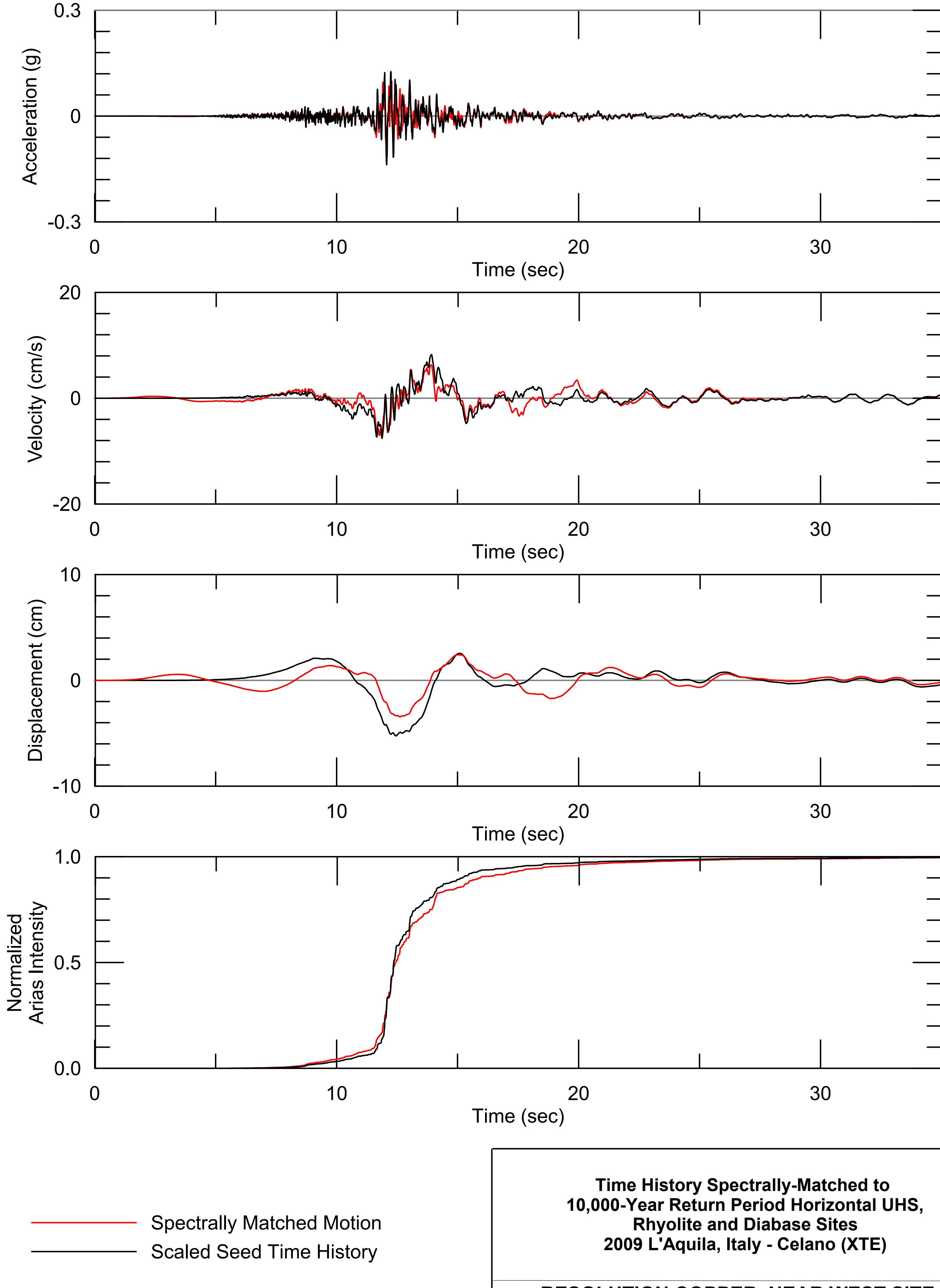

SEED: PEER RSN 4472

Time History Spectrally-Matched to 10,000-Year Return Period Horizontal UHS, Rhyolite and Diabase Sites 2009 L'Aquila, Italy - Celano (XTE)

RESOLUTION COPPER, NEAR WEST SITE

Lettis Consultants International, Inc.

Figure 83

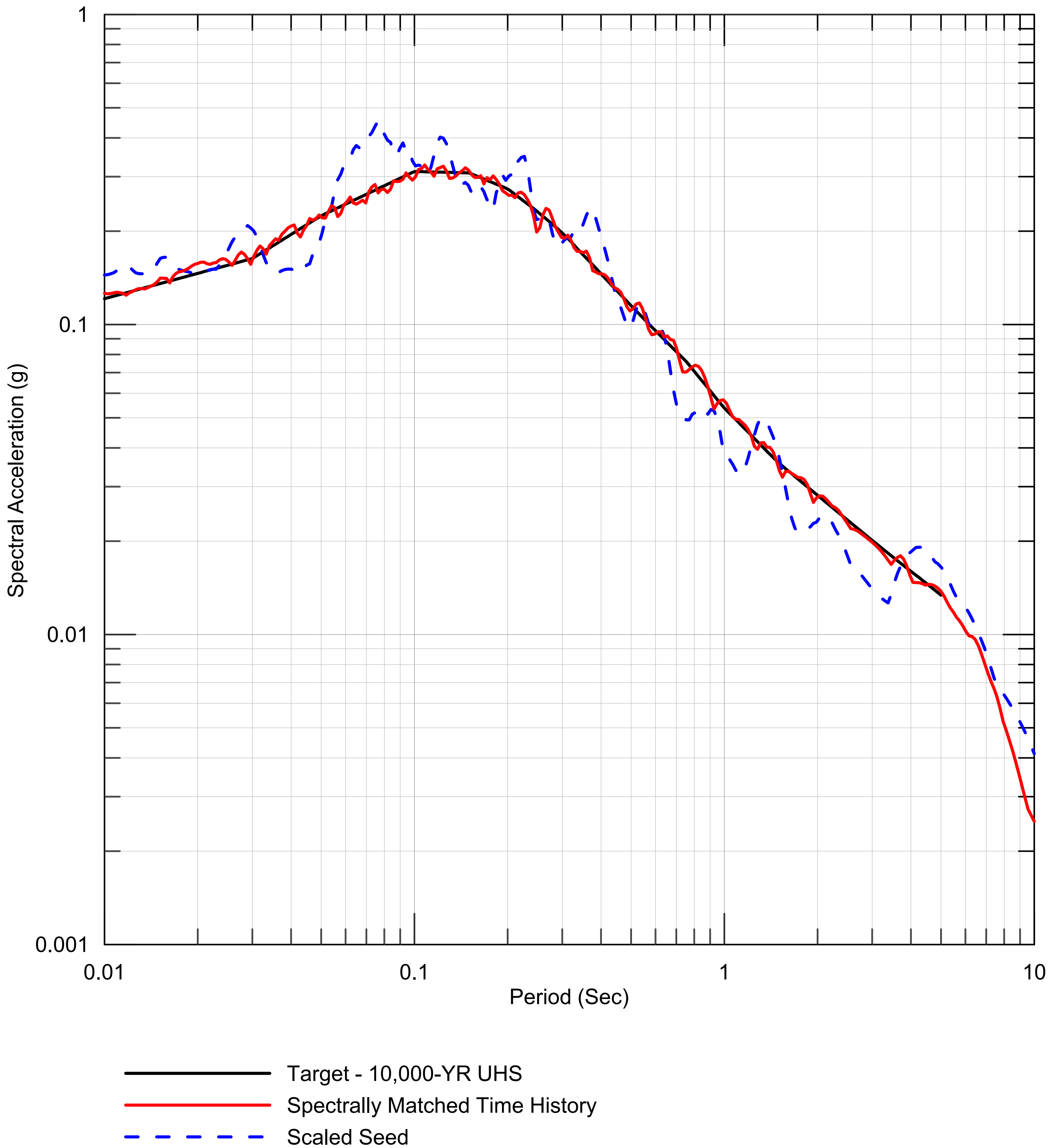

Response Spectra for Time History Spectrally-Matched to 10,000-Year Return Period Horizontal UHS, Rhyolite and Diabase Sites 2011 Christchurch, New Zealand - MQZ (N)

RESOLUTION COPPER, NEAR WEST SITE

Lettis Consultants International, Inc.

Figure 84

SEED: PEER RSN 8110

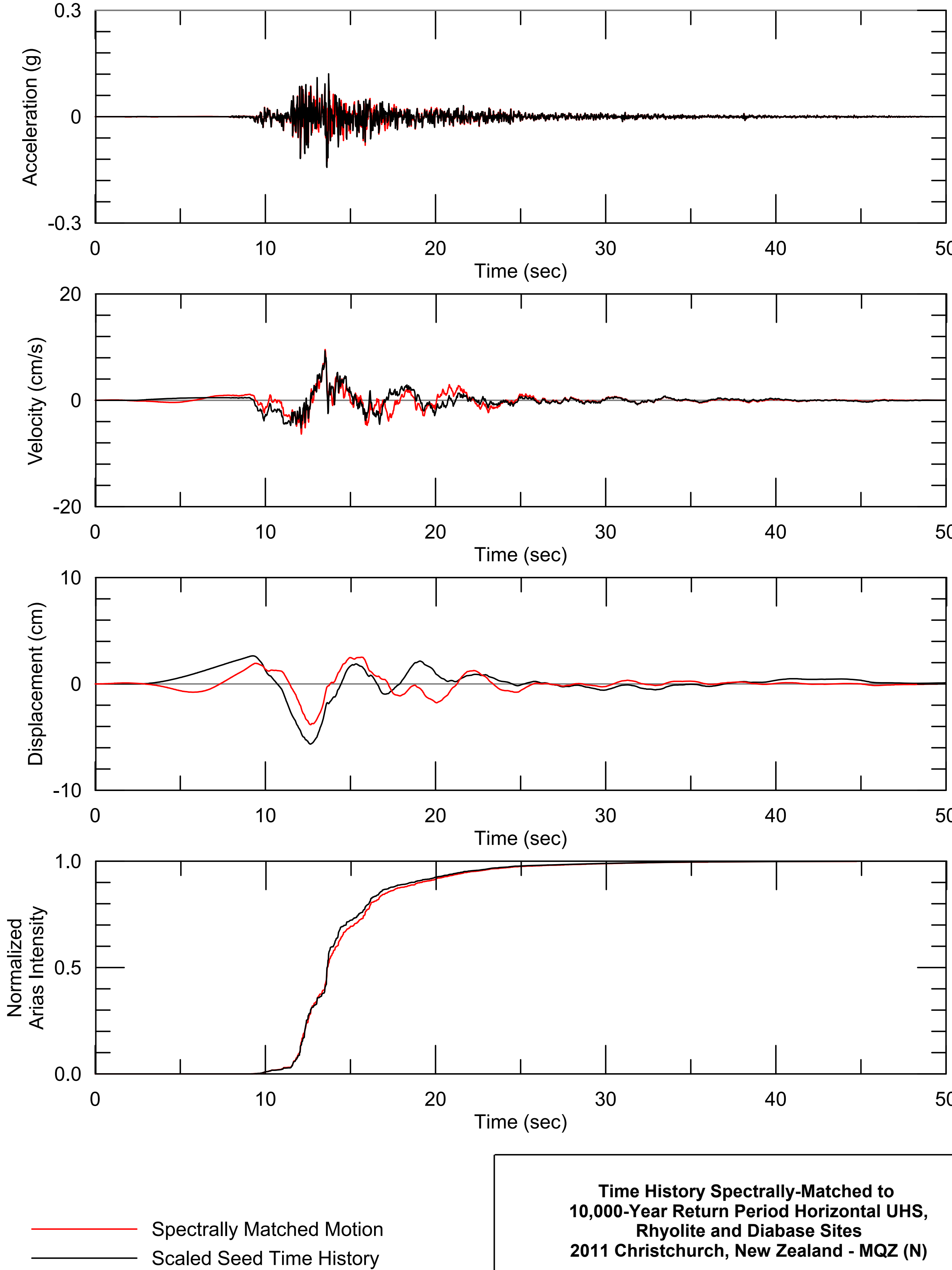

SEED: PEER RSN 8110

Time History Spectrally-Matched to
10,000-Year Return Period Horizontal UHS,
Rhyolite and Diabase Sites
2011 Christchurch, New Zealand - MQZ (N)

RESOLUTION COPPER, NEAR WEST SITE

Lettis Consultants International, Inc.

Figure 85

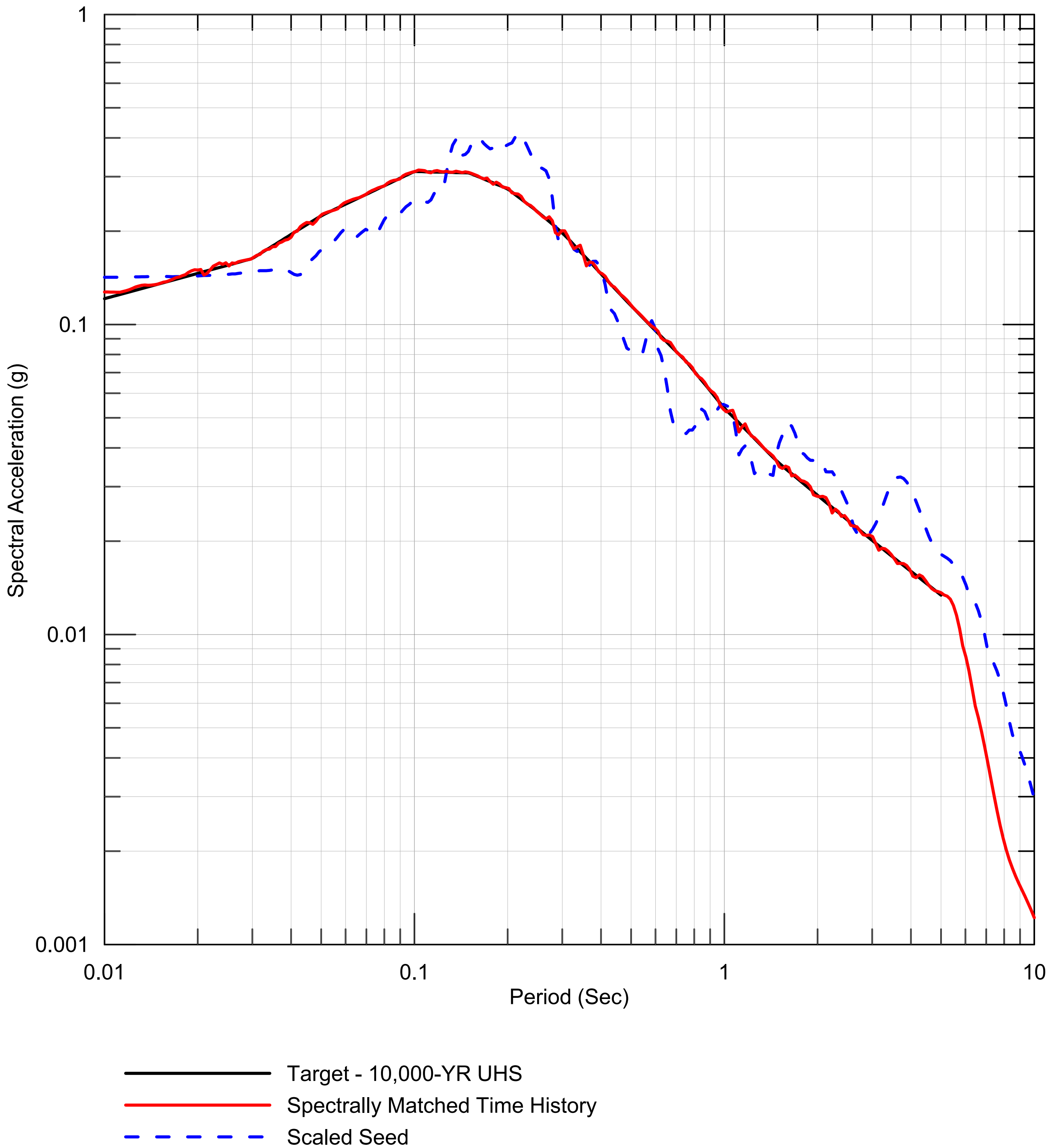

SEED: PEER RSN 8126

Response Spectra for Time History Spectrally-Matched to 10,000-Year Return Period Horizontal UHS, Rhyolite and Diabase Sites 2011 Christchurch, New Zealand - ROLC (61W)

RESOLUTION COPPER, NEAR WEST SITE

Lettis Consultants International, Inc.

Figure 86

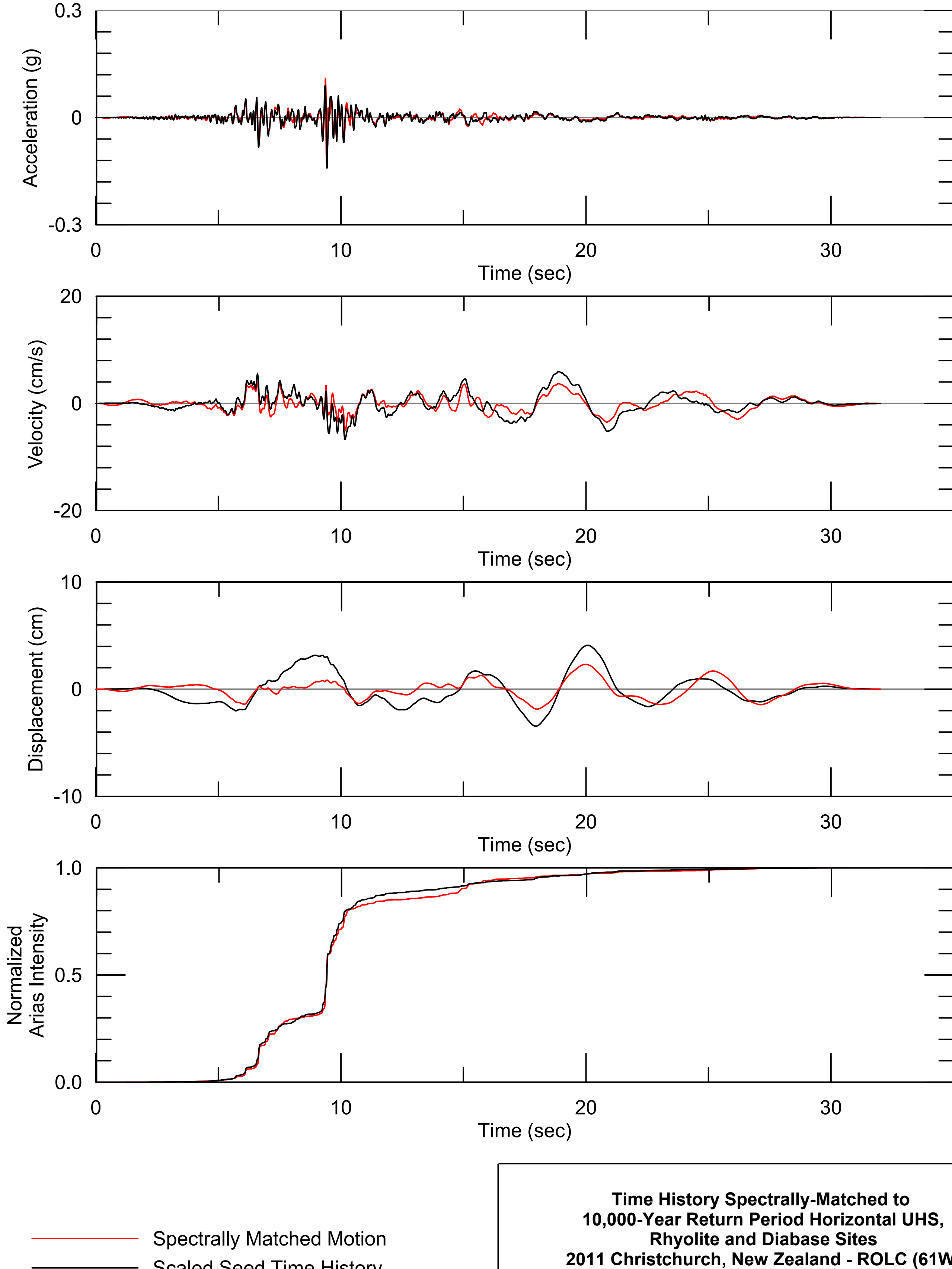

SEED: PEER RSN 8126

Time History Spectrally-Matched to 10,000-Year Return Period Horizontal UHS, Rhyolite and Diabase Sites 2011 Christchurch, New Zealand - ROLC (61W)

RESOLUTION COPPER, NEAR WEST SITE

Lettis Consultants International, Inc.

Figure 87